UCRL 9213

UNIVERSITY OF CALIFORNIA

Ernest O. Lawrence

Radiation Laboratory

FRACTIONAL CRYSTALLIZATION FROM MELTS

DISCLAIMER

UCRL-9213

UNIVERSITY OF CALIFORNIA

Lawrence Radiation Laboratory
Berkeley, California

Contract No. W-7405-eng-48

FRACTIONAL CRYSTALLIZATION FROM MELTS

William R. Wilcox

(Thesis)

June 1960

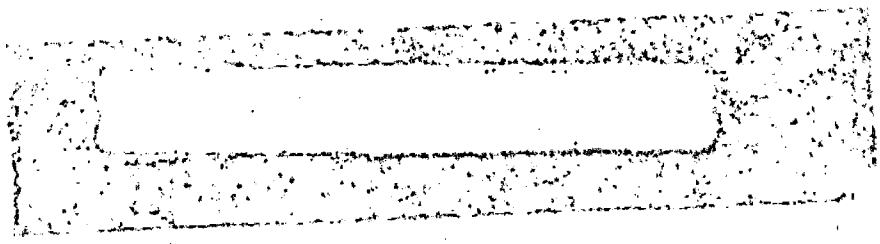

Printed in USA. Price $3.00. Available from the
Office of Technical Services
U. S. Department of Commerce
Washington 25, D.C.

FRACTIONAL CRYSTALLIZATION FROM MELTS

Contents

FRACTIONAL CRYSTALLIZATION FROM MELTS

William R. Wilcox

Lawrence Radiation Laboratory and Department of Chemical Engineering
University of California, Berkeley, California

June 1960

ABSTRACT

Studies of the separation process known as zone melting were made on 10% by weight (10%w) mixtures of β-naphthol and of benzoic acid in naphthalene. These systems were chosen as representative of the two simplest types of binary solid-liquid phase behavior, namely isomorphous and eutectic-forming. The solid mixtures were enclosed in 5 to 10 mm. glass tubes and pulled through a stationary heater, which generated a liquid zone. The separation attained in the process was significantly less than that predicted by assuming equilibrium between the bulk zone and the freezing solid. The separation increased as the zone travel rate decreased, as the size of the tube increased, and as the difference in liquid density between the bulk solid and the freezing interface increased. In addition, it was found that, for vertical tubes, the separation was much greater when the fluid of lower density (between the bulk zone and the freezing interface) was on the bottom than when it was on the top. Insertion of an axial tube or rod of metal or glass into the zone also increased the separation. These observations show conclusively that the separation was less than the equilibrium separation primarily because the zone was not completely mixed, especially near the freezing interface. By using the experimental data, a correlation was developed which enables estimation of the separation for various situations in zone melting.

Equations and principles were also developed which enable estimation of the thermal requirements for zone melting. A correlation of zone position, relative to the heater, was also developed from experimental measurements for low zone travel rates (less than 1 in/hr).

A theoretical study of pure diffusional mass transfer in zone melting was also made. In the present experiments, free convection was

sufficient so that mass transfer was not by molecular diffusion alone. However, for small tubes under proper conditions this condition would be realized. Consequently, a general expression for concentration profiles was derived for materials with a constant distribution coefficient. A method for the rapid estimation of these concentration profiles was also developed. Numerical results for eutectic-forming systems were obtained, and summarized in an analytical approximation.

Economic calculations were made for a separation in the multi-staged semi-continuous zone refiner known as a zone-void refiner. A cost on the order of $2.50 to $3.00 per pound was estimated for the separation of 500,00 pounds per year of 1%w β-naphthol in naphthalene into 0.1%w β-naphthol and 30%w β-naphthol. This is obviously uneconomical for a bulk chemical commodity, although it might be satisfactory for special, or ultra-high purity, chemicals. A capital investment of about four million dollars was also estimated to be necessary for this separation.

Exploratory experiments were made on a cooled-drum apparatus (modified drum-flaker), using NaCl-water as a system. These indicated that this equipment might be useful for large scale industrial separations, although further research and development are needed.

FRACTIONAL CRYSTALLIZATION FROM MELTS

William R. Wilcox

Lawrence Radiation Laboratory and Department of Chemical Engineering
University of California, Berkeley, California

June 1960

INTRODUCTION

A. Utility of Fractional Crystallization from Melts

Fractional crystallization from solutions has long been used for purification of materials. This method suffers from one great drawback, however. The mother liquor clings to the crystal and is often occluded by it.[1] Thus, in an attempt to purify a material in this manner, another impurity -- the solvent -- is introduced. Another disadvantage to crystallization from a solvent is the cost of the solvent. On an industrial scale, this ordinarily means additional equipment and operating costs for solvent recovery.

On the other hand, fractional crystallization from melts (or fractional solidification) uses no solvent, and so avoids these difficulties. In fractional solidification the material to be purified or separated is merely melted and then partially solidified. It is the purpose of this work to examine fractional solidification in general, and to study in detail two specific ways of carrying it out.

Fractional crystallization possesses advantages over other separation methods for some materials. For example, if a material is heat-sensitive with a low vapor pressure, distillation cannot be used. But if the melting point is below the heat-sensitive region, fractional solidification can be used. If a single pure crystal is desired, this can be accomplished in one step. To obtain ultrahigh purities in some materials, fractional solidification is the only method available.[2]

B. History

The use of solidification of melts for purification purposes is relatively new.[2] However, it was long used for the preparation of single crystals, e.g., by the Bridgman technique. Not until ultrahigh purity germanium was needed for semiconductor work was much thought given to purifying materials by growing crystals from a melt. At first, crystals were pulled from melts, or molten material was slowly solidified from one end to the other. This is called normal freezing and is illustrated in Fig. 1. The principal disadvantage of this process is that, in order to perform a multistage operation, the crystal must be sectioned between every pair of stages. This difficulty was overcome by Pfann, with his invention of zone melting.[2-5] In zone melting only a small zone in a bar of solid is melted. This zone is moved down the bar, with material melting into it on one side and freezing out on the other. This is illustrated in Fig. 2. The advantage here is that many passes of the zone (or several zones proceeding at once) can be made through a single bar. This gives a multistage effect without sectioning the rod. Zone melting of organic materials was studied theoretically and experimentally in this work.

Conventional zone melting, in turn, has a disadvantage -- it is a batch process. Each bar is processes individually. In order to avoid this difficulty, many variations of fractional crystallization from melts have been proposed and tried.[2,6-23] References to only a few of these are given here. One of these was investigated in an exploratory manner in this work. This was the modified drum flaker, or cooled-drum apparatus, which consisted of a cooled drum dipping into a stirred molten bath. Material solidifies on the rotating drum and is scraped off into the next tank. A series of these drums could be lined up into something analogous to a distillation column. Figure 3 shows a diagram of a possible multistage setup. The principal advantages of this system are:

(a) The melt can easily be mechanically stirred. This enables larger solidification rates to be obtained (see discussion on mass-transfer effects).

(b) It is readily adaptable to continuous, multi-stage operation.

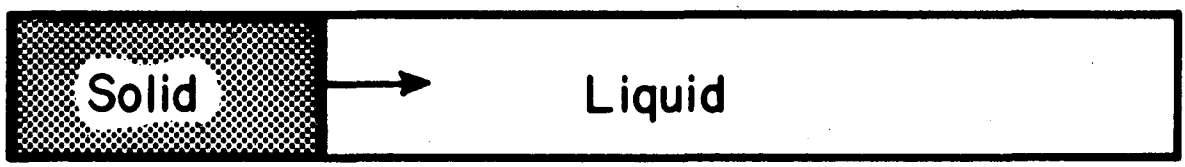

MU-20408

Fig. 1. Fractional solidification by normal freezing (schematic).

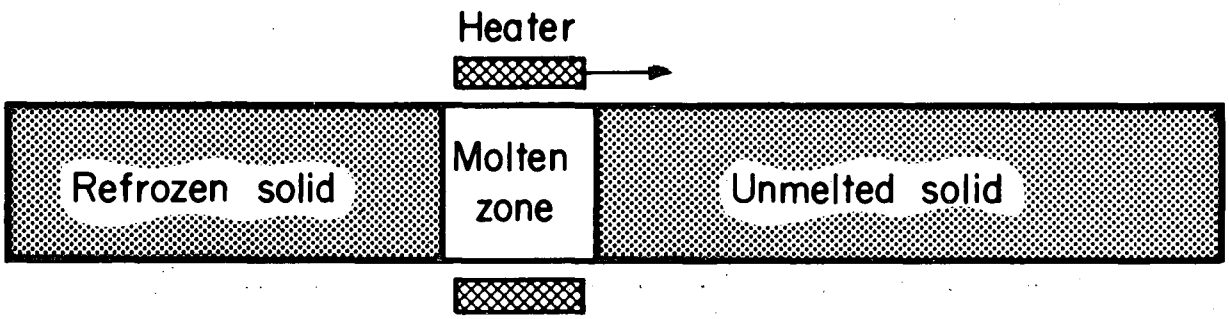

MU-20409

Fig. 2. Fractional solidification by zone melting (schematic).

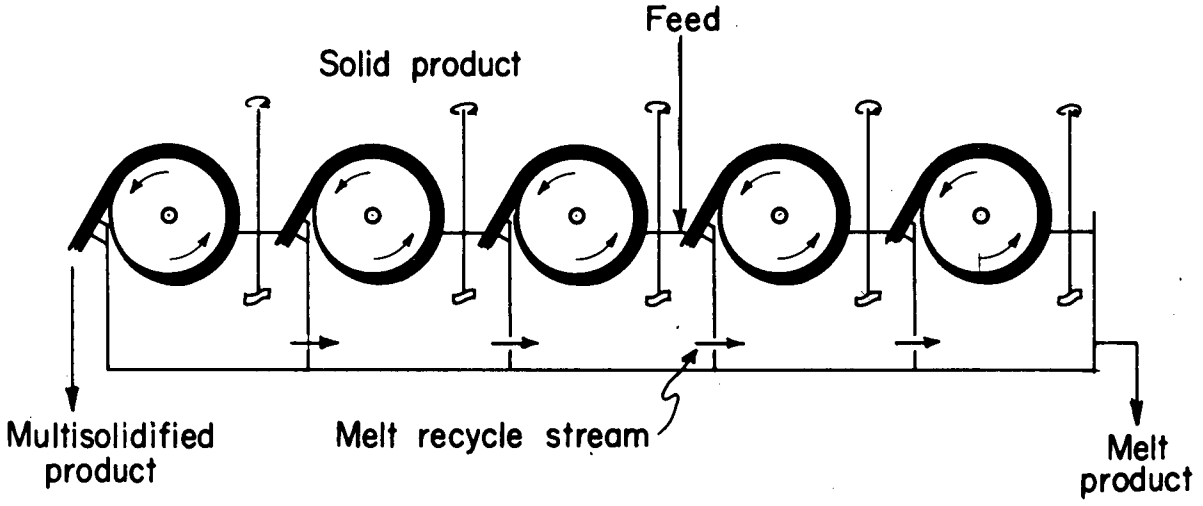

Fig. 3. Continuous, multi-staged, cooled-drum fractional solidifier (schematic).

The history of the cooled-drum apparatus is rather curious. Although Wilke, of this laboratory, conceived this apparatus independently, essentially the same idea was presented by Pfann in his excellent introductory book, Zone Melting.[2] Even more startling was the discovery that in 1943 Baron described a similar apparatus in his B.S. thesis.[24] He used a tin can for a drum and tried to separate waxes. He obtained no separation by solidification alone.

C. Design and Operational Considerations

In the design and operation of fractional-solidification equipment, many factors must be taken into account. These are discussed in the following pages.

Limiting Separation

The best separation that can be obtained is that in which the freshly frozen solid and the bulk liquid are in equilibrium. The relationship between compositions of solid and liquid in equilibrium may be read directly from a phase diagram.[2] (See Chapter III.) Usually this relationship is given in terms of a distribution coefficient, k, defined as the ratio of concentration of a component in the solid to that in the liquid. In many cases, especially when the concentrations are small, the distribution coefficient is constant over the concentration range of interest. In this work, concentration is expressed in weight fractions.

The concentration profile in a rod subjected to one zone pass may be easily calculated if the following assumptions are made:[2]

(a) Initial uniform concentration in rod
(b) Uniform cross-sectional area in rod
(c) Uniform zone size
(d) No solid-state diffusion
(e) Solid and liquid at equilibrium, at freezing interface
(f) Zone completely mixed and uniform
(g) Density same in liquid and solid
(h) Constant distribution coefficient
(i) Infinitely long rod.

With these assumptions, there is obtained

$$\frac{w_s}{w_0} = 1 - (1 - k)\ e^{-k\frac{z}{L}}, \qquad (1)$$

where w_s is the weight fraction of a component at a distance z from the first material frozen out of the molten zone, w_0 is the initial uniform concentration, k is the distribution coefficient (in weight fractions), L is the zone length, and z is the distance along the tube from the point where the solid first came out of the molten zone.

Needless to say many of these conditions are often not met in practice. Condition (e), equilibrium at the interface, has been shown to hold very closely.[24] The effects of removing conditions (a), (e), (f), and (i) have been studied.[26-34] The effects of removing conditions (f), (g), and (h) were investigated in this work.

Correction for different densities in the solid and liquid phases is rather simple and will be discussed now. Assume the rest of the conditions above hold. Imagine the zone moving through a differential length dz (see Fig. 4). The weight of the component coming out of the zone is $w\rho_s A dz$, where ρ_s is the density of the solid, and A is the cross-sectional area of the bar. Coming into the zone is $w_0\rho_s A dz$, The increase in the zone is $\rho_\ell AL\ dw_\ell$, where ρ_ℓ is the density of the liquid and w_ℓ is the weight fraction in the molten zone. A mass balance yields:

$$w_s\ \rho_s\ A\ dz - w_0\ \rho_s\ A\ dz = -\ \rho_\ell\ AL\ dw_\ell. \qquad (2)$$

But, by definition, w_ℓ equals w_s/k. With this, and rearranging, we have

$$\frac{k}{L}\ \frac{\rho_s}{\rho_\ell}\ dz = \frac{dw_s}{w_s - w_0}\ . \qquad (3)$$

Noting that $w_s = kw_0$ when $z = 0$ and integrating from 0 to z, we get

$$\frac{w_s}{w_0} = 1 - (1 - k)\ e^{-k\frac{z}{L}\ \frac{\rho_s}{\rho_\ell}}\ . \qquad (4)$$

Similar considerations apply for fractional solidification operations other than zone melting.

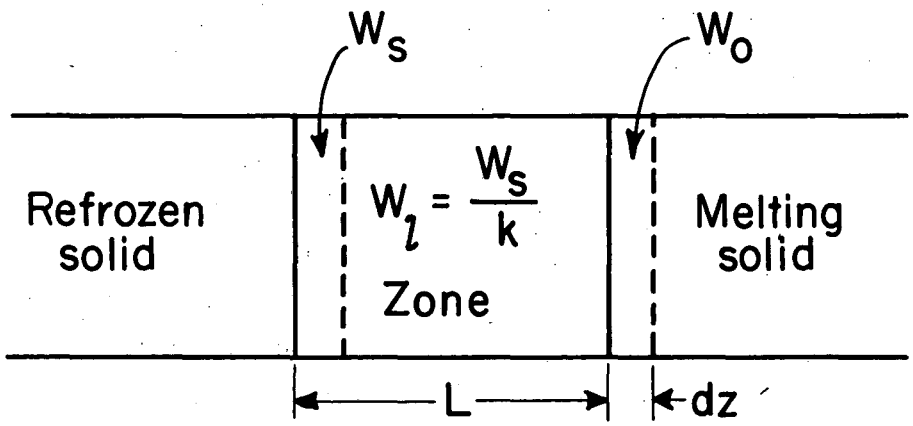

MU-20411

Fig. 4. Average concentrations (in weight fractions) in and near a moving zone, after it has moved a differential distance.

Actual Separations

In practice, of course, these ideal separations are seldom attained. As might be expected, the separation decreases as the speed of crystallization increases. Many workers, this author included, have observed this effect specifically for zone melting.[34-41] Several mechanisms that have been proposed to explain this are:

(a) Occlusion of the mother liquor. As the speed of solidification increases, the freezing interface tends to become rough and form dendrites.[1] These formations tend to trap the mother liquor. Usually, however, the interfaces are smooth at growth rates normally used for separations (about 0.1 to 4 cm/hr.).

(b) Adsorption on the growing crystal surface. Some materials are known to adsorb on the surface of a crystal in a concentration exceeding the equilibrium value.[1] The equilibrium value actually holds only between the bulk solid and liquid. This adsorption is merely a surface effect. If growth is occurring, these excess "impurity" molecules tend to diffuse back to the interface from the solid interior. If the crystal is growing fast, however, new molecular layers pile on top of the old too fast for this relaxation, or diffusion, to take place. Hall has derived an expression for the actual obtainable distribution coefficient at the crystal surface when adsorption occurs.[34] Unfortunately the parameters involved cannot, in general, be predicted. He also obtained data for growth of germanium crystals with antimony impurity in which the observed distribution coefficient behaved in the predicted manner. The observed distribution coefficients also depended on which lattice direction acted as the growing interface. This is what one might expect for a surface phenomenon. This whole theory is somewhat controversial, and in any case, appears to apply chiefly only at relatively high growth rates.

(c) Incomplete liquid mixing. Because of segregation, an excess of one component and a depletion of the other is created in the liquid immediately adjacent to the growing crystal. In order for further separation to occur, this excess must be transported away from the interface by some combination of diffusion and convection. As the velocity increases, new material arrives faster and faster at the freezing interface, making this transport against the current increasingly difficult.

The limiting cases of transport by diffusion only and by diffusion in a thin boundary layer outside which complete mixing prevails have been solved by the author and by others.[28,32,33,42-46] These derivations and further discussion are given in Chapter VII.

(d) Constitutional subcooling. As mentioned in (c) above, segregation leads to a concentration gradient at the freezing interface. This concentration gradient, in turn, produces a gradient in melting point (see phase diagrams in Chapter III). The imposed temperature gradient may actually fall below the melting point at a small distance from the interface (see Fig. 5). This phenomenon is known as constitutional subcooling. It is thought to be responsible for the cellular substructures observed in the growth of some metal alloy crystals.[47,48] It is also thought to be responsible for the cyclic impurity concentrations observed in many crystals grown from melts.[48-52] It is not certain, however, that this was not due to a variation in temperatures of heat sources and (or) sinks. This could also lead to a variation in growth rate and hence in impurity uptake. Constitutional subcooling could lead to a similar result by the following mechanism: As segregation occurs the concentration changes at the interface. This lowers the temperature of the interface and possibly increases the amount by which the melting point exceeds the imposed temperature adjacent to the interface. If this excess becomes large enough, solid nuclei actually form in the liquid. The layer of subcooled liquid rapidly freezes, entrapping the undesired component accumulated there. This process then repeats itself. As the velocity of solidification increases, the concentration gradient at the interface increases, and hence, the likelihood of such an intermittent flash freezing increases. Unfortunately, no quantitative results have been derived as yet.

These various mechanisms lead to different predictions for the effect of such variables as the geometry of the liquid layer, the degree of stirring, and various physical properties of the material. In Chapter VII these predictions will be compared with some experimental results on zone melting of organic compounds. In this way it is hoped to determine the best mechanism for fractional solidification of organic materials.

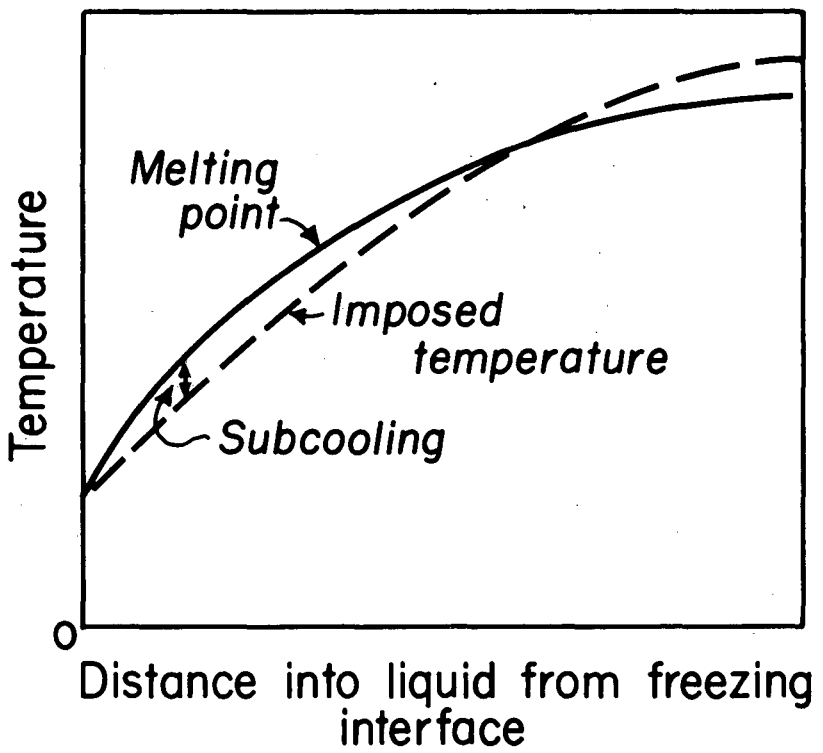

Fig. 5. Constitutional subcooling (schematic).

Thermal Considerations

To maintain a liquid region and a solid region, heat sources and sinks must be used. Among the types of heaters used are induction, electron-beam, radiant, and resistance. Normally these heaters are also moved relative to the melt in order to control the growth of the crystal. This may either take the form of a moving heater or a stationary heater with a moving working material.

For calculation of heat and temperature requirements several peculiarities must be noted. Usually the crystal is grown at a constant rate, and so only the steady-state operation need be analyzed. It is most convenient to take the solid-liquid interface as the origin for heat-transfer calculations. This, however, leads to a convection term in the conduction equations, since the material moves relative to the interface. One must also take into account the latent heat of fusion liberated at the freezing interface. These principles are all illustrated in the heat-transfer calculations in Chapters V and VIII.

One detail absolutely essential for these heat transfer calculations is knowledge of the interface temperature. It would be convenient if this were the melting point.* However, it is known that the actual interface is lower than this for freezing and higher for melting.[1,53] These temperature differences increase with increasing velocity of melting or freezing. Two methods have been used to measure subcoolings corresponding to certain growth rates:

(a) Direct measurement of the temperature of a growing interface. This method fails because the temperature probe conducts heat away from the interface, and thus is at a slightly different temperature from the interface. Because the temperature probe is usually in motion with respect to the moving interface, the experimental results are also difficult to interpret.

*Or more correctly the freezing point. For a multicomponent melt, the freezing point is properly defined as that temperature at which the solid is first formed. The melting point is the highest temperature at which the material is completely solid. In the discussion on constitutional subcooling, the term "freezing point" is also more correct than "melting point." See Chapter II on Experimental Equipment and Systems for sample phase diagrams.

(b) Measurement of the growth rate in a subcooled liquid. The temperature of the interface is assumed to be that of the liquid. Because of latent-heat liberation at the interface, however, it is actually warmer.[54] In spite of these errors and difficulties, many people have made measurements using the above methods, e.g. References 48 and 55. The bulk of these were made by using bethod (b), and are the ones described here. Because of the aforementioned latent heat error, these results may be considered to give conservative estimates for the growth velocity with a given interfacial subcooling. In general the results are of the form:[48]

$$V = A\ (\triangle T)^n \qquad (5)$$

where V is the velocity of crystal growth, n and A are constants characteristic of a particular material and lattice orientation, with n lying somewhere between 1.7 and 2.3 for most cases (with $\triangle T$ in $^{\circ}C$), and $\triangle T$ is the subcooling.

At this point it is interesting to look at the subcoolings required for various common materials for a growth velocity of 1 cm/hr (which is quite common in fractional crystallizations from melts). This is summarized in Table I.

Table I

Subcooling required for solid growth velocity of 1 cm/hr.

Material	Subcooling ($^{\circ}C$)	Reference
Benzene	0.03	56
Water	0.145	48
Tin	0.046	48
Phosphorus	0.0068	48

It is thereby apparent that, for many materials, the subcooling in freezing may be ignored for heat-transfer calculations in fractional crystallization from melts.

In zone melting, solid material is also melting. Here again, the temperature of the interface is not exactly that given by the phase diagram. It turns out, however, that the superheating necessary to melt a solid at a given rate is less than subcooling necessary to freeze it at that rate.[1] Therefore any melting interface may also be taken to be at the melting point for heat-transfer calculations.

General Design Considerations

In designing equipment for fractional crystallization from melts, the same sort of considerations must be made as for any other fractionation equipment design. For example, the container has to be corrosion resistant to the material being fractionated. Economic considerations are also important.

Some problems peculiar to this type of fractionation are:

(a) Difference in density between the solid and the liquid. In the case of zone melting this can lead to a net transport of material along a horizontal open boat.[2] This also makes it difficult to generate a molten zone in a closed container without breaking the container.

(b) Thermal expansion and contraction of the solid. If the solid adheres to the container it may break the container as it shrinks while cooling.

(c) Contamination by the container. Molten silicon, for example, dissolves impurities from all known containers. For purification of it, therefore, the technique known as "floating-zone refining" was developed.[2] In this process no container is used. Instead, the zone is held in position by surface tension and also possibly by magnetic suspension, for susceptible materials.

(d) Vapor pressure of the material. If the material being fractionated has an appreciable vapor pressure, the losses therefrom may be sufficient in an open container to make operation in a closed container essential.

(e) Release of dissolved gases. Many molten materials, even metals, dissolve appreciable quantities of gases. When the melt is solidified, the gases are released and may form undesirable pockets. This often necessitates considerable degassing.

(f) Sensitivity to thermal and mechanical shock. Because the separation is so sensitive to growth rates, slight periodic variations in pulling rates of heaters or in temperatures of heat sources and sinks can be very deleterious. Very close control and smooth pulling methods have therefore been developed for fractional solidification.[2]

One of the most important economic considerations in operation of these fractionaters arises from the sharp dependence of separation on growth velocity. In other words, is it better to grow a solid very slowly and have only a few stages, or grow it faster and have many stages? This of course depends on the type of equipment and materials to be purified. For zone melting, this and other economic factors have been considered by Pfann.[2] A detailed process design and cost estimate is given in Chapter IX of this work to illustrate some of the foregoing considerations.

II. EXPERIMENTAL EQUIPMENT AND SYSTEMS

A. Introduction

In the introductory chapter of this work it was mentioned that two variations of fractional crystallization from melts were studied -- zone melting and cooled-drum fractionating. In this chapter further details will be given on the particular experimental setups employed. In addition, the choice of systems to be studied will be discussed.

B. Systems

For simplicity it was decided to use binary mixtures in these fractionation studies.

Zone Melting

For zone melting, crystalline organic compounds were chosen for several reasons:

(a) They are, in general, low-melting. This simplifies equipment design considerably.

(b) Their melts are usually clear, enabling one to see the growing and melting interfaces.

(c) Many are cheap and readily available in a pure form.

In addition, a suitable system for a basic study of this type should:

(a) Be thermally stable to temperatures somewhat above the melting points.

(b) Have a phase diagram of one of the two elementary types, isomorphous and eutectic (see Figs. 6 and 7).

(c) Exhibit no difficulty in forming stable crystals.

(d) Be easily analyzable for composition.

Consequently the systems naphthalene-β-naphthol and naphthalene-benzoic acid were chosen. Naphthalene and β-naphthol are isomorphous, while naphthalene and benzoic acid form a simple eutectic. The phase

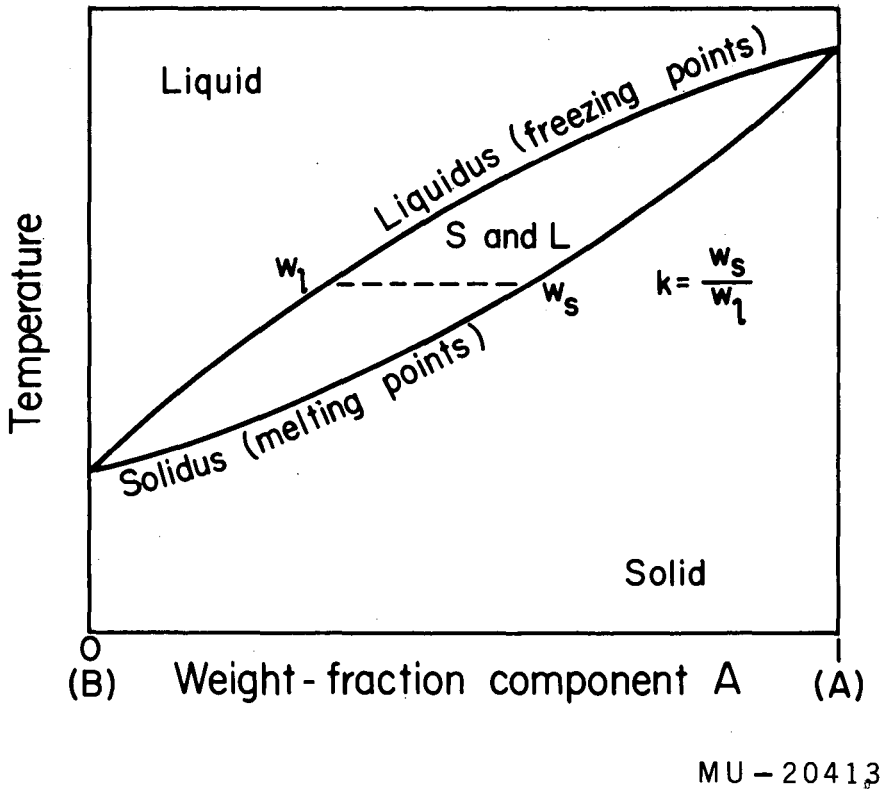

Fig. 6. Solid-liquid phase diagram for a completely isomorphous binary mixture (schematic).

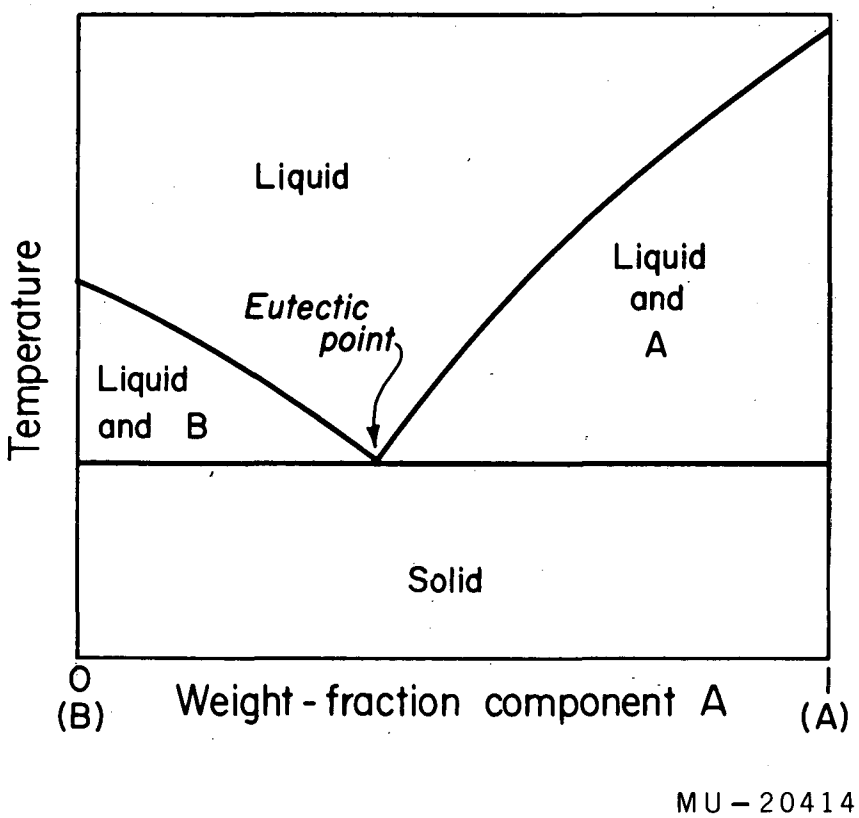

Fig. 7. Solid-liquid phase diagram for a simple eutectic-forming binary mixture (schematic).

diagrams are studied in detail in Chapter III. In order to simplify chemical analyses, mixtures were used that were fairly concentrated, by usual zone-melting standards. These were 10% by weight β-naphthol and benzoic acid, respectively. This means that the melting point of the materials in the zone often changed by several degrees during a run. This, however, is the sort of concentration one might expect in the bulk separations of the chemical process industry.

The purest available materials were used in the experimental work. These included Eastman's naphthalene recrystallized from alcohol, Mallinkrodt's N.F. β-naphthol, and Fisher's reagent-grade, A.C.S. benzoic acid.

To determine if these compounds were pure enough to use "straight from the bottle," they were actually subjected to zone melting (with the material enclosed in glass tubes and drawn through a stationary heater). Some slight amount of clarification occurred for benzoic acid and naphthalene. This was mostly due to the removal of small gas bubbles from the solid. No change occurred in their analyses and very little in the melting points. For β-naphthol, however, a striking color change occurred. The product as bought is a light tan color. After zone melting, however, it is completely colorless. Passage of samples from the zone, which contained the removed coloring matter and was dark brown, through a gas-liquid chromatographic column revealed no detectable amount of impurity. Analyses in the usual manner also showed no difference in composition beyond the usual range of variation in analytical response (see Chapter IV.).

Phenolic-type compounds, of which β-naphthol is one, typically undergo oxidation and polymerization in the presence of oxygen at elevated temperatures.[57] In order to determine if this might be the source of the coloring matter in β-naphthol, samples of molten β-naphthol were sealed in vials and held at a temperature well above the melting point. Some of the vials were only half-full, some completely full, and all had sealed lids. This meant that the amount of oxygen available in the half-full tubes was much greater than in the completely full ones (which had only dissolved oxygen). As time passed, the color in all tubes grew darker,

although much more so in the half-full tubes. The analysis also indicated a slight change after several days. Consequently it was decided to melt up the working mixtures and fill the zone-melting tubes in an atmosphere of nitrogen, to avoid producing any more impurity in this stage. The layer of solid between the zone and air in a filled tube effectively prevented the occurrence of any oxidation while zone melting.

In order to determine the effect that the amount of this unknown impurity present in the bottled product might have on the separation in zone melting, duplicate runs were made on "straight" β-naphthol and zone refined β-naphthol (mixed with naphthalene to 10% by weight). No detectable differences were noted. Therefore it was decided to use all the materials straight from the bottle, melting and filling the tubes in the aforementioned nitrogen atomsphere.

Since β-naphthol and benzoic acid dissolve in water, it is possible that they might absorb moisture from the air during weighing and handling. Over a period of several days, however, samples of these two kept a constant weight, showing no moisture absorption.

Cooled-Drum Apparatus

The high vapor pressure of naphthalene made it impractical to use the cooled-drum apparatus on the two systems used for the zone-melting studies. These systems were actually tried, however. When the drum continued to produce the product after the melt level had fallen below the drum level, it became apparent that the apparatus was acting as a better still than fractional crystallizer under these conditions. At any rate, since a refrigeration system became available at this point, it was decided to use the very convenient NaCl-water system instead. It is quite nonvolatile near the freezing point. Both components are very readily available in ultrapure forms.* The physical properties, at least for dilute enough solutions, are readily available.[58]

---

*The sodium chloride was Baker and Adamson's Reagent, A.C.S. grade, Code No. 2232.

C. Equipment

General Layout

To serve the need for a variable-temperature coolant, a special bath was constructed. The bath itself was in a stainless steel box enclosed in a wooden box with styrofoam insulation between the steel and the wood. The bath consisted of a stirred mixture of approximately 50% by weight ethylene glycol in water. Through this bath ran three coils. Through one coil was pumped a mixture of ethylene glycol and water* which was circulated either through the rotating drum of the cooled-drum apparatus or through one of the cooling chambers of the zone-melting equipment. One coil was attached to the cold-water supply from the laboratory cooling system. The third coil served as an expansion system for a Freon compressor. Also dipping into this tank were two 500-w electric heating spears and the necessary temperature controls. With this system the bath could be operated at any temperature from -40 to 100°C.

A photograph of one experimental area is shown in Fig. 8. On the right is a control panel for the bath, compressor, pump, and cooled-drum apparatus. Under the bench, from left to right, are the thermocouple cold junctions, compressor, and condensing unit, rotameter (to measure flow rate of circulating coolant), bath, and pump (not visible). On top of the bench are the melting-point apparatus (see Chapter III) and the cooled-drum apparatus.

For temperature measurement, copper-constantan thermocouples were used, with the reference junction in an ice bath.**

Thermocouple potentials were continually measured on a Leeds and Northrup Speedomax, Type G, 6-point recorder.

---

*A large quantity of this mixture was made up so that leaks and spills could be replaced with material of exactly the same composition throughout the experiments.

**Thermocouple leads were 0.020 in. in diameter.

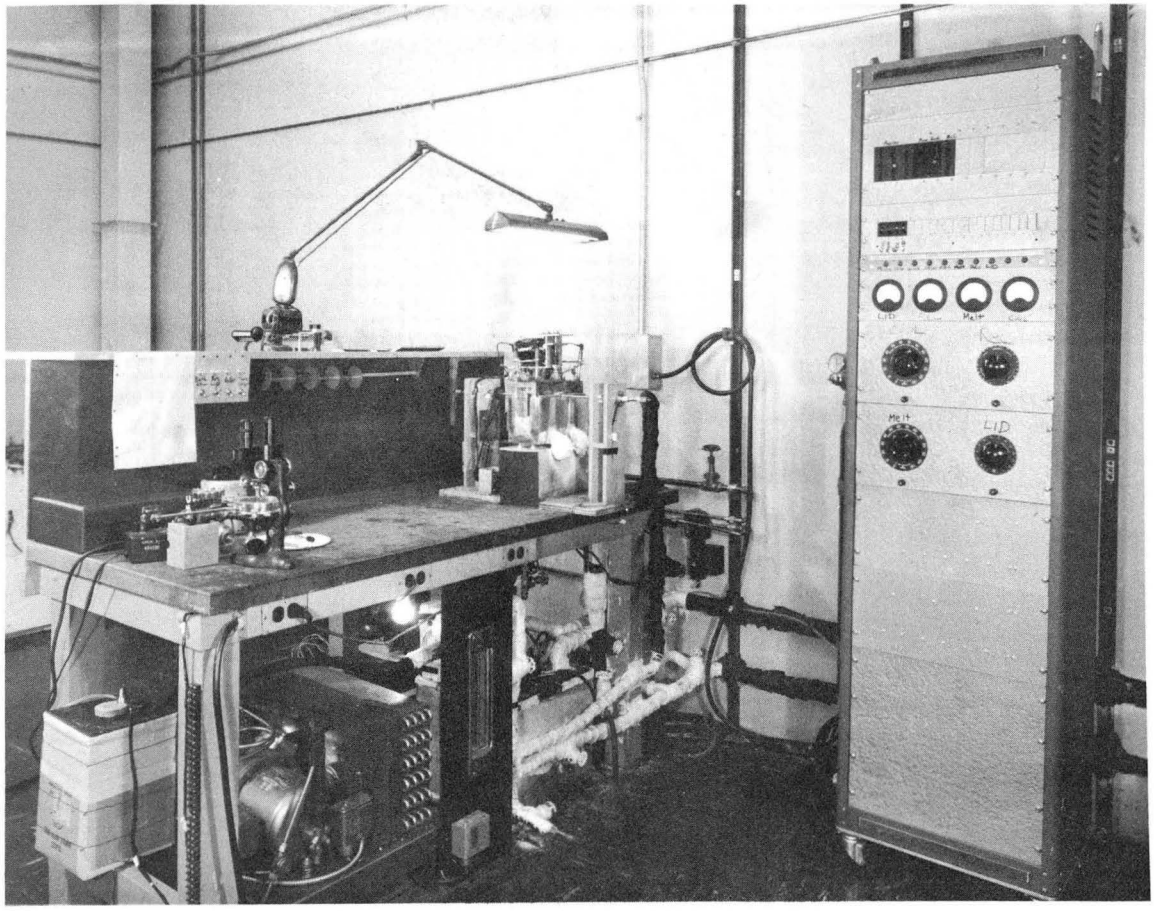

ZN-2502

Fig. 8. Photograph of one experimental area. On the bench, from left to right, are the melting-point apparatus and accessories (described in Chapter III), and the cooled-drum fractional solidifier. Under the bench, from left to right, are the thermocouple cold junction, compressor, rotameter, bath, and pump (not visible). On the right is a control panel.

Zone Melting - General Description

A photograph of the zone-melting equipment in a vertical position is shown in Fig. 9. In this position the material being processed was pulled down through a stationary heater. The pulling motor and gearbox are at the bottom of the picture. They were attached by a chain to a rod that passed through a seal into the interior of the zone melting chamber and hooked onto the tube being pulled. The black-covered pipelines carried coolant to the upper and lower cooling chambers. Between these lines (where they are in a horizontal position) is a window through which can be seen a heating tape (see Zone Melting -- Successful Modes of Operation). Out of the top emerges a thermocouple lead, since the run photographed was one in which a thermocouple wire ran through the tube.

Figure 10 shows a schematic sketch of the zone-melting apparatus. The main body was made of brass, with glass pipe on both ends. The heating chamber has two windows so that the zone can be watched. A removable plate allowed heaters to be inserted and held in place. Above and below the heating chamber are concentric chambers through which coolants flowed. The inside diameters of glass pipe, heating chamber, and coolant chambers were all approximately the same.

Coolant for one of the cooling chambers came from the aforementioned coolant bath. Coolant for the other was ordinary tap water. Although the tap water varied from about 17 to 25°C, the short-term (30 min.) variations, which are the ones affecting a separation of this type, were negligible. Temperature control on the coolant from the bath was very good (no detectable variation) for the range 20 to 100°C. The low-temperature control on the compressor, however, was quite poor. Consequently when the compressor was used, it was left on, the final temperature being a steady-state one and not directly controlled. In a like manner no temperature control for the heater was used. Instead the power input to the heater throughout any one run was kept constant. A constant-voltage transformer in conjunction with a variable transformer and watt meter were used to regulate the heater input.* In these ways variations in growth rate due to fluctuations in the heat source and sink temperatures were eliminated.

*The equipment included a Sola constant-voltage transformer (Cat. No. 30955, Ser. No. E328), a Powerstat type-116 variable transformer, and a Weston, 0 to 30, 0 to 15 watts, Model-432 wattmeter (No. 20690).

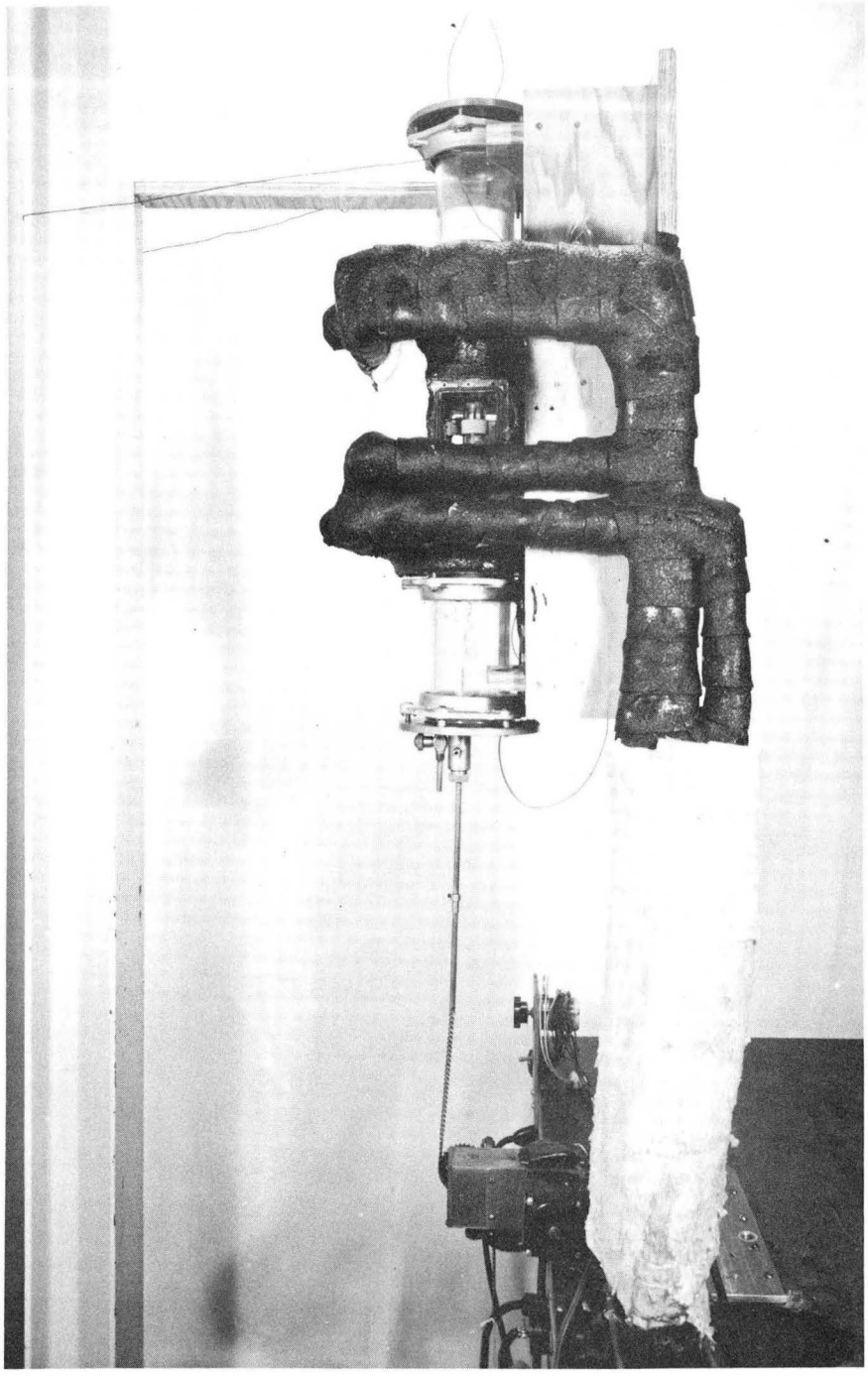

ZN-2503

Fig. 9. Photograph of the zone-melting apparatus in a vertical position, with the tube being pulled down. The puller motor and gear box are on the bottom and are connected by chain to the main chamber above.

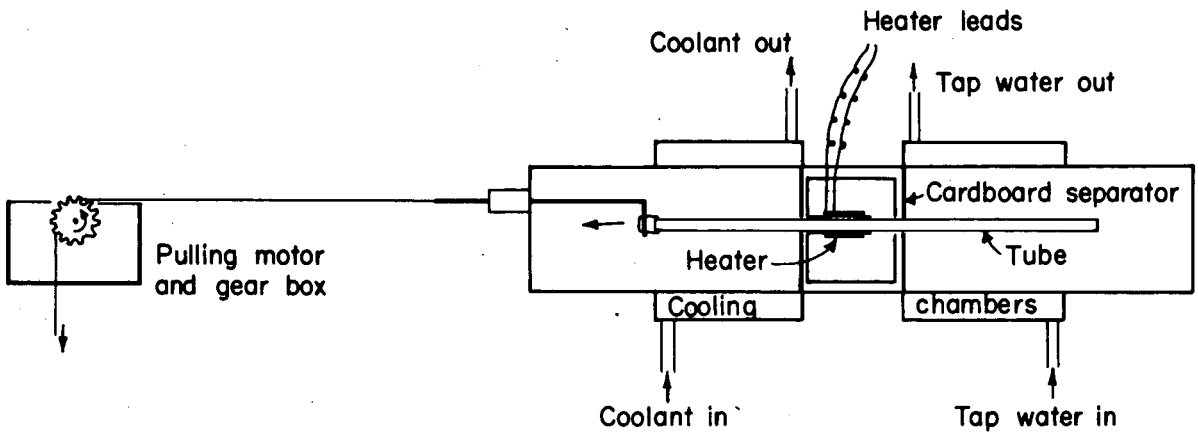

Fig. 10. Diagram of the zone-melting apparatus.

Zone Melting--Unsuccessful Modes of Operation

Resistance heaters were used for simplicity. It was decided to use glass containers for the working material for two reasons:

(a) Glass is transparent,

(b) The thermal conductivity of glass is of the same order of magnitude as that for most organic materials.

Because of the desirability of having a well-stirred zone, it was also decided to use a mechanical stirrer. This necessitated the use of an open-topped horizontal boat. The first one used is shown in Fig. 11.* This was used in conjunction with the first three heaters (from left to right) shown in Fig. 12. The first two were inserted into the zone, the third went around the outside of the boat. They were glass, wrapped with nichrome resistance wire. In operation, an inside heater was used in conjunction with the outside heater. The large diameter of the boat made such a heater arrangement necessary in order to completely melt the cross section. Vertical solid-liquid interfaces were never achieved, however, because free-convection effects made the zone spread out at the top. Stirring was also effected by a paddle stirrer inserted into the zone. Thermocouples were also inserted into the solid and into the molten zone, enabling temperature profiles to be taken.

The failure of this type of operation was due to the high volatility of naphthalene. Sometimes nearly all the zone would be gone by the end of the run. Narrowing the slot in the boat and covering it with various materials helped some, but never enough.

Zone Melting--Successful Modes of Operation

Because of the difficulties encountered above, it was decided to change over to closed-tube operation, abandoning the use of mechanical stirring. Consequently the experimental results and conclusions in this work are only for free-convection stirring of the zone.

---

*The white powder in the boat was merely used to make the boat show up better in the photograph. The boat was made from 70-mm glass tubing. The scale etched on it is in centimeters.

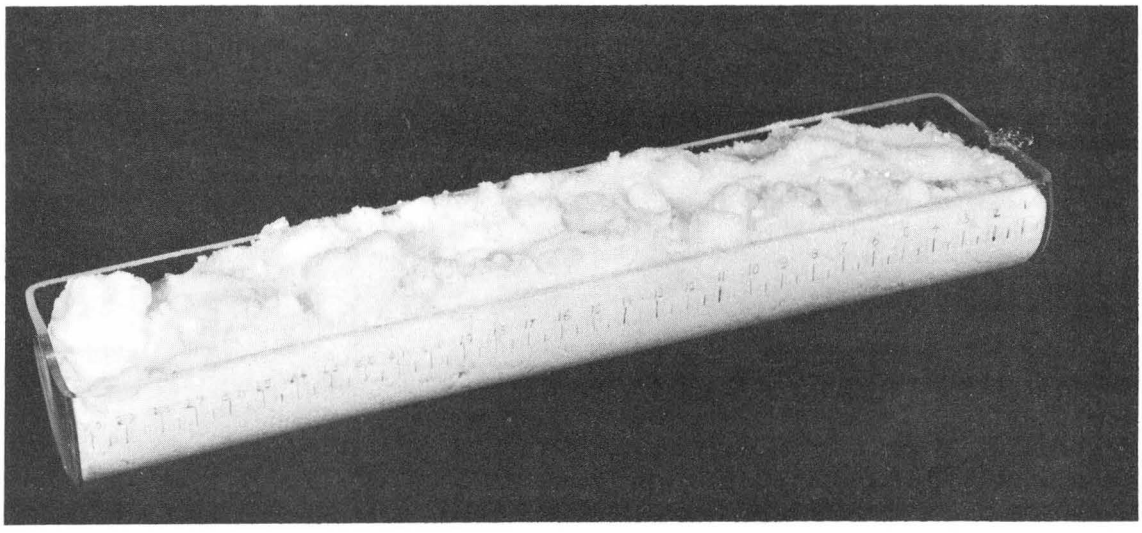

ZN-2504

Fig. 11. Photograph of an early open-top boat used for zone-melting studies. The white material was used to make the boat photograph better.

ZN-2505

Fig. 12. Photograph of various types of resistance heaters used in zone-melting studies. From left to right are the internal ring heater, probe heater, external ring heater, and heating-tape heater. The scale is graduated in inches.

The glass-tube containers were made from 5-mm, 10-mm, and 20-mm glass tubing.* The 10- and 20-mm tubes were filled by pouring the molten material in and allowing it to freeze rapidly to preclude the possibility of segregation. The 5-mm tube was hollow on both ends so that the melt could be sucked in and allowed to freeze. Tests showed the tube contents of all three tube sizes to be of uniform composition within the accuracy of analyses (see Chapter IV). The techniques used for sampling for analyses are also described in Chapter IV.

Some of the 10- and 20-mm tubes also had a glass tube, thermocouple, or stainless steel tube inserted in them. Examples of the filled tubes are shown in Fig. 13. The first tube on the left has thermocouple wire running through it. All tubes were approximately 1-ft long.

A very satisfactory type of resistance heater was found for these experiments. It consisted of two turns of heating tape around a glass tube of slightly larger diameter than the tube containing the material.** This outside tube was about the same length as the zone chamber itself (about 2 in.). The heater used for 10-mm tubes is on the far right in Fig. 13. The heater for 20-mm tubes is shown in operation in Fig. 14. A zone was actually developed for this photograph and extended from just below the tape to the top of the zone chamber. This 20-mm tube had a thermocouple lead running through it which is not clear in the photograph because of the distortion caused by the concentric tubes.

Pieces of cardboard, with holes for the tubes, were placed on both sides of the zone chamber to separate it from the cooling chambers and to act as guides for the tubes, keeping them centered in the chambers.

---

*Average inside and outside dimensions are given in Chapter V. A variation of up to 10% in diameter between various tubes is found, although the diameter along any one piece of tubing is quite constant.

**Briskeat heating tape, 1/2 in. and 1 in. wide was used. The exact dimensions of the tubes are given in Chapter V.

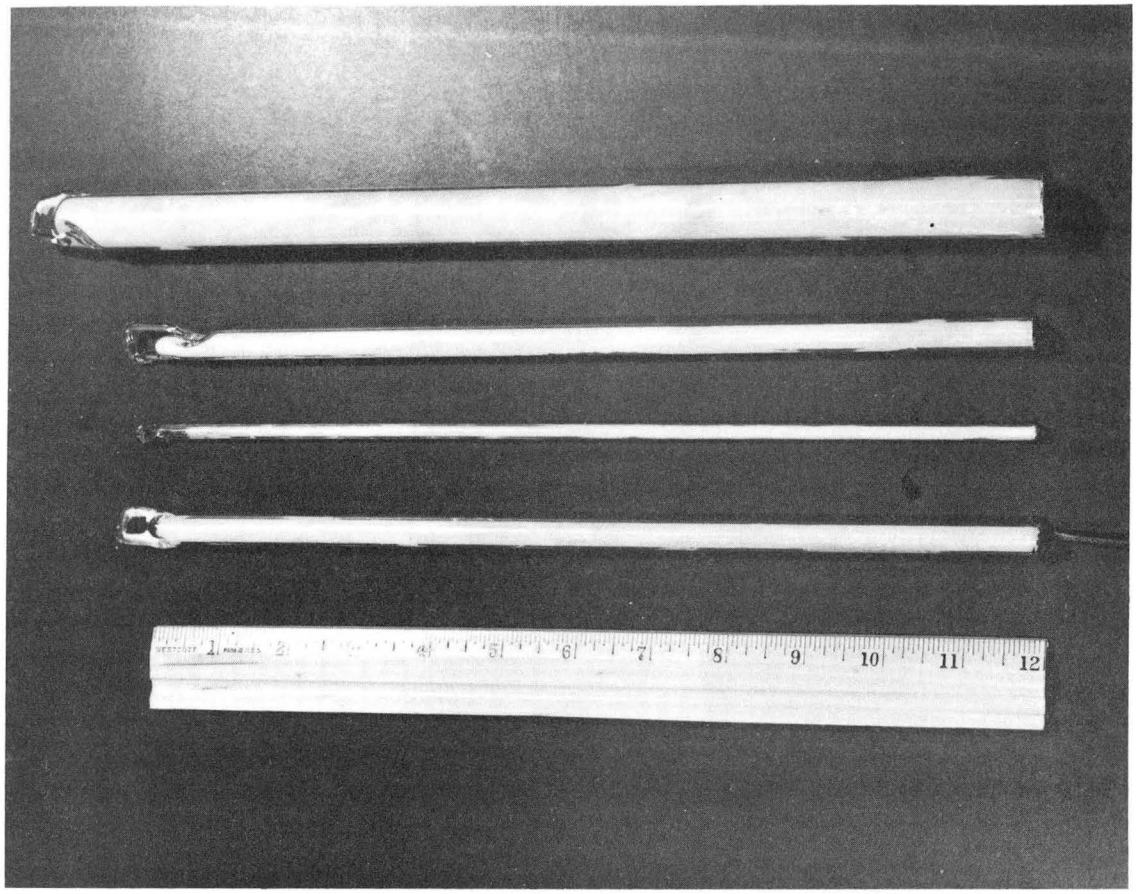

ZN-2506

Fig. 13. Photograph of various-sized glass tubes used in zone-melting studies. They have been filled and are ready for use. The scale is graduated in inches.

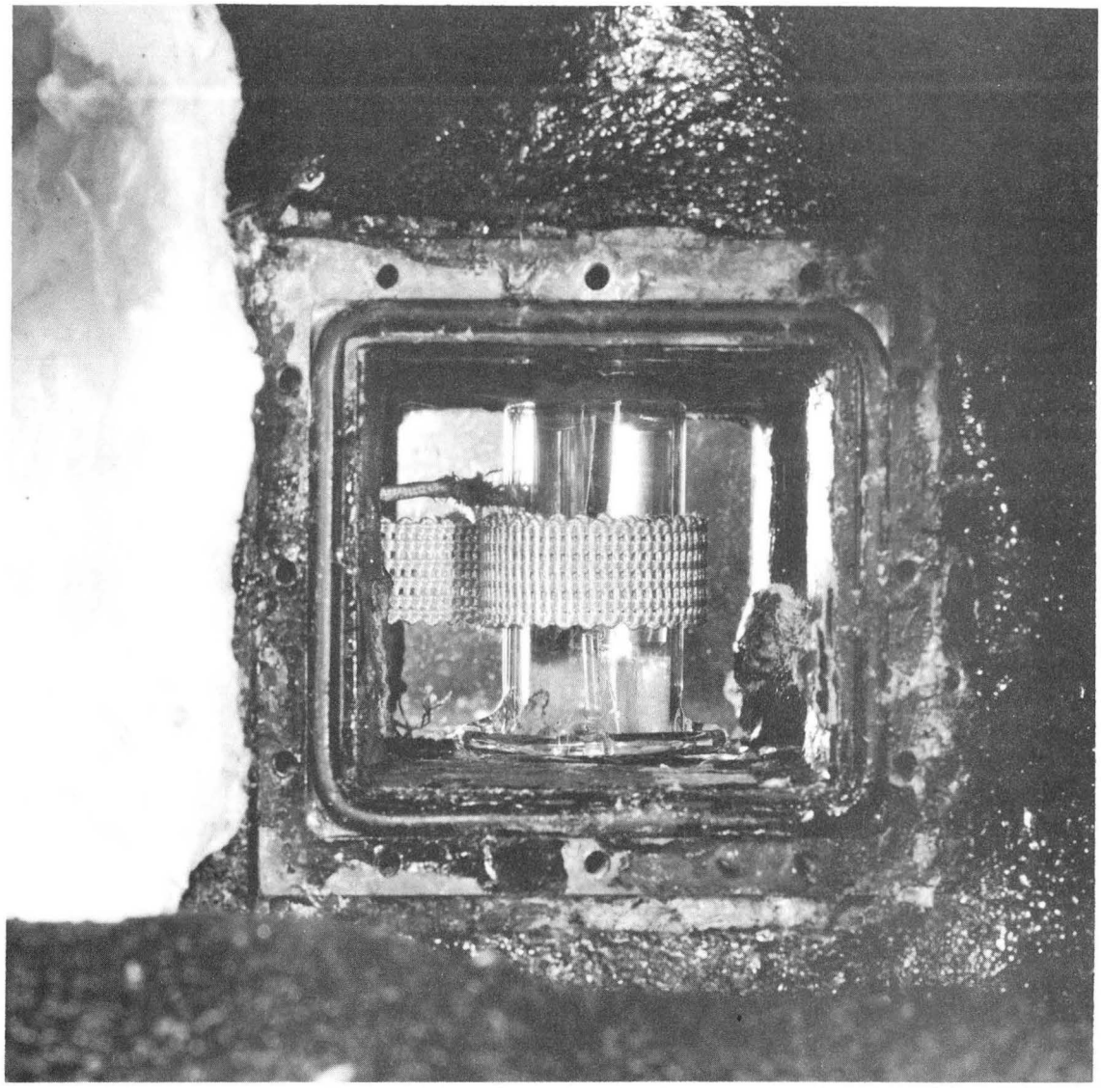

ZN-2507

Fig. 14. Close-up of a 0.5-in. heating-tape heater in action (close-up of Fig. 9) on a 20-mm tube with thermocouple leads running axially through it. The freezing interface is visible just below the heating tape.

Runs were made in both the vertical and horizontal position. In the vertical position the tubes were pulled both up and down.

The speed with which the tubes were pulled through was varied from 0.15 to 2.7 cm/hr. This was done by changing the gears on the gearbox attached to a 1 rpm synchronous motor (see bottom of Fig. 9). The pulling action of the rod seemed to be quite smooth -- the seal was well-lubricated. Measurements were made of position vs time and, insofar as could be measured, the pull rate was constant and smooth.

Cooled-Drum Apparatus

An over-all view of the cooled-drum apparatus is shown in Fig. 15. Coming out of both sides of it are stainless steel tubes which carried coolant to and from the drum and acted as a shaft for it. They passed through rotary seals to connect to the coolant system. Inserted from both sides were thermocouples which terminated at the drum itself. On the left side, two motors turned the shaft through chains. By interchange of gears and motors the drum rotation could be varied from 1/3 to 9 rpm. On top is a synchronous motor used for spinning the paddle stirrer in the melt. The speed of the stirrer could be varied from 0 to 900 rpm. On the right-hand side are two heated outlets for draining the melt tank and receiver tank. Windows on both sides enabled one to view the operation. A vertical scale was also etched in them so that the tank levels could be followed. The outside tank, which is visible, is actually separated from the inner tank by a 1/2-in. layer of insulation. Strip heaters were fastened onto this inside tank.

Figure 16 is a close-up of the heater lid. This was provided with two heaters (leads rising from both ends) which ran the full length of the lid. Thermon heat-transfer cement covered them and the lod, providing for efficient distribution of the heat. On the right, Tygon tubing delivered nitrogen for an inert atmosphere. Two plugs filled the holes used for filling the tanks. The stirrer motor, gears, and shaft seal are also shown.

Figure 17 is the underside of the lid. It shows the two thermocouple wells which dipped into the two tanks. The stirrer is visible,

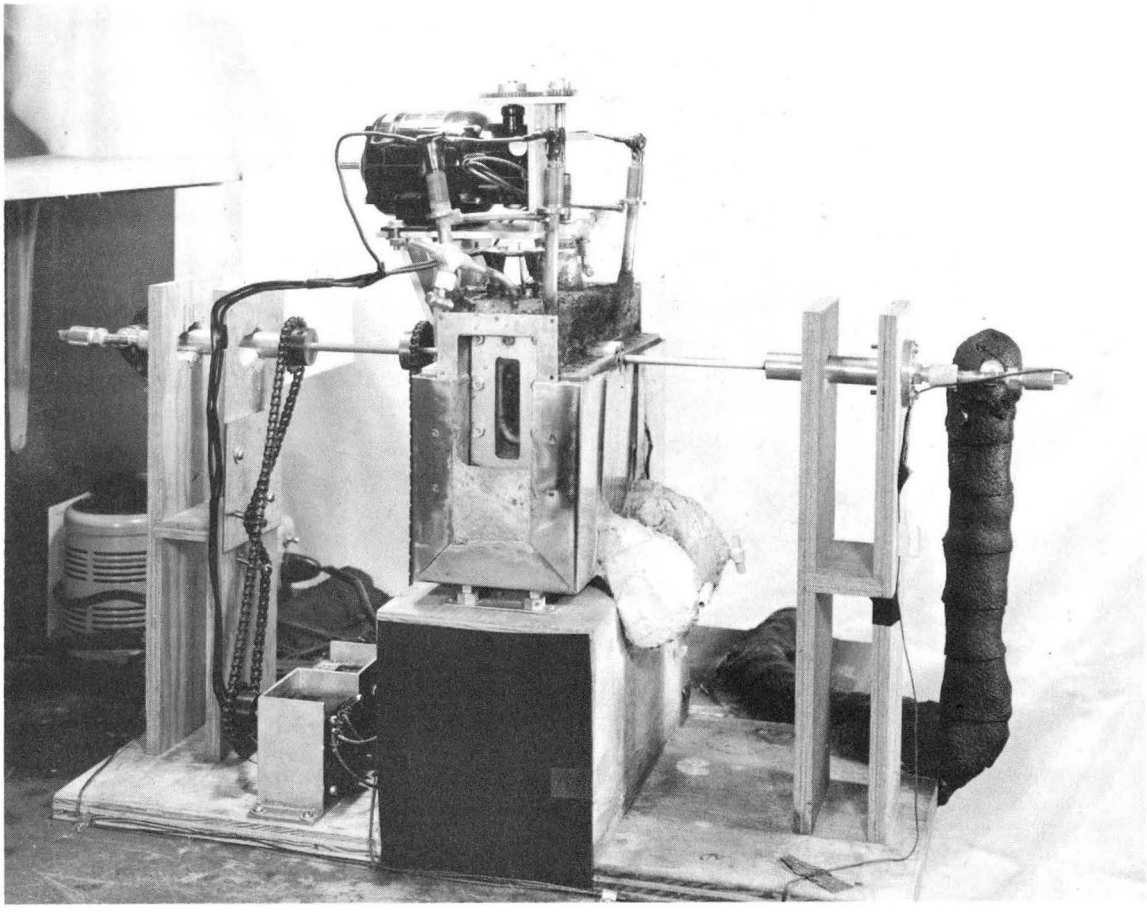

ZN-2508

Fig. 15. Photograph of the assembled cooled-drum apparatus.

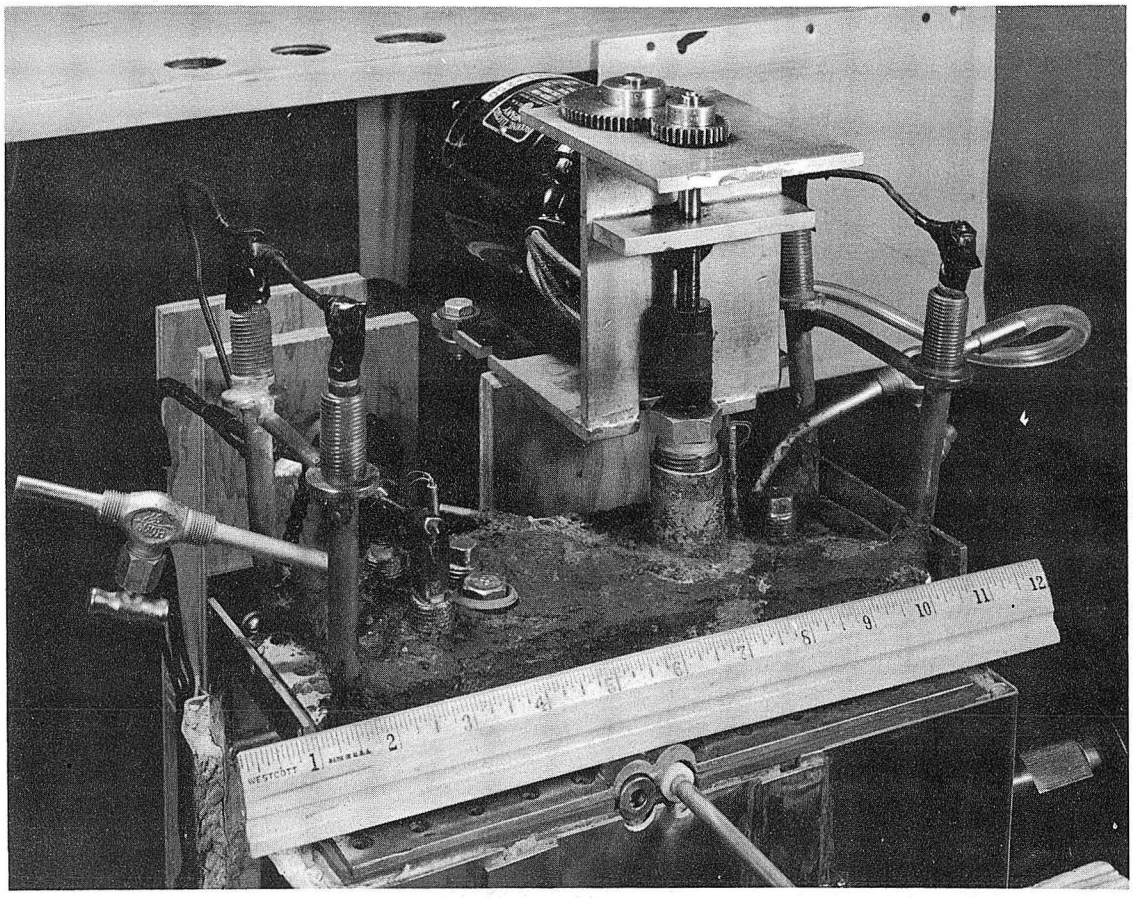

ZN-2509

Fig. 16. Top view of the cooled-drum apparatus. Outlets for thermocouple wells, inert gas, heaters, and the stirrer are shown. The scale is graduated in inches.

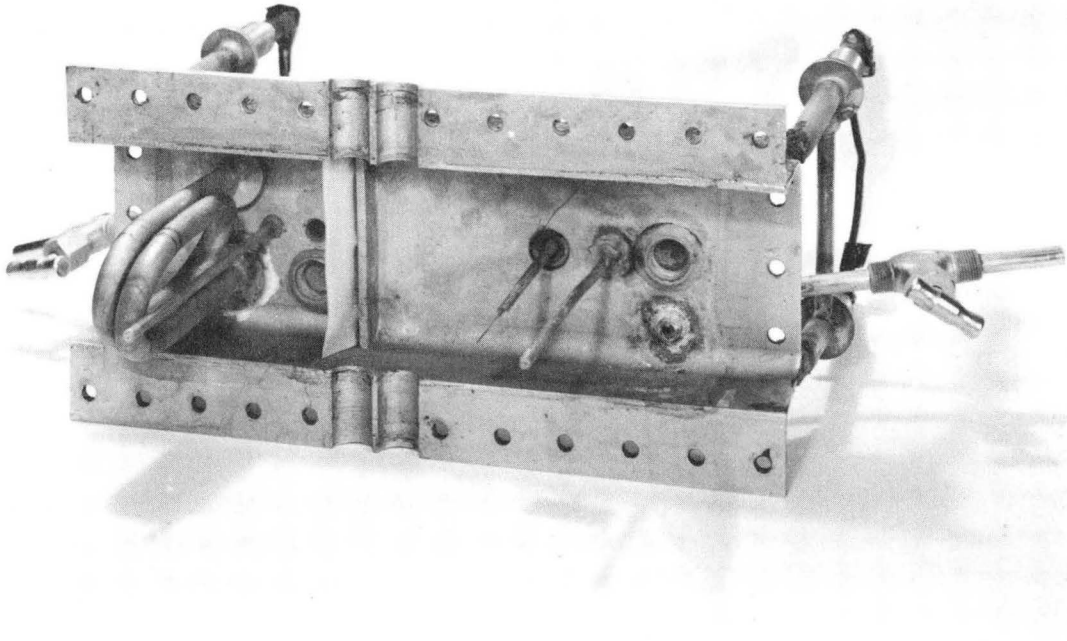

ZN-2510

Fig. 17. Bottom view of the lid to the cooled-drum apparatus. Shown are the thermocouple wells, heater for receiving chamber, Teflon chamber-separator, and stirrer (paddle edgewise to the camera).

although the blade was edgewise to the camera. The coil on the left is a heater for the receiving tank. The white strip in the center is a sheet of Teflon separating the two tanks.

Figure 18 is a top view of the tanks with the lid removed. The drum, of approximately 2-in.-diameter stainless steel, is in the center. Two Teflon bearings, with silicone rubber washers is shown on the tube-shafts. A stainless steel doctor blade rests on the drum. The tank on the top is for the melt, the one on the bottom received the solid product. The tube in the bottom of the melt tank was for a Fenwal temperature regulator. Actually the lid was only used for the preliminary runs with naphthalene-β-naphthol and naphthalene-benzoic acid. When NaCl-water was finally used the lid was not employed (although the stirrer was used). The stirrer was a stainless steel paddle 1-in. wide by 1/2-in. high, and located 1-5/8-in. from the drum (center line to center line). Both the motor for the stirrer and for the drum drive were synchronous, thus assuring constant speeds.

In operation, difficulty was encountered with material freezing on the ends of the drum. This continued until it was frozen to the sides of the tank and operation ceased. In order to avoid this, a thin layer of Epon resin was molded onto the drum ends. This effectively stopped freezing there.

A schematic drawing of the tank and accessories is shown in Fig. 19. The melt tank was 4-in. deep, 6-1/2-in. long, and 2-1/4-in. wide. It was made of brass and was silver-plated for corrosion resistance. The drum was 2-in. o.d. and 2-1/8-in. long (including 1/8-in. Epon layers on each end), and had a surface thickness of 1/32-in. It was of stainless steel.

Difficulty with uneven freezing on the surface of the drum was also encountered. This was partially eliminated by means of a distribution plate placed inside the drum near the inlet.

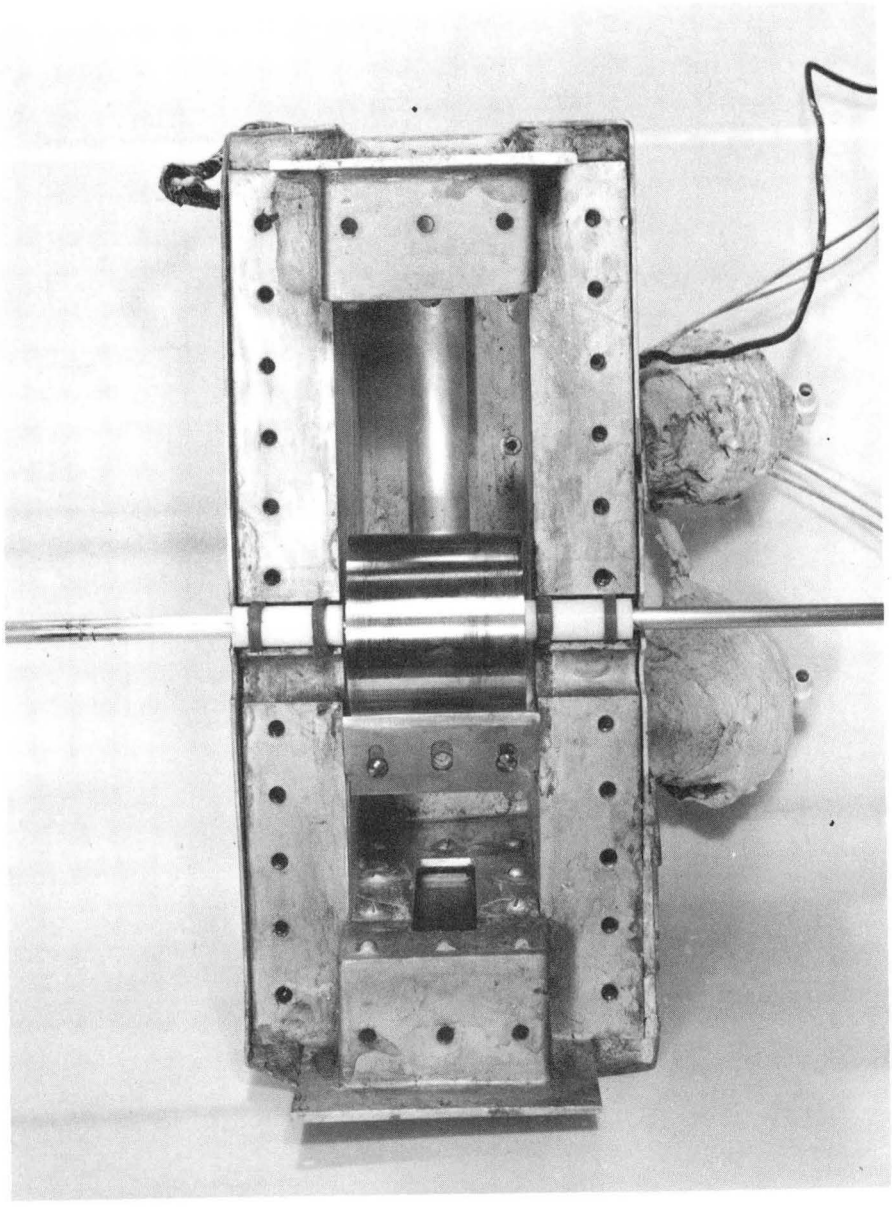

ZN-2511

Fig. 18. Top view of the cooled-drum apparatus with the lid removed. Shown are the drum, Teflon and silicone-rubber bearing, doctor blade, temperature-regulator well, and tank outlets (wrapped with heating tape).

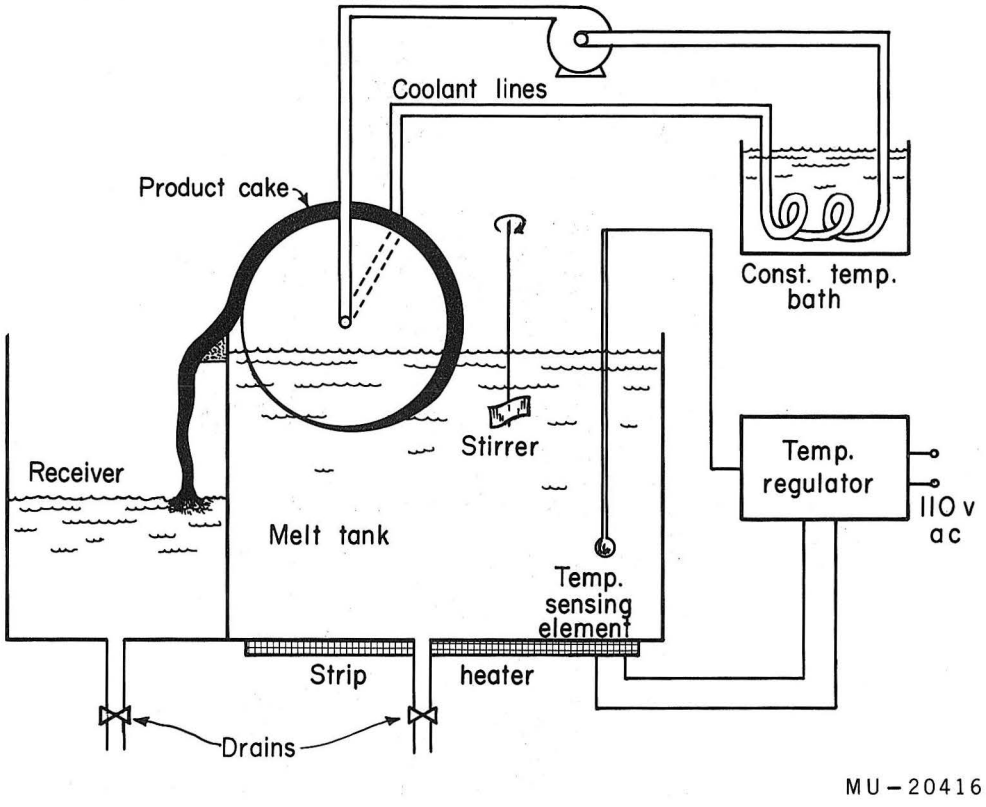

Fig. 19. Schematic diagram of the experimental setup for the cooled-drum apparatus.

III. PHYSICAL PROPERTIES

A. Introduction

The existing data on the desired physical properties of the organic systems studied here were quite meagre. Consequently, the more important physical properties for them were determined experimentally in this work. Adequate data exist for the NaCl-water system, however, so this will not be discussed further in this chapter. Suffice it to say here that NaCl-water is a eutectic-forming system with the physical properties given in the International Critical Tables.[58]

For the organic systems, the less-important thermal parameters were taken from the literature. Since data were available only for the pure components it was necessary to assume a relation between the thermal properties and composition. In view of the uncertainties in the data and the close proximity in values for the pure components, it seemed justifiable to assume nothing more complicated than straight proportionality relationships.

B. Phase Diagrams

Introduction

Solid-liquid phase diagrams are necessary in fractional solidification studies for two reasons:

(a) The melting points are needed for heat-transfer calculations.

(b) A knowledge of equilibrium separations -- the maximum separations attainable -- is desired.

There exists much data on the naphthalene-β-naphthol phase diagram.[58-65] Unfortunately, there is much less than complete agreement on the details, especially of the solidus. In this work the value of the distribution coefficient must be known and therefore determined with some accuracy.

The literature data on the naphthalene-benzoic acid system are very limited and of uncertain validity.[58] For this work we must

accurately know the eutectic concentration and the solid-phase solubility of benzoic acid in the naphthalene-rich portion of the phase diagram. Hopefully the latter is negligible, but this must be demonstrated.

Experimental Methods

In this work, melting points were determined on a Kofler Micro Hot stage.* The usual method of using this apparatus is described adequately in several places.[66-68] The apparatus is shown on the left side of Fig. 8, and close up in Fig. 20.

In practice, the temperature was rapidly brought near the melting point and then raised less than 0.5°C per minute.

The systems studied were so volatile that, unless the cover-glass edge was adequately sealed, the material was gone before melting began. Several sealing materials were tried. Nearly all were either too porous or absorbed the material. Of the seals tested, only Thermon T-3,** a black carbonaceous cement, was found to be satisfactory.

Therefore, the slides were prepared for use as follows. First the pure components were weighed out to give a mixture of the desired composition. This was melted in a closed container and then shaken thoroughly to mix. The material was then rapidly frozen. A piece of it was placed on a slide under a cover glass. This in turn was placed on a hot hot plate until the mixture began to melt. The slide was withdrawn and the cover glass pushed down, forcing the excess material out from under the cover glass. While this was being done, it was cooled by blowing until the mixture solidified.*** The excess material was then scraped off and the edge of the cover glass sealed to the slide with Thermon. The Thermon was allowed to dry and harden several hours before use. A typical slide ready for use is shown in Fig. 21.

---

*Purchased from the Arthur H. Thomas Company, Philadelphia, Pennsylvania.

**Manufactured by Thermon Manufacturing Company, Houston, Texas.

***The systems under investigation supercool very readily and in this case "flash-froze" when they cooled sufficiently.

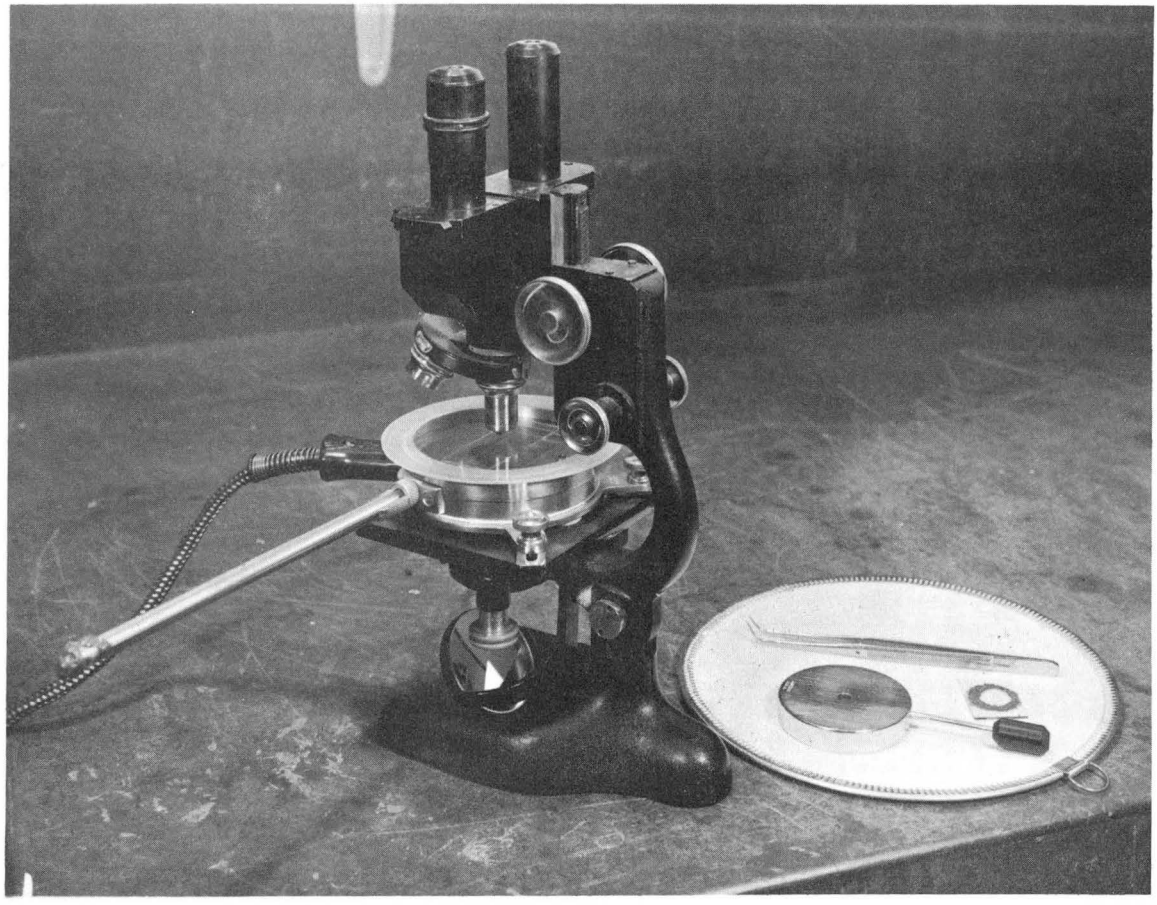

ZN-2512

Fig. 20. Photograph of the micro-hot-stage and accessories used for melting-point determinations.

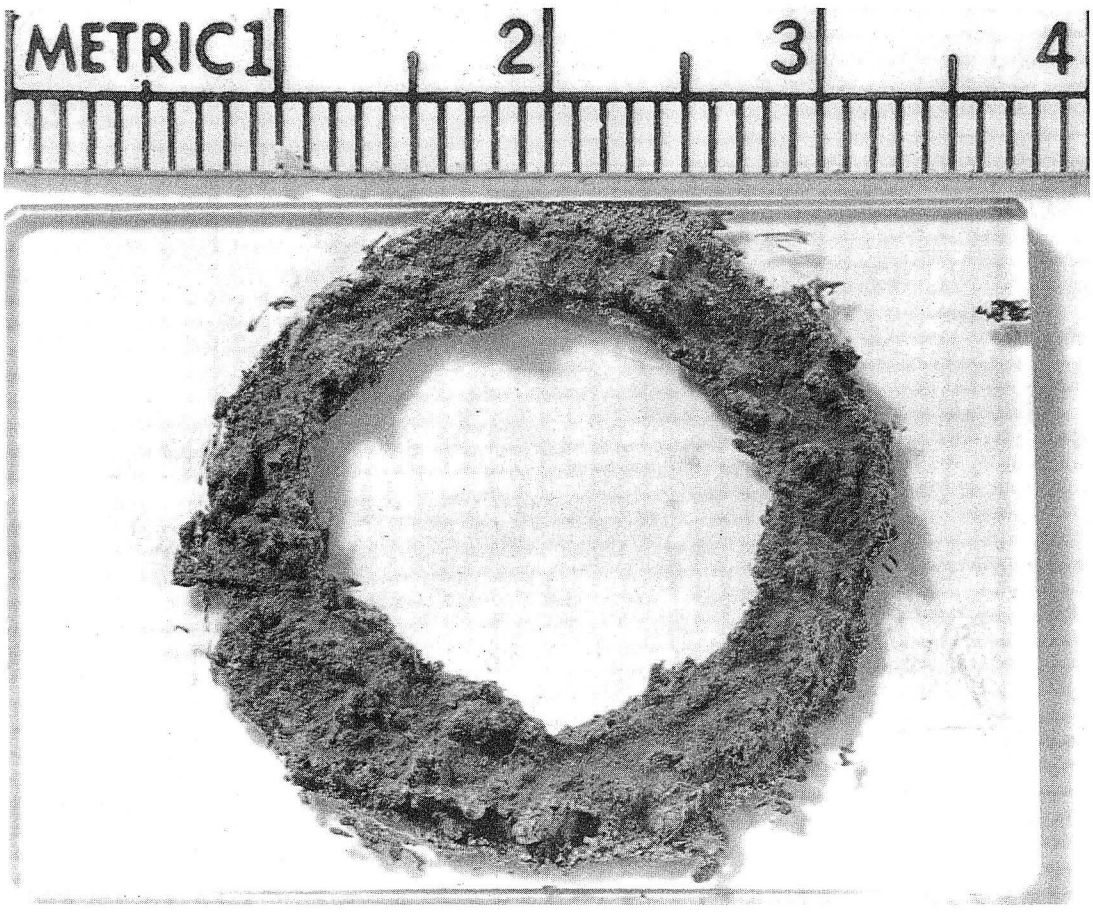

ZN-2513

Fig. 21. Close-up of a microscope slide prepared for a melting-point determination. The black material in a circle is Thermon, which seals the cover glass to the slide. The scale is graduated in centimeters.

To make the melting more discernable, polarized light with crossed polars was used. Under this condition, the solid was usually brightly colored because of the strains induced by sudden freezing. The liquid appeared dark, in strong contrast to the solid. Caution had to be exercised, however, as any bubbles also appeared dark.

Results

Contact-preparation fusions, as described by Kofler[66] and McCrone,[67] showed that naphthalene and β-naphthol are isomorphous and that naphthalene forms a simple eutectic with benzoic acid.

The melting points of the pure components, as determined in the manner herein described, are not the true melting points. For calculating distribution coefficients, this is immaterial.* For comparison with literature phase diagrams, however, the melting and freezing points obtained experimentally must be corrected. Actually, of course, the literature phase diagrams had to be corrected in the same manner, so that each phase diagram has the same singular points for the pure components.

The best literature value for the melting point of naphthalene is 80.25°C, for β-naphthol, 122.35°C, and for the naphthalene-benzoic-acid eutectic, about 70°C.[69-73] Tables II and III show the correction of the experimental data of this work obtained by using these figures. Each value is the average of two to four determinations. The temperature at which the material was half melted was also occasionally noted.

The corrected data of this work and of the literature are plotted in Figs. 22 and 23. The literature data for the solidus line of the naphthalene–β-naphthol phase diagram are unreliable. Only that of Forsyth and Wood for the region around 0.6 weight-fraction β-naphthol is considered trustworthy.[64] This was obtained by a near-equilibrium solidification.

---

*The distribution coefficient is an equilibrium relationship at constant temperature. As long as the melting and freezing points are the same, the absolute temperature is immaterial. See Fig. 6.

Table II

Experimental and corrected melting and freezing points of naphthalene – β – naphthol mixtures

Weight fraction β-nap.	Experimental			Corrected		
	M.p. (°C)	F.p. (°C)	Half-melted (°C)	M.p. (°C)	F.p. (°C)	Half-melted (°C)
0	83.0	83.9	--	80.25	80.25	--
0.05	83.2	84.9	84.3	80.5	81.4	81.2
0.10	85.3	87.7	--	82.8	84.3	--
0.15	86.0	89.7	87.5	83.7	86.4	84.7
0.20	87.2	91.0	89.5	85.1	87.9	86.9
0.50	93.0	101.0	96.5	91.6	99.0	94.6
1.00	122.0	123.0	--	122.35	122.35	--

Table III

Experimental and corrected melting and freezing points of naphthalene-benzoic acid mixtures

Weight fraction benzoic acid	Experimental			Corrected		
	M.p. (°C)	F.p. (°C)	Half-melted (°C)	M.p. (°C)	F.p. (°C)	Half-melted (°C)
0	83.0	83.9	--	80.25	80.25	--
0.01	73.0	83.0	82.0	70.2	79.3	78.3
0.03	72.5	82.2	81.2	69.8	78.6	78.1
0.10	72.5	82.0	--	70.9	79.0	--
0.319	71.0	73.0	--	70.0	70.5	--
0.310	71.0	72.0	--	70.0	71.5	--

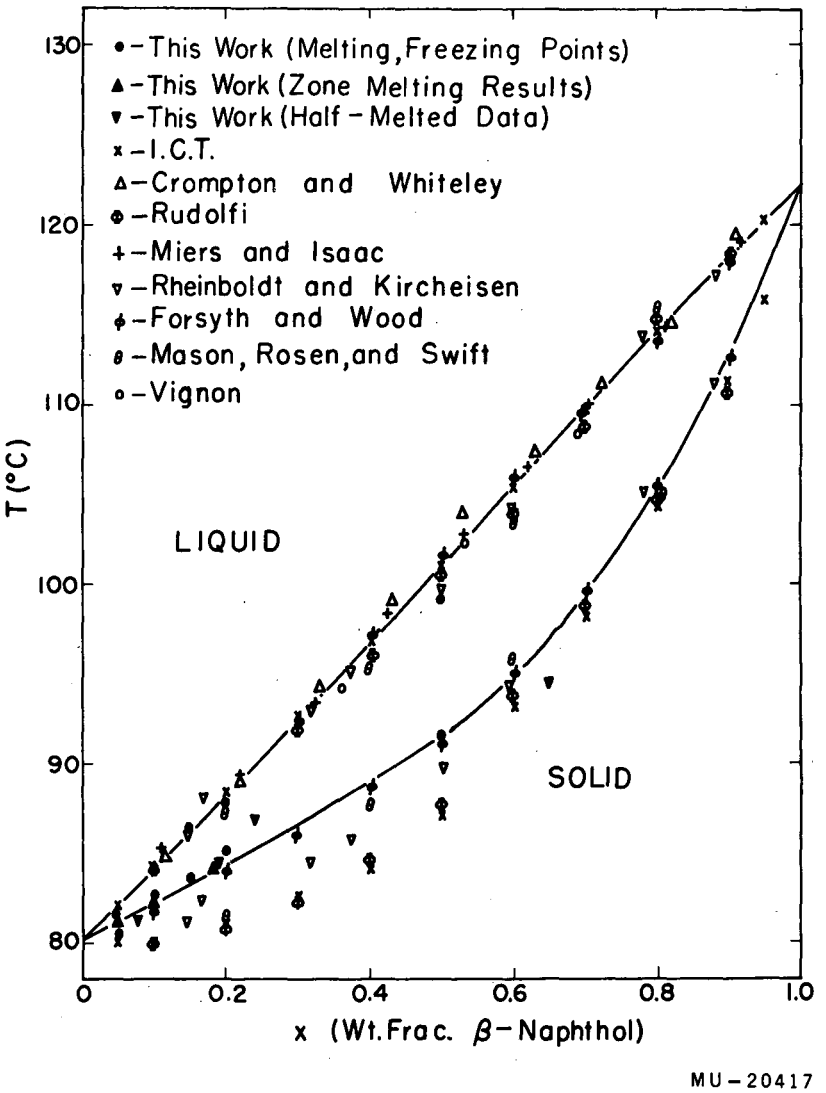

Fig. 22. Solid-liquid phase diagram for the system naphthalene–β-naphthol. Literature values are from references 58 to 65.

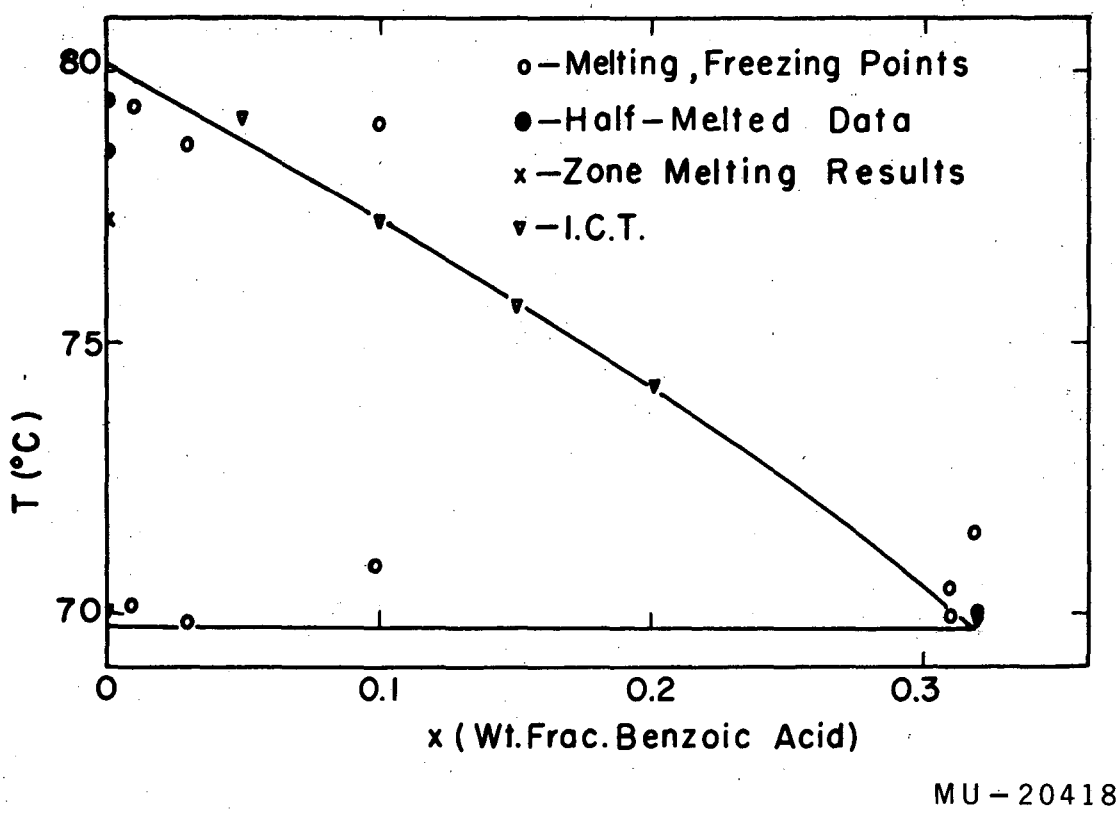

Fig. 23. Naphthalene-rich portion of the solid-liquid phase diagram for the system naphthalene-benzoic acid. Literature values are from reference 58.

Since the liquidi in both diagrams are fairly certain, the half-melted data were used in conjunction with the liquidi to yield a few more experimental points for the solidi.*

Some zone-melting results were also applied for the determination of the solidi. Under certain conditions** naphthalene (free of benzoic acid insofar as analyses could determine) was obtained from 0.10 weight-fraction benzoic acid mixtures. Under similar conditions the maximum separation of β-naphthol and naphthalene was also obtained. This yielded a distribution coefficient of 1.85 for 0.10 weight-fraction β-naphthol. There is some question about the validity of these runs, however, because a bubble was always present at the freezing interface. An experiment, in which a mixture was vaporized from an evaporating dish and crystallized onto a cover glass, showed that naphthalene vaporizes faster than both β-naphthol and benzoic acid in mixtures. Since the separations in the two systems are in opposite directions with respect to naphthalene, one must conclude that the equilibrium separation was obtained. Accordingly these results were used in completing the phase diagrams in Figs. 22 and 23.

It is important to point out now that, although zone melting looks promising as a method of determining phase diagrams, there is one major pitfall: it is never certain that the equilibrium separation has been obtained. Theoretically, lowering the zone travel rate until further lowering does not affect the separation should give the equilibrium condition. However, minute fluctuations in the growth rate nullify the effect of lowering the average growth rate below the magnitude of the fluctuations. Such fluctuations have been observed in this work in the thermostatted low-temperature runs*** and by many other workers.

---

*This is done by the standard method found in any elementary physical chemistry book. The half-melted point lies on an isotherm at the half-melted temperature and half way between the solidus and liquidus.

**This situation is described in greater detail in Chapter VII.

***See Chapter VII.

Conclusions

In the author's opinion, the best curves for the phase diagrams are those in Figs. 22 and 23. The points read from the curves for naphthalene–β-naphthol are summarized in Table IV.

The results for the naphthalene-rich portion of the naphthalene-benzoic acid phase diagram may be summarized by the following observations:

(a) The solid-phase solubility of benzoic acid is, for the purposes of this work, negligible.

(b) The eutectic composition is 0.317 weight fraction of benzoic acid.

(c) The eutectic temperature is 69.8°C.

C. Densities

Method

Densities were determined in the following fashion. A mixture of desired composition was weighed out and placed in a 10 ml graduated cylinder, which was then sealed with a ground-glass stopper. This was heated to melt the mixture and then shaken to make it uniform.

The stoppered cylinder was then placed in a constant-temperature bath (shown in Fig. 24), which could be controlled within 0.2°C at any temperature up to 130°C. This was allowed to stand for at least one-half hour until the volume of the melt no longer changed. The volume of the liquid was then read and divided into the weight of the mixture to give the density of the mixture at that temperature.

The density of the solid mixture was obtained as follows. The liquid was allowed to solidify slowly (by wrapping the cylinder with glass-wool insulation) in order to exclude as many bubbles as possible from the solid. Next, acetone was measured in, filling the cylinder to 10 ml. The volume of the solid was calculated by difference.

Results

The results of the experimental technique were corrected by using the very reliable literature data for pure naphthalene.[58,74-76] The crude

Table IV

Equilibrium solid-liquid relations for naphthalene—β-naphthol mixtures (read from Fig. 22)

T (°C)	Solidus (Wt. frac. β-nap.)	Liquidus (Wt. frac. β-nap.)	β-naphthol distribution coefficient
80.25	0.000	0.000	--
81	0.028	0.015	1.85
84	0.178	0.096	1.85
90	0.439	0.242	1.82
95	0.604	0.355	1.70
100	0.710	0.472	1.51
105	0.796	0.592	1.35
110	0.865	0.708	1.22
115	0.926	0.827	1.12
120	0.979	0.947	1.03
122.35	1.000	1.000	1.00

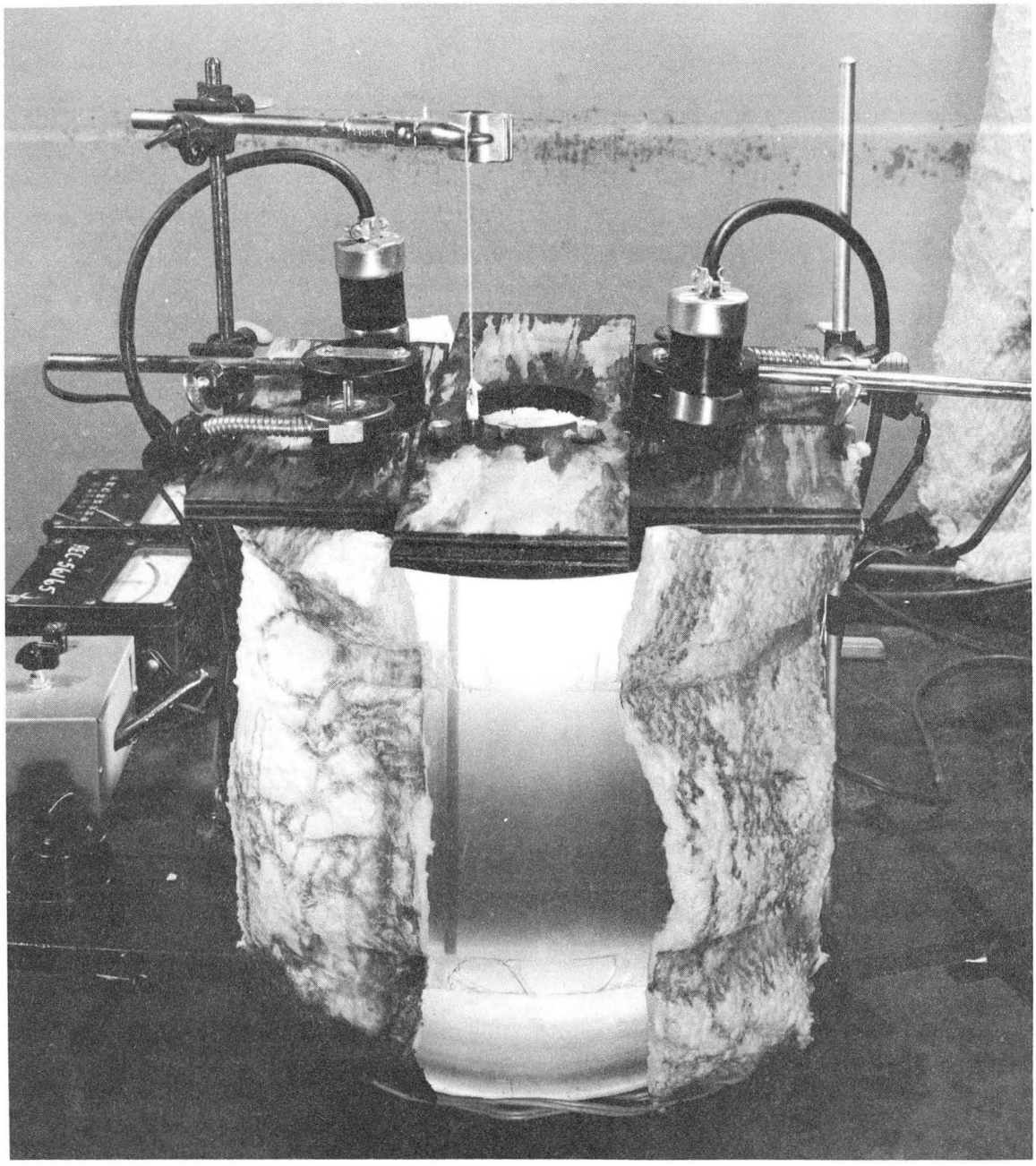

ZN-2514

Fig. 24. Photograph of the constant-temperature bath and accessories used in viscosity, density, and diffusivity determinations.

results for naphthalene from this work are compared with the literature values in Fig. 25. It is seen that the results of this work lie about 0.020 g/cc below the literature values. This discrepancy is mostly due to a combination of error in original calibration of the cylinders and the difference in behavior of the meniscus for naphthalene and water (for which the factory calibration was made). The error (2%), in any case, is small enough for the purposes of this work. Nevertheless, 0.020 g/cc was added to all the density data here obtained to bring them into line with the literature data for naphthalene. The results were then plotted vs temperature in Figs. 26 and 27.

Some of the filled cylinders tended to yield progressively higher experimental densities with extended use. This indicates a loss of material, probably caused by a "breathing" action as the cylinders alternately heated and cooled. Consequently runs at several concentrations were repeated, using cylinders in which the glass stopper had been thermally fused to it after filling. These runs were entirely reproducible after indefinite usage.

A common slope of $(\partial\rho/\partial T)_x = -7.80 \times 10^{-4}$ g/cc°C was found to fit the liquid-density data quite well. Lines of this slope were drawn through the data points. Density data read off these lines are summarized in Tables V and VI and plotted vs concentration in Figs. 28 and 29.

On the isothermal plots of liquid densities of benzoic acid mixtures, lines of slope $(\partial\rho^{-1}/\partial x)_T = -0.154$ cc/g represented the data well. On the isothermal plots for β-naphthol, lines of slope $(\partial\rho/\partial x)_T = 0.123$ g/cc looked best.

For mass-transfer calculations, molar concentration is usually used as a driving force. In this work, weight fraction is a much more convenient quantity. Consequently molar concentration at widely different temperatures is plotted vs weight fraction in Figs. 30 and 31. The fact that a straight line represents this data so well justifies the use of weight fractions instead of molar concentrations.

Both experimental and literature values[60] of the solid densities are plotted in Fig. 32. Because of the uncertainties in the present data,

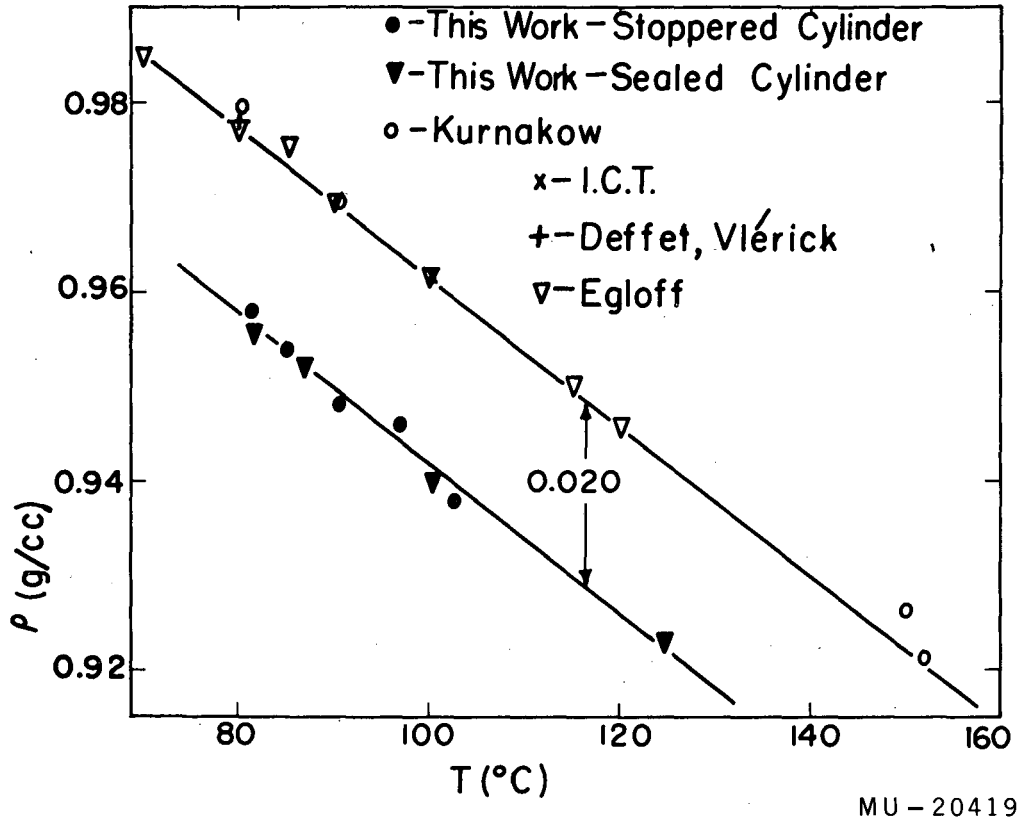

Fig. 25. Comparison of uncorrected experimental values for density of liquid naphthalene with literature values.[58,74,76]

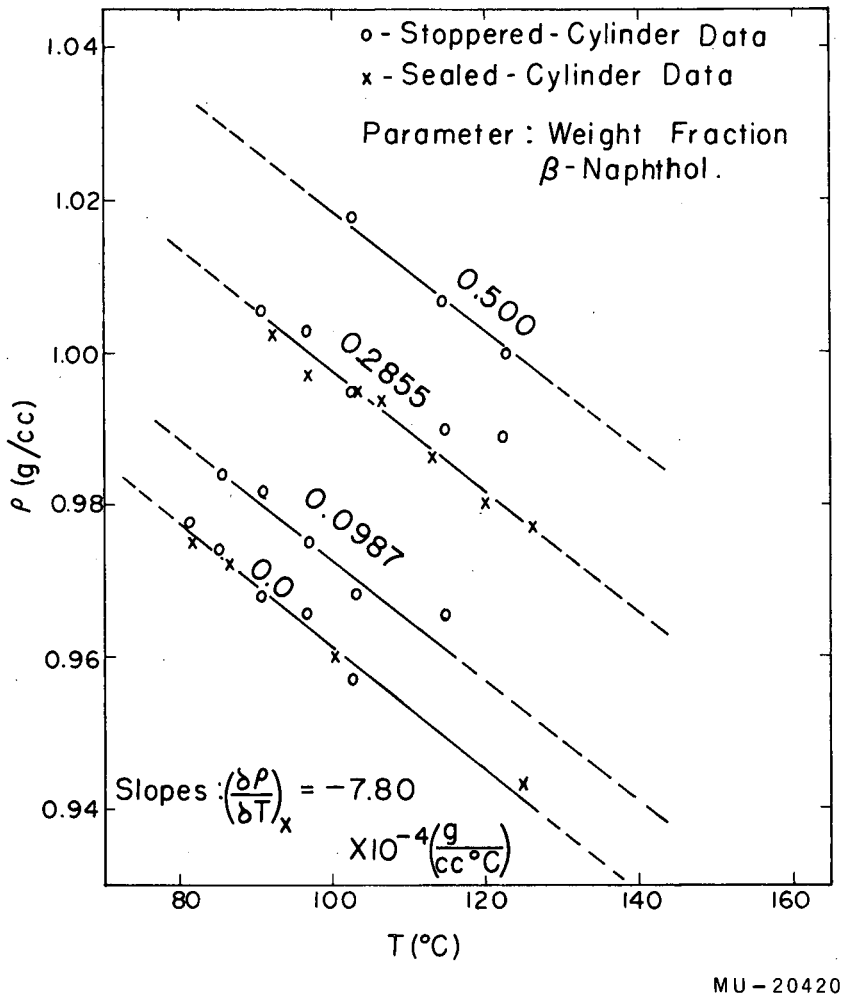

Fig. 26. Densities of liquid naphthalene–β-naphthol mixtures. Constant-concentration plots vs temperature.

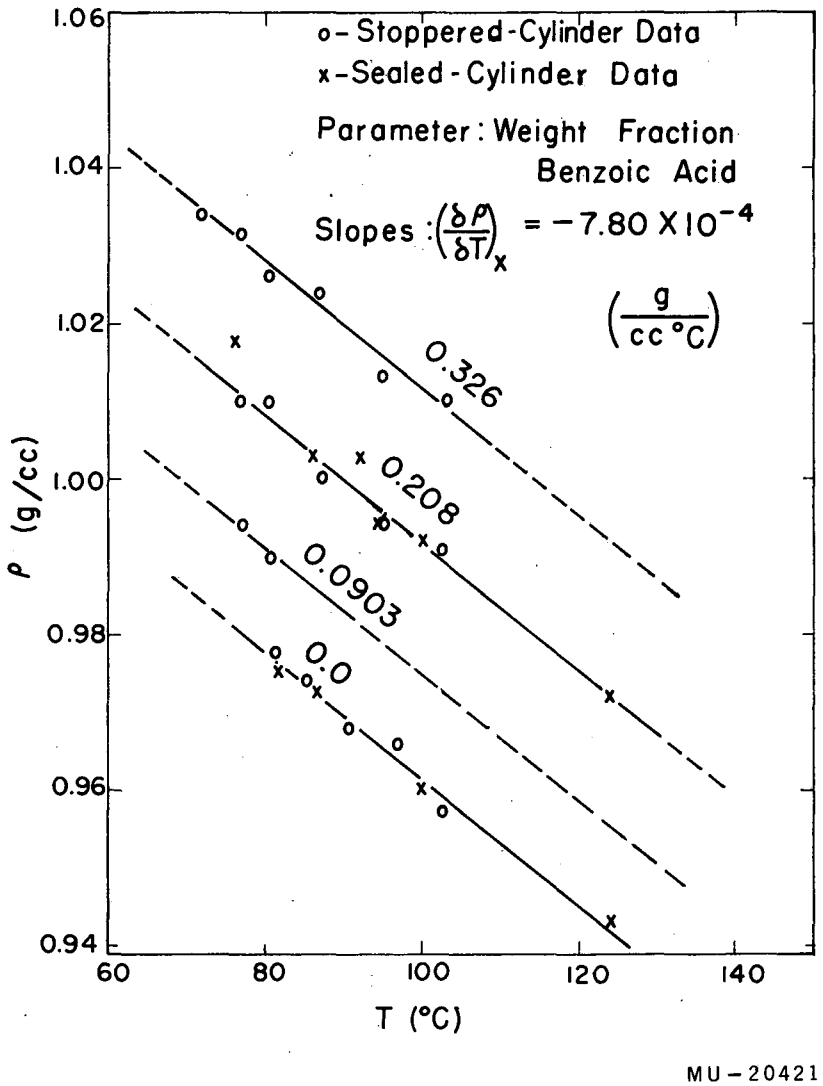

Fig. 27. Densities of liquid naphthalene-benzoic acid mixtures. Constant concentration plots vs temperature.

Table V

Corrected densities of liquid naphthalene-benzoic acid mixtures

Composition			
x, wt. fraction benzoic acid	C, M/l benzoic acid	ρ(g/cc)	T(°C)
0	0	0.986	70
0	0	0.978	80
0	0	0.969	90
0	0	0.961	100
0	0	0.953	110
0	0	0.945	120
0.0903	0.739	0.999	70
0.0903	0.733	0.991	80
0.0903	0.727	0.983	90
0.0903	0.722	0.975	100
0.0903	0.715	0.967	110
0.0903	0.710	0.959	120
0.208	1.730	1.017	70
0.208	1.719	1.008	80
0.208	1.704	1.000	90
0.208	1.690	0.992	100
0.208	1.678	0.984	110
0.208	1.661	0.975	120
0.326	2.76	1.036	70
0.326	2.74	1.028	80
0.326	2.72	1.020	90
0.326	2.70	1.012	100
0.326	2.68	1.003	110
0.326	2.66	0.995	120

Table VI

Corrected densities of liquid naphthalene–β–naphthol mixtures

Composition			
x, wt. fraction β-naphthol	C, M/l β-naphthol	ρ(g/cc)	T(°C)
0	0	0.978	80
0	0	0.969	90
0	0	0.961	100
0	0	0.953	110
0	0	0.945	120
0	0	0.937	130
0.0987	0.677	0.989	80
0.0987	0.670	0.980	90
0.0987	0.665	0.972	100
0.0987	0.660	0.965	110
0.0987	0.655	0.957	120
0.0987	0.650	0.949	130
0.2855	1.990	1.006	90
0.2855	1.977	0.998	100
0.2855	1.960	0.990	110
0.2855	1.944	0.982	120
0.2855	1.927	0.973	130
0.500	3.53	1.018	100
0.500	3.51	1.011	110
0.500	3.48	1.003	120
0.500	3.45	0.995	130

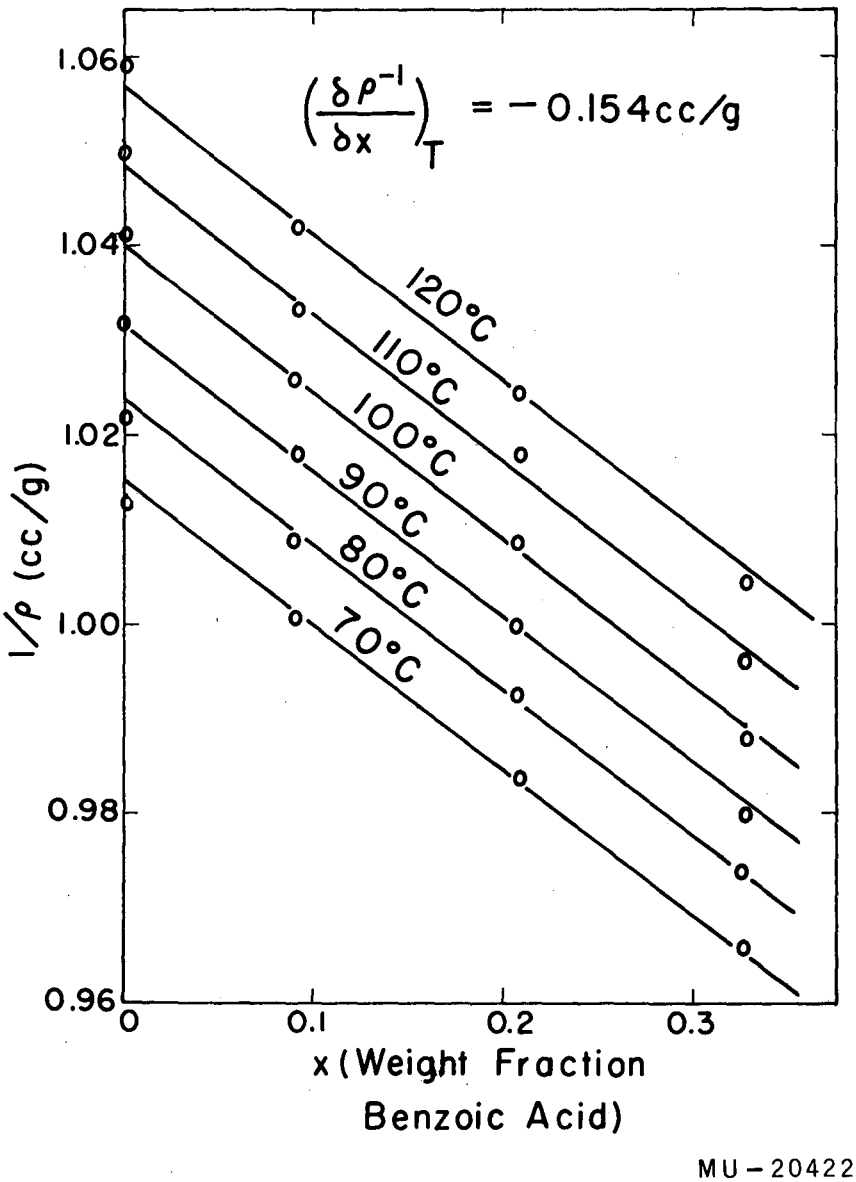

Fig. 28. Reciprocal densities of liquid naphthalene-benzoic acid mixtures. Isothermal plots vs concentration.

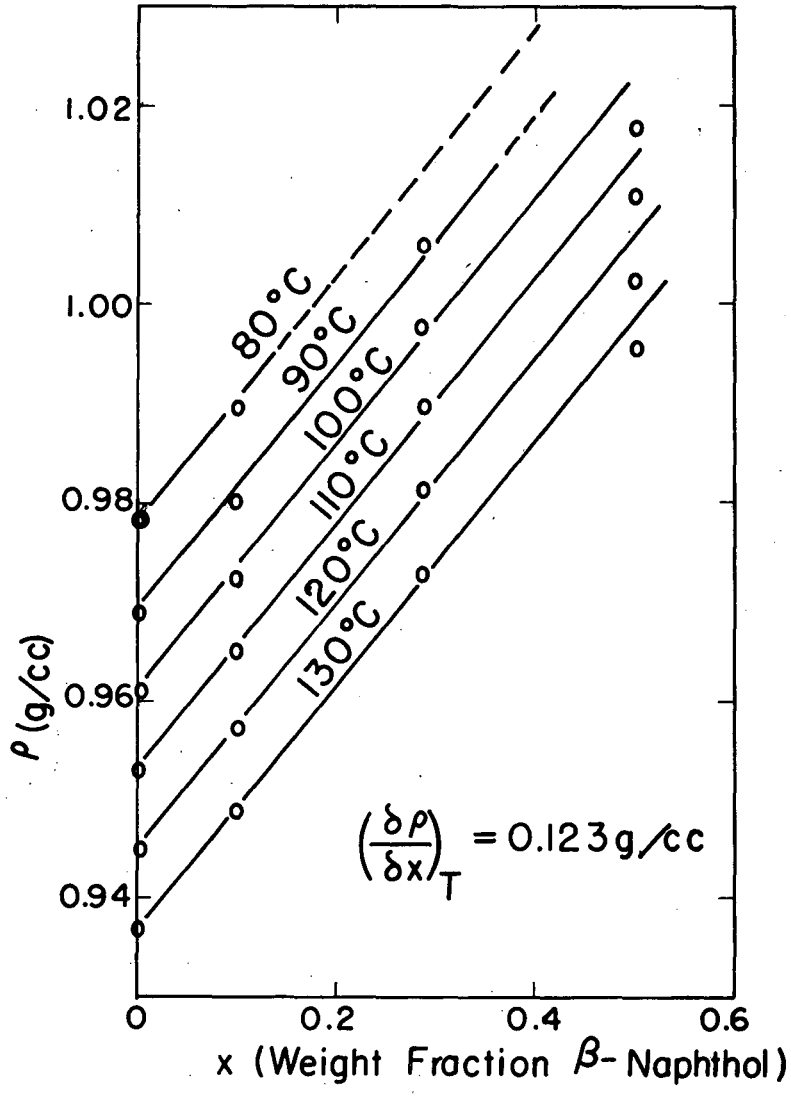

Fig. 29. Densities of liquid naphthalene–β-naphthol mixtures Isothermal plots vs concentration.

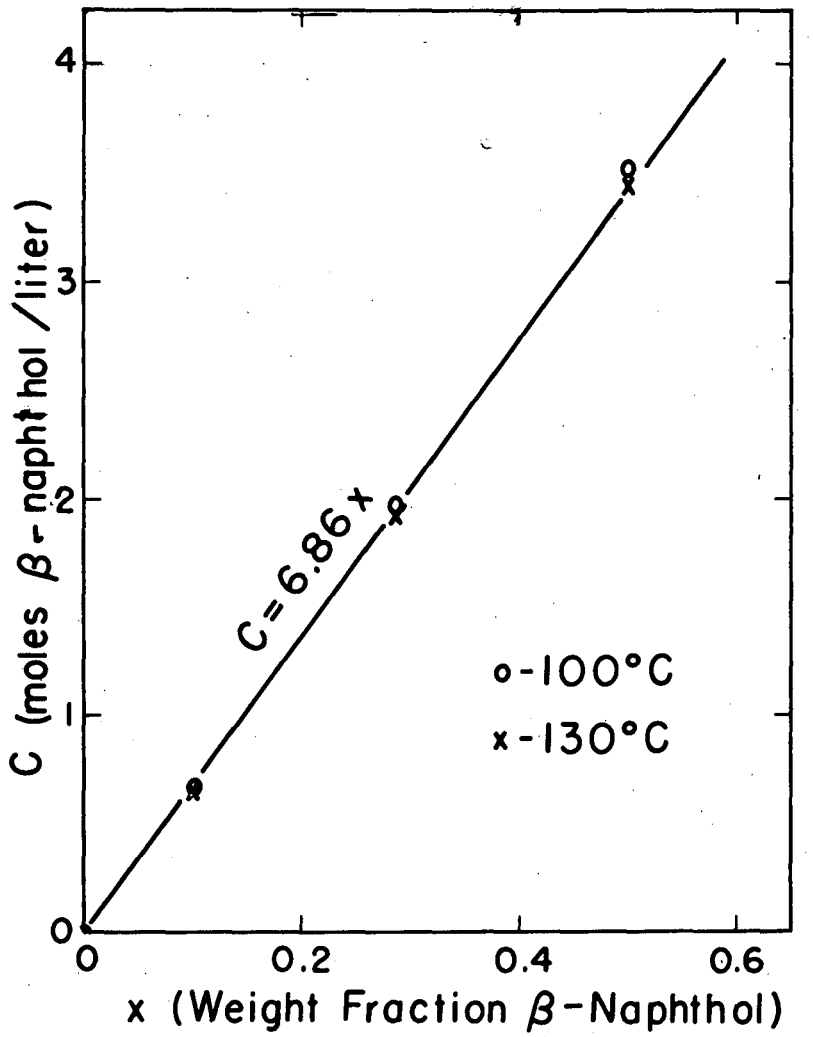

Fig. 30. Molar concentrations in liquid mixtures of naphthalene-β-naphthol plotted vs concentrations in weight fractions.

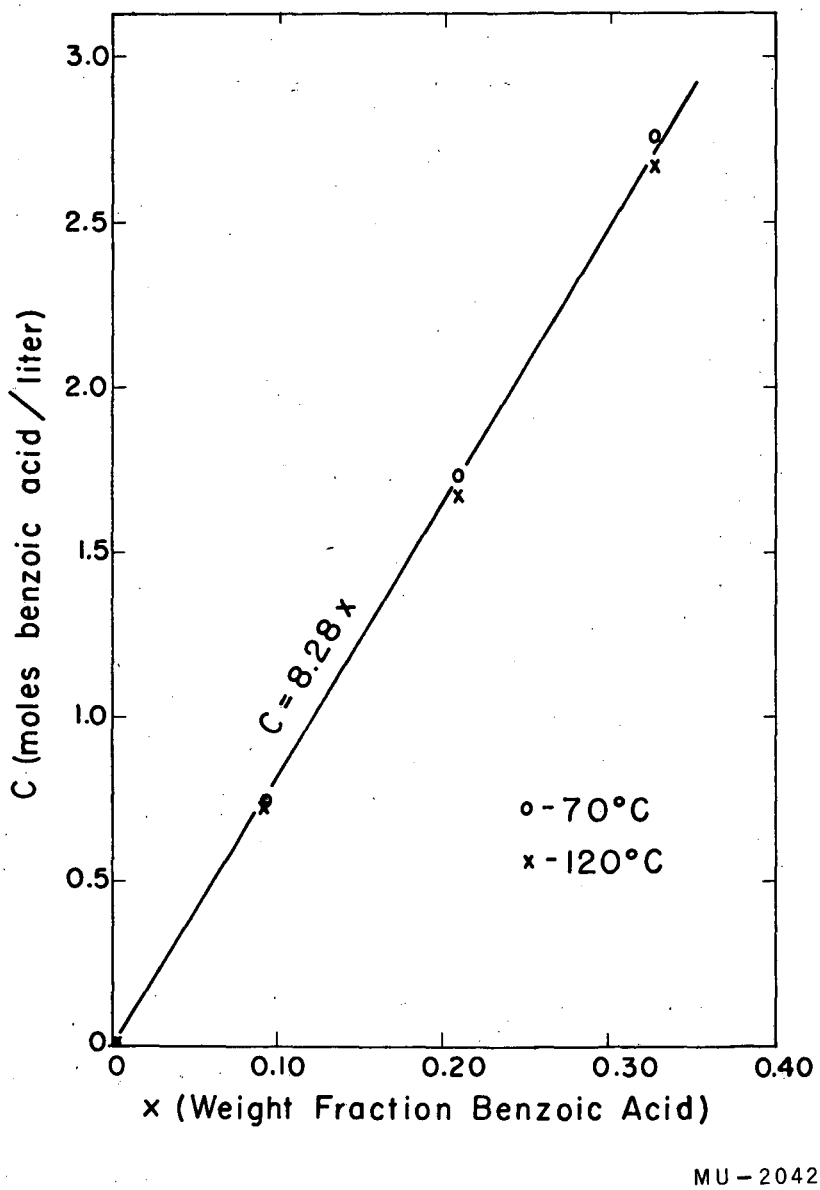

Fig. 31. Molar concentrations in liquid mixtures of naphthalene-benzoic acid plotted vs concentrations in weight fractions.

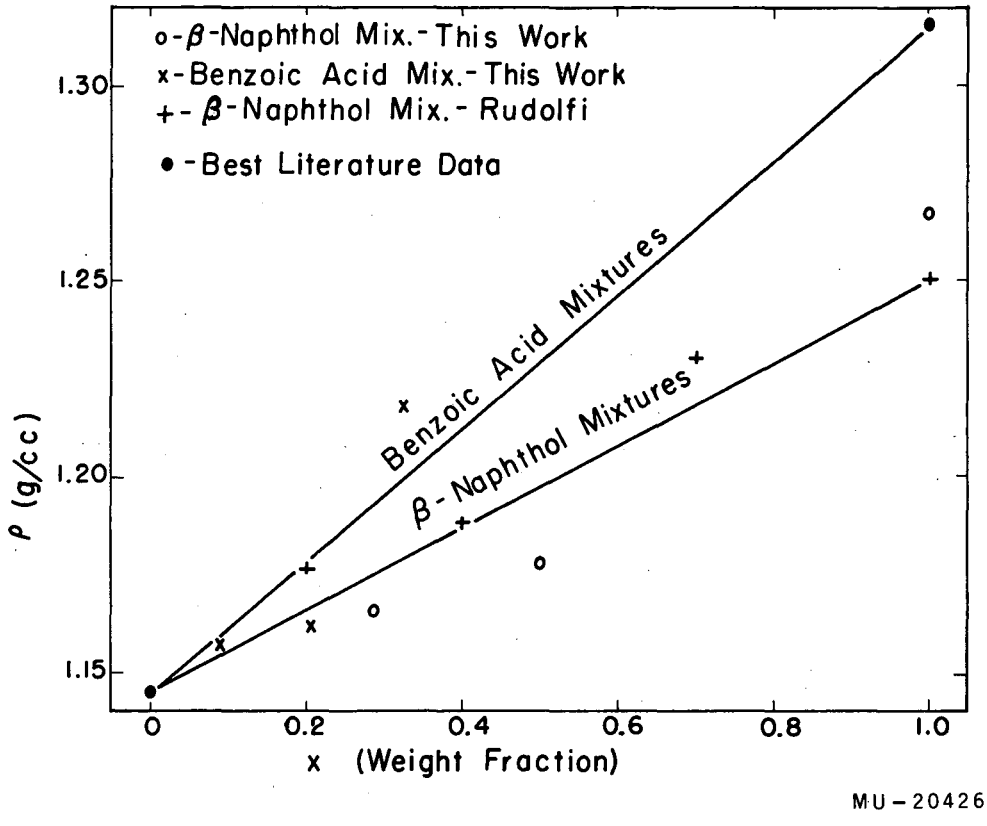

Fig. 32. Solid densities of mixtures of naphthalene-benzoic acid and of naphthalene-β-naphthol plotted vs weight fraction.

only straight lines were drawn between literature values for densities of the pure components.[58,69,70,77,78]

D. Viscosities

Method

Viscosities were determined with a Cannon-Fenske viscosimeter* by the standard ASTM method.[79,80] In use, the viscosimeter was placed in the constant-temperature bath mentioned previously in the discussion on densities. About 30 min was allowed for the temperature to equilibrate, which is supposed to be adequate.[80]

The viscosimeter was calibrated with water at various temperatures. Values for viscosity and density of water were taken from the Handbook of Chemistry and Physics.[70] The calibration curve (efflux time vs viscosity) was a straight line, with the data points superimposed on it.

Duplicate determinations were made in several cases. An average difference of about 0.2% resulted.

Because of tiny insoluble particles sometimes present in the naphthalene as purchased, the mixtures were filtered through very fine porous diaphragms before use. Any solid particles present would reduce the flow in the viscosimeter, and sometimes even completely clog it.

Results

The experimentally determined viscosity of naphthalene is compared with literature values in Fig. 33.[75,78,81-83] It compared quite well. The viscosities of the various mixtures are tabulated in Tables VII and VIII and plotted in Figs. 34 and 35.

*Size 50, No. A41, purchased from Arthur H. Thomas Co., Philadelphia, Pennsylvania.

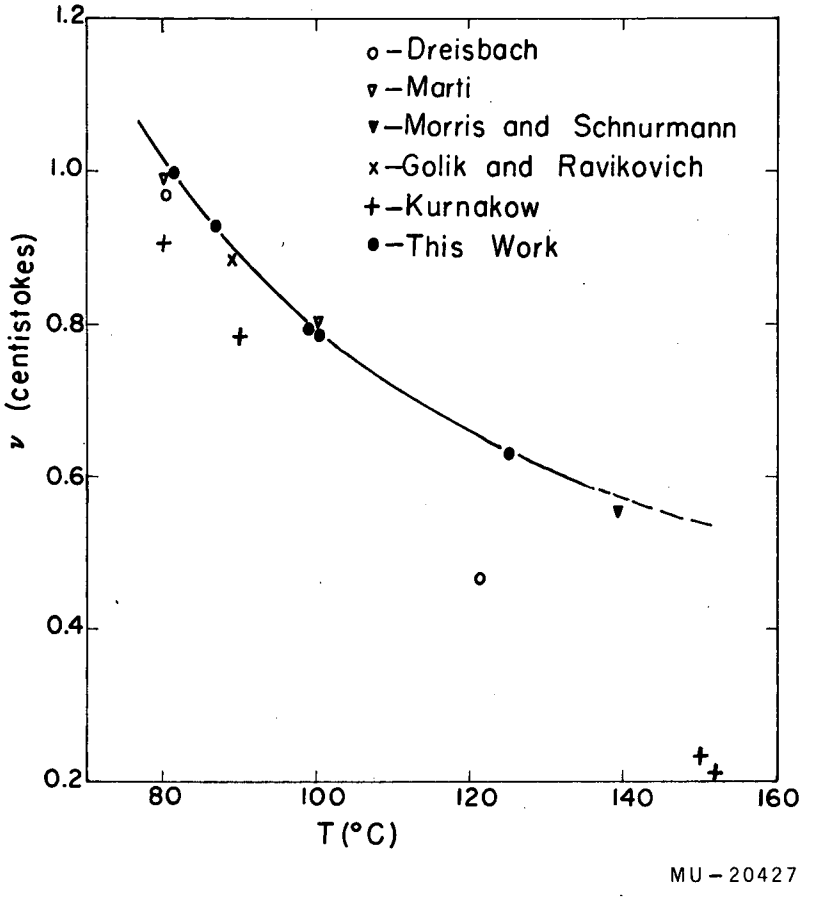

Fig. 33. Comparison of experimentally determined viscosities of naphthalene with literature values.[75,78,81-83]

Table VII

Viscosities of naphthalene-benzoic acid mixtures

x, wt. fraction benzoic acid	T(°C)	ν, Kinematic viscosity (centistokes)
0	81.4	1.000
0	86.6	0.933
0	99.0	0.794
0	100.0	0.788
0	125.0	0.632
0.1003	78.2	1.110
0.1003	87.0	0.982
0.1003	99.1	0.846
0.315	71.8	1.403
0.315	86.7	1.151
0.315	99.3	0.985
0.315	126.0	0.763

Table VIII

Viscosities of naphthalene-β-naphthol mixtures

x, wt. fraction β-naphthol	T(°C)	ν, Kinematic viscosity (centistokes)
0	81.4	1.000
0	86.6	0.933
0	99.0	0.794
0	100.0	0.788
0	125.0	0.632
0.0995	86.6	1.023
0.0995	100.3	0.860
0.0995	125.0	0.679
0.200	100.0	0.956
0.200	125.0	0.730
0.500	125.0	1.058

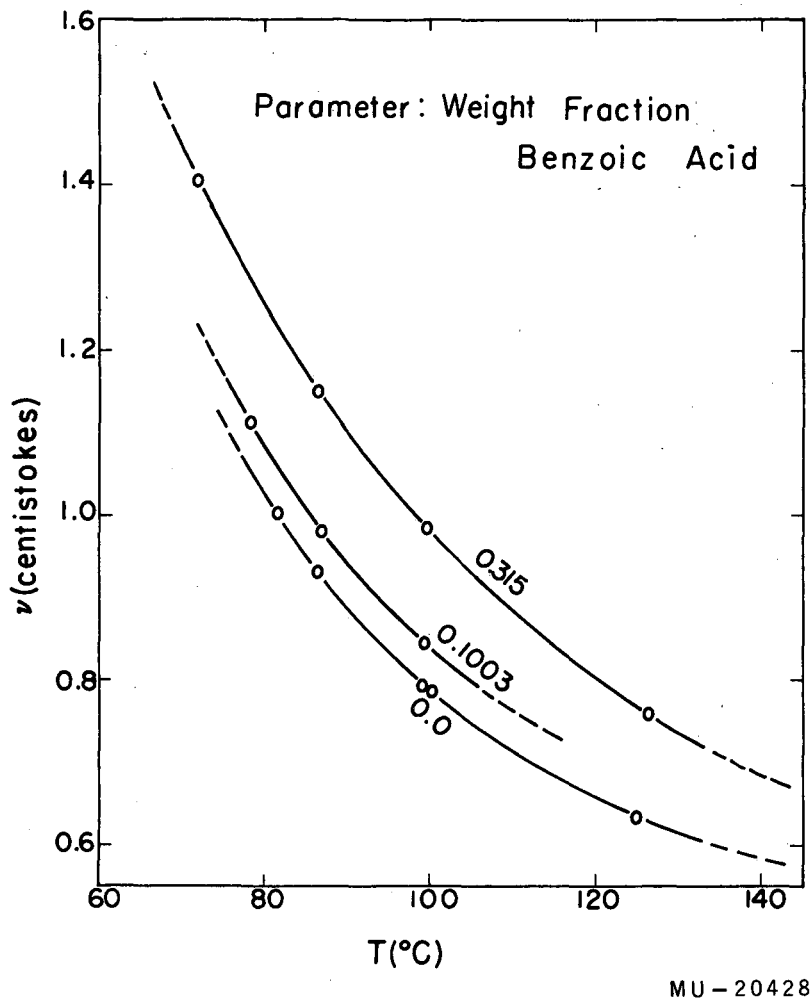

Fig. 34. Kinematic viscosity of naphthalene-benzoic acid mixtures. Constant concentration plots vs temperature.

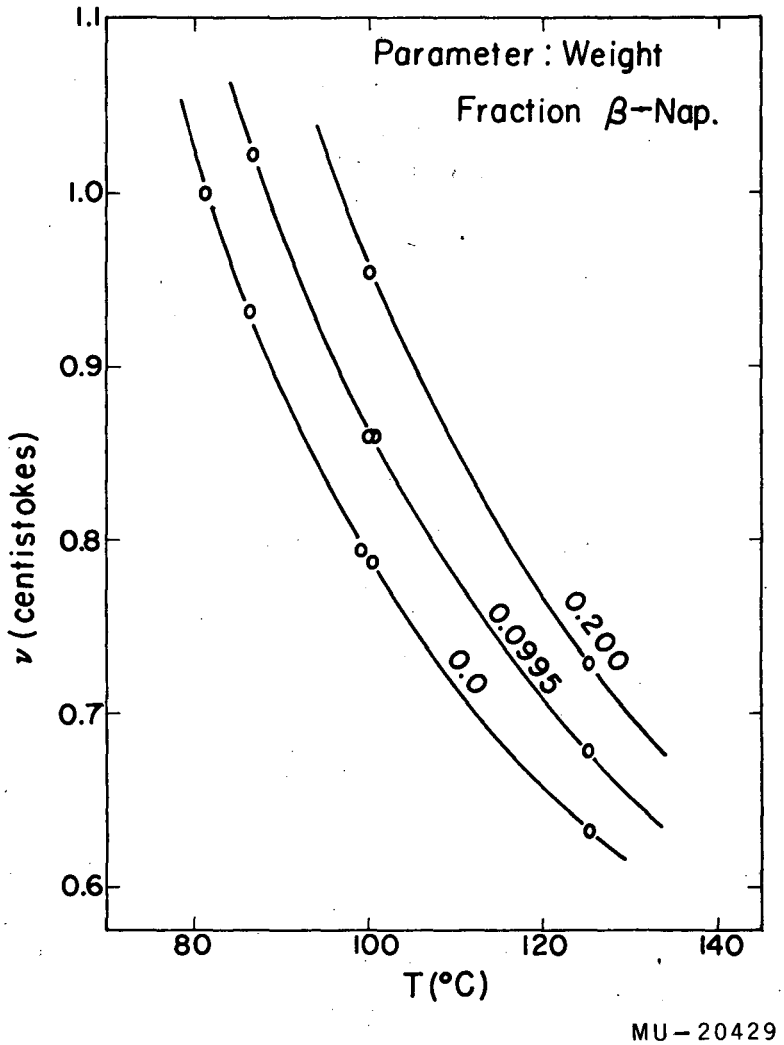

Fig. 35. Constant concentration plots of kinematic viscosity vs temperature for naphthalene–β-naphthol mixtures.

E. Diffusivities

Method

Diffusivities were determined by the capillary-tube method. In this method a uniform mixture is placed in a capillary sealed at one end. This is then placed in a stirred mixture of another composition and allowed to diffuse for a time. Knowledge of the average composition in the tube at the end of this time enables one to calculate an average diffusion coefficient. The solution for this situation is given by Carslaw and Jaager.[84] In terms of weight fractions (use of which was justified in the density discussion) it is:

$$\frac{X_{av} - X_{bulk}}{X_0 - X_{bulk}} = \frac{8}{\pi^2} \sum_{n=0}^{\infty} \frac{1}{(2n+1)^2} \exp\left[-\frac{(2n+1)^2 \pi^2}{4} \frac{Dt}{L^2}\right] \qquad (6)$$

where X_{av} is the average concentration in the tube at time t, X_{bulk} is the concentration of medium into which contents of the tube are diffusing, X_0 is the initial concentration in the tube at time 0, D is the diffusion coefficient, L is the length of the tube, and t is the time of diffusion.

In this work 4 mm (2.5 mm i.d.) glass tubes were used. Initially the concentration in the tubes differed from the bulk concentration by about 0.1 weight fraction.

The tubes were prepared by sucking a mixture of known concentration up into the tubes. The tubes were then broken at an intermediate point, some of the material was removed from the freshly-broken end, and the ends were then fitted with silicone rubber plugs which fit into the tubes about 2 mm. These plugs were sealed in place with Thermon T-3,* which was allowed to dry and hardened for several hours. (Incidentally, this type of seal was tested and found to be leakproof under the conditions for which it was employed.) When the Thermon had set, the tube was broken again at a desired length and the distance between the plug and broken end was measured and recorded. The tubes were then fastened

*This material was described in the phase-diagram discussion.

to a stirring rod in such a manner that density gradients would not cause bulk flow out of the tubes. The stirrer was lowered into the molten bath and stirring was begun. The time at which the contents of the tubes were melted was recorded.

The runs were made in a 100-ml round-bottom flask fitted with a tapered-joint mercury-seal stirrer. The flask was held in the constant-temperature bath described in the density discussion. The stirrer, and attached tubes, were rotated at about 60 rpm. The runs took place over several days. The bulk concentration was found to change a negligible amount during a run.

At the end of a run the tubes were removed from the bath and the time was recorded. The contents were frozen by blowing on them, they were scraped and rinsed with acetone, and the distance between their seals and open ends were again measured. The seals were then removed and the contents of the tubes were analyzed in the usual manner.*

Results

Tube lengths from 1.5 to 4.5 cm were tried, with substantially no difference in the results. This indicates the absence of appreciable end effects. Runs were also tried with the higher concentration both inside the tubes and in the bulk melt. Again the results were about the same. The temperature control also failed once and the temperature fluctuated wildly for part of one run. Even in this case results agreed fairly well with those of well-controlled runs. The results are shown in Table IX. The values of $T/D\eta$ for any given concentration appeared to be nearly single-valued. Consequently, averages were taken, compiled in Table X, and plotted in Fig. 36.

---

*See Chapter IV.

Table IX

Results of diffusion experiments

$\frac{X_0 + X_{bulk}}{2}$ (wt. frac.)	D x 10^5 (cm^2/sec)	Number of runs	Maximum deviation from average D (%)	T(°K)	ν(cs)	ρ(g/cc)	$\frac{T}{D\eta} \times 10^{-7}$ $\left(\frac{°K\ sec}{cm^2\ cp}\right)$
β-naphthol							
0.05	2.91	3	28	358	1.00	0.9790	1.258
0.05	3.00	3	17	363	0.932	0.9747	1.332
0.05	3.50	3	12	373	0.824	0.9670	1.338
0.15	2.84	2	7	363	1.026	0.9863	1.262
Benzoic acid							
0.05	2.39	4	5	359	0.965	0.9795	1.589
0.05	3.00	2	25	373	0.810	0.9682	1.584
0.15	3.20	3	12	363	0.970	0.9910	1.180
0.15	2.58	3	8	353.2	1.110	0.9990	1.231
0.26	2.66	2	4	353.2	1.220	1.0171	1.070

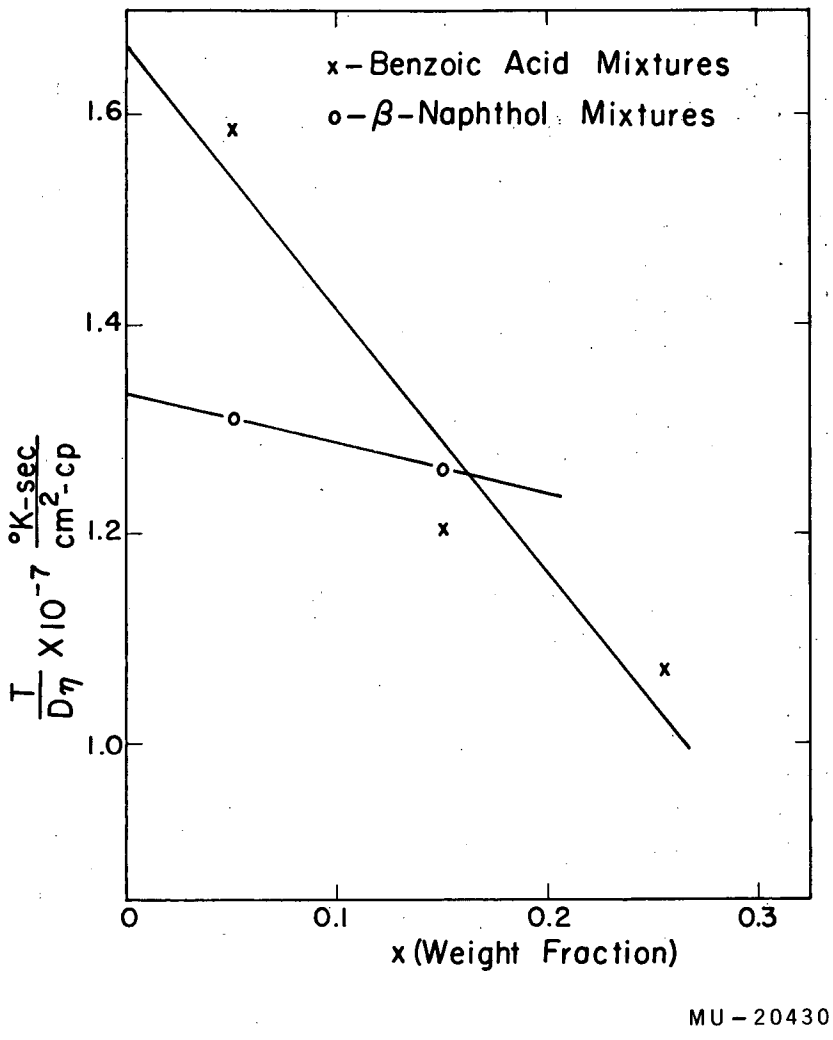

Fig. 36. Values of T/Dη vs concentration in weight fraction for naphthalene-benzoic acid mixtures and for naphthalene–β-naphthol mixtures.

Table X

Average wt. fraction	Average $T/D\eta \times 10^{-7}$
0.05 β-naphthol	1.309
0.15 β-naphthol	1.262
0.05 benzoic acid	1.586
0.15 benzoic acid	1.205
0.26 benzoic acid	1.070

F. Thermal Parameters

As stated in the introduction to this chapter, only values of the thermal parameters for the pure components are available from the literature, but these are sufficient. Table XI summarizes what are believed to be the best data available in the literature.[58,69,70,85-90] When values at several temperatures were given, those nearest the melting point were chosen. The liquid-phase thermal conductivities were estimated by the use of Eq. (7-55) from Sherwood and Reid.[85]

Table XI

Literature values of thermal parameters[a,b]

Material	Liquid c_p (cal/g°C)	Solid c_p (cal/g°C)	Liquid k,x10^4 (cal/sec-cm-°C)	Solid k,x10^4 (cal/sec-cm-°C)	λ (cal/g)
Naphthalene	0.381	0.372	2.63	6.80	35.9
β-naphthol	0.478	0.400	3.28	5.62	31.6
Benzoic acid	0.518	0.360	4.47		34.0

[a]Data were obtained from references 58, 69, 70, and 85-90.

[b]Here c_p is the heat capacity at constant pressure, k is the thermal conductivity, and λ is the heat of fusion.

IV. ANALYSES

A. Introduction

In order to determine separations, samples were taken by the author and analyzed by the Analytical Group of the Lawrence Radiation Laboratory, Berkeley. The methods of analyses were suggested by the author and the details worked out by the Analytical Group. The methods used and the sampling techniques are described in the following pages.

B. Sampling Techniques

In the zone-melting runs each sample consisted of the entire contents of the tube between two points several millimeters apart. Distances were measured from the point where material had first crystallized from the zone to these points. The point of first recrystallization was usually obvious, as the recrystallized material was clearer than the original material.* At times, especially at rapid pull rates, this point was not too clear, so it had to be estimated later from the analytical results.

For the 10- and 20-mm tubes, the glass tubes were chipped off with a small hammer, exposing the solid product. A sample was then removed with a sharpened spatula. Samples were about 3 to 6 mm long for 10-mm tubes and 1 to 3 mm long for 20-mm tubes.

For the 5-mm tubes, a diamond scribe was used and the tubes containing the product were broken into 8- to 12-mm lengths. These were weighed, the product was dissolved out with absolute alcohol, and the tube was reweighed. The weight of product for analyses was obtained by difference.

For the salt-water experiments on the cooled-drum apparatus, samples were taken directly from the doctor blade with tweezers. They

---

*Zones were formed somewhere in the middle of the tube, so that recrystallized material was immediately adjacent to untouched original material.

were placed in a sample vial before they melted. Samples from the "melt" chamber were taken by means of the drain in the bottom of the tank. Care was taken, of course, to flush the line and valve with melt before taking a sample.

C. Analysis of β-Naphthol–Naphthalene Mixtures

Mixtures of β-naphthol and naphthalene were analyzed by means of a spectrophotometer.* This method was suggested by the data of Marchlewski and Moroz, which showed that β-naphthol absorbed heavily at a wavelength of 330A, while naphthalene absorbed negligibly.[91] These absorptions were roughly confirmed by the Analytical Group. Figure 37 shows the data of Marchlewski and Moroz. Figures 38, 39, and 40 show the absorption curves obtained by the Analytical Group. On the basis of these curves a wavelength of 331A was selected for use in analyses. Figure 41 shows the standard curve used for analyses.

The analytical technique, then, was to dissolve a known weight of mixture in a known volume of absolute ethyl alcohol. The concentration of β-naphthol was then obtained from the spectrophotometric reading (naphthalene was assumed to be nonabsorbent). The fraction of β-naphthol in the original mixture was then calculated.

In order to check the analytical accuracy, samples of known concentration (10%w β-naphthol) were submitted periodically. It was found that the average percent error of these analyses was 6.16%. For standard samples analysed consecutively, however, the error was only 3.05%. This shows that the analytical results tended to vary from one analytical period to another. Thus the results were recalibrated for each analytical period on the basis of the analyses of the standard samples. For example, if the standard sample analyzed 9.0%, all other results were multiplied by 9/10.

---

*Beckman DU, Serial No. 567.

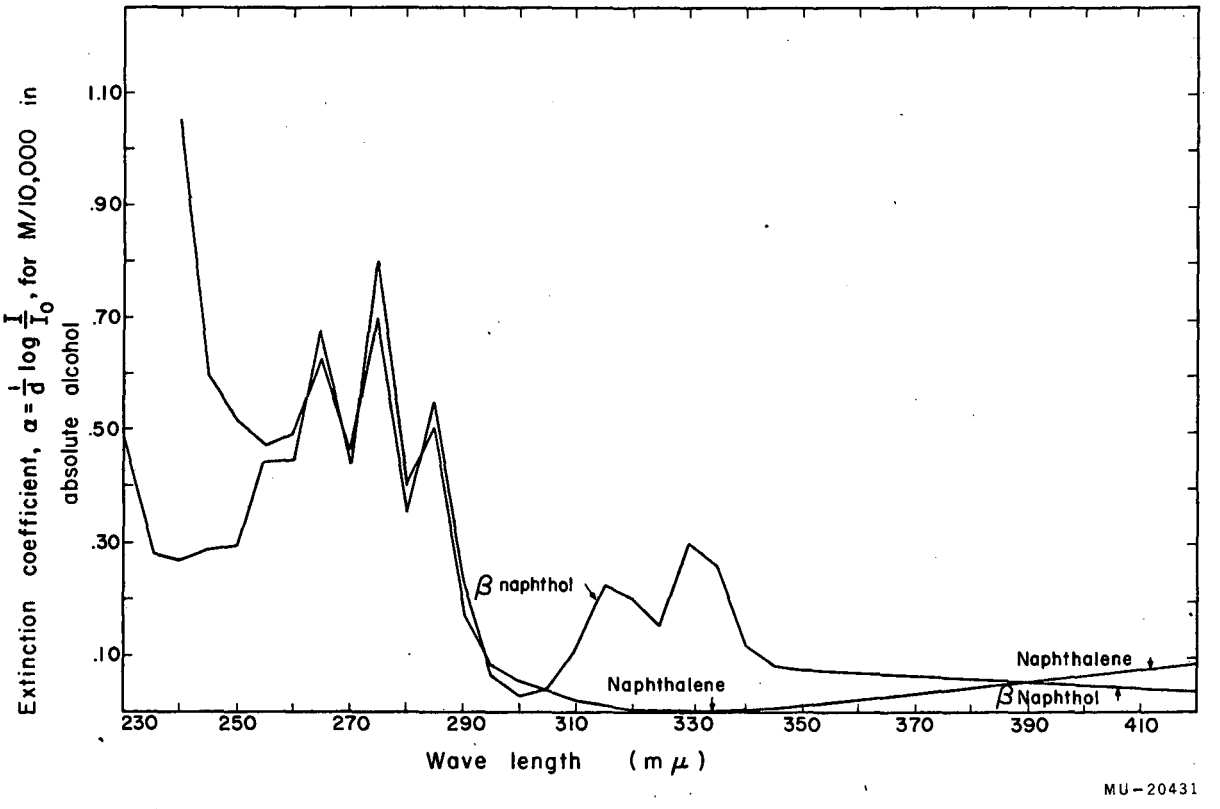

Fig. 37. Literature values of the extinction coefficient plotted vs wavelength for 0.0001 M solutions of naphthalene and of β-naphthol in absolute alcohol.[91]

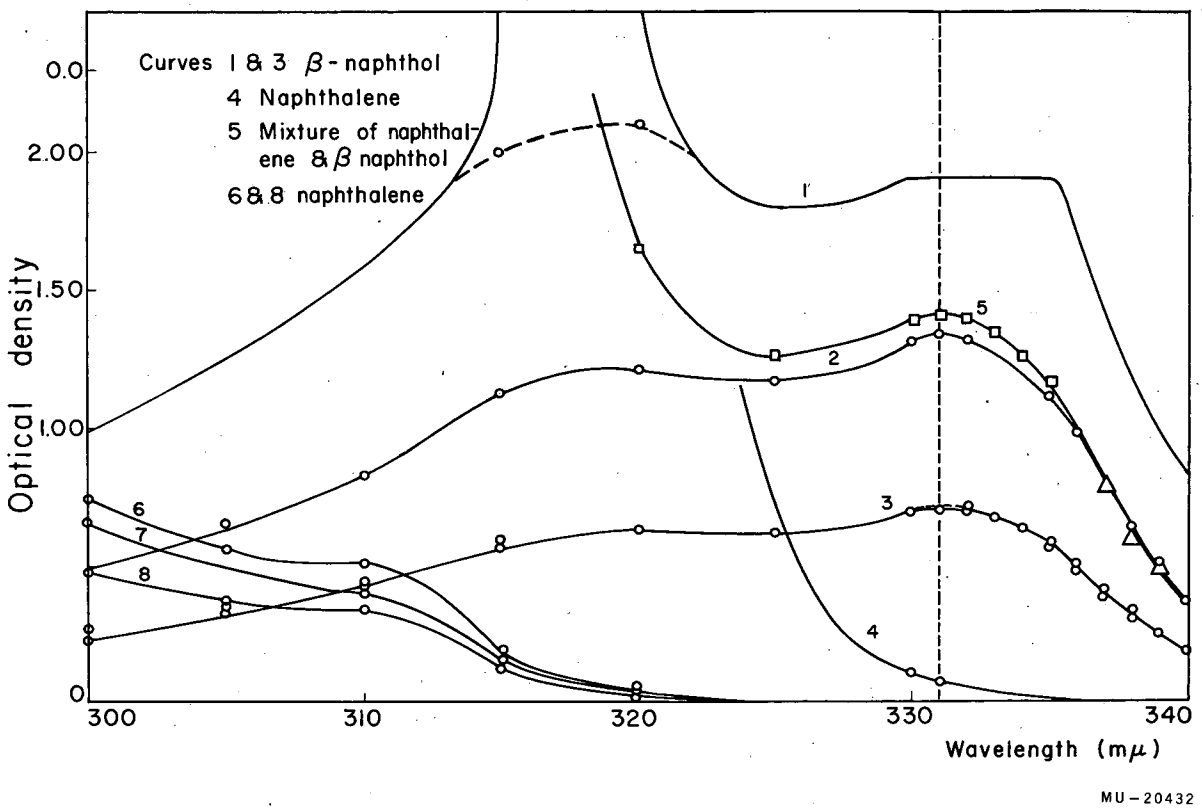

Fig. 38. Optical densities vs wavelength for solutions of naphthalene and β-naphthol in absolute alcohol. Curves are for 25-ml alcoholic solutions of

(1) 5.096 mg β-naphthol,
(2) 2.548 mg β-naphthol,
(3) 1.274 mg β-naphthol,
(4) 1.0376 g naphthalene,
(5) 2.548 mg β-naphthol, and 86.47 mg napthalene,
(6) 8.96 mg naphthalene,
(7) 7.87 mg naphthalene, and
(8) 5.79 mg naphthalene.

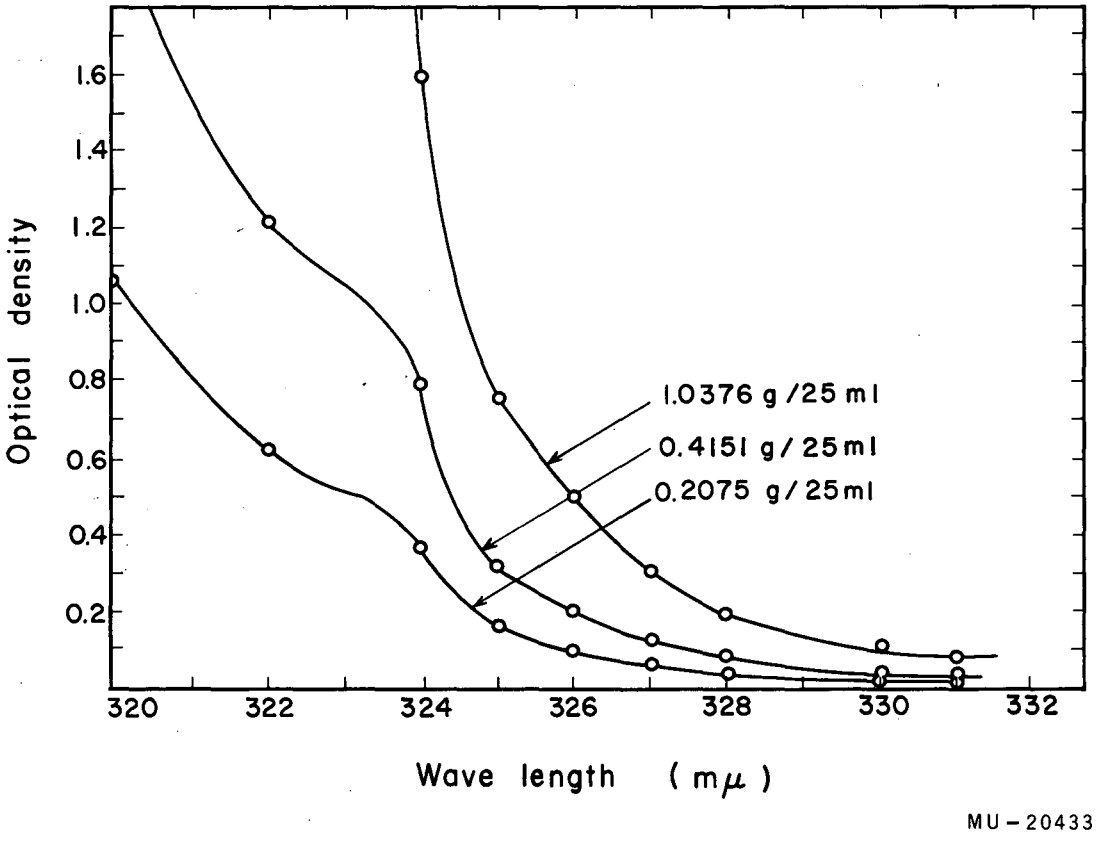

Fig. 39. Optical density vs wavelength for solutions of naphthalene in alcohol.

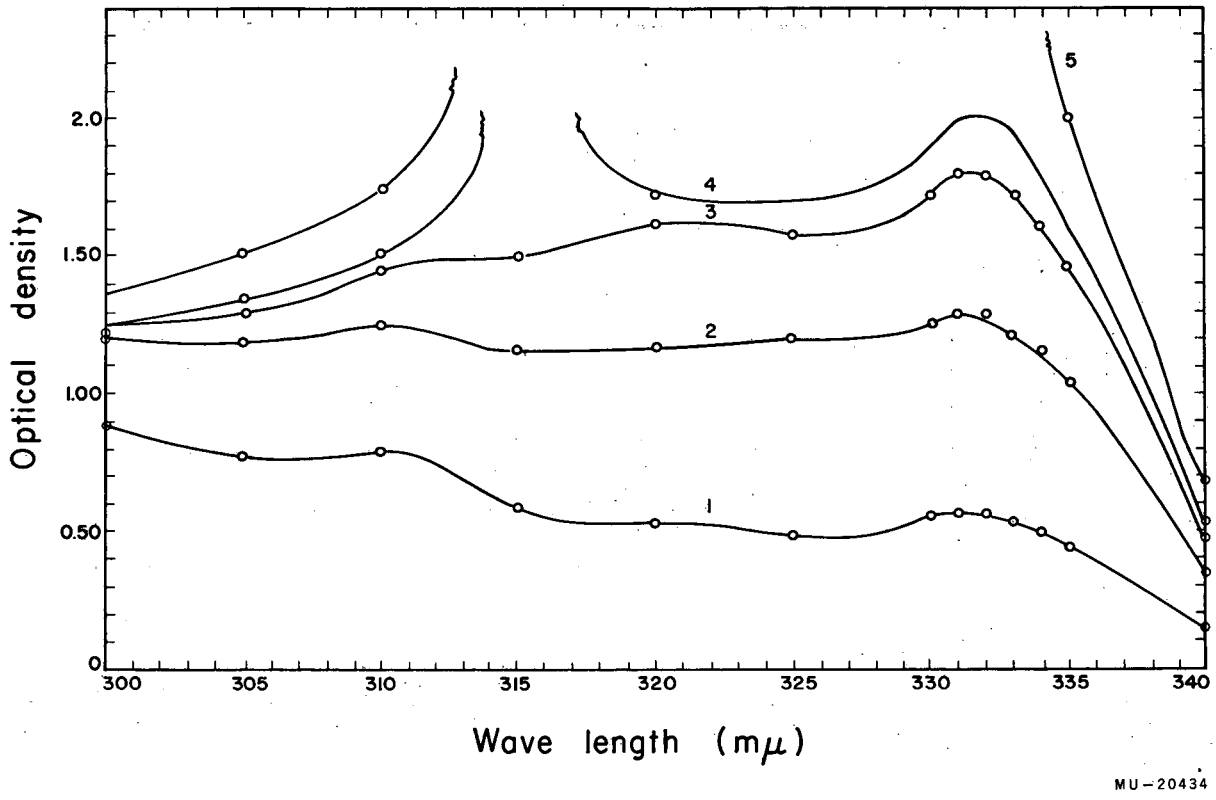

Fig. 40. Optical densities vs wavelength for 25-ml alcoholic solutions of
(1) 0.91 mg β-naphthol and 8.35 mg naphthalene,
(2) 2.36 mg β-naphthol and 9.50 mg naphthalene,
(3) 3.41 mg β-naphthol and 7.29 mg naphthalene,
(4) 3.80 mg β-naphthol and 6.34 mg naphthalene, and
(5) 4.96 mg β-naphthol and 5.35 mg naphthalene.

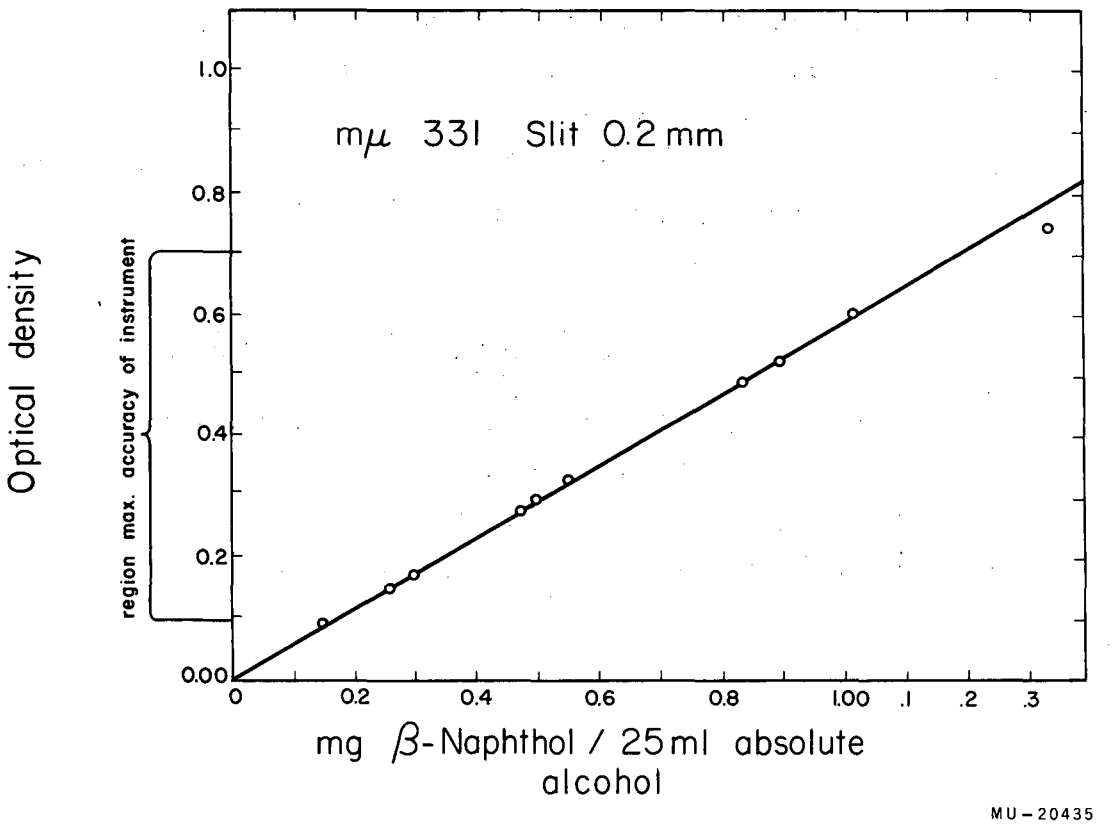

Fig. 41. Standard curve for the spectrophotometric analyses of mixtures of β-naphthol in naphthalene. Optical density vs mg β-naphthol per 25 ml of alcoholic solution.

D. Analysis of Benzoic-Acid-Naphthalene Mixtures

Mixtures of benzoic acid and naphthalene were dissolved in absolute alcohol. The general procedure was the same as for β-naphthol mixtures, except that the amount of benzoic acid present was found by a standard acid-base titration using a standard sodium hydroxide titrant and phenolphthalein indicator. The average error was 6.24%, while the average deviation from standard in any analytical period was 2.57%.

E. Analyses of Salt-Water Solutions

The fraction of salt in the salt-water mixtures was found gravimetrically. A silver nitrate solution was used to precipitate silver chloride, which was then dried and weighed. Both the average error and deviation in a single analytical period were less than 1%.

V. HEAT TRANSFER IN ZONE MELTING

A. Introduction

Two pieces of information needed to design a zone melter are: (a) Zone size as a function of heater input, geometry, and coolant temperature, and, (b) Position of the zone relative to the heater. Detailed heat-transfer calculations will be carried out in this section for zone melting in a vertical tube under free-convection conditions. It is hoped that this will serve as a model for other situations.

B. Heat Balance

The logical way to arrive at the size of the zone is by a heat balance. Fig. 42 is a diagram of the experimental layout in the region of the zone. For purposes of discussion, the following heat flux rates are defined:

1. Q_{tot} is the rate of heat transfer from heater to zone.
2. Q_{waste} is the rate of heat transfer from the zone through the side of the tube to the surroundings.
3. q_{glass} is the rate of axial heat conduction through the glass tube at the bottom and top of the zone.
4. q_t is the rate of axial conduction into the upper (top) solid interface from the zone.
5. q_b is the rate of axial conduction into the lower (bottom) solid interface from the zone.

An over-all heat balance yields the equation:

$$Q_{tot} = Q_{waste} + q_{glass} + q_t + q_b. \qquad (7)$$

It is easily seen that the size of the zone may be calculated if the following are known:

(a) heat into the zone (Q_{tot}).

(b) heat out the top and bottom of the zone ($q_{glass}+q_t+q_b$).

(c) heat transfer coefficient from the zone to the surroundings (h_c), and temperature of the surroundings (T_c).

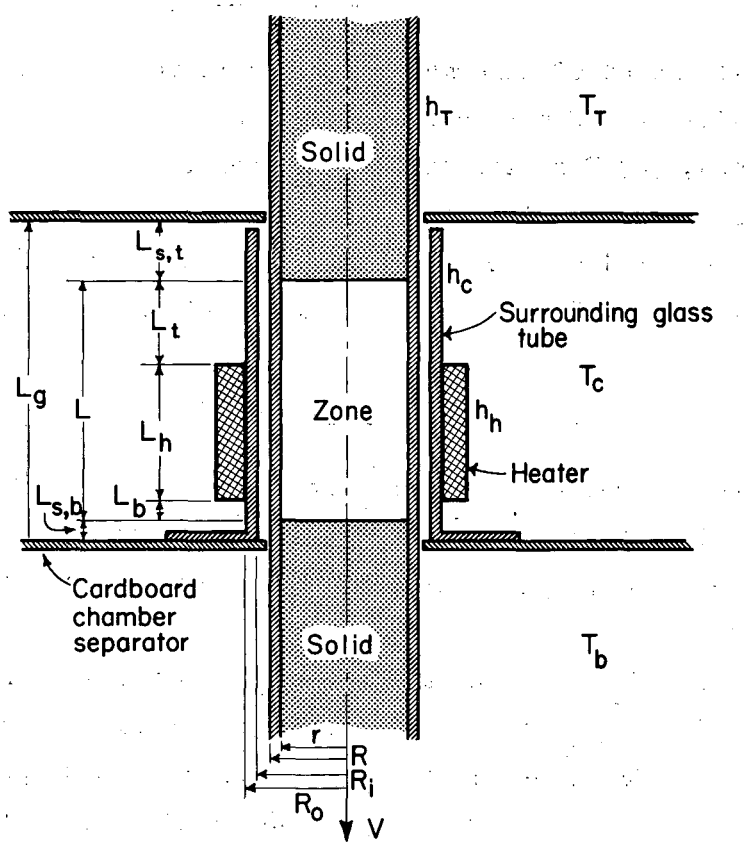

Fig. 42. Diagram showing various thermal parameters in zone-melting apparatus.

Thus Q_{waste} is obtained by difference. The magnitude of h_c determines the heat-transfer area necessary to produce Q_{waste}. This area must be the surface area of the zone outside the heater. In the following pages and calculations the use and validity of this principle is demonstrated.

Assumptions

The following assumptions were made in order to simplify the calculations. They are listed here for convenience, although some are discussed later in this section.

(a) There is only radial heat transfer from the tape to the zone.

(b) There is only radial heat transfer from the zone to the surroundings.

(c) The interfaces are planar.

(d) There is only axial heat conduction in the solid.

(e) The solid is effectively infinite in length.

(f) The free convection from a cylindrical solid is the same as from a vertical plane.

(g) The solid-liquid interfaces are at the melting point.

(h) The zone is at the melting point.

(i) Average thermal parameters may be used in the solid and surrounding tube.

Heater Properties

The heater used in these experiments consisted of two wraps of heating tape* around a glass tube, which surrounds the glass tube with the product enclosed. In the zone-melting experiments, only the total power input to the heater was measured. In order to calculate the actual heat transferred to the zone, the heat-transfer characteristics of the tape must be known. Accordingly, the following experiment was performed. A "sandwich" of 7 layers of heating tape was made, with current applied

* Briskeat heating tape, which consists of nichrome resistance wire wrapped with glass fiber and woven into tape.

to only the central tape. Small thermocouples were inserted between each layer of tape with about two inches of the thermocouple lead also embedded between the layers. This assembly was held in mid-air, with the edges of the tapes on the top and bottom. Glass-wool insulation was applied to the top and bottom. The steady-state temperature distribution was measured as a function of power input to the central tape.

In order to interpret these experiments, one observation about the character of these tapes should be noted. The strands of wire run back and forth across the tape. This means that the thermal resistance is much greater from one tape to the next than from one side of the tape to the other. Thus it was assumed that the tape behaves as very thin sheets of metal separated by insulation and that the temperature in each tape layer is uniform. The thermocouple measures the average temperature of adjacent layers of tape. From this data, the heat-transfer coefficient between layers of tape and the heat-transfer coefficient from the outside layers to the surroundings was calculated. It was found that the surface coefficient was independent of temperature and tape size. This is probably due to the cellular nature of the surface, which does not allow a smooth boundary layer to build up.

The heat-transfer coefficient between layers of tape, h_t, was found to be 0.00796 $w/cm^2\ ^oC$. The heat-transfer coefficient from the surface, h_h, was 0.00248 $w/cm^2\ ^oC$.

Since the edges of the tape were not insulated in the zone-melting runs, these experiments were repeated without glass-wool insulation on the edges. The heat-loss rate per unit length of tape per ^oC temperature difference was found to be

$$(2hA/L)_o = 0.00057\ w/cm\ ^oC.$$

The next piece of information needed about the heater is the heat-transfer coefficient between the tape and the zone. For this calculation it was necessary to assume a temperature for the zone, since this is not known. The most obvious temperature to assume is the melting point. If the zone is well-stirred and the resistance to heat transfer from the tape to the zone is large, this assumption is reasonable.

To measure this resistance, a thermocouple was inserted in between the layers of tape while a zone was generated in the usual manner. From the measured temperature in the tape, and the heat transfer characteristics of the tape, the heat transferred to the surroundings can be calculated. By subtracting this heat from the power input to the tape, we obtain the heat transferred to the zone. It is difficult to measure the temperature of the tape accurately, so the results are somewhat rough. The coefficients obtained in this manner, however, correspond closely to coefficients calculated from elementary considerations. In the latter method, the conductive resistances of heating tape, glass tubes, and air-gap are added to yield an over-all resistance. The coefficient resulting from this is added to the coefficient for radiative heat transfer to give the effective over-all heat-transfer coefficient. This indicates that the air gap between the two glass tubes is stagnant. The data of Table XII show this gap, $(R_i - R)$, to be small (about 1 mm), and so it would be expected to be stagnant. Consequently, this calculated heat-transfer coefficient was used in the calculations to follow.

With these results the total heat transferred from heater to tube is given by

$$q_{total} = 2\, r_3 L_h\, \pi\, (T_3 - T_m)\, h_z, \tag{8}$$

where r_3 is the radius of the heating-tape layer closest to the tube, h_z is the coefficient of heat transfer from the tape to the zone, T_m is the melting point of the material in the zone, and T_3 is given by:

$$T_3 = \frac{(q/A)r_3 + h_t r_2 b + (hA/L)_0 (r_3/L_h) T_c + T_m h_z r_3}{h_z r_3 + h_t r_2 (1-a) + (hA/L)_0 (r_3/L_h)} \tag{9}$$

where r_2 is the radius of the gap between the first and second layers of heating tape, (q/A) is the heat input per unit area to the heating tape,

$$a = \frac{h_t r_2}{h_h r_1 + h_t r_2 + (hA/L)_0 (r_1/L_h)},$$

$$b = \frac{(q/A)r_1 + (hA/L)_0 (r_1/L_h) T_c + h_h r_1 T_c}{h_h r_1 + h_t r_2 + (hA/L)_0 (r_1/L_h)},$$

and r_1 is the radius of the outside layer of tape.

Table XII

Heating tape and tube dimensions

Tube diam. (mm)	Tape width (in.)	Tape area, A (cm^2)	L_h (cm)	$L_t+L_{s,t}$ (cm)	r (mm)	R (mm)	R_i (mm)	R_o (mm)
5	1/2	8118	1.37	1.25	1.75	2.50	2.85	3.65
5	1	144.3	2.32	1.10	1.75	2.50	2.85	3.75
10	1/2	80.0	1.37	1.23	4.00	5.00	5.45	6.70
10	1	144.3	2.32	1.20	4.00	5.00	6.60	7.55
20	1/2	81.8	1.37	1.70	8.75	10.00	11.00	12.60

By means of addition of resistances and conductances, h_z was found to be given by

$$h_z = \frac{1}{(1/h_t) + \frac{2(R_o - R_i)r_3}{k_g(R_o + R_i)} + \frac{2(R_i - R)\ r_3}{k_a(R_i + R)} + \frac{2(R-r)\ r_3}{k_g(R+r)}}$$

$$+ (0.173)\ \epsilon\ (R/r_3)\ \frac{(T_3/100)^4 - (T_m/100)^4}{(T_3 - T_m)}\ , \qquad (10)$$

where: R_o, R_i, R and r are the radii shown in in Fig. 42; k_a and k_g are the thermal conductivities for air and glass, respectively, and ϵ is the emissivity of the tube and its surroundings (about 0.9). The heat transferred to the zone, Q_{tot}, is given by

$$Q_{tot} = q_{total}\ (L_h/L_{h,zone}), \qquad (11)$$

where $L_{h,zone}$ is the length of heating tape directly adjacent to the zone (which equals L_h if no solid is directly beneath the tape).

Heat-Transfer Coefficients from Solid

For the solid within the surrounding heater tube, the heat-transfer coefficient from the surface was taken to be the same as that from the heater to the zone, since the conditions are nearly the same. The only difference is transfer from the tape to the heater tube in one case as compared with transfer from the tube to the surroundings in the other. Since all resistances are negligible compared to the air-gap resistance, these two resistances (tape-to-tube and tube-to-air) are likely to be close enough to make little difference in the over-all coefficient.

The heat-transfer from the surface of the container tube beyond the heater tube is by free convection and by radiation. For simplicity the correlations for free convection from a vertical plane are assumed

to apply.[92] The difficulty now is that this coefficient depends on the temperature difference, which, in this case, will vary greatly. It was necessary to correct for this variation by using a theoretical result by E. M. Sparrow for linear temperature variations.[93] The length parameter used in this correlation was that length along the tube over which the temperature variation deviated only 1% from being linear. To a first approximation this was equal to the zone length. The heat-transfer coefficient calculated in this manner was assumed to apply over the entire length of the tube.

Heat Transfer in Solid

In order to simplify the mathematics, assumptions c, d, e, and g must now be made. The assumption of axial heat conduction alone (d) is reasonable because of the insulating effect of the heating tube. For large tubes this assumption will break down, of course. The same statements can be made concerning the assumption of planar interfaces (c). The assumption of infinite tubes (e) is reasonable because the solid temperature drops off to very near the surrounding temperature at the tube ends. This was observed in runs with a thermocouple imbedded in the solid.

By using the foregoing assumptions, the differential equations governing heat transfer in the solid may be derived. For purposes of illustration, only the differential equation for heat transfer in the solid below the heater tube will be derived in detail. A heat balance over a differential element, as shown in Fig. 43, yeilds:

$$-k\left(\frac{dT}{dx}\right)_x \pi R^2 + V\rho c_p T_x \pi R^2 = h_b (T_x - T_b) 2\pi R \Delta x$$

$$\left(-k\left(\frac{dT}{dx}\right)_{x+\Delta x} \pi R^2 + V\rho c_p T_{x+\Delta x} \pi R^2 \right). \qquad (12)$$

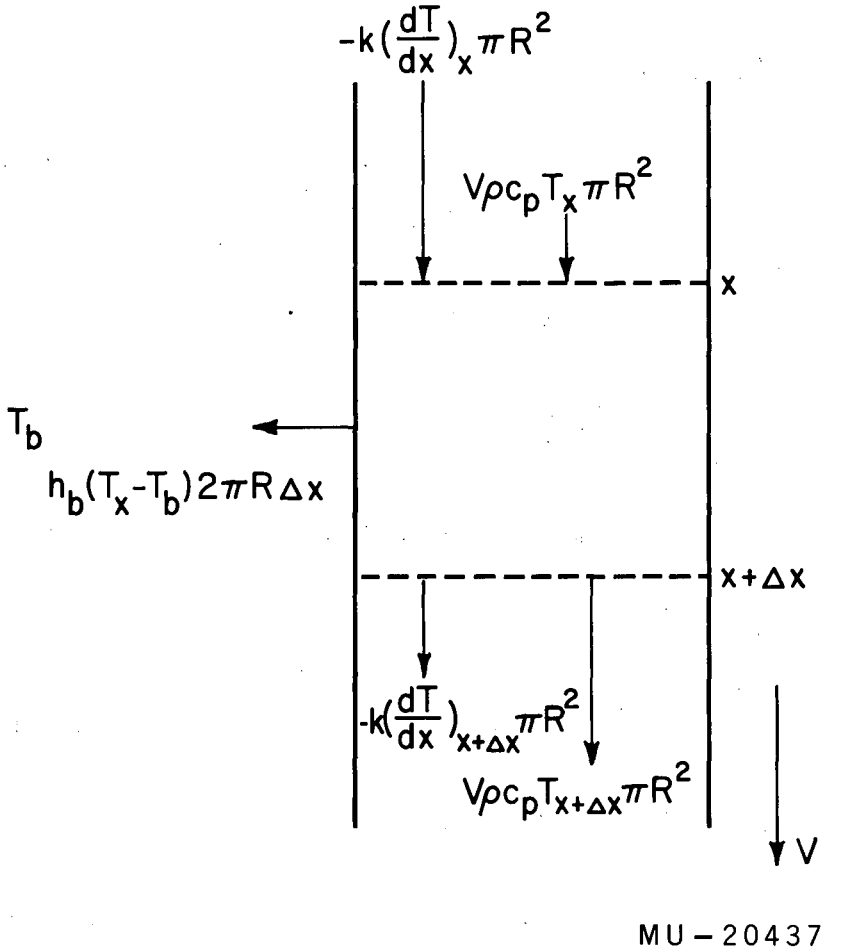

Fig. 43. Differential element of solid, showing heat fluxes.

Dividing through by $k\pi R^2 \Delta x$ and taking the limit as $\Delta x \longrightarrow 0$, we obtain the differential equation,

$$d^2T/dx^2 - \alpha_s \, dT/dx - \beta_b (T-T_b) = 0 \tag{13}$$

where $\alpha_s = V(\rho c_p/k)_{eff}$ and $\beta_b = 2 h_b/Rk_{eff}$. The general solution to this is:

$$T = T_b + C_3 \exp\left(\frac{\alpha_s + \sqrt{\alpha_s^2 + 4\beta_b}}{2} x\right) + C_4 \exp$$

$$\left(\frac{\alpha_s - \sqrt{\alpha_s^2 + 4\beta_b}}{2} x\right), \tag{14}$$

where C_3 and C_4 are constants to be determined from the boundary conditions.

The equations for heat transfer in the solid inside the heater tube are the same, except that h_b is replaced by h_c. For a solid that lies inside the heater itself, the differential equation is

$$d^2T/dx^2 - \alpha_s \, dT/dx + H = 0. \tag{15}$$

Where $H = q_{total}/L_h k_{eff} \pi R^2$, where q_{total} is the total rate of heat transfer from the tape to the tube (molten zone and solid), and L_H is the length of the heater (see Fig.42).
The general solution to this is

$$T = C_1 + C_2 \exp(\alpha_s x) + H x/\alpha_s, \tag{16}$$

where C_1 and C_2 are constants to be determined from the boundary conditions.

The equations for heat transfer above the heater tube are the same, except V is replaced by -V and h_b by h_t. If the tube is being pulled up instead of down, as has been supposed here, then V is replaced

by -V everywhere. It should be noted that the k_{eff} and $(\rho c_p/k)_{eff}$ used are area-weighted averages for the glass tube and the solid product.

The boundary conditions necessary for a complete solution are as follows:

(a) As $x \longrightarrow \infty$, $T \longrightarrow T_b$ (or T_T on top).

(b) Matching conditions where different solutions meet, i e.

$T_a(x) = T_b(x)$, or $dT_a(x)/dx = dT_b(x)/dx$,

where $T_a(x)$, $T_b(x)$ are different solutions that have to be the same where they meet.

(c) At $x = 0$, $T = T_m$, i e., at the interfaces the temperature is the melting point.

When the problem of heat transfer in the solid has thus been solved, the flux at the interface must be calculated. From the foregoing, T (x) is known. The heat transferred along the glass is given by

$$q_{glass} = -k_g \left(\frac{dT}{dx}\right)_0 \pi (R^2 - r^2). \qquad (17)$$

The heat transferred from the liquid into the lower interface (q_b) is derived from a heat balance at that interface, as shown in Fig. 44. It yields

$$q_b = \left[-k\left(\frac{dT}{dx}\right)_0 - V\rho\ \Delta H_f\right] \pi\ r^2\ , \qquad (18)$$

where ΔH_f is the latent heat of fusion (taken as positive for heat absorbed in melting or liberated in freezing).

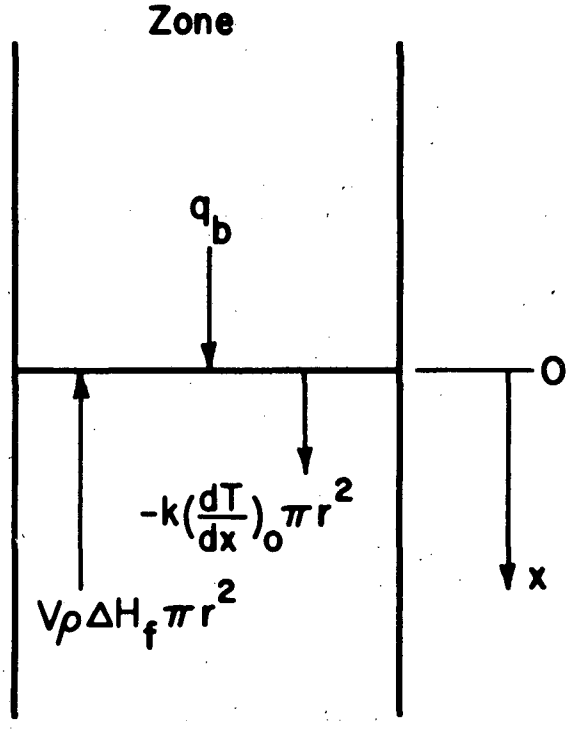

Fig. 44. Heat fluxes at the freezing interface.

Particular Solutions

1. When part of the solid is in the heater and part is outside the heater but still in the heater tube, the heat out of the bottom of the zone is given by

$$q_b = \pi r^2 \left[-k_s\left(\frac{H}{\alpha_s} + C_2\alpha_s\right) - V\rho_s\Delta H_f\right] \qquad (19)$$

where k_s is the thermal conductivity of the solid material,

$$c_2 = \left\{\left(da_5e^{-a_5L_b - H/\alpha_s}\right)\left(be^{-a_5L_b} + e^{-a_6L_b}\right) + \left(ba_5e^{-a_5L_b} + a_6e^{-a_6L_b}\right)\right.$$

$$\left.\left(T_m - T_c - de^{-a_5L_b - HL_b/\alpha_s}\right)\right\} \div \left\{\alpha_s e^{-\alpha_s L_b}\left(be^{-a_5L_b} + e^{-a_6L_b}\right) + \right.$$

$$\left.\left(1 - e^{-L_b\alpha_s}\right)\left(ba_5e^{-a_5L_b} + a_6e^{-a_6L_b}\right)\right\},$$

$$b = \left(\frac{a_4 - a_6}{a_5 - a_4}\right)\frac{\exp\left[a_6(L_{s,b} + L_b)\right]}{\exp\left[a_5(L_{s,b} + L_b)\right]},$$

$$d = \frac{a_4(T_c - T_b)}{(a_5 - a_4)\exp\left[a_5(L_{s,b} + L_b)\right]},$$

$$a_4 = \frac{\alpha_s\sqrt{\alpha_5^2 + 4\beta_b}}{2},$$

$$a_5 = \frac{\alpha_s + \sqrt{\alpha_s^2 + 4\beta_c}}{2},$$

$$a_6 = \frac{\alpha_s - \sqrt{\alpha_s^2 + 4\beta_c}}{2},$$

$$b_c = \frac{2h_z}{k_{eff}R}\left(\frac{r_3}{R}\right).$$

2. When no solid is inside the heater, but some is inside the heating tube, the heat out of the bottom of the zone is:

$$q_b = \pi r^2 \left[-k_s (C_5 a_5 + C_6 a_6) - V\rho\Delta H_f\right], \qquad (20)$$

where $C_5 = T_m - T_c - C_6$, a_4 and a_5 are as defined before, and

$$C_6 = \frac{(T_m - T_c)(a_5 - a_4)\exp(a_5 L_{s,b}) - a_4(T_c - T_b)}{(a_4 - a_6)\exp(a_6 L_{s,b}) + (a_5 - a_4)\exp(a_5 L_{s,b})} .$$

3. When no solid is inside the heating tube, the heat out of the bottom of the zone is

$$q_b = \pi r^2 \left[-k_s (T_m - T_b) a_4 - V\rho\Delta H_f\right] , \qquad (21)$$

where a_4 is as before.

Analogous expressions for the heat out of the top of the zone may be obtained by making the following substitutions in the above results:

$-V$ for V
q_t for q_b
h_T for h_b
T_T for T_b
L_t for L_b
$L_{s,t}$ for $L_{s,b}$

Heat-Balance Comparisons

By the methods described above, calculations were carried out for 41-zone melting runs, with the tube being pulled down. The crude data are shown in Tables XIII and XIV. These calculations are obviously very tedious and complicated, and involve trial-and-error calculations of h_T and h_b (since these are interdependent with the temperature profile).

Table XIII

Heat-transfer data for benzoic acid-naphthalene runs

Run no.	Nominal tube size (mm)	Nominal tape size (in.)	V (cm/hr)	Power input to tape (w/cm^2)	T_b (^oC)	T_t (^oC)	L_t (cm)	L (cm)
B-7	10	0.5	0.45	0.1281	20.0	34.6	0.40	1.90
B-7	10	0.5	0.00	0.1281	20.0	34.6	1.10	1.90
B-8	5	0.5	0.15	0.1090	20.0	34.6	0.95	2.78
B-10	5	0.5	0.15	0.1410	-9.1	18.0	0.60	2.10
B-11	5	0.5	0.15	0.1180	20.0	20.0	0.80	2.40
B-13	5	1.0	0.15	0.0949	20.0	20.0	0.96	3.31
B-15	5	1.0	0.225	0.0935	20.0	20.0	0.40	3.00
B-17	5	1.0	0.45	0.0935	20.0	20.0	0.50	3.10
B-18	10	0.5	1.35	0.1258	20.0	20.0	0.30	1.65
B-19	10	0.5	0.15	0.1552	-9.1	20.0	0.55	1.80
B-20	10	0.5	0.15	0.1590	-9.1	20.0	0.45	1.90
B-21	10	0.5	0.45	0.0986	59.4	23.0	1.00	2.70
B-22	10	0.5	0.15	0.0986	59.4	23.0	1.00	2.80
B-23	20	0.5	0.45	0.1230	59.4	22.0	1.70	3.90
B-25	10	0.5	0.45	0.1701	-11.0	20.0	0.85	2.05
B-26	10	1.0	0.15	0.1161	-11.0	20.0	0.90	2.90
B-27	20	0.5	0.45	0.2026	-11.0	20.0	0.85	2.20
B-28	5	0.5	0.45	0.1362	-11.0	20.0	0.40	1.70
B-29	5	0.5	0.15	0.1772	-11.0	20.0	1.00	2.80
B-30	5	0.5	0.45	0.0687	65.3	20.4	0.30	1.95
B-31	20	0.5	2.70	0.2040	20.0	20.0	1.60	4.20
B-32	20	0.5	0.45	0.2040	20.0	20.0	2.50	4.30
B-33	20	0.5	0.15	0.1361	20.0	20.0	0.20	1.30
B-34	10	1.0	1.35	0.1189	20.0	20.0	1.80	4.48
B-35	5	1.0	0.225	0.1169	20.0	20.0	1.70	4.25
B-36	5	0.5	0.00	0.0929	20.0	20.0	0.20	1.40

Table XIII (cont'd.)

Run no.	$Q_{tot,calc}$ (w)	$Q_{tot,corr}$ (w)	$(q_t+q_b)_{calc}$ (w)	$(q_t+q_b)_{corr}$ (w)	$(q_t)_{corr}$ (w)	$(q_{glass})_{corr}$ (w)
B-7	0.445	0.468	0.0559	0.0533	0.0355	0.124
B-7	0.309	0.454	0.0323	0.0245	0.0109	0.0571
B-8	0.248	0.358	0.0111	0.00852	0.00385	0.0367
B-10	0.251	0.354	0.0199	0.0155	0.00717	0.0666
B-11	0.244	0.341	0.0146	0.0113	0.00571	0.0489
B-13	0.319	0.368	0.0131	0.0116	0.00567	0.0499
B-15	0.309	0.312	0.0144	0.0143	0.00817	0.0615
B-17	0.309	0.329	0.0142	0.0134	0.00870	0.0578
B-18	0.364	0.398	0.0714	0.0658	0.0658	0.147
B-19	0.474	0.547	0.0660	0.0582	0.0286	0.136
B-20	0.544	0.580	0.0693	0.0653	0.0313	0.152
B-21	0.457	0.458	0.0315	0.0315	0.0315	0.0703
B-22	0.457	0.468	0.0289	0.0283	0.0227	0.0659
B-23	0.824	0.900	0.132	0.122	0.122	0.106
B-25	0.532	0.684	0.0624	0.0510	0.0310	0.119
B-26	0.302	0.366	0.0500	0.0425	0.0212	0.0990
B-27	1.10	1.11	0.205	0.202	0.143	0.257
B-28	0.220	0.258	0.0196	0.0171	0.00968	0.0737
B-29	0.397	0.589	0.0179	0.0135	0.00555	0.0582
B-30	0.144	0.156	0.00979	0.00905	0.00755	0.0390
B-31	1.29	1.79	0.455	0.356	0.356	0.180
B-32	1.29	1.65	0.154	0.127	0.112	0.161
B-33	0.482	0.525	0.188	0.174	0.110	0.221
B-34	0.497	0.558	0.0586	0.0528	0.0528	0.0872
B-35	0.480	0.612	0.0125	0.0103	0.00516	0.0443
B-36	0.125	0.136	0.0145	0.0134	0.00696	0.0580

Table XIV

Heat-transfer data for β-naphthol-naphthalene runs

Run no.	Nominal tube size (mm)	Nominal tape size (in)	V (cm/hr)	Power input to tape (w/cm^2)	T_b (^oC)	T_t (^oC)	L_t (cm)	L (cm)
N-31	10	0.5	0.15	0.1357	20.0	34.6	0.10	1.30
N-33	5	0.5	0.15	0.1204	20.0	20.0	0.58	1.60
N-35	5	1.0	0.15	0.1059	20.0	20.0	0.30	2.40
N-36	5	1.0	1.35	0.1059	20.0	20.0	0.60	2.80
N-37	10	0.5	1.35	0.1553	20.0	20.0	0.70	2.30
N-38	10	0.5	2.70	0.1453	20.0	20.0	0.20	1.75
N-39	10	0.5	2.70	0.1453	20.0	20.0	0.45	2.05
N-40	10	0.5	0.15	0.1614	-11.0	20.0	0.10	1.15
N-41	10	0.5	0.15	0.1232	59.4	25.4	1.40	2.95
N-42	10	0.5	0.45	0.1232	59.4	25.0	1.00	2.60
N-44	20	0.5	0.15	0.1810	20.0	20.0	1.30	2.70
N-45	20	0.5	0.45	0.1810	20.0	20.0	1.20	2.70
N-46	20	0.5	2.70	0.1809	20.0	20.0	0.25	2.65
N-47	5	0.5	0.15	0.0820	65.3	20.0	0.25	1.60
N-48	5	0.5	0.00	0.1170	20.0	20.0	0.40	1.60

Continued

Table XIV (Continued)

Run no.	$Q_{tot,calc}$ (w)	$Q_{tot,corr}$ (w)	$(q_t+q_b)_{calc}$ (w)	$(q_t+q_b)_{corr}$ (w)	$(q_t)_{corr}$ (w)	$(q_{glass})_{corr}$ (w)
N-31	0.344	0.326	0.0706	0.0748	0.0407	0.174
N-33	0.140	0.246	0.0171	0.0120	0.00694	0.0516
N-35	0.224	0.237	0.0191	0.0182	0.0105	0.0783
N-36	0.277	0.321	0.0176	0.0155	0.0140	0.0669
N-37	0.542	0.710	0.0707	0.0571	0.0571	0.130
N-38	0.477	0.513	0.112	0.105	0.105	0.161
N-39	0.477	0.618	0.112	0.0914	0.0914	0.141
N-40	0.345	0.353	0.0814	0.0796	0.0427	0.186
N-41	0.524	0.654	0.0424	0.0354	0.0238	0.0824
N-42	0.523	0.586	0.0439	0.0396	0.0341	0.0924
N-44	0.965	1.20	0.203	0.170	0.102	0.215
N-45	0.965	1.20	0.204	0.171	0.137	0.216
N-46	0.964	1.35	0.494	0.384	0.384	0.235
N-47	0.128	0.140	0.0143	0.0132	0.00817	0.0570
N-48	0.152	0.216	0.0186	0.0144	0.00738	0.0620

Consequently, the detailed calculations were actually carried out on an IBM-650 digital computer according to the following process:

1. Heat transfer from the heater to the tube was calculated by using Eqs. (8), (9), and (10).
2. The heat input to the zone (results tablulated in Tables XIII and XIV) was calculated by Eq. (11).
3. Heat-transfer coefficients (h_T and h_b) from solid to surroundings were assumed.
4. The temperature profile was calculated from these coefficients and the proper forms of Eqs. (14) and (15).
5. New heat-transfer coefficients were calculated from the results of step (4) and Sparrow's results.[93]
6. Steps (4) and (5) were repeated as often as necessary.
7. Heat fluxes out of the top and bottom of the zone were calculated from Eqs. (19), (20), or (21), whichever is applicable. Results are shown in Tables XIII and XIV.
8. Heat fluxes out of the glass were calculated from Eq. (17) and the previously calculated temperature profiles. The results are shown in Tables XIII and XIV.

The parameters of concern were varied over the following ranges:

T_m : 77 to 84 °C

V : 0 to 2.70 cm/hr

T_b : -11.0 to 65.3 °C

L_h : 1.37 to 2.32 cm

L : 1.30 to 4.48 cm

r : 1.75 to 8.75 mm.

The quality of heat balance obtained in this manner may be judged by comparison of the $Q_{tot,calc.}$ and $Q_{tot,corr.}$ columns in Tables XII and XIV. The first is the Q_{tot} as calculated by the above method. This is supposed to be equal to the sum of the other heat fluxes, as shown in Eq. (7). In general it was not, so it was modified by taking

the average between it and the heat flux sum. This is what is shown in the $Q_{tot,corr.}$ columns of Tables XII and XIV. It is seen that the heat-balance error is sometimes pretty high— an indication that some of the assumptions used may not be too good. For a first approximation, however, the calculation method described here should be quite useful— if for nothing other than an order-of-magnitude calculation of heat requirements. It is also seen that the sum of the calculated heat fluxes out of the zone was generally greater than the heat input to the zone, i.e. $Q_{tot,calc.} \leq Q_{tot,corr.}$. This is a strong indication that the values of h_T and h_b used were too high. Undoubtedly a better estimate of h_T and h_b would have been obtained if a larger length of solid had been considered in conjunction with Sparrow's[93] results. (Free-convection heat-transfer coefficients increase as the length of the transfer surface decreases.[92] See Illustrative Problem in Section VE for further details.)

C. Position of Zone

Now that the size of the zone can be calculated, where will it be with respect to the heater? In general, because free convection carries heat up, more of the zone will be above the heater than below it. In an attempt to answer this question quantitatively and develop a method for prediction purposes, several correlations were tried, using the data just calculated on the 41 vertical zone-melting runs. What is desired is the distance from the center of the portion of the heater adjacent to the zone to the top of the zone, L_{ch}. Intuitively, the following factors might be thought to influence the zone's position for the present systems:* rate of zone travel, size of heater, size of tube, size of zone, and the various heat fluxes. Because of the interrelation of the various heat fluxes, as given in Eq. (7), one of the heat fluxes

---

*Obviously the effects of various physical properties could not be investigated, since they were not varied appreciably in these experiments.

is not independent. In addition, the flux of heat from the zone to the surroundings depends strongly on the size of the zone, and only slightly on its position. Consequently, this flux, and likewise the flux of heat conducted out the ends of the zone in the glass, were not considered further. The effect of the remaining variables could only be determined by an analysis of variance. Therefore, the constants in various forms of correlations utilizing these parameters were determined by means of a multiple linear-regression routine on the IBM-650 digital computer. Some of the resulting correlations are:

$$1.\ L_{ch} = -1.657 + 0.379\ Q_{tot} + 1.644\ (q_t + q_b) - 5.569\ q_t$$

$$-0.1274\ L_h + 0.00369r + 0.682L + 0.0321\ V_\ell, \qquad (22)$$

where Q_{tot}, $(q_t + q_b)$, q_t are in watts, and L_h, L, r are in centimeters. The average error is 5.4%, the maximum error 13.7%.

$$2.\ L_{ch} = 0.469 \left[\frac{Q_{tot}^{0.216}\ q_t^{0.0190} L_h^{0.159}\ r^{0.381}\ L^{0.772}}{(q_t + q_b)^{0.310}\ V_\ell^{0.0283}} \right] \qquad (23)$$

Here the average error is 7.08%, and the maximum error is 44.7%.

$$3.\ \left(\frac{L_{ch}}{L}\right)\ \frac{L}{r}\left[\frac{(q_t + q_b)}{Q_{tot}}\right]^{1/4} = -0.0284 + 0.699\ \exp\ (-q_t/Q_{tot})$$

$$-0.146\ \exp\left[-q_t/(q_t+q_b)\right] - 0.103\ \exp\ (-10r/L)$$

$$-0.0154\ \exp(-L_h/L) \qquad (24)$$

The average error is 12.5%; the maximum error, 26.4%.

$$4.\left(\frac{L_{ch}}{L}\right) = -0.01355 + 0.5395\left[\frac{r}{L}\,\frac{Q_{tot}}{(q_t+q_b)}\right]^{1/4} \qquad (25)$$

The average error is 7.9%, the maximum error, 55%.

By inspection of the various coefficients and exponents in the foregoing correlations, it is seen that the velocity of zone travel and length of the heater do not significantly affect the position of the zone. Certainly at high zone-travel rates, the zone will be shifted in the direction of zone travel, and this will not be true. In this work, then, apparently the zone-travel rates were small enough so that the latent-heat liberation and absorption rates were negligible with respect to the other heat flows. The best correlation among the foregoing is believed to be No. 4, because of its simplicity and the fact that it includes only the significant variables. The average error (7.9%) is not significantly greater than that of the much more complicated expressions, No. 1 (5.4%), and No. 2 (7.1%). The appearance of the 1/4 power is most curious, especially since a 1/4 power often appears in free-convection heat-transfer correlations.[94] At present no explanation of this correlation is known. An interpretation of the terms involved proves interesting, however. The fraction of the zone above the center of the heating tape adjacent to the zone is (L_{ch}/L), and $\left[r\ Q_{tot}/4L(q_t+q_b)\right]$ is the ratio of heater input per unit area of tube around the zone to the heat per unit area removed to the solid at both ends of the zone. Note also that from both correlations 1 and 2, V_ℓ has very little influence. This is because the velocity of zone travel is small, i e. the heat carried by free convection in the zone is much larger than that carried by bulk movement of material through the zone.

The absence of a q_t term in correlation 4 incidates that the rate latent heat liberation and absorption is negligible in comparison to the conduction and convection heat fluxes. At higher zone-travel rates, this would not be true.

The 1/4 power in correlation 4 actually dropped out of a linear regression of (L_{ch}/L) vs $\left[rQ_{tot}/L(q_t + q_b)\right]$. The exact power obtained in this manner was 0.2575. The value of $\left[rQ_{tot}/L(q_t + q_b\right]$ varried from 0.985 to 1.406. The 75% confidence limits in the constants of correlation 4 are: $- 0.01355 \pm 0.13174$, and 0.5395 ± 0.1138.

Plots of $(L_{ch})_{calc.}$ vs $(L_{ch})_{expt}$ obtained by using correlation 4 are shown in Fig. 45, 46, and 47. These serve to demonstrate that apparently no systematic error exists in the correlation. Of the points, 95.1% have an error less than 20%, 83% less than 10%, and 41.4% less than 5%.

When the zone lies within the heater, these correlations all break down, as in this case where $L_{ch} = 0.5L$ exactly, by definition. Correlation (4) can also be expected to break down for high zone-travel rates, as the travel rate does not appear in it, and at high travel rates the zone will certainly be shifted some in the direction of zone travel.

D. Horizontal Runs

Although heat-transfer data were not calculated for horizontal zone melting, the same principles as enunciated here could be applied. The zone size could be calculated by a heat balance. For slow enough travel rates, the zone would be of equal size on both sides of the tube. In some cases, however, the same effect of free convection that tended to make the portion of zone above the heater larger than that below it in vertical runs will tend to make the zone spread at the top in horizontal runs.

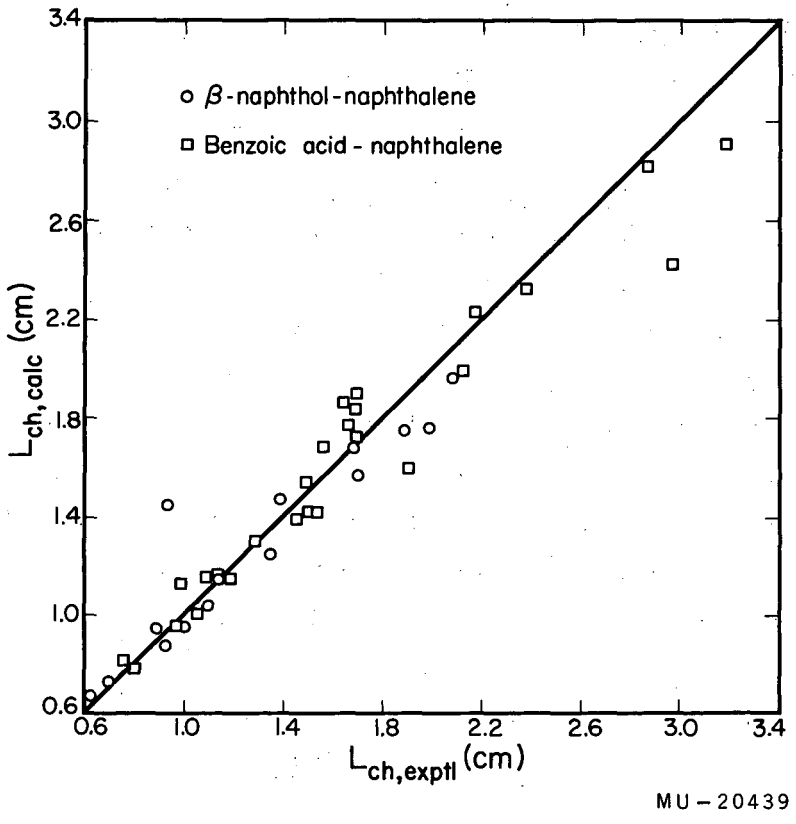

Fig. 45. Comparison of calculated (Eq. 25) with experimental zone locations for vertical zone melting.

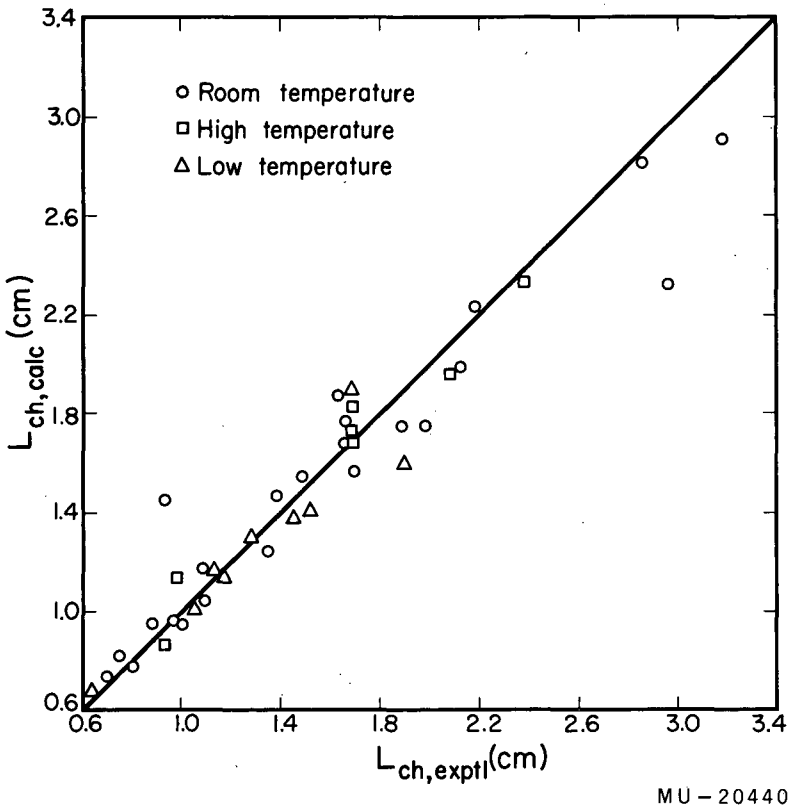

Fig. 46. Comparison of calculated (Eq. 25) with experimental zone locations for vertical zone melting.

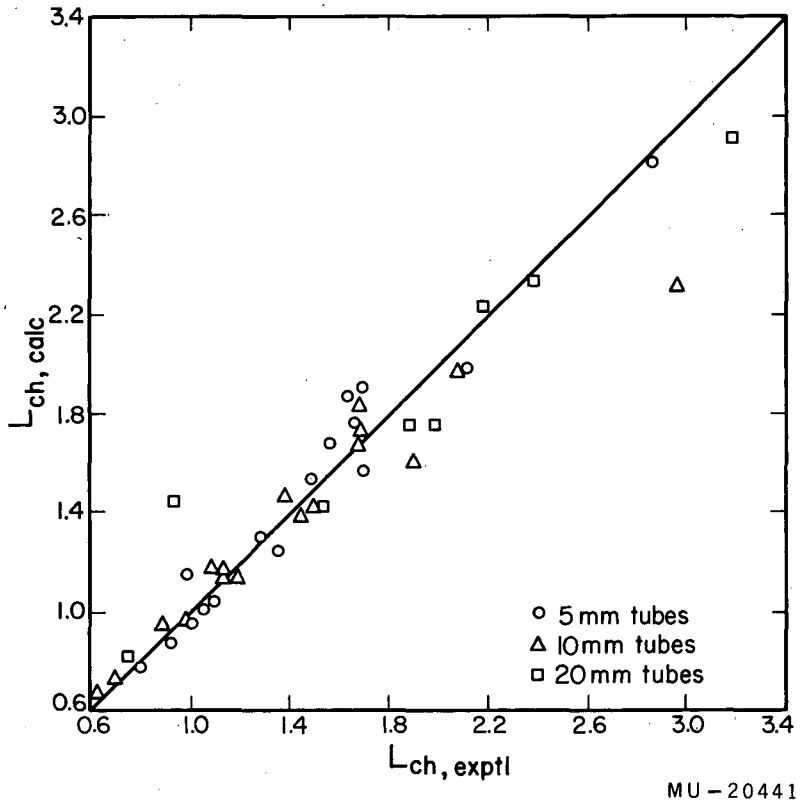

Fig. 47. Comparison of calculated (Eq. 25) with experimental zone locations for vertical zone melting.

E. Design

Recommended Procedure

Based on the foregoing considerations, the following step-by-step procedure is recommended for design of zone melters. It is assumed that the velocity of zone travel, size of tube, zone size, type of heater and cooler, etc., have been fixed either by mass transfer considerations (See Chapter VII) or practical design considerations. The procedure consists of five basic steps:

(a) Based on the design factors cited above, calculate the heat flows out both sides of the zone. Assume the zone is located equally on both sides of the heater.

(b) Add these heat losses which are equal to the difference in heater input to the zone and heat loss from the zone to the surroundings. The size of the heater determines the area available for heat loss to the surroundings, and therefore the necessary heater input to the zone.

(c) If the tube is vertical, use correlation (4) to calculate the position of the zone relative to the heater. If the position is horizontal, assume no change in position.

(d) If a new zone position affects heat fluxes, recalculate them.

(e) Based on the heater design, calculate the fraction of heater power that is absorbed by the zone. Using this and necessary heat input to the zone, calculate the total necessary heater power.

This design procedure is of general applicability, although the specific equations used here are subject to the following restrictions:

(a) The zone length must be of the same order of magnitude as the diameter of the tube or larger.

(b) The thermal conductivity of the tube must be of the same order of magnitude as the material being refined.

(c) The heater must be shorter than the zone (this is important for the calculation of zone location, but not for the heat balance, although having a larger heater will complicate the heat-balance calculations).

(d) The length of the solid on both sides of the zone must be much larger than the diameter of the tube (over about five tube diameters).

Illustrative Problem

In order to demonstrate the foregoing principles and results, the following simple problem will be solved:

> Calculate the heater input and zone position necessary to maintain a stationary 3-cm zone of naphthalene in a vertical 1-cm glass tube, using a 1-cm-long heater. The heater makes close contact with the tube and is well-insulated so that it loses only 25% of the total heat input to the surroundings. The tube is surrounded by stagnant air at $0^{\circ}C$.

Offhand, the fluxes should be an order of magnitude higher than the ones obtained in this work, because of the absence of the insulating heater tube and the much lower temperature of the surroundings.

The temperature profile for the solid is given by:

$$T = T_b + (T_m - T_b) \exp(-\sqrt{\beta_b}\, x)$$

$$= T_b + (T_m - T_b)(1 - \sqrt{\beta_b}\, x + 1/2\, \beta_b x^2 - \text{------}) \qquad (25)$$

where x is the distance into the solid from the solid-liquid interfaces, T_b is the temperature of the surroundings, and all other parameters are as before.

Therefore, the heat fluxes out of the ends of the zone are:

$$(q_b + q_t + q_{glass}) = -2 k_{eff}(dT/dx)_{x=0} \pi R^2$$

$$= 2 k_{eff} \sqrt{\beta_b} (T_m - T_b) \pi R^2 \qquad (27)$$

But, according to Sparrow*,[93] h_b is given by:

$$h_b = \frac{0.67 h_0 (T - T_b)_x}{(T - T_b)_{x/2}} + \frac{0.33 h_0 (T_m - T_b)}{(T - T_b)_{x/2}} \qquad (28)$$

where h_b is an average heat-transfer coefficient between 0 and x (assuming T is linear in x), h_0 is the heat-transfer coefficient that would be found if T equalled T_m over the entire interval (See McAdams[92]). It is seen, from Eq. (25) that the temperature profile is linear in this case as long as the following is true:

$$x \ll \frac{2}{\sqrt{\beta_b}} .$$

If, in order to obtain a numerical result, the profile can be allowed to depart slightly from linear, then x may be taken as, for example:

$$x = 1/\sqrt{\beta_b}$$

This calculation, then, is one necessitating successive approximations with initial assumptions for x, $(T-T_b)_x$, $(T-T_b)_{x/2}$. The calculations for this problem are summarized in Table XV. The value of k_{eff} is 0.00605 $w/cm^2(^oC/cm)$;[58,70] T_m is 80°C, and T_b is 0°C.

---

*This ignores radiation, i e. it is for free convection only. In the heat balances performed on the experimental data, radiation was considered, but its inclusion here would only complicate the calculations and not serve to illustrate a new point.

Table XV

Calculation of temperature profiles by successive approximations

x (cm)	h_o (w/cm ^oC)	$(T-T_b)_x$ (^oC)	$(T-T_b)_{x/2}$ (^oC)	h_b (w/cm ^oC)	β_b ($1/cm^2$)
2	0.00216	80	80	0.00216	1.43
0.838	0.00256	29.5	48.5	0.00248	1.63
0.795	0.00259	28.7	48.1	0.00244	1.62

Therefore, the heat losses out of the zone's ends are

$$(q_b+q_t+q_{glass}) = 2(0.00605)(1.62)^{1/2}(80)(0.5)^2 = 0.97 \text{ w.}$$

The value for the heat-transfer coefficient from the zone to the surroundings will be composed of the resistance due to free convection from the glass surface and to conduction through the glass tube (ignoring radiation, which would actually be appreciable here):

$$h_z = \frac{1}{\frac{1}{h_o} + \frac{2(R-r)R}{(R+r)k_g}} = \frac{1}{\frac{1}{0.00259} + \frac{2(0.1)(0.5)}{(0.9)(0.0116)}}$$

$$= 0.00253 \text{ w/cm}^2\ ^oC. \qquad (29)$$

Therefore, the heat transferred radially from zone to surroundings is

$$Q_{waste} = h_z(L-L_h)2\pi R(T_m-T_h) \qquad (30)$$

$$= (0.00253)(2)(2\pi)(0.5)(80) = 1.27 \text{ w,}$$

and so the heater input to the tube is

$$Q_{tot} = Q_{waste} + q_t+q_b+q_{glass} = 2.24 \text{ w.} \qquad (7)$$

Including the 25% loss to the surroundings, then, 2.99 w must be generated in the heater to maintain this zone. Likewise, the position of the zone is given by Eq. (24) as

$$L_{ch} = \left\{ - 0.0136 + 0.54 \left[(0.4)(2.99)/(3)(0.302) \right]^{1/4} \right\} 3$$

$$= 1.78 \text{ cm}$$

which means that about 1.28 cm of zone will be above the heater and 0.72 cm below.

VI. THEORETICAL DEVELOPMENTS FOR MASS TRANSFER IN ZONE MELTING

A. Introduction

In the introductory chapter to this work, it was noted that several mechanisms may account for dependence of separation on rate of solidification. The case of incomplete mixing in the liquid will be examined in this chapter. The differential equations and boundary conditions are derived for pure diffusional mass transfer in zone melting.* These were solved both for constant distribution coefficient and for eutectic-forming systems. In addition, solutions were derived for diffusion in a thin boundary layer with complete mixing in the bulk liquid.

B. Derivation of the Differential Equation and Boundary Conditions

The most convenient coordinate system for analysis of this problem is one in which the position of the zone is fixed and material flows through it. This is illustrated in Fig. 48.

The interface at which crystallization is taking place is chosen as the origin. The interfaces are assumed planar and the cross-section uniform, so that the problem becomes a one-dimensional one. Furthermore, the density and diffusivity are assumed to be independent of concentration and temperature, although the density may be different in the solid and liquid. The diffusivity in the solid, of course, is assumed to be negligible. With these assumptions, the fluxes in and out of a cross-sectional element of the zone are shown in Fig. 49.

A material balance over this element of the zone yields:

$$DA\rho_{\ell}\left[\left(\frac{\partial w}{\partial x}\right)_{x+\Delta x} - \left(\frac{\partial w}{\partial x}\right)_{x}\right] + G(w_{x+\Delta x} - w_{x}) = A\rho_{\ell}\left(\frac{\partial w}{\partial t}\right)\Delta x, \qquad (31)$$

*Many of the equations are valid, however, for other methods of fractional crystallization from melts.

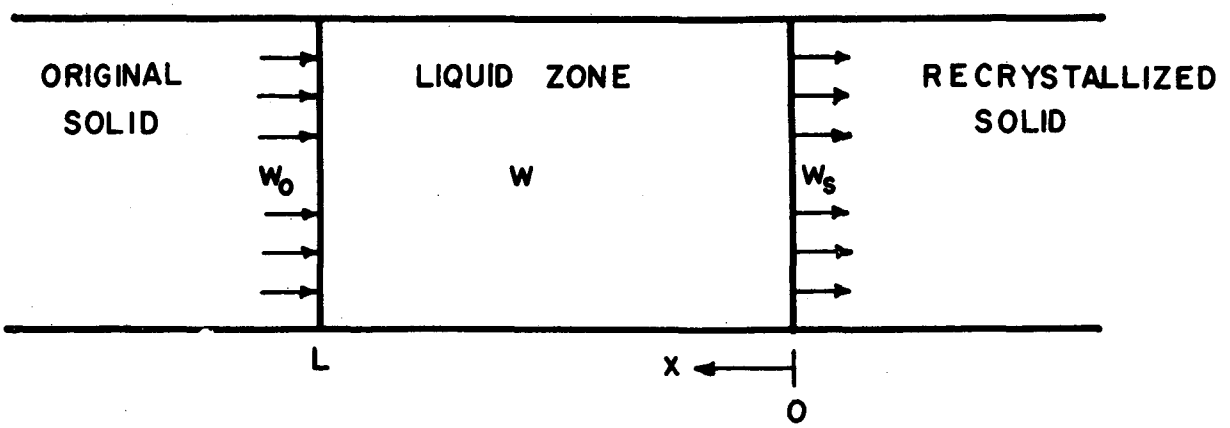

Fig. 48. Concentrations (in weight fractions) and coordinate system for zone-melting mass-transfer theory.

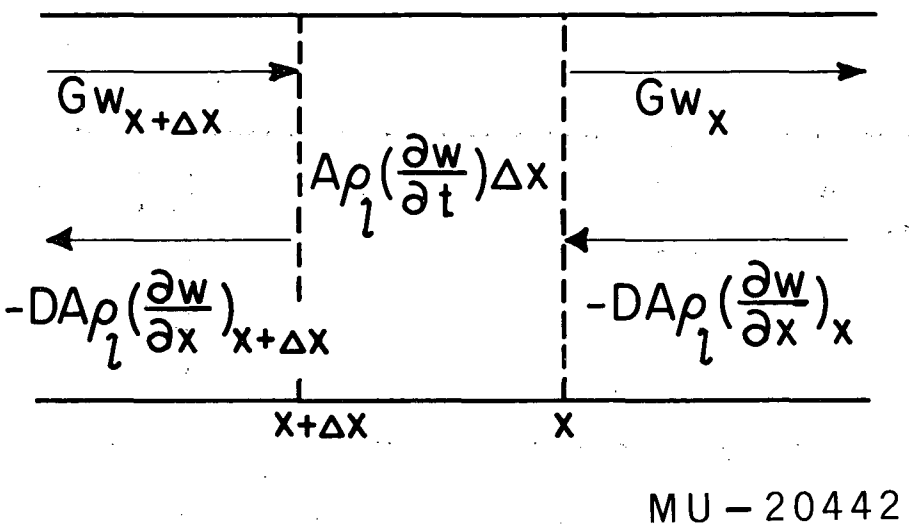

Fig. 49. Differential element of zone showing material fluxes in pure diffusional mass transfer.

where D is the diffusivity, A is the cross-sectional area, ρ_ℓ is the density of the liquid, w is the weight fraction of the component, G is the mass rate of flow, t is the time, Δx is the elemental distance along the zone, and x is the distance from the freezing interface into the zone.

By dividing Eq. (31) by Δx and taking the limit as Δx goes to zero, the following results:

$$DA\rho_\ell \frac{\partial^2 w}{\partial x^2} + G \frac{\partial w}{\partial x} = A\rho_\ell \frac{\partial w}{\partial t} . \tag{32}$$

Now let $\eta = xG/DA\rho_\ell$, $\phi = w/w_0$, and $\tau = (t/D)(G/A\rho_\ell)^2$, where w_0 is the initial concentration in weight fraction. Substituting these in Eq. (32) there is obtained:

$$\frac{\partial^2 \phi}{\partial \eta^2} + \frac{\partial \phi}{\partial \eta} = \frac{\partial \phi}{\partial \tau} . \tag{33}$$

which is the desired differential equation governing diffusive mass transfer in zone melting.

Boundary Conditions

Figures 50 and 51 show the fluxes at the freezing and melting interfaces of the zone. Making mass balances at the interfaces, there is obtained:

$$- D\rho_\ell A \frac{dw}{dx} = G(w-w_s) \tag{34}$$

at x = 0, and

$$- D\rho_\ell A \frac{dw}{dx} = G(w-w_0) \tag{35}$$

at x = L, where w_s is the weight percent of the component in the recrystallized material at the interface. Note that no assumption as to the relationship between w_s and w at x = 0 has been made yet. Also note that w does not necessarily equal w_0 at x = L, the melting interface.

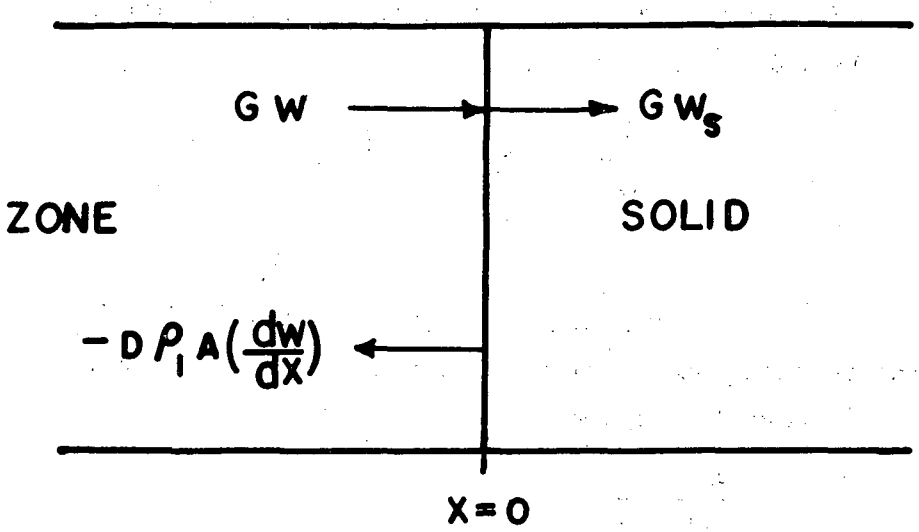

Fig. 50. Freezing interface showing material fluxes in pure diffusional mass transfer.

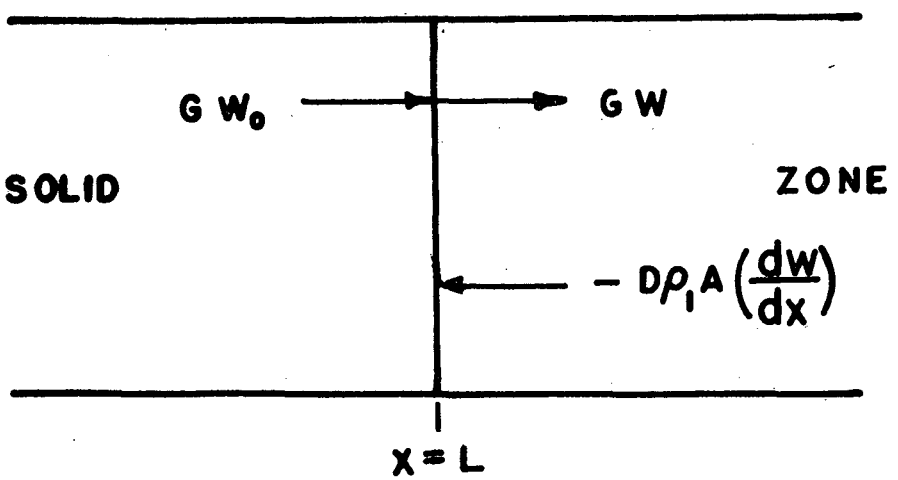

Fig. 51. Melting interface showing material fluxes in pure diffusional mass transfer.

Now again make the substitutions for η, ϕ and τ and let $p = LG/DA\rho_{\ell}$, and $\phi_s = w_s/w_0$.

Then there results:

$$\frac{d\phi}{d\eta} = \phi_s - \phi \tag{36}$$

at $\eta = 0$, and

$$\frac{d\phi}{d\eta} = 1 - \phi \tag{37}$$

at $\eta = p$.

In addition, there is the condition that the initial concentration in the zone is the same as the over-all initial solid concentration, or, at $\tau = 0$,

$$\phi = 1. \tag{38}$$

Eqs. (36), (37), and (38) are thus the general boundary conditions for diffusion in zone melting.

Constant-Distribution Coefficient

It is the usual assumption in zone-melting theory that the solid concentration is always proportional to the liquid concentration when solid and liquid are in equilibrium. It is further assumed that equilibrium is attained at the freezing interface. Thus at $x = 0$, $w_s = kw$ holds, where k is the distribution coefficient. Therefore Eq. (36) becomes

$$\frac{d\phi}{d\eta} = \phi(k-1) \tag{39}$$

at $\eta = 0$. Eqs. (33), (37), and (38) remain unchanged.

Eutectic-Forming Systems

Before investigating the proper boundary conditions for the zone melting of a binary mixture that forms a simple eutectic, a deep look will be taken into what a eutectic is and how it crystallizes physically. For this purpose, refer to Fig. 52, which is a schematic phase diagram for this type of system. The eutectic point e is usually taken to be the point at which solid and liquid in equilibrium have the same composition.

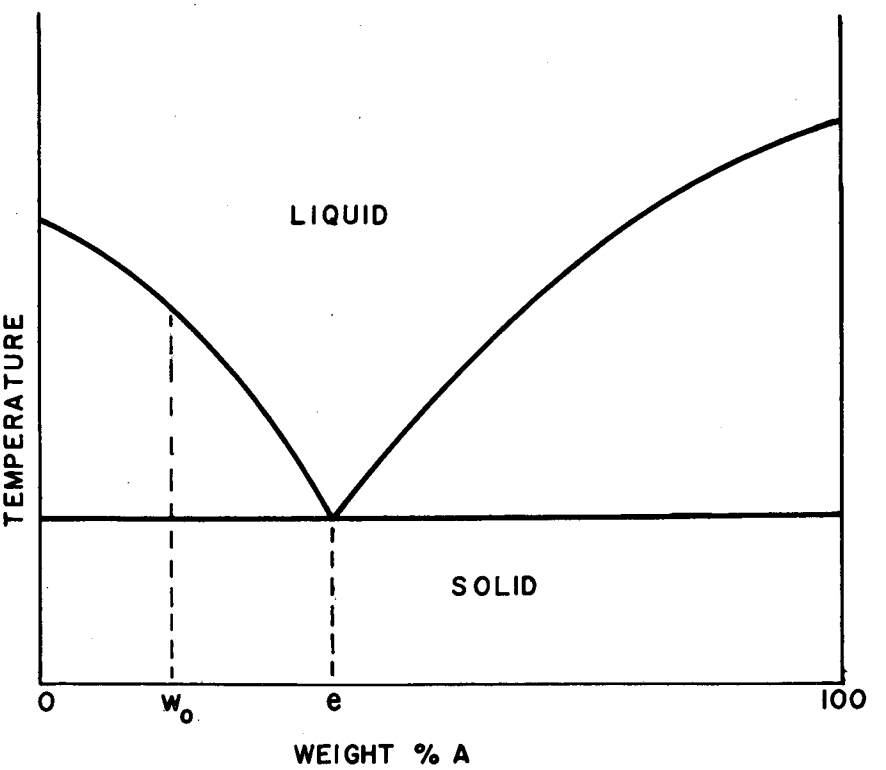

Fig. 52. Schematic solid-liquid phase diagram for systems forming simple eutectics, showing original weight fraction, w_o, and eutectic weight fraction, e.

Compounds which form a eutectic do so because their basic crystal structure is sufficiently different that molecules of one cannot fit into a crystal of the other. In other words a eutectic mixture of the two is not really a homogeneous mixture, but instead consists of microscopic crystals of the separate components.[95,96]

But what happens when a liquid mixture of eutectic composition e begins to crystallize? For some reason (e.g. a statistical fluctuation in concentration, or perhaps the greater tendency of one component to nucleate) a microscopic crystal of one component will form first. This, however, depletes the surrounding melt in that component. The melt, now being rich in the other component, will then yield a microscopic crystal of it. This in turn makes the surrounding melt richer in the first component, and so the process repeats. Thus it is seen that on the microscopic scale this type of crystallization is not a continuous and smooth process, but actually a cyclic one. Note that the concentration fluctuations in the melt are unobservably minute and extend only an extremely short distance into the melt that surrounds the growing solid.

We are now ready to investigate what happens when a eutectic-forming mixture is subjected to zone melting. Referring again to the schematic phase diagram, let us suppose that the initial composition is w_0. If equilibrium is attained at the freezing interface, the first solid to come out will be pure B (0%A). This will cause the liquid to become richer in A. Thus while pure B comes out, the liquid composition moves towards the eutectic composition e. What happens when the liquid composition at the freezing interface reaches e? It might be expected that now the solid will come out at composition e, and that this is the steady-state condition. This, however, would mean that material of composition w_0 was being fed into the zone and material of composition e was being removed. This is plainly impossible for a steady-state condition. What must really happen is that when the liquid at the interface first exceeds e a small amount of pure A comes out. When this happens, however, the liquid composition moves slightly below e, and so pure B comes out. Again the cyclic crystallization process occurs. The difference here is that there is a convective flux of material to the

interface and a diffusive flux away. The balance between these two regulates the relative amounts of A and B that come out. In the steady state, the average concentration coming out must be w_0.

The foregoing discussion necessitates a revision of the meaning customarily attached to the eutectic point of the phase diagram. Since liquid at the eutectic composition can yield solid of virtually any overall average composition, the eutectic point e on the diagram must not indicate a point at which a solid and liquid in equilibrium must have the same composition. Instead it is a point above which pure A comes out and below which material without A comes out.

The boundary conditions for the zone melting of a system of this type can now be stated. At $\eta = 0$ the average conditions are obviously

$$\frac{d\phi}{d\eta} = -\phi \tag{40a}$$

and

$$\phi_s = 0 \tag{40b}$$

for $\phi < e/w_\theta$, and

$$\frac{d\phi}{d\eta} = \phi_s - \frac{e}{w_\theta} \tag{40c}$$

for $\phi = e/w_\theta$.

This means that until ϕ at $\eta = 0$ reaches e/w_θ, ϕ_s is zero and ϕ is calculated from Eq. (40a). When ϕ reaches e/w_θ it remains there (on the average) and the average ϕ_s is given by Eq. (40c).

The other boundary conditions are the same as for constant distribution coefficients, namely Eq. (37) and (38).

C. Solutions for Pure Diffusional Mass Transfer

Steady-state

At steady state, the differential Eq. (33) becomes

$$\frac{d^3\phi}{d\eta^2} + \frac{d\phi}{d\eta} = 0 \tag{41}$$

The general solution to this is

$$\phi = a + be^{-\eta}, \tag{42}$$

where a and b are constants. For a constant distribution coefficient, the boundary conditions, Eqs. (34) and (37), yield

$$-b = (a+b)(k-1)$$

at $\eta \neq 0$, and

$$-be^{-p} = 1-a - be^{-p}$$

at $\eta = p$, from which there is obtained: $a=1$ and $b=(1-k)/k$. Therefore the steady-state solution is:

$$\phi = 1 + \frac{1-k}{k} e^{-\eta}. \tag{43}$$

As a check, note that at steady state, ϕ should equal $1/k$ at $\eta = 0$. At $\eta = 0$, Eq. (43) gives $\phi = 1 - (1-k)/k = (k+1-k)/k = 1/k$, and so it checks.

For eutectic-forming systems, the steady-state solution is found in a like manner. It is

$$\phi = 1 - \left(\frac{e}{w_0} - 1\right) e^{-\eta}. \tag{44}$$

There are several things to be noted from these solutions.

(a) Eq. (43) is the same for a variable distribution coefficient, provided that the k for $w_s = w_0$ is used.

(b) The concentration profile in the zone does not depend on the size of the zone at steady state.

(c) The concentration w at the melting interface does not equal w_0, although it approaches w_0 as the size of the zone increases.

Computer Solutions for Unsteady State

The unsteady-state problem may be solved analytically only for a constant distribution coefficient (see following section). In order to solve the problem for a eutectic-forming system, an IBM-650 electronic computer was used. The problem was solved on the computer for constant-distribution coefficient as a check (by comparison with the exact

analytical solution). The problem for constant distribution coefficient was also solved in this manner by Landau for normal freezing.[46]

The finite difference equation corresponding to the differential Eq. (33) is

$$\phi_{\eta,\tau+\Delta\tau} = \frac{\Delta\tau}{(\Delta\eta)^2}\left[\phi_{\eta+\Delta\eta,\tau}\,(1+\Delta\eta) + \phi_{\eta,\tau}\,(-2-\Delta\eta+\frac{(\Delta\eta)^2}{\Delta\tau}) + \phi_{\eta-\Delta\eta,\tau}\right], \tag{45}$$

where $\phi_{\eta,\tau}$ equals ϕ at any particular η and τ, $\Delta\tau$ is the size of the interval of τ, and $\Delta\eta$ is the size of the interval of η.

For simplicity, let

$$-2-\Delta\eta+\frac{(\Delta\eta)^2}{\Delta\tau} = 0.$$

Then Eq. (45) becomes

$$\phi_{\eta,\tau+\Delta\tau} = \frac{1}{2+\Delta\eta}\left[\phi_{\eta+\Delta\eta,\tau}(1+\Delta\eta) + \phi_{\eta-\Delta\eta,\tau}\right] \tag{46}$$

The boundary conditions result in a similar manner. For constant distribution coefficient they are

$$\phi_{0,\tau} = \frac{\phi_{\Delta\eta,\tau}}{1+(k-1)\Delta\eta} \tag{47}$$

at $\eta = 0$, and

$$\phi_{p,\tau} = \frac{\phi_{p-\Delta\eta,\tau} + \Delta\eta}{1+\Delta\eta} \tag{48}$$

at $\eta = p$.

Thus in the actual solution ϕ was initially set equal to one over the whole interval of the zone. The $\phi_{\eta,\tau}$ were all calculated by Eq. (46) except for the end points, which were found from Eqs. (47) and (48). This process was repeated over and over until a sufficient amount of τ had been covered. The value of ϕ_s was calculated from the fact that $\phi_s = k\,\phi_{0,\tau}$ at any particular τ.

These calculations were made for k from 0.1 to 5 and for p from 0.1 to ∞. In general $\Delta\eta$ had to be approximately 0.05, since solutions for smaller $\Delta\eta$ were the same, but for larger $\Delta\eta$ were different.

A correct solution to any mass-transfer problem must satisfy an over-all material balance. For the case of zone melting, this means that the total amount of material added to (or taken from) the zone must equal the total amount of material taken from (or added to) the recrystallized solid. At the steady state, this is expressed by the condition

$$\int_0^p (1-\phi)d\eta = \int_0^\infty (\phi_s-1)\, d\tau \tag{49}$$

It was found that the computer results of the previous paragraph for a constant distribution coefficient did not satisfy this condition. Because the cause of the error was suspected to be the assumption of a linear concentration profile at the freezing interface, a cubic equation was tried instead. This yielded results that satisfy Eq. (49) and compare closely with the analytical results.

In a like manner numerical solutions were made for eutectic-forming systems. A typical result is shown in Fig. 53. The curved portion of the plot was found to be exponential, as shown in Fig. 54.

The computer solution for eutectic-forming systems were found to satisfy the over-all material balance very well. Using this fact and several observations from the computer results, we can now summarize the results very completely and in a convenient form.

It has been found that after $\phi = e/w_0 = \epsilon$ is obtained at the freezing interface, the following is approximately true

$$(\phi-1) = (\epsilon-1)\, e^{-r\eta}, \tag{50}$$

where $r = r(\tau)$. Noting from the boundary condition at $\eta = 0$ that

$$\frac{d\phi}{d\eta} = \phi_s - \epsilon, \tag{51}$$

there results:

$$\phi_s = -r(\epsilon-1) + \epsilon. \tag{52}$$

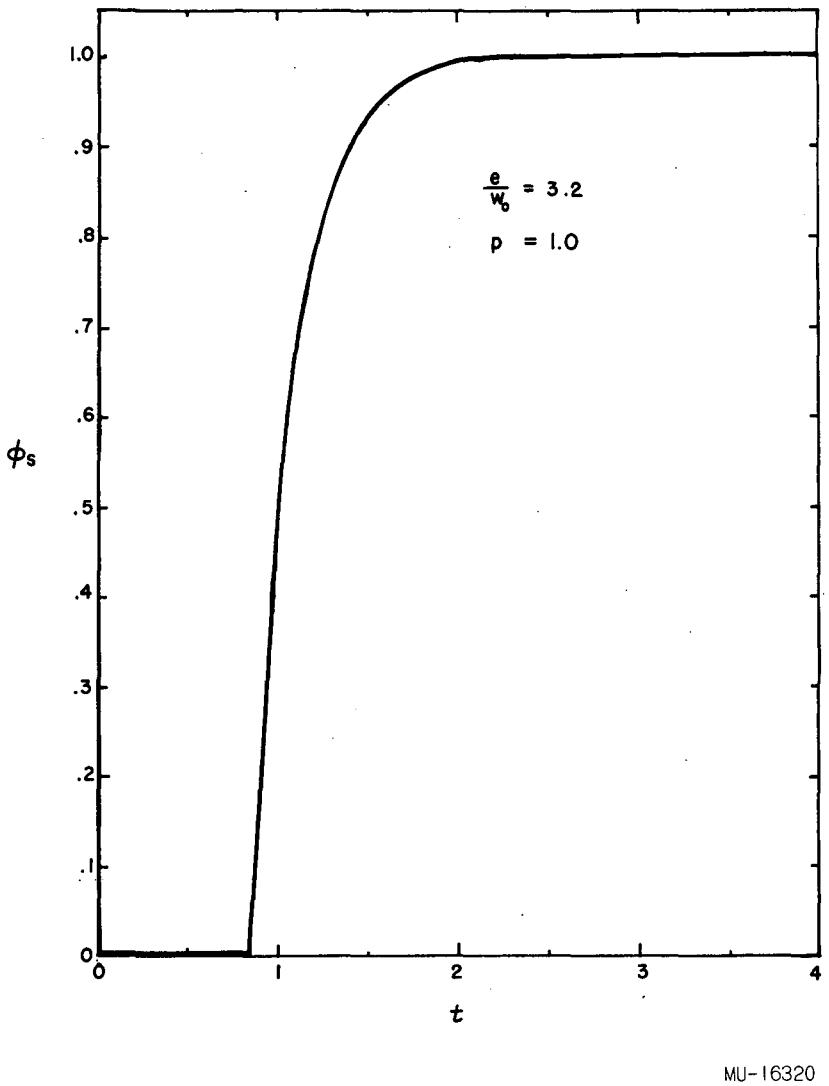

Fig. 53. Sample finite-difference solution for pure diffusional mass transfer in zone melting of eutectic formers.
ϕ_s vs τ for ϵ = 3.2 and p = 1.0.

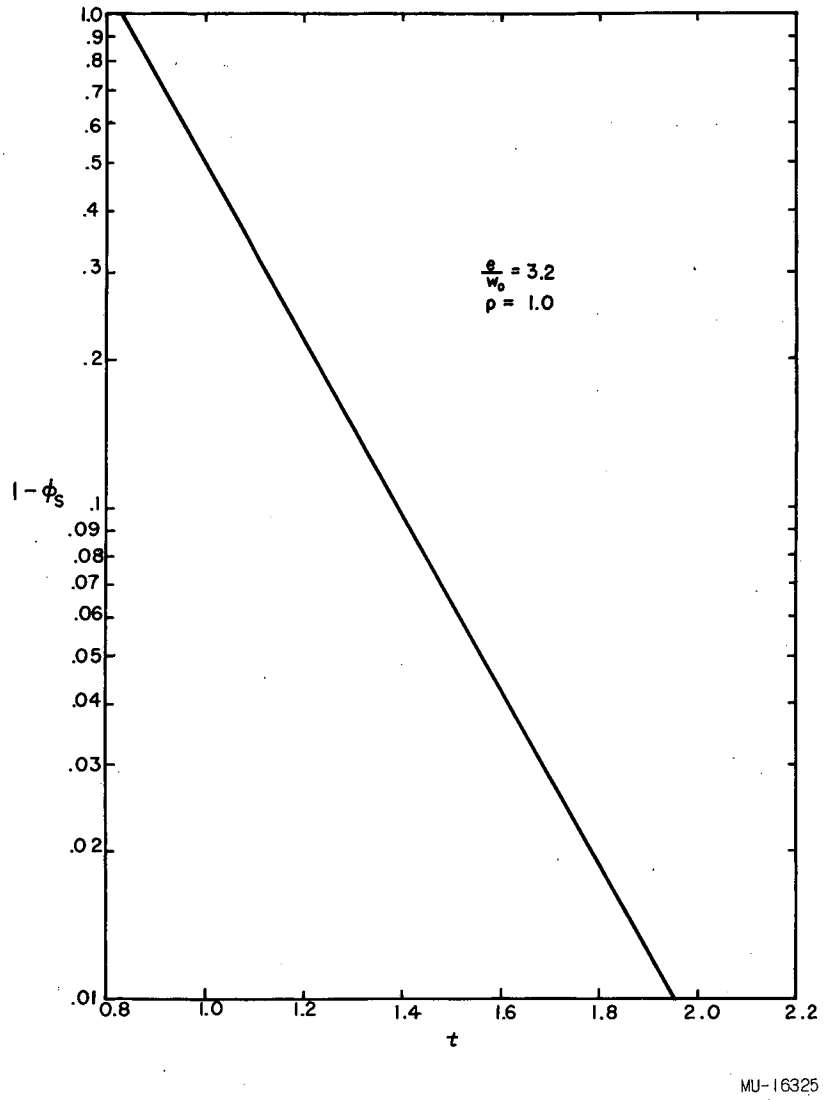

Fig. 54. Exponential portion of a finite-difference solution for pure diffusional mass transfer in zone melting of eutectic formers.
$\ln (1 - \phi_s)$ vs τ for $\epsilon = 3.2$, $p = 1.0$.

However at the time parameter, τ_θ, when at $\eta = 0$, $\phi = \epsilon$ for the first time, $\phi_s = 0$, and

$$r(\tau_\theta) = \frac{\epsilon}{\epsilon-1} \ . \tag{53}$$

But it is known that $\phi_s = 0$ for $\tau \leq \tau_\theta$,

$$(1-\phi_s) = e^{-(\tau-\tau_\theta)q}, \tag{54}$$

and, at the steady state, $(\phi-1) = (\epsilon-1)e^{-\eta}$.
An over-all material balance for $\tau \geq \tau_0$ yields

$$\int_{\tau_0}^{\infty} e^{-q(\tau-\tau_0)} \, d\tau = \int_{\theta}^{p} (\epsilon-1)(e^{-\eta} - e^{-r(\tau_\theta)\eta}) d\eta. \tag{55}$$

From Eqs. (53), (54), and (55), there finally results:

$$\frac{1}{q} = (\epsilon-1) \left[(1-e^{-p}) - \frac{\epsilon-1}{\epsilon} \left(1-e^{-\frac{\epsilon}{\epsilon-1} p} \right) \right] \ . \tag{56}$$

Likewise a material balance for $0 \leq \tau < \tau_0$ yields

$$\tau_0 = \int_0^p (\epsilon-1)e^{-r(\tau_\theta)\eta} d\eta = \frac{(\epsilon-1)^2}{\epsilon} (1 - e^{-\frac{\epsilon}{\epsilon-1} p}). \tag{57}$$

These expressions correlate well the computer results.

In order to exemplify the concentration vs distance behavior that this theory predicts, calculations were carried out for the benzoic acid-naphthalene zone-melting runs. Here $\epsilon = 3.17$. A plot of w_s/w_0 vs τ/p is shown in Fig. 55.* Notice the sharpness with which w_s/w_0 departs from 0 and reaches 1. A plot of the average value of w_s/w_0 (from $\tau = 0$ to τ) vs τ/p is given in Fig. 56.

---

*Note that since $z = tV$, by definition we have

$$\frac{\tau}{p} = \frac{z}{L} \left(\frac{\rho_s}{\rho_\ell} \right)$$

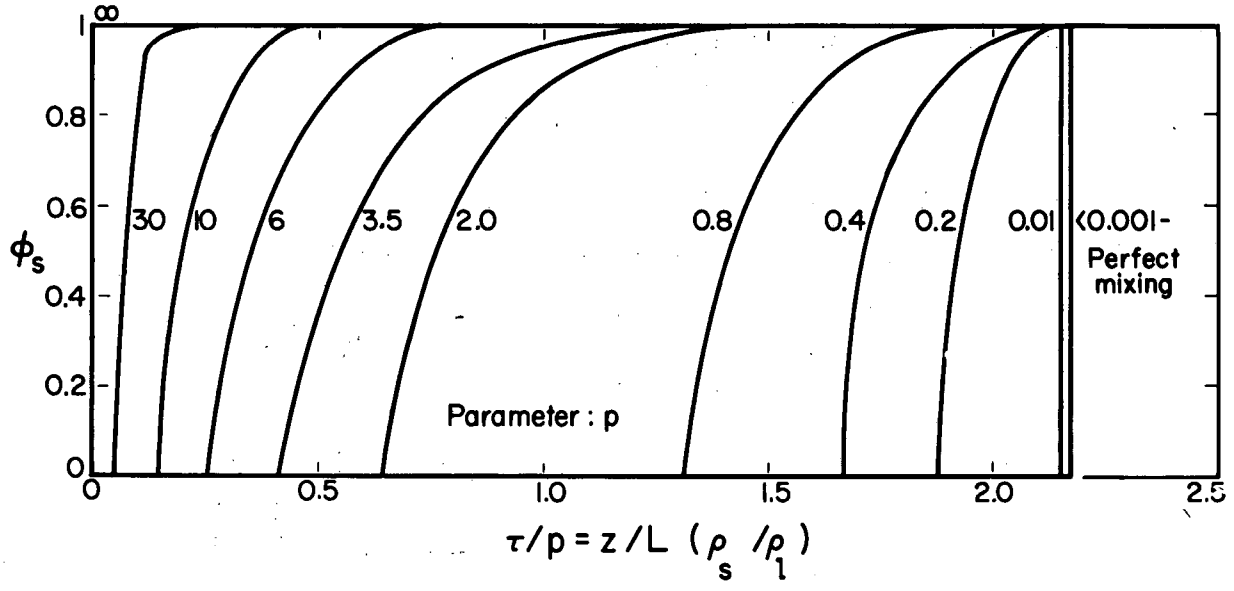

Fig. 55. Concentration profiles resulting from a single zone pass of a eutectic former with $\epsilon = 3.17$, with pure diffusional mass transfer.
ϕ_s vs $\tau/p = z/L\ (\rho_s/\rho_\ell)$.
Calculated from Eqs. (54), (56), and (57).

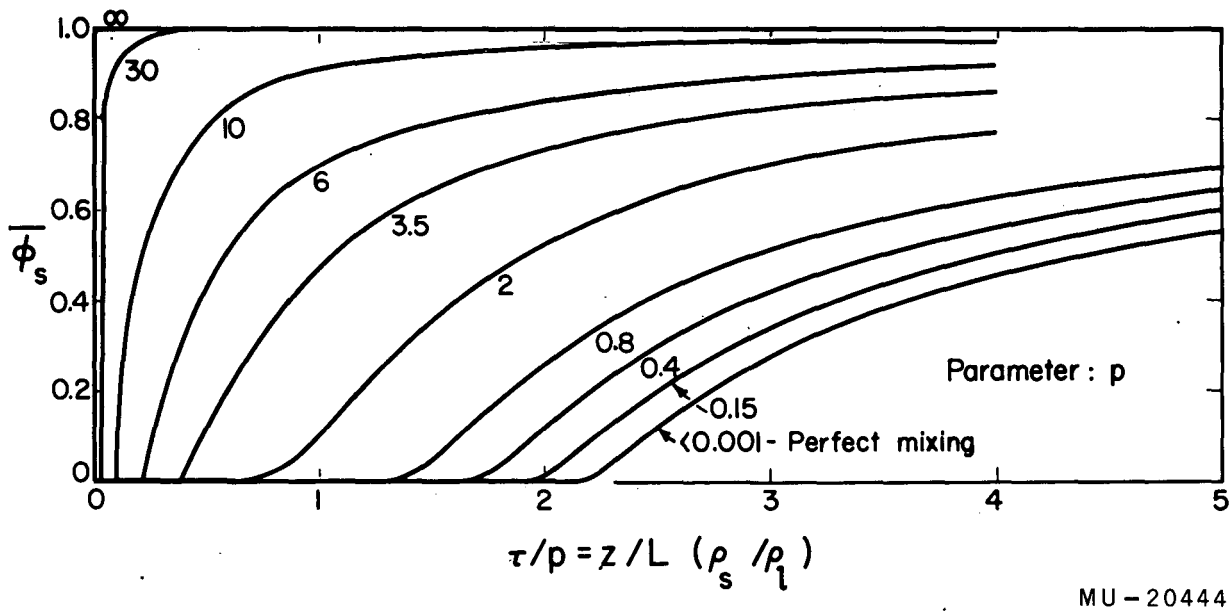

Fig. 56. Average concentrations from 0 to τ resulting from a single zone pass of a eutectic-former with ϵ = 3.17, with pure diffusional mass transfer.
ϕ_s vs τ/p.
Calculated from Fig. 55.

Analytical Solution for Constant-Distribution Coefficient

In order to solve the unsteady-state problem exactly, the differential equation and boundary conditions must form a Sturm-Liouville system. As they stand, they do not. To remedy this, the following transformation is made:

$$\phi = e^{-\eta/2}\,\psi.$$

Then Eqs. (33), (37), and (39) become respectively,

$$\frac{\partial^2\psi}{\partial\eta^2} - \frac{1}{4}\psi = \frac{\partial\psi}{\partial\tau}\,, \tag{58a}$$

$$\frac{\partial\psi}{\partial\eta} = \psi\left(k - \frac{1}{2}\right) \tag{58b}$$

at $\eta = 0$, and

$$\frac{\partial\psi}{\partial\eta} + \frac{1}{2}\psi = 0 \tag{58c}$$

at $\eta = p$. Letting $T = \tau/p^2$ and $S = \eta/p$, there results

$$\frac{\partial^2\psi}{\partial S^2} - \frac{p^2}{4}\psi = \frac{\partial\psi}{\partial T}\,, \tag{59a}$$

with

$$\psi = e^{\eta/2} \tag{59b}$$

at $T = 0$,

$$\frac{\partial\psi}{\partial S} = p\left(k - \frac{1}{2}\right)\psi \tag{59c}$$

at $S = 0$, and

$$\frac{\partial\psi}{\partial S} = -\frac{1}{2}p\psi \tag{59d}$$

at $S = 1$.

The method of separation of variables yields

$$\psi_j = C_j\left(\cos m_j S + b_j \sin m_j S\right) e^{-\lambda_j^2 T}\,, \tag{60}$$

where λ_j are eigenvalues, b_j and c_j are constants, and we have

$$m_j = \left[\lambda_j^2 - (p^2/4)\right]^{1/2} \text{ and } \lambda_j^2 = m_j^2 + p^2/4.$$

Application of the boundary conditions at S = 0 and 1, yields

$$\tan m_j = \frac{4m_j\ pk}{4m_j^2 - p^2\ (2k-1)}\ , \tag{61a}$$

and

$$b_j = p(k - \tfrac{1}{2})/m_j . \tag{61b}$$

Addition of the steady-state and unsteady-state solutions yields

$$\phi = 1 + \frac{1-k}{k}\ e^{-pS} + e^{-pS/2} \sum_{j=1}^{\infty} C_j(\cos m_j S + b_j \sin m_j S) e^{-\lambda_j^2 T} . \tag{62}$$

Utilization of the condition at T = 0, the fact that Eq. (59) is Strum-Liouville, and Eq. (61) yields

$$C_j = \frac{16\ pm_j(k-1)}{(p^2+4m_j^2)\ [\ 2m_j(1+b_j^2)+\sin 2m_j(1-b_j^2)+4b_j \sin^2 m_j\ ]} . \tag{63}$$

Thus, using m_j as the really useful eigenvalue, substituting for S and T, and noting that $\phi_s = k\phi(0,\tau)$, the final result is obtained:

$$(\phi_s - 1) = k \sum_{j=1}^{\infty} C_j \exp[-(\tfrac{1}{4} + \frac{m_j^2}{p^2})\tau] , \tag{64}$$

where C_j, m_j are given by Eqs. (61) and (63).

As the size of the zone gets larger (i.e. p increases), the number of terms needed for the exact solution increases rapidly. It would be convenient, therefore, to have a solution for an infinite-sized zone, i.e. for infinite normal freezing. Fortunately this problem has already been solved by using Laplace transforms by Pohl,[42] Hulme,[44] Smith et al.,[33] and Memelink.[43] Pohl's solution, however, holds only for small k; it is given quite well anyway by the approximate solution of Tiller et al.[45] The solutions of Hulme, Smith, and Memelink are basically the same, i.e.

$$\phi_s = \frac{1}{2}\left\{1 + \text{erf}\left(\frac{\sqrt{\tau}}{2}\right) + (2k-1)e^{-k(1-k)\tau}\ \text{erfc}\left(\frac{2k-1}{2}\sqrt{\tau}\right)\right\}. \quad (65)$$

Smith[33] also gives solutions for a sudden change in the rate of solidification in infinite normal freezing, and for the terminal transient in finite normal freezing.

In a sample calculation it was found that the solution for zone melting expressed in Eq. (64) is approximately the same as that in Eq. (65) for $p = 8$. This was suspected from the results of the computer calculations, which showed that the concentration change in the zone did not reach the melting interface for $p \geq 8$, and reached very little for $p = 5$.

Calculations based on Analytical Results

In order to illustrate the analytical results, concentration profiles were calculated for $k = 1.85$.* These are shown in Fig. 57. The averages from $\tau = 0$ to τ are shown in Fig. 58.

It is apparent that the calculation of concentration profiles is a rather tedious process. Consequently certain characteristics of these profiles have been calculated and plotted for the convenience of future users. A schematic profile of $|\phi_s - 1|$ vs τ is shown in Fig. 59. All curves begin at $\tau = 0$ with $(\phi_s - 1) = (k-1)$ and infinite slope (except for $p = 0$, perfect mixing). After sufficient time, all but the first term in the infinite series of the analytical solution become negligible. At this time the equation of the profile simplifies to

$$(\phi_s - 1) = (\phi_{s,ext} - 1)\, e^{-s\tau}, \quad (66)$$

where $|\phi_{s,ext} - 1|$ is the intercept at $\tau = 0$ of the straight line portion of a semi-logarithmic plot of $|\phi_s - 1|$ vs τ. By comparison with the analytical solutions, the following is obtained:

$$(\phi_{s,ext} - 1) = kc_1, \quad (67)$$

---

*This value is for 10%wβ-naphthol in naphthalene. See Chapter III.

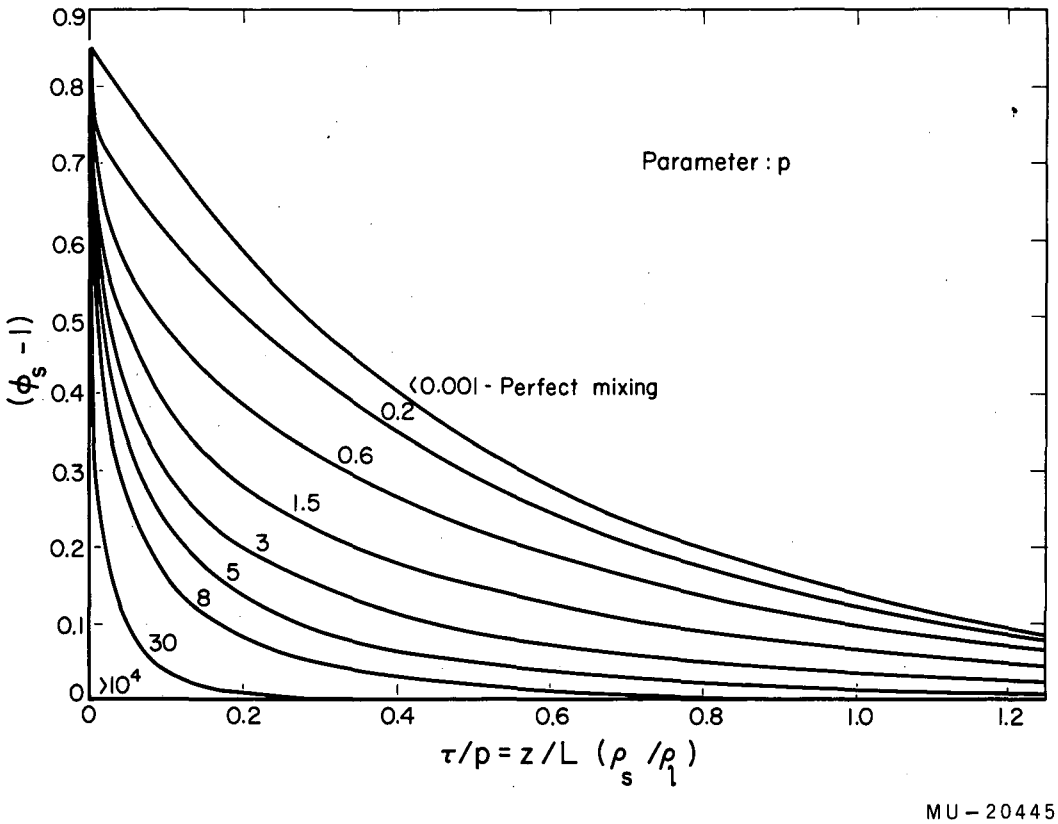

Fig. 57. Concentration profiles resulting from a single zone pass of a material with constant k of 1.85, with pure diffusional mass transfer. $(\phi_s - 1)$ vs τ/p. Calculated from Eq. (64).

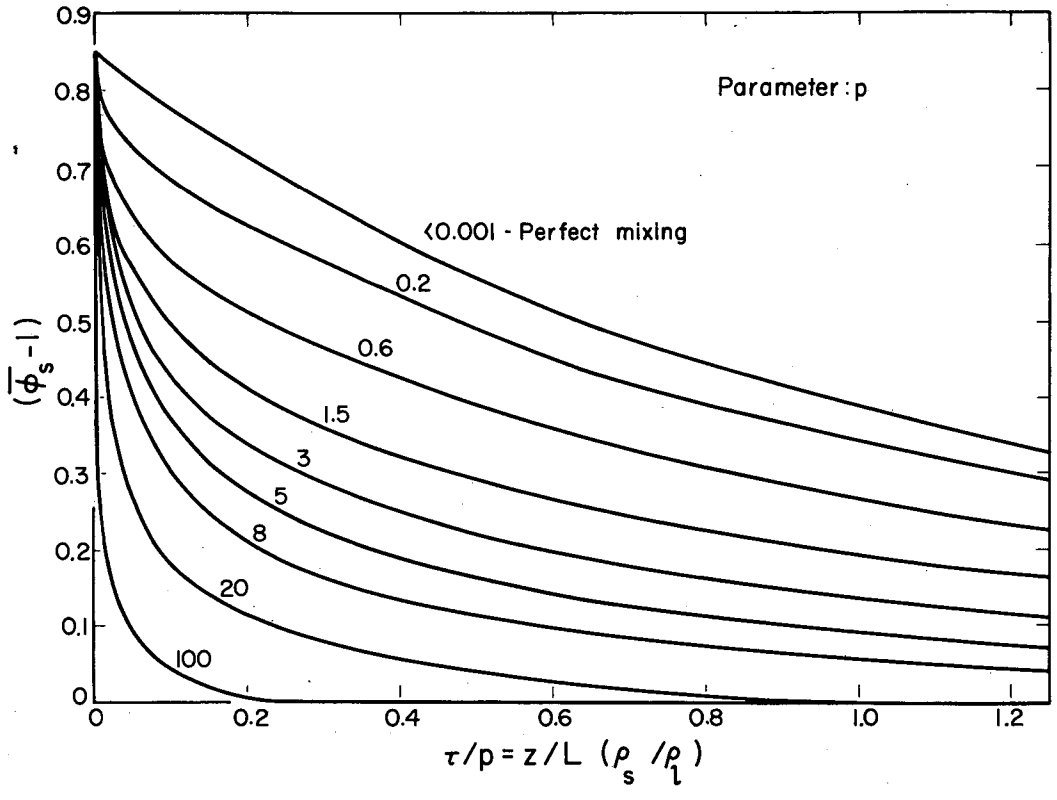

Fig. 58. Average concentrations from 0 to τ resulting from a single zone pass of a material with constant k of 1.85, with pure diffusional mass transfer. $(\phi_s - 1)$ vs τ/p. Calculated from Fig. 57.

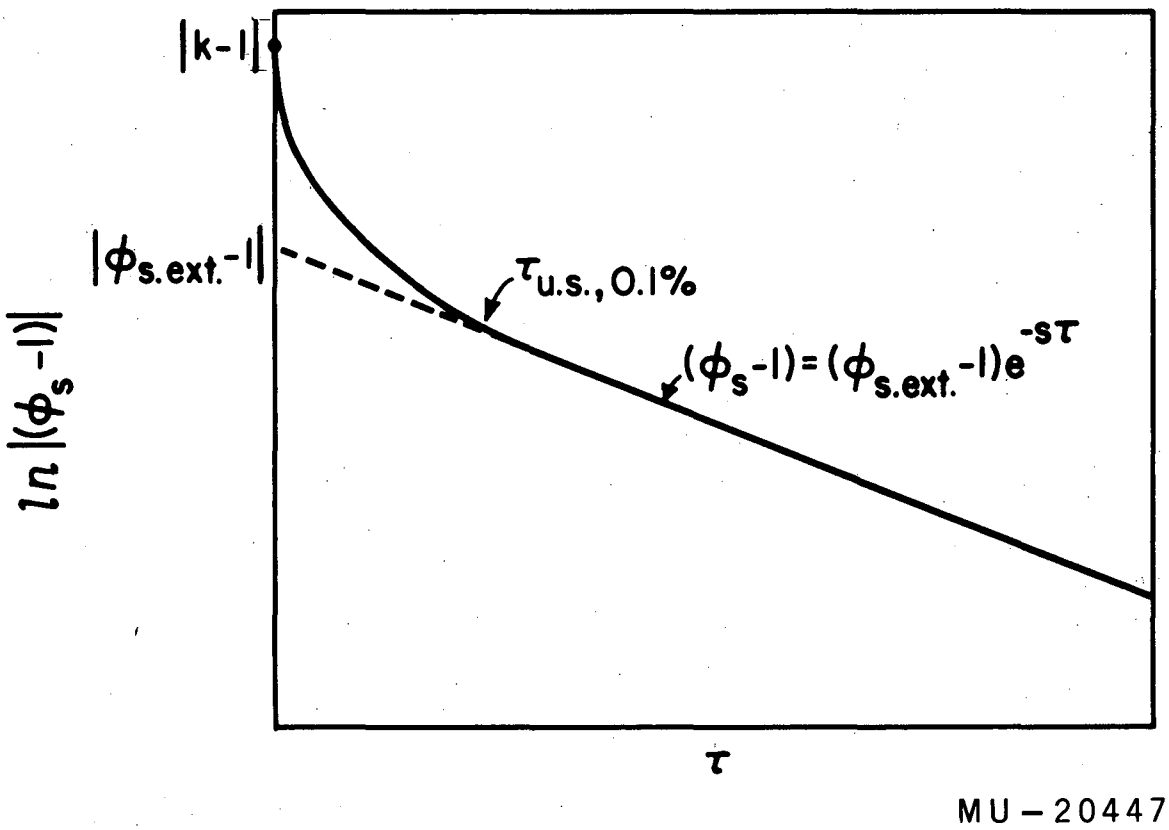

Fig. 59. Schematic sketch of a concentration profile for a single zone pass of a material with constant distribution coefficient, with pure diffusional mass transfer, showing the parameters characterizing the curve. $\ln |\phi_s - 1|$ vs τ.

and

$$s = \left(\frac{1}{4} + \frac{m_1^2}{p^2} \right). \tag{68}$$

As p approaches infinity, however, s approaches zero, and the usefulness of this approach vanishes. Instead, the value of s, the slope of the semi-logarithmic plot, at some low value of $|\phi_s - 1|$ was calculated. This was chosen to be $(\phi_s - 1) = 0.1\ (k - 1)$.

Another valuable parameter would be the value of τ at which the concentration profile first deviated significantly from an exponential form. For convenience, this was chosen as the value of τ at which the constant C_2 of the second term of the infinite series was equal to 0.1% of C_1. At this point τ was designated as $\tau_{us,0.1\%}$, which is given by

$$\tau_{us,0.1\%} = \left[\frac{p^2 \ln \left(\frac{C_2}{0.001 C_1} \right)}{m_2^2 - m_1^2} \right] \tag{69}$$

Values of these various parameters were calculated for k = 0.1, 0.5, 1.00, 1.85, and 5.00. They are plotted in various fashions vs p in Fig. 60, 61, 62, and 63. It is seen that the analytical solution reduces to perfect mixing for $p < 0.01$ and effectively* to infinite normal freezing for $p > 6$. These plots enable production of a quick sketch of the expected concentration profile for zone melting, with mass transfer only by diffusion. In making these calculations it was noted that the first eigenvalue m_1 becomes imaginary for $k < 0.5$ with $p > 4k/(1-2k)$.

Effective Diffusion Coefficient

Needless to say, pure diffusional mass transfer is seldom realized in fluids. Only in fine capillary tubes would you expect to find no free convection. If the convection is small, however, it is

*Deviation occurs only at values of $|\phi_s - 1|$ so low that it does not effect the result significantly.

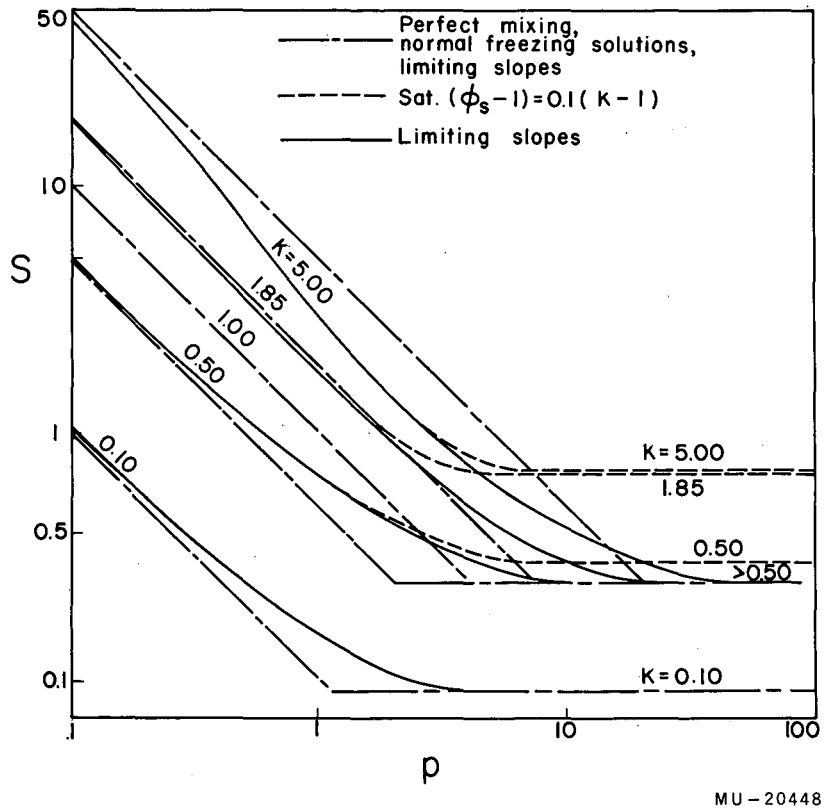

Fig. 60. Plot of ln s vs ln p.

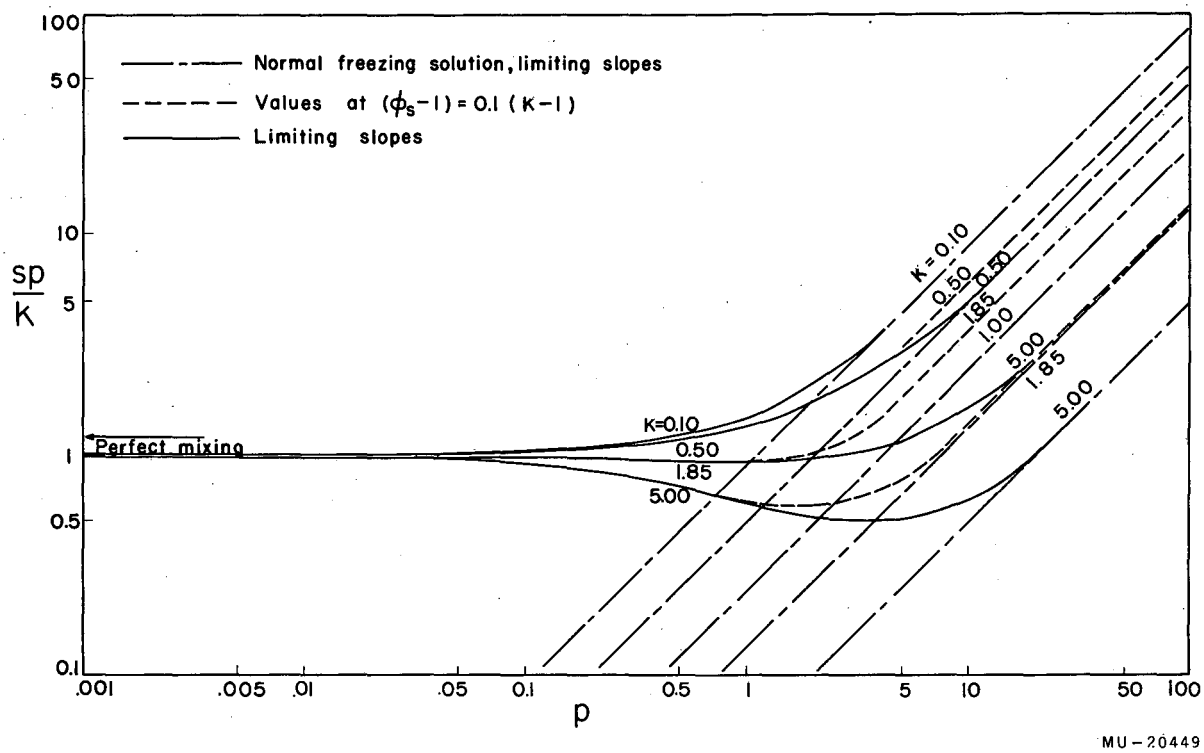

Fig. 61. Plot of ln (sp/k) vs ln p.

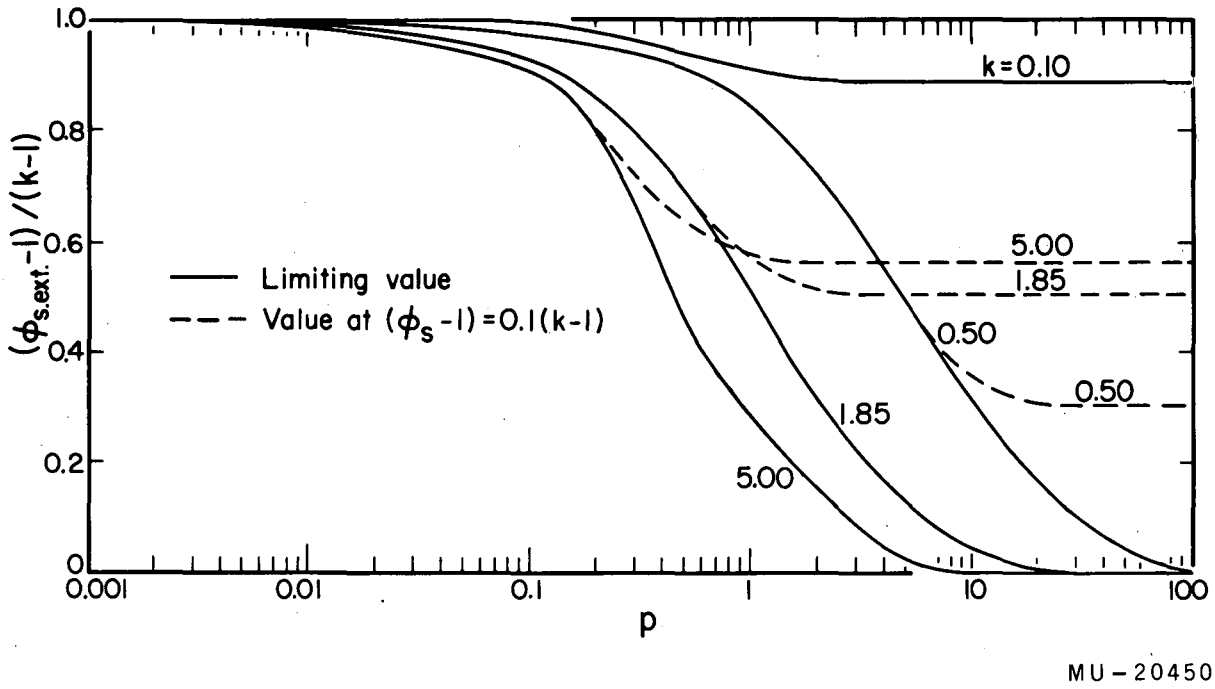

Fig. 62. Plot of $(\phi_{s,ext} - 1)/(k - 1)$ vs ln p.

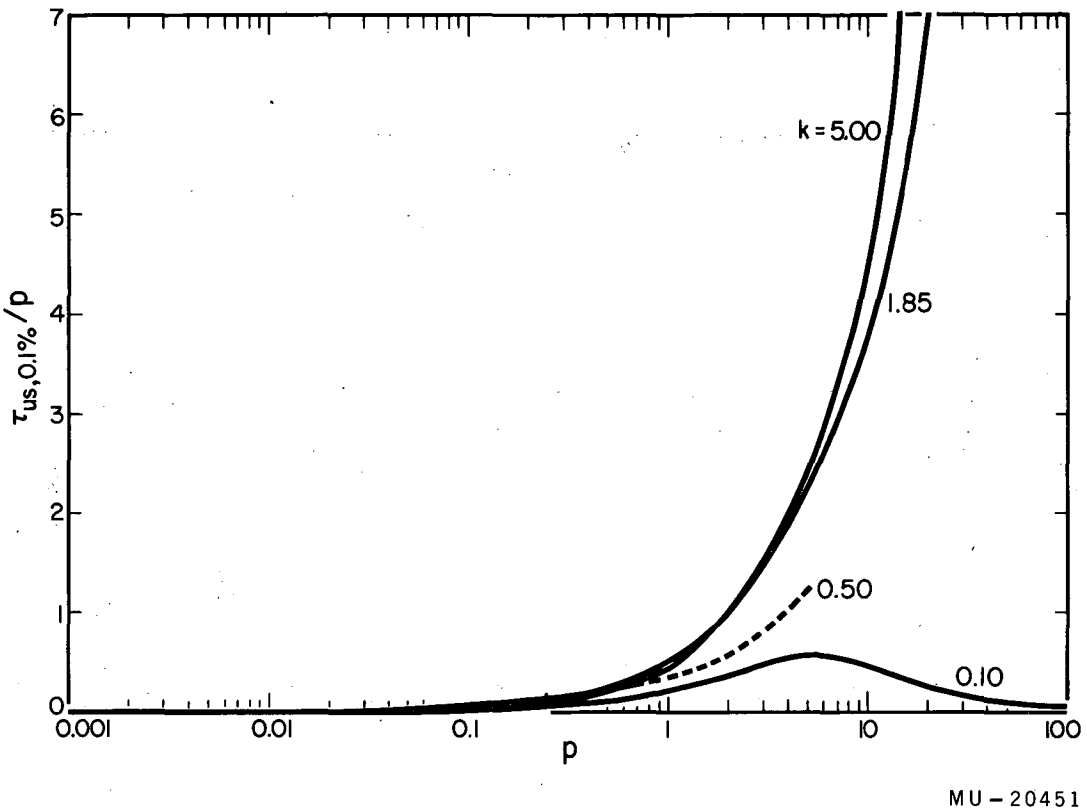

Fig. 63. Plot of $\tau_{us,0.1\%}/p$ vs ln p.

conceivable that the resistance to mass transfer may be distributed throughout the zone. In such a case, an effective diffusion coefficient, larger than the true diffusion coefficient, might serve to make the results derived here applicable. This is the idea that remains to be tested in Chapter VII, EXPERIMENTAL RESULTS FOR MASS TRANSFER IN ZONE MELTING.

D. Boundary-Layer Solutions

Instead of the resistance to mass transfer being distributed throughout the zone, it may be concentrated in a thin boundary-layer near the freezing interface.* Burton, Prim, and Slichter have used such an analyses for normal freezing.[2,32] Its basic usefulness is that it yields an effective distribution coefficient k_{eff} which may be used in place of the equilibrium distribution coefficient k in Eqs. (1) and (4).

Constant Distribution Coefficient

If the boundary-layer is small, changes in the amount of material in it may be ignored. We suppose that inside the boundary layer, mass transfer is by diffusion only, while outside it, complete mixing prevails. Inside the boundary layer, then, Eq. (42) applies. Thus, this is a quasi-steady-state situation.

Applying the following boundary conditions

$$\phi = \frac{\phi_s}{k} \quad , \quad \frac{d\phi}{d\eta} = \phi(k-1) \tag{70}$$

at $\eta = 0$, and

$$\phi = \phi_\ell \tag{71}$$

at $\eta = \frac{\delta V}{D} \frac{\rho_s}{\rho_\ell}$,

*Conditions near the melting interface are immaterial as long as the boundary layer there contains a negligible amount of material with respect to that in the whole zone.

where δ is the boundary-layer thickness, and ϕ_ℓ is the ratio of concentration in the bulk zone to the original solid concentration, one obtains

$$k_{eff} = \left(\frac{w_s}{w_\ell}\right) = \left(\frac{\phi_s}{\phi_\ell}\right) = \frac{k}{k+(1-k)\exp\left(-\frac{\delta V}{D}\frac{\rho_s}{\rho_\ell}\right)} \qquad (72)$$

This is the desired expression. In order to exemplify the predicted behavior, concentration profiles were calculated and plotted in Fig. 64, where (ϕ_s-1) is plotted vs τ/p for $k = 1.85$. Curves are shown for various values of $\delta V/D$ (with $\frac{\rho_s}{\rho_\ell} \doteq 1$). Note, in particular, that these curves do not have an intercept at $\tau = 0$ of $(\phi_s-1) = 0.85$, as did the curves for uniform mass-transfer resistance throughout the zone (Fig. 57).

Eutectic-Forming Systems

As noted previously, the concentration profiles resulting from the zone-melting of eutectic-forming mixtures have three regions, viz.:

1. A region in which one of the components comes out pure.
2. A region in which both components come out at a concentration different from the original concentration.
3. A steady-state region, with the same composition leaving the zone as entering it.

No solution could be obtained for regions (1) and (2) by using the boundary-layer approach. It is certain, however, that region (2) will be small, i.e. the transition from one component coming out pure to the steady-state condition is rapid and sharp. From the steady-state solution given by Eq. (44), is obtained

$$(\phi_\ell-1) = (\epsilon-1)\exp\left(-\frac{\delta V}{D}\frac{\rho_s}{\rho_\ell}\right). \qquad (73)$$

Calculation of δ

The hope in this approach is that δ will be relatively independent of the growth rate. Unfortunately however, it cannot, in general, be theoretically calculated. The presence of a flow through the boundary layer makes an exact theoretical analyses extremely difficult, even for

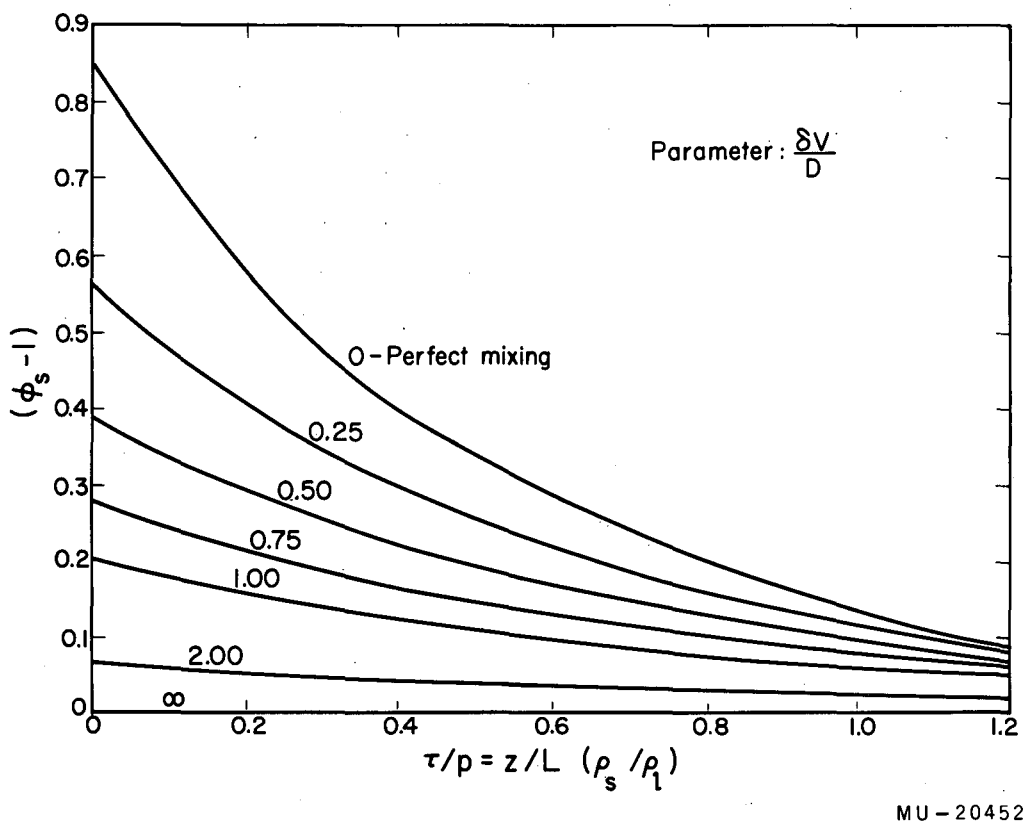

Fig. 64. Concentration profiles resulting from a single zone pass of a material with constant k = 1.85, with the bulk of the zone well-mixed. $(\phi_s - 1)$ vs τ/p.

relatively simple situations. In free convection, there is the additional complicating factor of simultaneous temperature and concentration gradients. Both temperature and concentration give rise to density changes--the driving force for free convection.

It would be nice, however, to have some idea of the parameters involved in simultaneous heat and mass transfer in free convection. Accordingly a theoretical analysis was made of simultaneous heat and mass transfer in free convection from a vertical flat plate with no flow into the plate.[47] The results are summarized here in terms of the predicted boundary-layer thickness for mass transfer. For heat transfer controlling $[|Gr| > |(Pr/Sc)^{1/2}\ Gr'|]$*,

$$\frac{\delta}{L_P} = 1.476\ (Pr+0.952)^{1/4}\ (Sc)^{-1/2}\ [Gr+(Pr/Sc)^{1/2}\ Gr']^{-1/4} \qquad (74)$$

For mass transfer controlling ($|Gr| < |(Pr/Sc)^{1/2}\ Gr'|$),

$$\frac{\delta}{L_P} = 1.476\ (Sc+0.952)^{1/4}\ (Sc)^{-1/2}\ [Gr'+(Sc/Pr)^{1/2}\ Gr]^{-1/4}. \qquad (75)$$

Here L_P is the length of the plate, Pr is the Prandtl number (ν/a), Sc is the Schmidt number (ν/D), Gr is the Grashof number for heat transfer:

$$Gr = \left(\frac{g\ L_P^3\ \beta\ (T_o-T_\infty)}{\nu^2} \right),$$

and Gr' is the Grashof number for mass transfer:

$$Gr' = \left(\frac{g\ L_P^3\ \alpha\ (w_i-w_\ell)}{\nu^2} \right),$$

*In the aforementioned work, it was found that it was necessary to define separate Grashof numbers for heat transfer, Gr, and for mass transfer, Gr' (defined in detail below), in order to complete the theoretical solution of the problem. Indeed, it turned out, that, in this problem, use of the usual Grashof number $[g\ L_p^3(\rho_o-\rho_\infty)/\rho\nu^2 = Gr+Gr']$ to characterize the driving force for free-convection mass transfer is incorrect. Instead Gr and Gr' must be weighted as shown in Eqs. (74) and (75).

where a is the thermal diffusivity of fluid ($k/c_p \rho$), w_i, w_l are the concentrations of the concerned component in the bulk fluid at the wall respectively, c_p is the heat capacity of the fluid, D is the diffusivity of the concerned component, g is the accleration due to gravity (taken as positive for flow up the plate and negative for flow down), k is the thermal conductivity of fluid, T_∞, T_0 are the temperatures in the bulk fluid and at the wall, respectively, α is the concentration densification coefficient, $(1/\rho)(\partial\rho/\partial w)_T$, β is the temperature densification coefficient, $(1/\rho)(\partial\rho/\partial T)_w$, and ν is the kinematic viscosity.

For most liquids Pr and Sc are much greater than 0.952, and so the constant 0.952 may be dropped from the first term in parenthesis in Eq. (74) and (75).

In zone melting there is not only generation of convection currents at the solid-liquid interfaces but also at the inner surface of the glass tube which transmits heat from the heater to the fluid. The relative magnitude of these effects remains to be determined by experiment. This is done in the following chapter.

VII. EXPERIMENTAL RESULTS FOR MASS TRANSFER IN ZONE MELTING

A. Introduction

The objectives of the work described in this chapter were:

(a) To pick the best mechanism to explain variation with zone travel rate of separation in zone melting.

(b) To develop a correlation that will enable prediction of separation in zone melting.

The various mechanisms that could explain the variation of separation with zone travel rate were outlined in Chapter I. They are also listed below, along with the various side effects expected to accompany the operation of each mechanism. It is by comparison of the experimental results with these side effects, that the choice of the best mechanism is to be made from the following:

(1) Occlusion of mother liquor. The interface will appear rough -- probably with needles growing out from it.

(2) Adsorption on the growing crystal surface. If this mechanism is controlling, the zone's mixing parameters (geometry of zone, heat input, direction of zone travel, etc.) will not affect the separation.

(3) Incomplete liquid mixing. The zone's mixing conditions will affect separation. The final solid-concentration profile will lie between the two limiting cases discussed in the preceding chapter, and listed below. There are however, differences in the predictions of these limiting cases:

(a) The mass-transfer resistance is spread uniformly throughout the zone. Separation will be affected strongly by the zone length, i.e., as the zone length increases, separation decreases rapidly.

(b) The mass-transfer resistance is confined to a thin boundary at the freezing interface. The size of the zone is immaterial (except that a larger zone is able to contain more impurity, so that a given rate of separation will occur over a larger length of solid).

(4) Constitutional subcooling. Unfortunately the same conditions affect separation for this mechanism as for mechanism (3), since constitutional subcooling depends on the concentration gradient at the freezing interface. One would expect, however, that the imposed temperature gradient would have a larger effect for mechanism (4), a steeper gradient causing less subcooling. The principal difference between mechanisms (3) and (4), however, is in the prediction of the recrystallized-solid concentration profile for eutectic-forming systems. As noted in the preceding chapter, mechanism (3) predicts a sharp transition from a situation in which one component is obtained pure to a steady-state region. Constitutional subcooling, on the other hand, predicts a gradual transition. It is apparent that the large separation that results when one component comes out pure induces a large concentration gradient at the freezing interface, and hence makes possible a large subcooling.

B. Data

The experimental procedure has been discussed in Chapters II and IV. Mixtures of 10%w benzoic acid in naphthalene and 10%w β-naphthol in naphthalene were subjected to zone melting. The mixtures were in glass tubes which were pulled through a stationary heater made of heating tape wrapped around a glass tube slightly larger than the moving tube. Runs were made by pulling the tubes up, down, and horizontally. Sometimes the tubes also had thermocouple leads, a glass tube, or a stainless steel tube running through them.* Most of the runs were made with the tubes pulled down. The ranges of the other variables were:

Zone travel rate: 0.15 to 2.70 cm/hr

Tube size (internal radius): 0.178 to 0.875 cm

Zone length: 0.5 to 4.5 cm

---

*The thermocouple leads were 0.020-in. wires covered with fiberglass insulation. The glass tube measured 4mm o.d. and 3mm i.d. The stainless steel tube measured 1/8-in. o.d. with 1/64-in. wall thickness.

Heating tape widths: 1/2-in. and 1-in.

Mean temperature difference between coolants and melting point: 34.8 to 78.0°C.*

From the experimental results for each run, a plot of solid composition vs distance was made. Several of these are shown in Figs. 65 through 71. Note that the runs are long enough for the steady state to be reached.

Two things about the concentration changes wrought by zone melting are important:

(1) The total amount of separation that has occurred (see Eq. 49).

(2) The shape of the concentration vs distance curves.

Only (1), the total separation, will be examined at this point.

The total separation (relative to w_0) can be calculated from both the experimental recrystallized-solid concentration profile and from the experimental zone concentration profile. For the solid this is given (in terms of zone density) by**

$$P_s = \int_0^\infty \left| \phi_s - 1 \right| \frac{\rho_s}{\rho_\ell} \, dz \, . \tag{76}$$

For the zone it is given by

$$P_z = \int_0^L \left| \phi - 1 \right| dx \, . \tag{77}$$

---

*This is a mean temperature between the temperatures of the coolants in the two cooling chambers, which was calculated and subtracted from the melting point of the average mixture in the zone during the run. This is believed to be the temperature difference of most significance to free convection in the zone (other than the temperature difference between melting point and zone, which was not measured), since the various heat fluxes in the zone are roughly proportional to it.

**Actually the total separation in g per unit cross-sectional area of rod is $P_s \rho_\ell w_0 = P_z \rho_\ell w_0$.

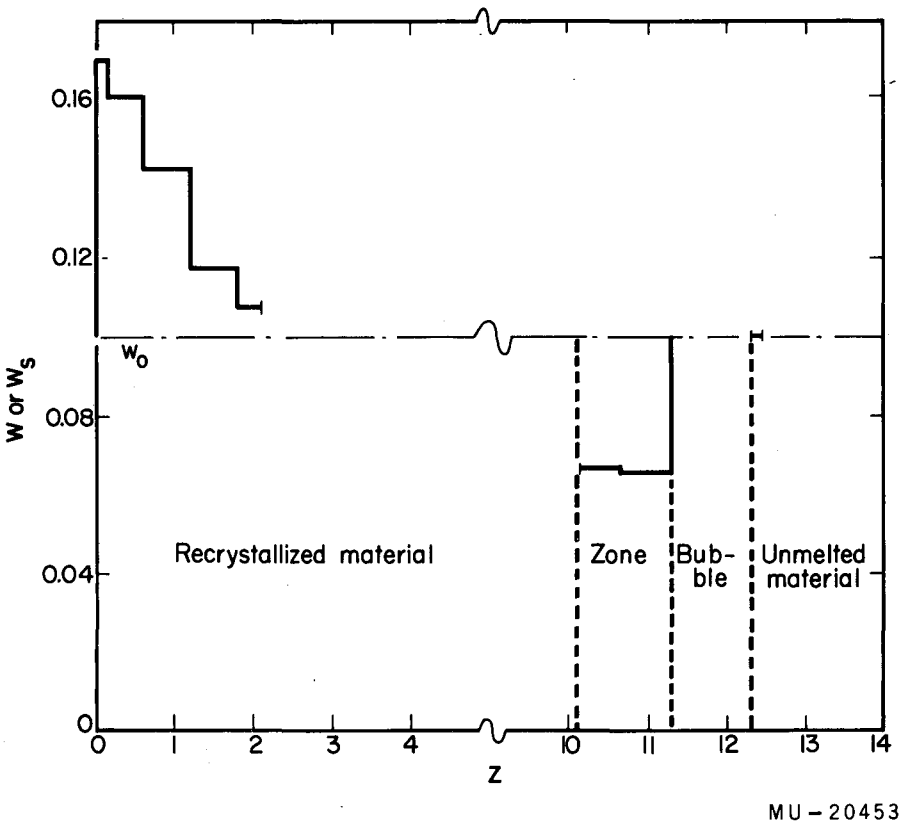

Fig. 65. Experimental concentration (in weight fractions) profile resulting from a single zone pass of 10%w β-naphthol in naphthalene. Run N-44 (0.15 cm/hr zone travel rate, 20-mm glass tube pulled down).

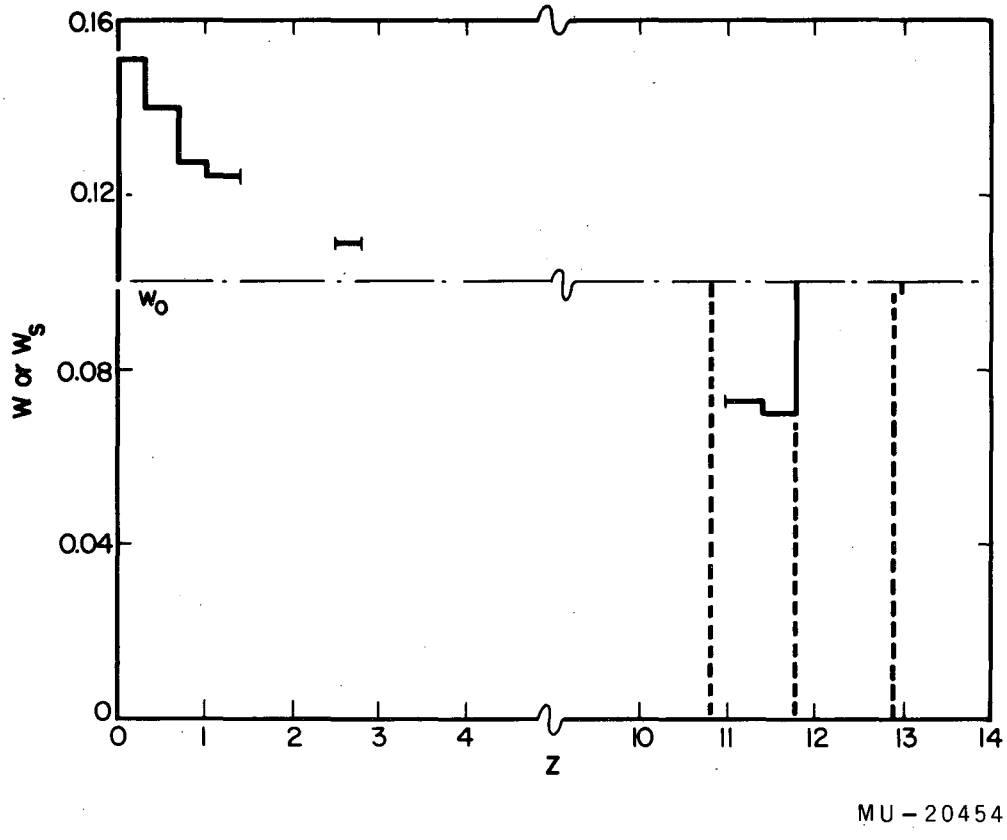

Fig. 66. Experimental concentration (in weight fraction) profile resulting from a single zone pass of 10%w β-naphthol in naphthalene. Run N-45 (0.45 cm/hr zone travel rate, 20-mm glass tube pulled down).

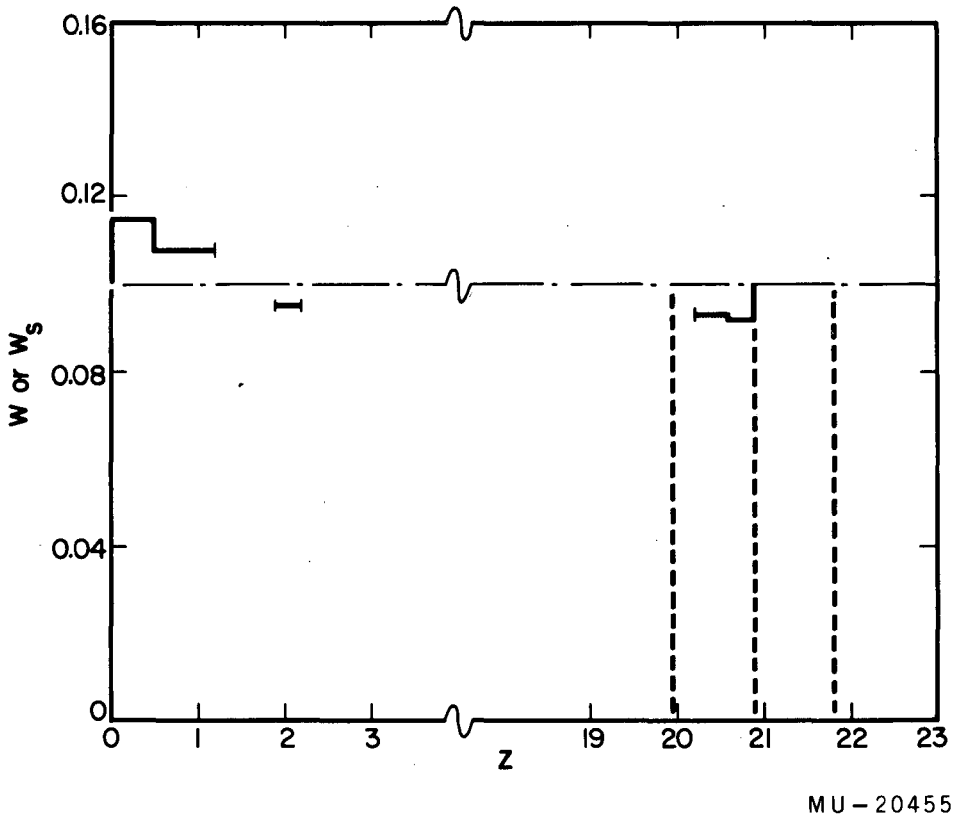

Fig. 67. Experimental concentration profile resulting from a single zone pass of 10%w β-naphthol. Run N-46 (2.7 cm/hr, 20-mm tube pulled down).

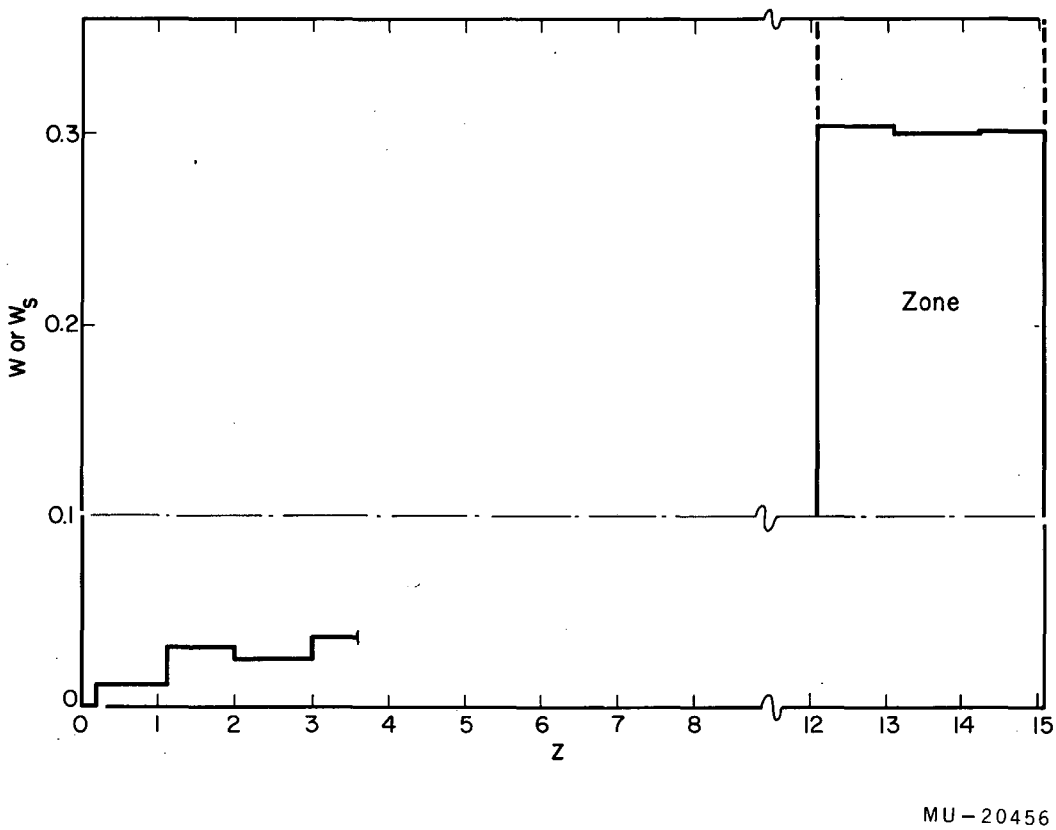

Fig. 68. Experimental concentration profile resulting from a single zone pass of 10%w benzoic acid in naphthalene. Run B-1 (0.15 cm/hr, 10-mm tube pulled up).

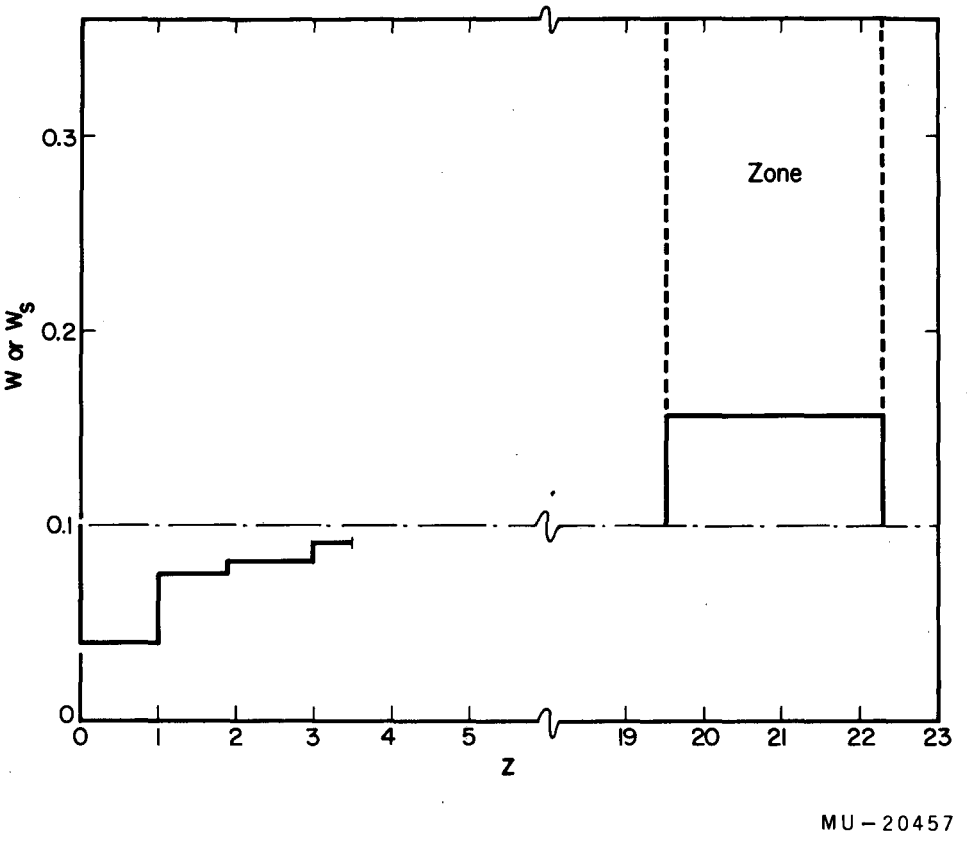

Fig. 69. Experimental concentration profile resulting from a single zone pass of 10%w benzoic acid. Run B-3 (1.35 cm/hr, 10-mm tube pulled up).

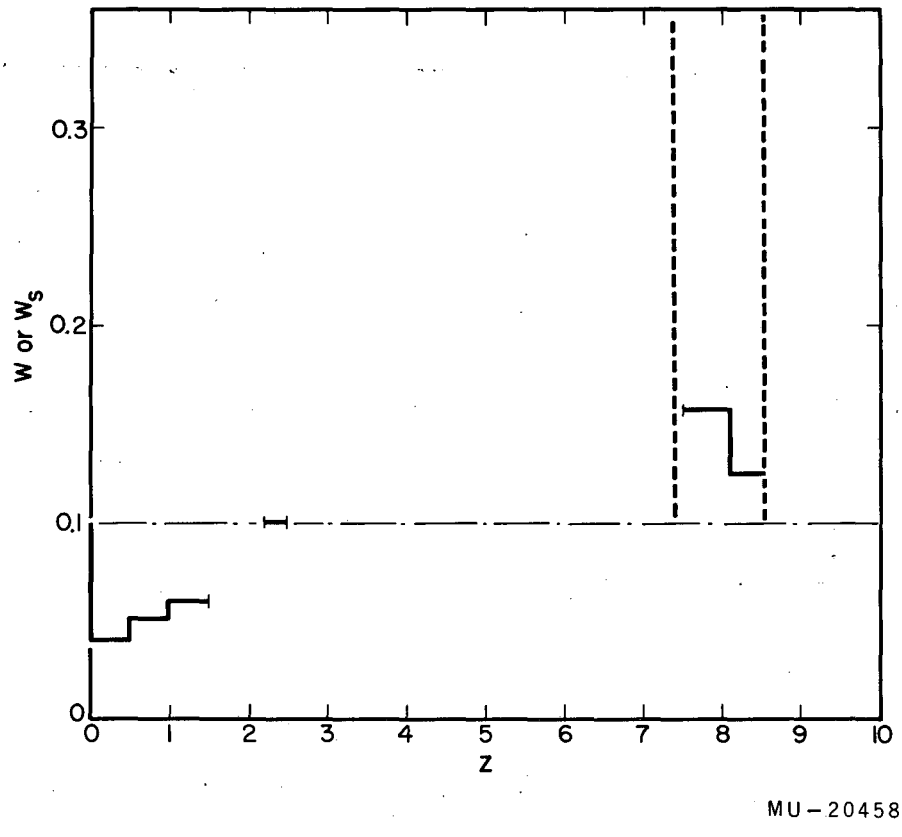

Fig. 70. Experimental concentration profile resulting from a single zone pass of 10%w benzoic acid. Run B-19 (0.15 cm/hr, 10-mm tube pulled down).

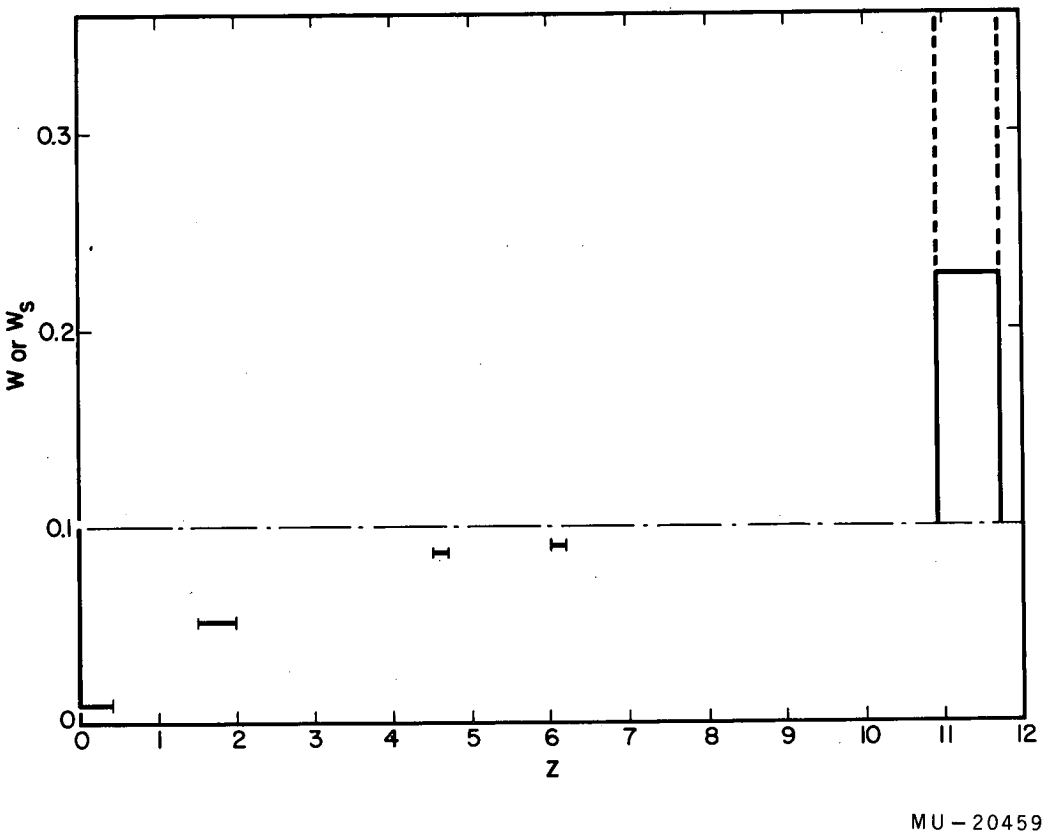

Fig. 71. Experimental concentration profile resulting from a single zone pass of 10%w benzoic acid. Run B-40 (0.45 cm/hr, 20-mm glass tube with a 4-mm axial glass tube in the zone pulled horizontally).

From these may be calculated either a value of $p = \frac{LV}{D}\left(\frac{\rho_s}{\rho_\ell}\right)$ or of $\frac{\delta V}{D}\frac{\rho_s}{\rho_\ell}$ for the zone melting of a very long rod. Integration of Eqs. (43) and (44) and inspection of Eqs. (77) and (73) [noting that $P = L\,(1 - 1/k_{eff})$] shows these to be, in terms of $P = P_s$ or P_z, the following. For a constant distribution coefficient, this yields

$$\frac{V\delta}{D}\frac{\rho_s}{\rho_\ell} = \ln \frac{P}{L\,|1 - 1/k|} , \tag{78}$$

and for eutectic-forming systems,

$$\frac{V\delta}{D}\frac{\rho_s}{\rho_\ell} = \ln \frac{P}{L\,|\epsilon - 1|} . \tag{79}$$

Likewise the values for p are given by

$$P = |1/k - 1|\, L\left(\frac{1 - e^{-p}}{p}\right) \tag{80}$$

for a constant-distribution coefficient, and by

$$P = |\epsilon - 1|\, L\left(\frac{1 - e^{-p}}{p}\right) \tag{81}$$

for eutectic-forming systems.

In the actual runs, the zone size often varied during the course of a run. However, the tubes were pulled far enough and the changes in zone size were gradual enough, that the final zones could be considered to be at their steady-state concentrations. Because of this, separate values of P_z and P_s are to be expected, in general, for any one run. The data were worked up in this manner, down to the point of finding values for δ for both the solid separation and the zone separation in each run.* These are tabulated in Tables XVI and XVII. The uncertainty in the experimental separations is actually quite large. This is due to the inaccuracies in the technique used for analyzing the compositions

*Sample calculations are shown in Appendix I.

Table XVI

Experimental boundary-layer thicknesses for zone melting of β-naphthol-naphthalene mixtures

Run no.	δ(zone) (cm)	L(zone) (cm)	δ(solid) (cm)	L(solid) (cm)	r (cm)	V (cm/hr)	ΔT (°C)
			Pulling tube down				
N-31	0.1502	1.2	0.1594	1.4	0.400	0.15	55.7
N-33	0.1871	1.3	0.1780	1.8	0.175	0.15	63.0
N-34	0.2440	1.0	0.2090	1.8	0.175	0.225	63.0
N-35	0.1934	3.0	0.0313	2.4	0.175	0.15	63.0
N-36	0.0768	1.5	0.0951	2.8	0.175	1.35	63.0
N-37	0.0419	0.5	0.0631	1.5	0.400	1.35	63.0
N-39	0.0687	1.5	0.0791	1.9	0.400	2.70	63.0
N-40	0.4130	0.65	0.4480	1.1	0.400	0.15	78.0
N-41	0.1062	1.8	0.1062	2.5	0.400	0.15	40.6
N-42	0.1038	1.3	0.1163	2.5	0.400	0.45	40.6
N-44	0.1980	1.2	0.1690	2.3	0.875	0.15	63.0
N-45	0.0945	1.0	0.0903	2.3	0.875	0.45	63.0
N-46	0.0480	0.95	0.0541	2.2	0.875	2.70	63.0
N-47	0.1154	1.2	0.1130	1.6	0.175	0.15	40.3
			Pulling tube down; thermocouple in zone				
N-43	0.0938	1.3	0.1720	1.7	0.875	0.15	63.0
			Pulling tube down; glass tube in zone				
N-32	0.1270	1.0	0.1411	1.7	0.400	0.15	55.7
N-38	0.0745	1.5	0.0742	1.8	0.400	2.70	63.0
			Pulling tube up; stainless steel tube in zone				
N-21	0.0644	2.2	0.0408	2.4	0.875	0.45	55.0
N-29	0.0721	2.9	0.01038	3.5	0.400	0.45	55.0

(continued)

Table XVI (cont'd.)

Run no.	δ(zone) (cm)	L(zone) (cm)	δ(solid) (cm)	L(solid) (cm)	r (cm)	V (cm/hr)	ΔT (°C)
			Pulling tube up				
N-22	0.44700	3.9	0.3650	4.3	0.400	0.15	55.0
N-23	1.03000	2.1	0.3990	2.4	0.400	0.15	55.0
N-24	0.13810	2.2	0.1536	2.5	0.400	0.225	55.0
N-25	0.01514	2.3	--	--	0.400	0.45	55.0
N-26	0.01514	2.1	--	--	0.175	0.45	55.0
N-28	0.04000	3.5	0.0235	3.5	0.175	0.45	55.0
N-30	0.37600	1.2	0.2020	1.6	0.400	0.15	78.0
			Horizontal run				
N-50	--	--	0.2610	2.0	0.175	0.15	63.0
			Horizontal run; glass tube in zone				
N-51	0.72000	4.3	0.6700	3.7	0.875	0.15	78.0

Table XVII

Experimental boundary-layer thicknesses for zone melting of benzoic acid-naphthalene mixtures

Run no.	δ(zone) (cm)	L(zone) (cm)	δ(solid) (cm)	L(solid) (cm)	r (cm)	V (cm/hr)	ΔT (°C)
			Pulling tube down				
B-6	0.618	1.40	--	--	0.400	0.15	46.7
B-7	0.415	1.85	--	--	0.400	0.45	46.7
B-8	0.666	2.40	1.36	2.5	0.175	0.15	46.7
B-10	0.888	0.80	1.97	1.6	0.175	0.15	69.5
B-11	0.889	1.80	1.05	2.3	0.175	0.15	54.0
B-12	0.975	1.90	--	--	0.175	0.45	54.0
B-13	3.870	2.65	1.45	3.21	0.175	0.15	54.0
B-15	1.020	2.46	1.00	2.70	0.175	0.225	54.0
B-17	--	--	0.973	3.20	0.175	0.45	54.0
B-18	--	--	1.624	1.65	0.400	2.70	54.0
B-19	0.738	1.15	0.685	1.80	0.400	0.15	69.0
B-20	0.308	1.40	0.603	1.90	0.400	0.15	69.0
B-21	--	--	0.513	2.50	0.400	0.45	34.8
B-22	0.933	2.00	1.202	2.60	0.400	0.15	34.8
B-23	0.697	2.60	0.874	3.80	0.875	0.45	34.8
B-25	0.408	1.45	0.385	1.90	0.400	0.45	69.5
B-26	0.922	1.10	0.879	2.90	0.400	0.15	69.5
B-27	0.350	1.65	0.393	2.00	0.875	0.45	69.5
B-28	0.557	1.50	--	--	0.175	0.45	69.5
B-29	0.695	1.75	0.957	3.00	0.175	0.15	69.5
B-30	--	--	0.551	1.80	0.175	0.45	31.2
B-31	--	--	0.0894	4.10	0.875	2.70	54.0
B-32	--	--	0.475	4.30	0.875	0.45	54.0
B-33	--	--	0.1738	1.30	0.875	0.15	54.0
B-34	--	--	0.201	4.45	0.400	1.35	54.0
B-35	0.961	3.10	0.944	4.25	0.175	0.225	54.0
			Pulling tube down; thermocouple in zone				
B-24	0.277	1.70	0.524	2.20	0.400	0.15	54.0

(continued)

Table XVII (cont'd.)

Run no.	δ(zone) (cm)	L(zone) (cm)	δ(solid) (cm)	L(solid) (cm)	r (cm)	V (cm/hr)	ΔT (°C)
			Pulling tube up				
B-1	0.0277	3.04	--	--	0.400	0.45	69.0
B-3	0.0737	3.00	0.0908	3.20	0.400	1.35	69.0
B-5	0.1076	2.20	--	--	0.400	0.15	69.0
			Horizontal runs				
B-38	0.1100	1.70	0.3070	1.70	0.175	0.45	54.0
B-39	--	--	0.1221	2.50	0.175	0.90	54.0
B-41	0.0434	1.80	0.0555	1.80	0.400	0.90	54.0
			Horizontal runs; glass tube in zone				
B-37	0.0573	3.20	0.0306	2.70	0.400	0.225	54.0
B-40	0.0884	0.80	0.0674	2.00	0.875	0.450	54.0

(see Chapter IV.). Since it is the difference between the final composition and initial composition that is desired, the effect of the errors of analyses are magnified. This magnification of error may be even more severe in the calculating of δ if the separation is nearly that for perfect mixing. For example, if the final average zone concentration in a β-naphthol–naphthalene run is 7%w β-naphthol, then an error of 5% in the analyses will result in an error of 12% in the total separation, and an error of 26% in δ. These values are actually fairly typical. The values of zone length, tube radius, velocity, and mean temperature difference can be expected to have errors of about 5%, 3%, 1%, and 5%, respectively.

C. Preliminary Conclusions

At this point several of the proposed mechanisms for limitation of separation can be eliminated. It was observed that the freezing interfaces were smooth, so that no occlusion of mother liquor could have been expected to take place. Examination of the data in Tables XVI and XVII shows that, in a qualitative way, the free-convection parameters do affect the separation. Therefore adsorption on the freezing interface is not the controlling mechanism. This means that either incomplete mixing and/or constitutional subcooling are responsible for the separation limitations. The shape of the concentration profiles in Figs. 68 to 71 indicate that cyclic freezing due to constitutional subcooling was occurring.*

---

*No cyclic variation of appearance was observed in the recrystallized solid, however. In two runs in which the refrigeration unit was used there were periodic variations in the appearance of the solid. It was discovered, however, that the length (about 1 mm) of the variations corresponded to the period of cyclic operation of the compressor, (and therefore cyclic variation of coolant temperature and growth rate) which was under poor control at that time. From this, one must conclude that the variations in growth rate caused by constitutional subcooling were of a relatively high frequency, since they were not visible in the product. It is interesting to comment at this point also, that roughly the same total separations were obtained for these cyclic coolant-temperature runs as for corresponding constant coolant-temperature runs.

For the moment, however, only the total separation is under consideration. It is still an open question as to whether or not this is controlled primarily by incomplete mixing in the zone.

For the present, it is supposed that the total separation is regulated only by mixing conditions in the zone. Examination of the data in Tables XVI and XVII shows that the separation does not depend on zone length. This is most easily seen in those runs in which values for δ were calculated both from the solid concentration and the zone concentration and in which the zone size changed radically. Notice that the two values for δ in each case are about the same. Moreover, values of D_s (not shown) calculated for these runs were widely different.* Figures 65 to 71 also show that the concentration gradient is mostly confined to a region near the freezing interface. Therefore, the boundary layer results will be used for correlation purposes.

It should be noted at this point that the zone did not leak back around the cooling solid in these experiments, as some workers have observed.[98] The solid appeared to adhere well to the glass wall. As noted previously,** the recrystallized material from naphthalene-β-naphthol runs was colorless while the zones were yellowish-brown. If leakage had occurred this could have made it visible. None was observed.

D. Correlation

Preliminary Correlations

Because the majority of the data were for runs with the tube pulled down, the effect of the variables will be found by using that case. Consequently, a multiple linear-regression calculation was made for the β-naphthol–naphthalene and separately for the benzoic acid-naphthalene runs. An equation of the following form was used:

---

*This point is illustrated in the sample calculations of Appendix A.

**See Chapter II.

$$\delta = a\, L^{b}\, r^{c}\, V^{d}\, \Delta T^{e} \,. \tag{82}$$

For β-naphthol–naphthalene the constants were found to be:

$a = 0.000305 \pm 0.0005$

$b = 0.318 \pm 0.072$

$c = 0.170 \pm 0.099$

$d = -0.400 \pm 0.050$

$e = 1.41 \pm 0.29.$

For benzoic acid-naphthalene they were:

$a = 2.075 \pm 1.5$

$b = 0.063 \pm 0.123$

$c = -0.539 + 0.102$

$d = -0.239 \pm 0.082$

$e = -0.522 \pm 0.247.$

Several things that are to be noted from these results and from the data in Tables XVI and XVII are:

1. The relative separation for β-naphthol–naphthalene is much better than for benzoic acid-naphthalene. (Relative separation decreases with increasing boundary-layer thickness.)

2. Increasing the mean temperature difference decreases the separation markedly for β-naphthol–naphthalene and increases it for benzoic acid-naphthalene.

3. The boundary-layer thickness decreases with increasing velocity.

These observations can be rationalized only on the basis of free convection caused by heat and mass transfer.* The physical situation here is one with the freezing interface on the bottom of the zone. If, by some combination of temperature and concentration gradients, the density is lower at the interface than in the bulk fluid, then free convection is enhanced. The boundary layer in this case is decreased and separation increased. If, on the other hand, density is increased, free convection

*The results for a theoretical analyses of simultaneous heat and mass transfer in free convection are given in Chapter VI.

is seriously hampered. This is accentuated by the glass-tube walls surrounding the freezing interface, which make it impossible for liquid of increased density merely to slip away from the interface along a horizontal surface. These concentrations lead to the following conclusions:

(a) For these two systems, the boundary layer is enriched in the benzoic acid and depleted in β-naphthol, respectively. Density increases with increasing concentration of both of these.* Therefore, the density gradient induced by concentration is favorable to free convection for β-naphthol–naphthalene, and unfavorable for benzoic acid-naphthalene. On the other hand, the density gradient induced by the temperature drop across the boundary layer is unfavorable to free convection for both systems. Hence, the concentration density gradient is dominant, and thus we have:

$$|Gr'| > |(Sc/Pr)^{1/2}\ Gr| \quad \text{[see Eqs. (74) and (75)]}.$$

(b) The effect of the mean temperature difference on the total separation is explained by the reasoning in (a) above. The effects of temperature gradient and concentration gradient are additive for benzoic acid-naphthalene, and opposed for β-naphthol–naphthalene. Increasing the mean temperature difference between melting point and coolant temperatures naturally tends to increase the heat flow and hence the temperature drop across the boundary layer. Therefore, increasing the mean temperature difference increases separation for benzoic acid-naphthalene and decreases it for β-naphthol–naphthalene.

(c) As the velocity of zone travel increases, separation decreases. But as separation decreases, the steady-state concentration difference between bulk liquid and liquid at the freezing interface increases (since the steady-state concentration at the interface is the

---

*See Chapter III.

same for any separation, while the liquid concentration approaches w_o for decreasing separation). As the concentration difference increases, the density difference caused by it increases, the induced free convection increases, and the boundary-layer thickness decreases.

It is not certain, a priori, that the free-convection currents induced by the heater are not felt at the freezing interface. However, a multiple-regression calculation using the heat-transfer parameters calculated in Chapter V did show that, to the first approximation, their effects may be neglected in this case. It will be shown later, however, that this is not always true.

Final Correlations

On the basis of the foregoing, the following equation was used for a multiple linear regression:

$$\frac{\delta}{r} \left| \left[Sc \left(Gr' + \sqrt{Sc/Pr}\, Gr \right) \right] \right|^{1/4} = a \left(\frac{r}{L}\right)^b \left(\frac{LV}{D}\right)^c, \quad (83)$$

with r instead of L_p being used in Gr and Gr'. The last two terms are actually corrections for any mass-transfer resistance that may lie outside the boundary layer. The 1/4 power on the term in brackets is from the theoretical analyses of free convection in simultaneous heat and mass transfer discussed in the preceding chapter, Eq. (75). It appears in all laminar free-convection correlations of experimental work.[99] The present data were not sufficiently accurate, and the term in brackets was not varied widely enough, to confirm this 1/4 power, so it was taken as given.

In order to make this correlation calculation, two assumptions has to be used:

(a) In order to calculate Gr, the temperature difference across the boundary-layer must be known. The zone temperature, however, is not known. Accordingly, it was assumed that this temperature difference was proportional to the mean temperature difference, ΔT. Various values were tried for this constant of proportionality. The one giving the best results was 0.001. Needless to say this assumption will hold

only very roughly, but it is necessary to complete the calculations. This demonstrates further the necessity of assuming the 1/4 power in Eq. (83), as the term in brackets is not really known accurately because of the errors in the present assumption.

(b) No expression is available for free convection from enclosed horizontal surfaces facing up into a liquid. For open horizontal surfaces facing up into a liquid, however, empirical expressions for heat transfer are available.[99] These show that the boundary-layer thickness is about twice as large when fluid of lower density is on the bottom than when fluid of higher density is on the bottom. This is to be expected, as fluid of lower density tends to rise while fluid of higher density tends to fall. When the higher density is on the bottom, therefore, convection must occur by movement of the denser fluid along the surface away from the area where density is increased (e.g., by cooling). When this area is enclosed by vertical walls, however, the denser fluid cannot escape in this manner, and, in fact, escape in any manner would seem improbable. Indeed, in the present experiments, it was found that the boundary-layer thickness is about 10 times greater (instead of two times for open surfaces) when the density is larger on the bottom than when it is smaller. Accordingly, in order to find the best values of the constants a, b, and c, by using a linear regression calculation, the boundary layer thicknesses were divided by a constant when the liquid of higher density was on the bottom. The best value for this constant was found to be approximately 10.

With these assumptions, the values for the constants in Eq. (83) were found to be

$$a = 6.64 \pm 1,$$

for higher density liquid in bulk zone,

$$a = 66.4 \pm 15,$$

for higher density liquid on bottom, at the freezing interface,

$$b = -0.439 \pm 0.052,$$

and

$$c = -0.258 \pm 0.046,$$

where the limits shown are the 50% confidence limits (i.e., there is a

50% chance that the correct and true values for the constants lie within the specified limits).

Using these results, values of δ were calculated and compared with the experimental values in Fig. 72. Observe that the errors (deviation of points in Fig. 72 from the 45-deg line) are larger when the boundary-layer thickness is larger. This is because the errors in analyses cause greater errors in the total separation (and, hence, in the boundary-layer thickness) for small separations (and, hence, for large boundary-layer thicknesses). The average error, based on the calculated δ is 37% for 68 points (40 points for benzoic acid-naphthalene, and 28 for β-naphthol–naphthalene). Twenty-two percent of the calculated points had an error of less than 5%, 31% less than 10%, 49% less than 20%, 87% less than 50%, and 94% less than 100%. As mentioned previously, errors of over 25% are to be expected from uncertainties in the raw data. It should be noted that <u>all</u> the data obtained were used. None were thrown out. In view of the various assumptions and experimental difficulties, the correlation is believed to be a fairly good one. From this expression, it can be seen that the relative separation increases with:

(a) increasing radius
(b) decreasing zone length
(c) decreasing velocity of zone travel
(d) increasing diffusivity.

The parameters of concern were varied over the following ranges:

(a) experimental δ : 0.0313 to 3.87 cm
(b) calculated δ : 0.0356 to 0.990 cm
(c) $|Gr'/r^3|$: 1.01×10^4 to 2.06×10^5 cm^{-3}
(d) $|Sc/Pr)^{1/2}\ Gr/r^3|$: 905 to 2402 cm^{-3}
(e) (r/L) : 0.0412 to 0.921
(f) (LV/D) : 1.10 to 130.

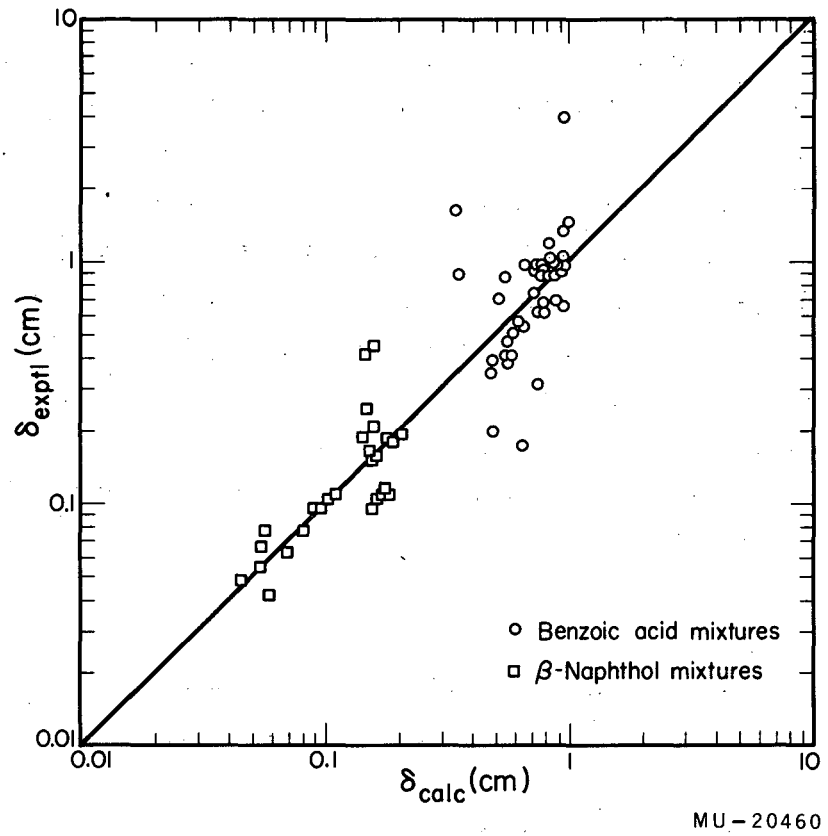

Fig. 72. Comparison of experimental with calculated boundary-layer thicknesses [Eq. (83)] for zone melting runs, with the tube pulled down and with no axial tubes or rods.

Extension of Correlation to Other Geometries

It was assumed that the form of the correlation found for vertical zone melting with the tube pulled down, holds for other geometries. Values of the constant a were calculated to make the best fit for each situation. These are summarized in Table XVIII. The value of $(Gr' + \sqrt{Sc/Pr}\ Gr)$ is taken as positive for cases where the induced density gradient aids free convection, and negative where it hinders free convection. The general form of the equation is

$$\frac{\delta}{r} = \frac{a}{|F|\ (r/L)^{0.439}\ (LV/D)^{0.258}} \quad , \tag{84}$$

where

$$F = Pr^{-1/4}\ Sc^{1/2}\ [Gr + (Pr/Sc)^{1/2}\ Gr']^{1/4} \tag{85a}$$

for $|Gr| > |(Pr/Sc)^{1/2}\ Gr'|$, and

$$F = Sc^{1/4}\ [Gr' + (Sc/Pr)^{1/2}\ Gr]^{1/4} \tag{85b}$$

for $|Gr| < |(Pr/Sc)^{1/2}\ Gr'|$.

Where the $(w_i - w_\ell)$ in Gr' is given by

$$(w_i - w_\ell) = (1/k - 1)\ w_0\ \left[1 - \exp\left(-\frac{\delta V}{D}\ \frac{\rho_s}{\rho_\ell}\right)\right] \tag{86}$$

for a constant-distribution coefficient, and

$$(w_i - w_\ell) = (\epsilon - 1)\ w_0\ \left[1 - \exp\left(-\frac{\delta V}{D}\ \frac{\rho_s}{\rho_\ell}\right)\right] \tag{87}$$

for eutectic-forming systems.

A plot of calculated δ vs experimental δ for these remaining geometries is shown in Fig. 73. An average error of about 39% was obtained, with 33% of the points having less than 10% error, 43% less than 20%, 68% less than 50%, and 95% less than 100%. The parameters of concern were varied as follows:

Table XVIII

Values of the constant a in Eq. (84) for various conditions

Condition	$(Gr' + \sqrt{Sc/Pr}\ Gr)$ > 0	$(Gr' + \sqrt{Sc/Pr}\ Gr)$ < 0
Vertical, pulling down	6.64	66.4[a]
Vertical, pulling up	6.64[a]	9.95
Horizontal	9.61	impossible
Vertical, pulling down, glass tube inside	6.24	--
Horizontal, glass tube inside	3.98	impossible
Vertical, pulling down, thermocouple inside	5.98	30.2[a]
Vertical, pulling up stainless steel tube inside	--	3.32

[a]These values are probably somewhat high because of solid-state diffusion in the benzoic acid-naphthalene runs. This is discussed further in section F2.

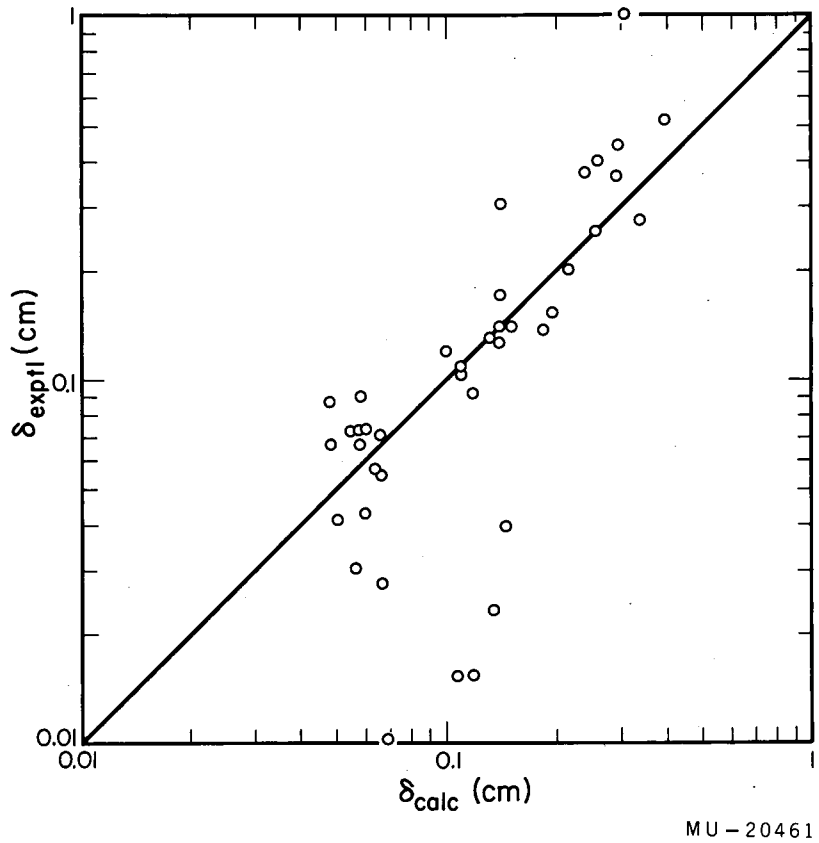

Fig. 73. Comparison of experimental with calculated boundary-layer thicknesses [Eq. (84)] for zone melting runs other than when the tube was pulled down with no axial tubes or rods in it.

(a) experimental δ : 0.0104 to 1.03 cm

(b) calculated δ : 0.042 to 0.386 cm

(c) $|Gr'/r^3|$: 9.36×10^3 to 1.75×10^5 cm^{-3}

(d) $|(Sc/Pr)^{1/2}\ Gr/r^3|$: 1.40×10^3 to 2.40×10^3 cm^{-3}

(e) (r/L) : 0.0497 to 1.09

(f) (LV/D) : 1.69 to 54.7.

Several things are to be noted from the results of this section:

(a) Nearly all the highly deviant points in Fig. 73 are for vertical runs, pulling the tube up. This is partially due to the formation of a bubble on the freezing interface (this will be discussed in greater detail shortly). It is also partially due to other experimental difficulties. These runs were the early ones in the experimental program. In several, heating tape was wound directly around the zone melting tube, which tended to cause a jerky pulling motion.

(b) Table XVIII shows that the presence of rods, or tubes, of highly conducting material increases the separation. These tubes conduct heat axially, removing it from the zone, and inducing greater-than-normal convection currents at the freezing interface. The stainless steel tube was particularly efficient in this respect.

(c) The effect of negative $(Gr' + \sqrt{Sc/Pr}\ Gr)$ is less when the tube is pulled up than down. This is due to the nature of the convection currents. The heater generates currents which rise adjacent to the outside surface and go down the center of the tube. They tend to die out, however, near the bottom interface. An experiment was performed to verify this. A very fine powder of aluminum lactate (insoluble in naphthalene) was mixed in molten naphthalene and frozen into a tube. A zone was formed in the usual manner. The powder moved with the convection currents and, in effect, made them visible. A schematic diargam of these observations is shown in Fig. 74. Therefore, it is seen that the heat input of the heater is important only in cases where either of the following are true:

(a) $(Gr' + \sqrt{Sc/Pr}\ Gr) < 0$,

with freezing at the top interface, or

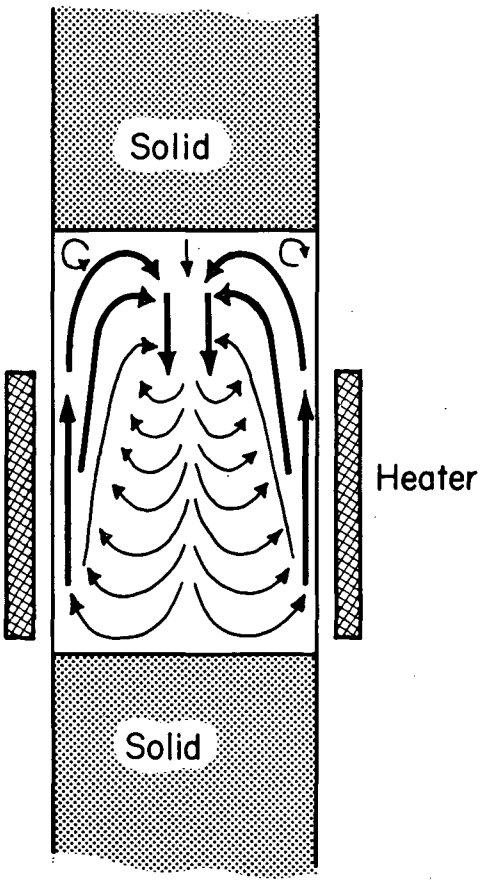

Fig. 74. Diagram of observed laminar free-convection currents in a zone of naphthalene in a 10-mm glass tube. Currents were made visible with a suspension of fine aluminum lactate powder.

(b) there is insufficient heat input to keep the bulk zone fairly well mixed, especially for very small tubes.

E. Concentration Profiles

Let us return now to the question of prediction of the concentration profile in the recrystallized solid. We have seen that the total separation is primarily a function of free convection conditions in the zone. For β-naphthol–naphthalene runs, Eq. (4) (with k_{eff} instead of k) fits the data satisfactorily. Of course $(w_i - w_\ell)$, and hence δ, and k_{eff} vary during a run. Thus Eq. (4) (using k_{eff} instead of k) is only an approximation of what one would actually expect.

For benzoic acid-naphthalene, however, the situation is different. It has already been shown that constitutional subcooling must have been occurring here, and that no method exists for predicting concentration profiles for such a situation. Empirically, however, a certain trend in the length of solid over which a separation can be discerned has been observed. If this length is designated as L_{eff} then it was found that

$$\frac{L_{eff}}{P_s}\left(\frac{\rho_s}{\rho_\ell}\right) = \frac{L_{eff}}{\int_0^\infty |\phi_s - 1|\, dz} \approx 3.89 . \qquad (88)$$

If the transition from pure component to original concentration was very sharp, this ratio would be 1.00. The average error in the ratio is 35%, but shows no trend for high or low values of L_{eff}. Needless to say the evaluation of L_{eff} is subjective and somewhat uncertain. Nevertheless, Eq. (88) is believed to be useful for semi-quantitative prediction of concentration profiles when constitutional subcooling is likely to occur. (Methods are available for prediction of this.[47])

F. Miscellaneous Experimental Difficulties

Bubble Formation

As mentioned previously, gases dissolve in molten materials. Upon freezing they are liberated. If freezing is rapid, small bubbles are entrapped in the solid. In zone melting, however, the freezing is sufficiently slow so that the gases collect on top of the zone. In vertical zone melting, pulling down, the gas bubble (nitrogen in this case) collects at the melting interface and does no harm other than to change the size of the zone as the run progresses. When the tube is pulled up, however, gas collects at the freezing interface. Fortunately, however, the bubble is small in the early part of the run when the major part of the separation is taking place. Later it tends to form bubbles or a hollow chimney in the solid. This bubble formation is believed to cause many of the large differences between calculated and experimental boundary-layer thicknesses observed for these runs. In horizontal runs the gas collects on the surface.

Solid-State Diffusion

One difficulty caused by the use of concentrated mixtures, is that at any temperature between the freezing point and melting point there is really a mixture of solid and liquid. In the solid adjacent to the melting interface this situation exists. This leads to an extraction of material of high concentration from the melting solid to the zone, thus effectively cutting down the separation. This was actually observed in separate experiments in 5-mm tubes. A zone was formed and held stationary. After a certain period, the zone and solid on both sides were analyzed. Indeed, low melting material was diffusing into the zone. After about 12 hr, equilibrium was reached and no more separation occurred. The separation was much less for β-naphthol–naphthalene than for benzoic acid-naphthalene, since the spread between melting point and freezing point is less for the former than for the latter. The data are shown in Table XIX. In zone melting, this reduces the total separation obtainable. The amount of this diffusion is small, and no method of

correcting for it is known. Consequently, it was neglected in the total-separation calculations on the preceding pages. It does make the predicted separations for benzoic acid-naphthalene somewhat conservative, however.

Table XIX

Separations by diffusion for stationary zones

Original material	Zone size (mm)	Zone concentration after			
		75 min	150 min	12 hr	24 hr
10%w β-naphthol	18	9.8	9.9	9.3	9.4
10%w benzoic acid	14	11.0	10.8	12.5	12.1

G. Conclusions

It has been shown that the total separation by zone melting depends primarily on the mixing conditions in the zone. Empirical correlations have been derived for free convection in zones of various geometries.

Especially interesting is the discovery that the location of the freezing interface makes a significant difference on the separation, and that the optimum position depends on the characteristics of the mixture being refined. Also somewhat surprising is the fact that increasing the heat input to the zone may or may not increase the separation, depending on the other parameters involved. As might be expected, running a rod of high-thermal-conductivity material through the zone increases the separation, sometimes very significantly.

A further understanding of some phenomena occurring in zone melting has been obtained. These observations may be useful as a basis for improved designs of zone-melting equipment.

VIII. EXPERIMENTAL RESULTS FOR THE COOLED-DRUM APPARATUS

A. Introduction

The purpose of the exploratory work described in this chapter was to determine the feasibility of using a modified drum-flaker for fractional crystalizations.

B. Experimental Procedure

The equipment used here has been described and shown in Chapter II. Note that in all the runs, the top edge of the stirrer was 0.55 cm lower than the bottom of the drum. In operation, the melt temperature was controlled to within 1°C. Coolant was sent through the rotating drum. When steady-state was reached, tank levels vs time were read. Calibration of tank levels vs tank volumes enabled calculation of production rates. The sampling procedure was described in Chapter IV.

Freezing tended to occur chiefly on the center 10 to 20 mm of the drum. Consequently, the width of the freezing band was also measured. Because of adhesion and subsequent freezing of the mother liquor in the drum, the freezing band was not sharply defined, however. Knowledge of the production rate, rate of drum rotation, size of drum, and width of freezing band enabled calculation of an average cake thickness. This is needed for heat-transfer calculations, and possibly for correlation of the separation efficiency.

The data for these experiments are recorded in Table XX. The parameters of concern were varied over the following ranges:

(a) concentration of melt: 0, 1, 3, and 10%w NaCl
(b) drum speed: 1/3, 1, and 3 rpm
(c) drum immersion: 0.4 to 2.45 cm
(d) stir speed: 0, 90, 360, 600 rpm
(e) melt temperature: -1.9 to 25.1 °C
(f) coolant temperature: -13.1 to -20.0 °C
(g) production rate: 0.180 to 3.580 ml/min
(h) average cake thickness: 0.060 to 0.980 mm.

Table XX

Cooled-drum apparatus data

Run no.	Initial NaCl conc. (wt %)	Drum Speed (rpm)	Drum immersion (cm)	Stir speed (rpm)	Melt temp. (°C)	Coolant temp. (°C)	Rot. reading	Prod. rate (ml/min)	Av. cake thickness (mm)	Eff. (%)	h $\left(\frac{\text{Btu}}{\text{hrft}^2\,^\circ\text{F}}\right)$
11-B	3	1/3	2.05	360	19.0	-20.0	25.4	0.270	0.180	26.0	233
13-A	3	1/3	2.20	90	24.0	-17.0	25.1	0.195	0.130	20.3	198
17-A	3	1/3	2.05	360	7.6	-18.0	25.2	1.070	0.582	8.1	364
17-B	3	3	2.15	360	14.4	-17.2	28.7	0.217	0.136	10.3	291
17-C	3	3	1.65	360	8.3	-16.9	28.8	0.750	0.205	6.6	434
17-D	3	3	1.95	0	25.1	-16.9	28.8	0.354	0.183	10.4	197
21-A	10	1/3	2.35	360	7.7	-15.9	38.5	0.180	0.130	11.0	235
21-B	10	1/3	0.45	360	6.8	-15.9	38.9	0.450	0.188	8.7	235
21-C	1	1	2.40	360	18.9	-15.6	38.9	0.322	0.126	28.0	299
21-D	1	1	0.40	360	13.1	-15.6	38.9	0.732	0.230	10.0	388
21-D	10	3	2.40	360	5.9	-16.7	38.9	0.400	0.180	0.8	273
22-E	10	3	0.55	0	17.9	-16.4	38.9	0.222	0.127	0.5	145
24-A	10	3	2.45	600	10.6	-17.8	38.9	0.214	0.142	2.0	233
27-A	3	1/3	2.35	600	16.5	-15.6	40.7	1.220	0.616	6.3	426
27-B	3	1/3	2.40	600	2.6	-15.2	40.7	3.300	0.827	10.8	670
27-C	10	1/3	2.25	600	-1.9	-15.9	40.7	2.190	0.980	0.5	369
28-A	1	1	2.15	600	7.1	-16.9	40.2	1.500	0.484	12.5	630
28-B	3	1	2.25	600	7.7	-16.9	40.2	0.692	0.377	8.0	486
28-C	3	1	0.45	600	3.7	-17.5	40.2	3.580	0.607	5.4	725
18-A	0	3	1.50	360	8.0	-18.6	9.4	--	0.066	--	350
18-B	0	3	2.00	360	14.9	-15.6	28.5	--	0.085	--	350
18-C	0	3	1.75	360	17.2	-13.1	47.5	--	0.060	--	350

C. Heat-Transfer Calculations

The heat-transfer situation here is quite complex. When the drum first dipped into the melt, it was below the freezing point of the melt. However, in this case the subcooling was not sufficient to nucleate the liquid. Consequently, freezing was propagated along the drum from the previously frozen material. Thus the first layer of solid was frozen very rapidly, and so the separation was small. This layer, however, greatly increased the thermal resistance between the coolant and the solid surface, and hence, decreased the freezing rate. Eventually steady state was reached and freezing ceased.

In the equipment used here, the situation was further complicated by the presence of the stirrer. This caused the heat-transfer coefficient from the solid on the drum to the melt to vary with position. Consequently, freezing occurred on the side of the drum away from the stirrer, melting in the region near the stirrer, and freezing again as the surface of the melt was approached. Fortunately, the thickness of the final product was observed to be almost completely independent of the speed of drum rotation. In other words, it was the steady-state thickness. In this situation (ignoring the curvature of the drum):

$$\frac{q}{A} = \frac{T_f - T_{cool}}{\frac{1}{h_{cool}} + \frac{L_{drum}}{k_{drum}} + \frac{L_{cake}}{K_{cake}}} = h_{melt}\,(T_{melt} - T_f). \qquad (89)$$

Here q/A is the heat rate per unit area transferred through the solid cake, T_f is the freezing point of the melt, T_{cool} is the temperature of the coolant (given in Table XX), T_{melt} is the temperature of the melt (given in Table XX), L_{drum} is the thickness of the drum wall (1/32 in.), L_{cake} is the thickness of the cake (given in Table XX), k_{drum} is the thermal conductivity of the drum material (stainless steel here, given in Perry[69]), k_{cake} is the thermal conductivity of the cake (given in the International Critical Tables[58]), h_{cool} is the heat-transfer coefficient between the coolant and the inside of the drum wall, and h_{melt} is the heat-transfer coefficient between the solid-liquid interface and the bulk melt.

It is known that heat-transfer coefficients for turbulent flow in pipes vary with $(DV/\nu)^{0.8}$, where D is the diameter, V is the velocity, and ν is the kinematic viscosity.[100] It is assumed here that this is also true for heat transfer in the drum. On the other hand, it was found here that (DV/ν) is proportional to the reading of the rotameter in the coolant line. This means that

$$h_{cool} = a\,(Rot)^{0.8}, \qquad (90)$$

where a is a constant of proportionality, and Rot is the rotameter reading (given in Table XX).

The raw data are shown in Table XX. Note that runs 18-A, B, and C differ only in the rotameter reading, coolant temperature, and melting temperature. Since h_{melt} depends primarily on the stirrer speed, it is, therefore, roughly the same for each run. If it is assumed to be identical for each of the three runs, this leaves two unknowns (a and h_{melt}) and three equations (data of three runs plugged into Eqs. (90) and (91)). This enabled average values for a and h_{melt} to be obtained. These were found to be 26.7 Btu/hr ft^2 ^oF and 350 Btu/hr ft^2 ^oF, respectively. If h_{melt} was taken to be the above value and substituted back into Eqs. (90) and (91) along with the data of these three runs, values of 26.8, 26.8, and 26.4 Btu/hr ft^2 ^oF were obtained for a. The small deviations of these values from the mean indicates that the foregoing assumptions are good.

From this value of 26.7 Btu/hr ft^2 ^oF for a and Eqs. (90) and (91), values for h_{melt} were calculated for all the NaCl-water runs. The results are shown in Table XX, and plotted in Fig. 75. By inspection of these, it is seen that h_{melt} increases as:

(a) The stirring speed increases.

(b) The drum speed increases.

(c) The melt level falls.

More quantitative statements are not justified because of:

(a) Adhesion and subsequent freezing of the mother liquor onto the drum and frozen product.

(b) A non uniform heat-transfer coefficient on the immersed surface of drum.

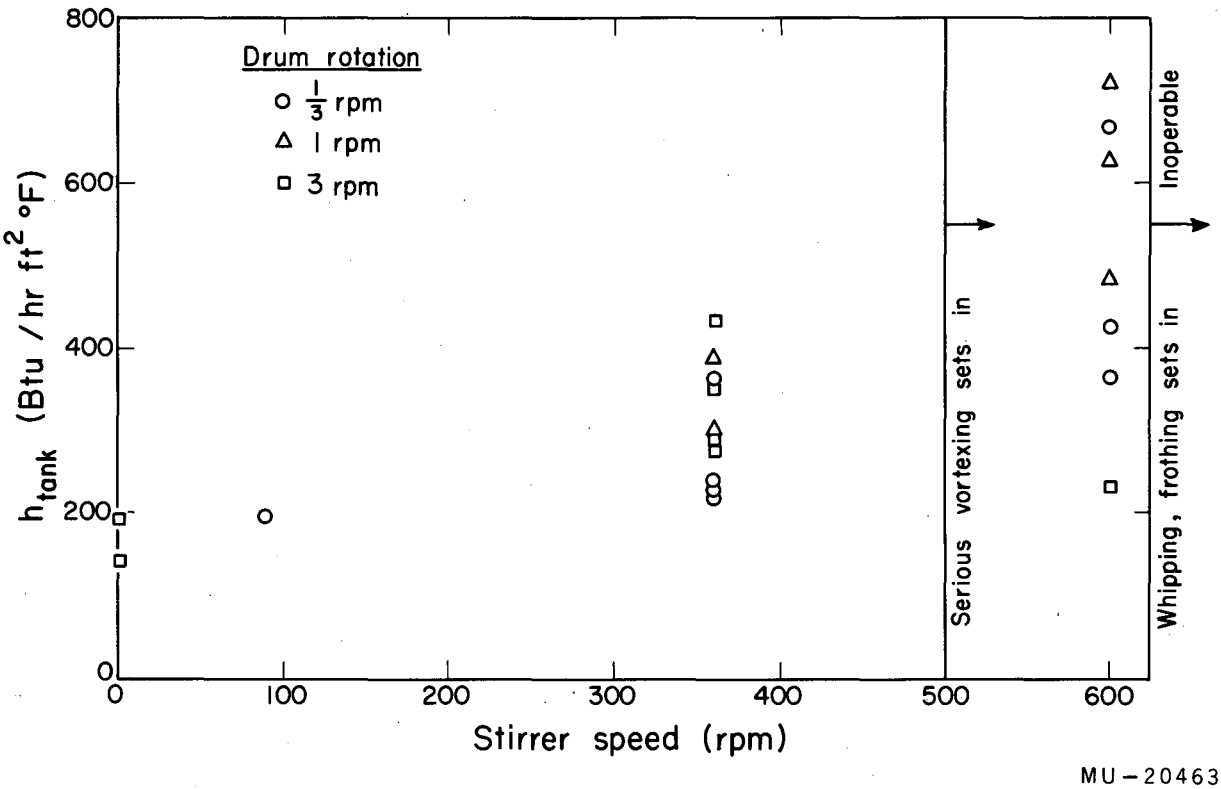

Fig. 75. Observed heat-transfer coefficients between cake surface and molten bath in NaCl-water cooled-drum experiments.

D. Separation

Ideally, salt-free ice can be obtained from salt water. Needless to say, this goal was not attained here. A stage-efficiency was defined as $(w_0 - w)/w_0$ where w_0 is the original %w NaCl, and w is the w% NaCl in the solid product. Accordingly, this was calculated for each run. The results are shown in Table XX and plotted in Fig. 76. Stage efficiencies varied from 0.5 to 28.0%. By inspection, it may be observed that efficiency increases as (a) the production rate decreases, (b) the salt content decreases, (c) stirring increases, and (d) the melt-level increases.

E. Conclusion

In this chapter, general trends were established for heat transfer and separation in the cooled-drum apparatus. As noted, several improvements would be necessary before such an apparatus could be really practical. These include: (a) a better baffle design in the drum to get uniform freezing on the surface, (b) improved mixing in the melt to get uniform heat- and mass-transfer coefficients over the drum surface, (c) prevention of adhesion of the mother liquor to the drum, perhaps by a squeegee just above the melt surface, (d) reduction of occluded mother liquor in product. Perhaps this could be accomplished by a combination of squeezing and partial-remelting of the product, as Baron did with waxes.[24] (e) Accomplishing a more uniform freezing rate around the drum. Perhaps it could be done by using several coolants at different temperatures fed into a compartmented drum with the warmest being where the drum first dips into the melt. Or perhaps it could be done by placing the stirrer near the point where the drum first dips into the melt, so as to produce a higher heat-transfer coefficient there [this would be in opposition to point (b)].

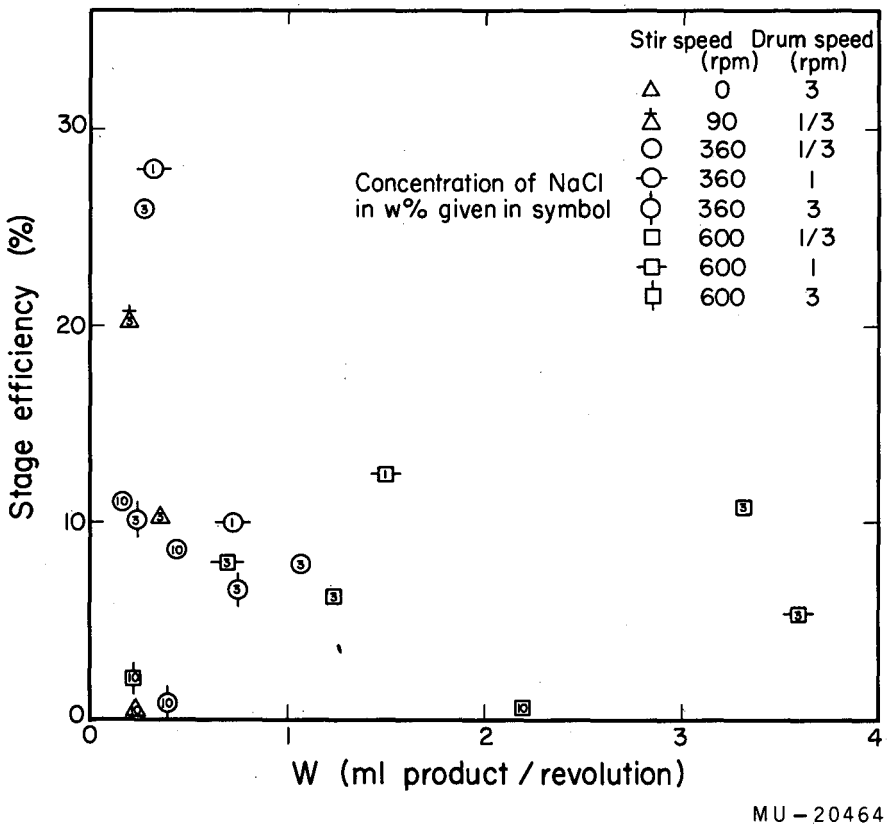

Fig. 76. Stage efficiencies in cooled-drum runs with NaCl-water.

For purposes of illustration, an example will be calculated using 10%w β-naphthol in naphthalene. Typical values for the parameters found in Chapter VII are $D = 0.1\ cm^2/hr$, $\delta = 0.05$ cm, $(\rho_s/\rho_\ell) = 1.165$, and $k = 1.85$. By trial and error, the optimum value of the zone travel rate, V_{opt}, was found to be $V_{opt} = 0.995$ cm/hr, for which $k_{eff} = 1.346$, which is considerably below the equilibrium value of 1.85.

C. Sample Design and Economic Calculations

The Problem

Roughly 550 million pounds of naphthalene are produced yearly.[101] Of this, about 430 million is crude material (melting about 78°C), selling for about 5¢/lb. About 80 million pounds of refined naphthalene (redistilled or sublimed), selling at 13¢/lb, are also produced yearly.[102] Small lots (kg.) of naphthalene recrystallized from alcohol sell for several dollars a pound. In order to determine where the cost of refining by zone-melting would fit into such a picture, calculations were made on the following hypothetical separation. The starting material is assumed to be 500,000 lb/year of 1%w β-naphthol in naphthalene, and the products are 0.1%w β-naphthol in naphthalene and 30%w β-naphthol in naphthalene.

Equipment

For a large-scale separation such as this, use of a conventional batch-type zone melter is generally impractical. Consequently, in this work it was decided to use a zone-void refiner instead. This is described in detail by Pfann.[2,4,5] Briefly, it consists of an inverted U tube with zones moving up one side and down the other. The feed stream enters the top region, which is kept in a molten state. Material flows down both legs of the tube by movement of void spaces up the legs. These void spaces are created at the bottom of each leg by the drainage of zones from the bottoms of the legs. On the leg where zones move up, each void moves by following (or, more precisely, preceding) the zone up the leg. The zone and void move together, with the material melting at the top of

the void, flowing through it into the zone, and subsequently freezing out at the bottom of the zone. On the other hand, the movement of voids in the other leg, where zones move down, is discontinuous. Each time a zone reaches a void, the void (actually a vapor space) bubbles up through the zone to the top of it. Thus, every time a zone passes a void the void moves up the leg by one zone length. When the voids reach the top of the legs and, hence, reach the feed chamber, they bubble up through the liquid feed and thereby permit more feed to enter the legs. It is seen, therefore, that the operation of a zone-void refiner is semicontinuous and multistaged, and possesses the advantages of such operations.

The most economical cross-sectional geometry for the legs of the U tube appears to be rectangular, as sketched in Fig. 77. The principal advantage of this over a circular cross section is that fewer distinct pieces of apparatus are needed for a given production rate. This is true because of the practical limitation imposed on the zone surface-to-volume ratio by heat-transfer considerations.

A diagram of the entire plant layout is shown in Fig. 78. Crude naphthalene in solid form is kept in a storage tank. From there it is melted and pumped to a series of zone-void refiners in parallel. The two product streams issuing from these are packaged, reprocessed, stored, or otherwise disposed of.

Design Considerations

To minimize production per piece of equipment, the wall spacings in the refiner should be as large as possible. From the experimental work described in Chapter VII, the upper limit is seen to be about 2 in. The zone size and interzone spacing are both approximately the same size as the wall spacing. Consequently, the wall spacing, the sum of the void space and zone size, and the interzone spacing were all taken to be 2 in. If the zones travel at the same rate in both legs, the size of the void space will be much larger in the side producing 0.1% β-naphthol than in the side producing 30% β-naphthol.*

*This is derived from a simple material balance (the production rate out each side being proportional to the void size).

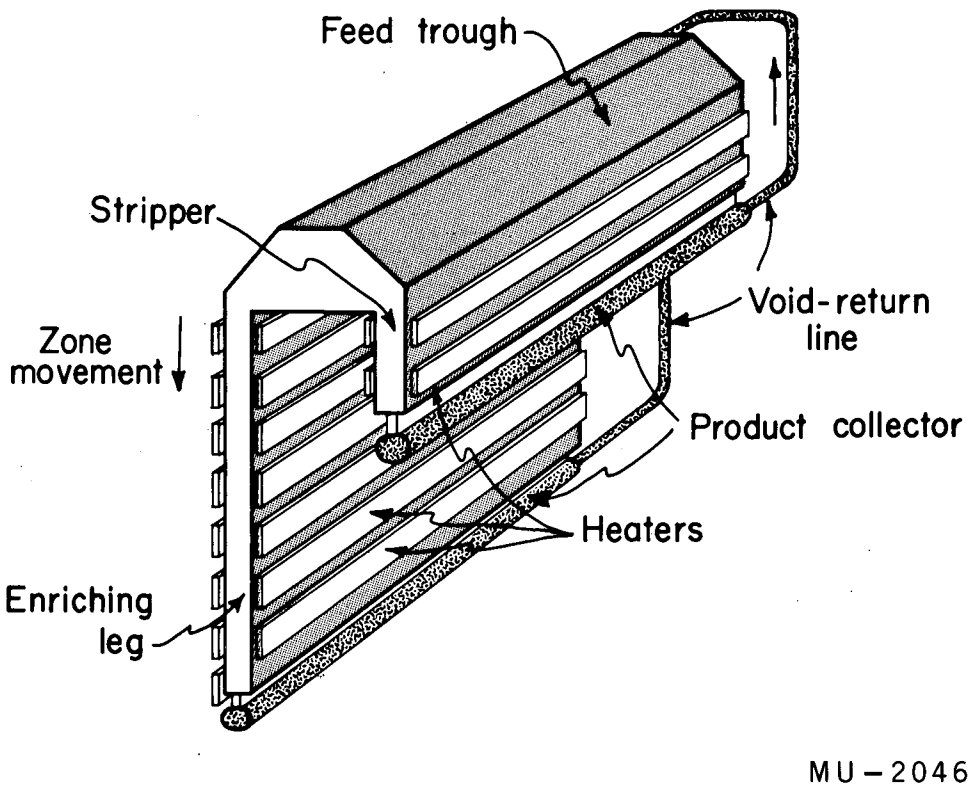

Fig. 77. Diagram of proposed zone-void refiner.

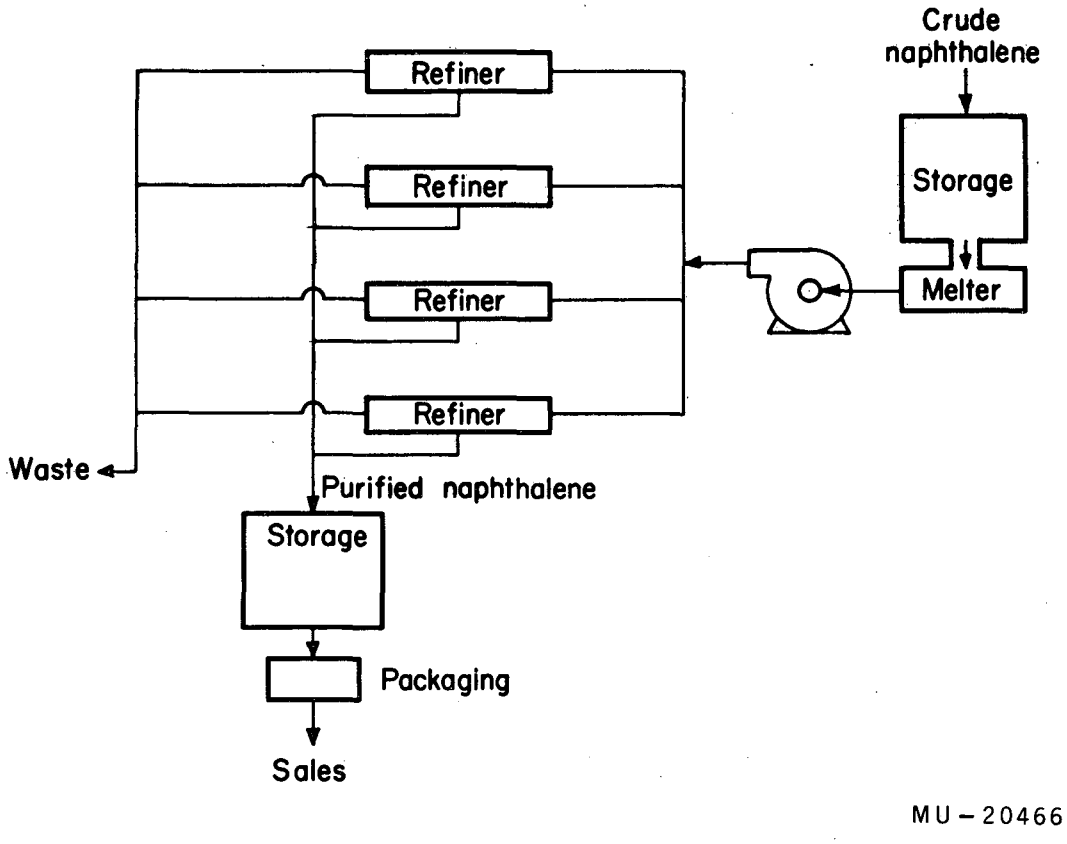

Fig. 78. Schematic diagram of proposed plant for bulk separation by zone-void refining.

The problem now is to calculate the length of the legs needed to produce the desired separation. As shown by Pfann[2] and later here, the most difficult separation to obtain is that in the leg producing 30% β-naphthol (called the enriching section). Consequently, most calculations will be carried out on it. Pfann has given the equations for the length of the legs.*

For the enriching section, the void size is negligible with respect to the zone size, and Pfann's equations reduce to

$$\frac{L_v}{L} = (k_{eff} - 1)\left[\frac{1}{\alpha} - \frac{1}{k_{eff}} \exp\ (B_e L_e/5.3)\right], \qquad (93)$$

where L_v is the void length, L is the zone length, α is the separation ratio (which is 30 here), L_e is the length of the enriching section, and B_e is given by $\exp\ (B_e L) \doteq 1 + B_e\ L/k_{eff}$.

For a given L_e it is desirable to maximize the production rate from a single unit. The production rate is proportional to

$$\frac{L_v}{L} = (k_{eff} - 1)\ VA, \qquad (94)$$

where

$$A = \left[\frac{1}{\alpha} - \frac{1}{k_{eff}} \exp\ (B_e L_e/5.3)\right].$$

This parameter was calculated for L_e = 40 in., 60 in., 80., and 120 in. by using δ = 0.05 cm,** and D = 0.1 cm^2/hr. The results are plotted vs δ V/D in Fig. 79. Notice how sharp the peaks are.

---

*These equations are reproduced in Appendix B.

**This was chosen from Table XVI as a typical value for the boundary-layer thickness with 10%w β-naphthol. Since the conditions here (metallic walls, rectangular cross sections, 2-in.-wide zones) are not at all the same as those investigated experimentally in Chapter VII (glass walls, circular cross section, 1-in.-zones), the value of δ is rather uncertain. Because it was not deemed profitable to make an approximate and questionable calculation of δ merely for purposes of cost estimation and illustration of design procedures, the value of 0.05 cm is only a guess.

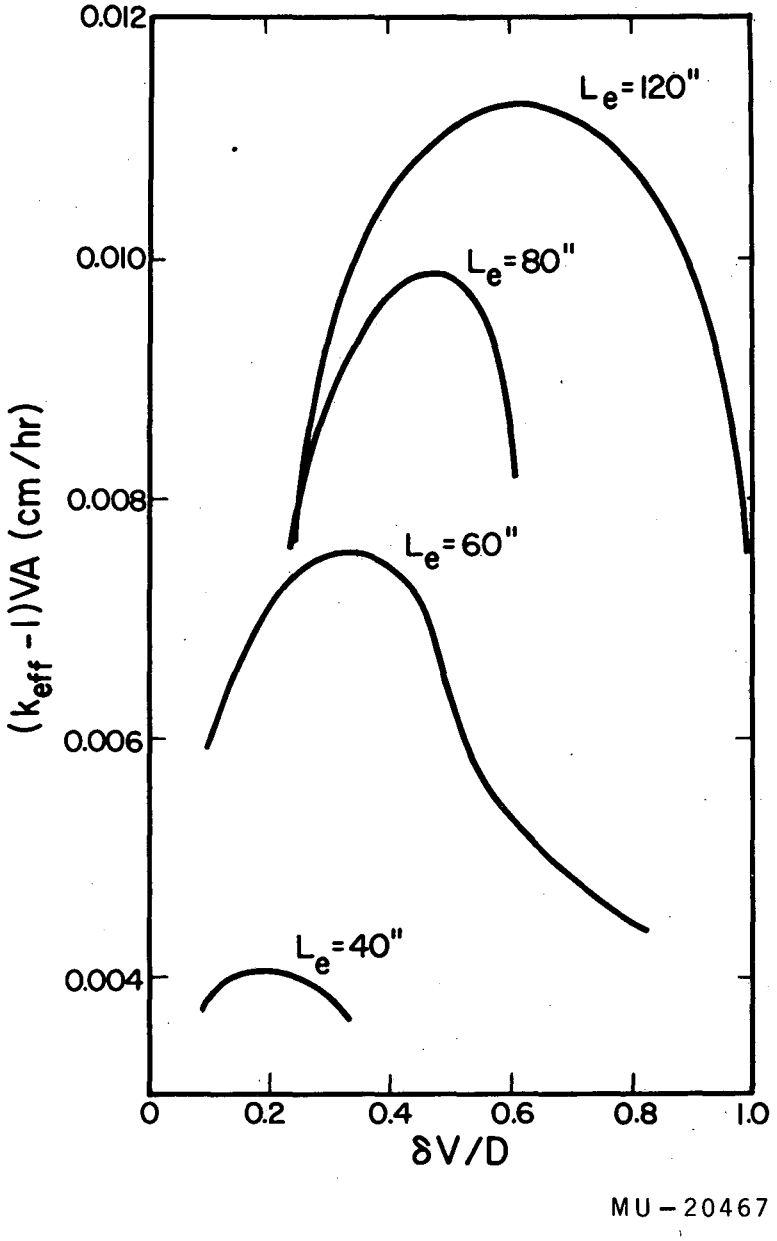

Fig. 79. Relative production rate per zone-void refiner. $(k_{eff} - 1)$ V A vs δ V/D, for δ = 0.05 cm.

From an economic standpoint, it is also desirable to minimize the capital expenditure of the whole plant. It is therefore assumed that the cost is proportional to (no. units) x (size of each unit)$^{0.8}$. Use of the usual 0.6 power[103] is not justified here, since the cost per unit will also decrease as the number of units increases. On the other hand, savings are made in larger units since the cost of the feed chamber and pulling device does not vary appreciably with size. A 0.8 power is felt to be a good compromise. In any case, the above expression is also seen to be proportional to

$$(L_e)^{0.8}/(k_{eff} - 1)\ VA.$$

Accordingly, the results of the preceding calculations were used to calculate values of $(L_e)^{0.8}/(k_{eff} - 1)$ VA *vs* L_e. These are plotted in Fig. 80. Note here that the peak (or valley) is not sharp. The optimum leg length was found to be 84 in., which corresponds to 21 zones. Consequently, the optimum design features were found to be:

L_e = 84 in.
no. zones = 21
δ V/D = 0.478
V = 0.821 cm/hr
k_{eff} = 1.399
L_v = 0.0253 in.

Note how close the velocity is to the optimum found earlier for a single zone-melting pass (0.995 cm/hr).

From these results and the equations of Pfann* the calculated sizes for the leg producing 0.1%w β-naphthol (called the stripping section) are 0.815 in. for L_v and 2.47 in. for L_s. Note that the length of the stripping section (which is $L_s + L_v + L$ here) is negligible compared to the length of the enriching section.

From the above results, the calculated total length of the refiner needed to process 500,000 lb/year of crude naphthalene is 1100 ft. If each refiner is 20 ft long, 56 refiners would be required (allowing for one extra).

*See Appendix II.

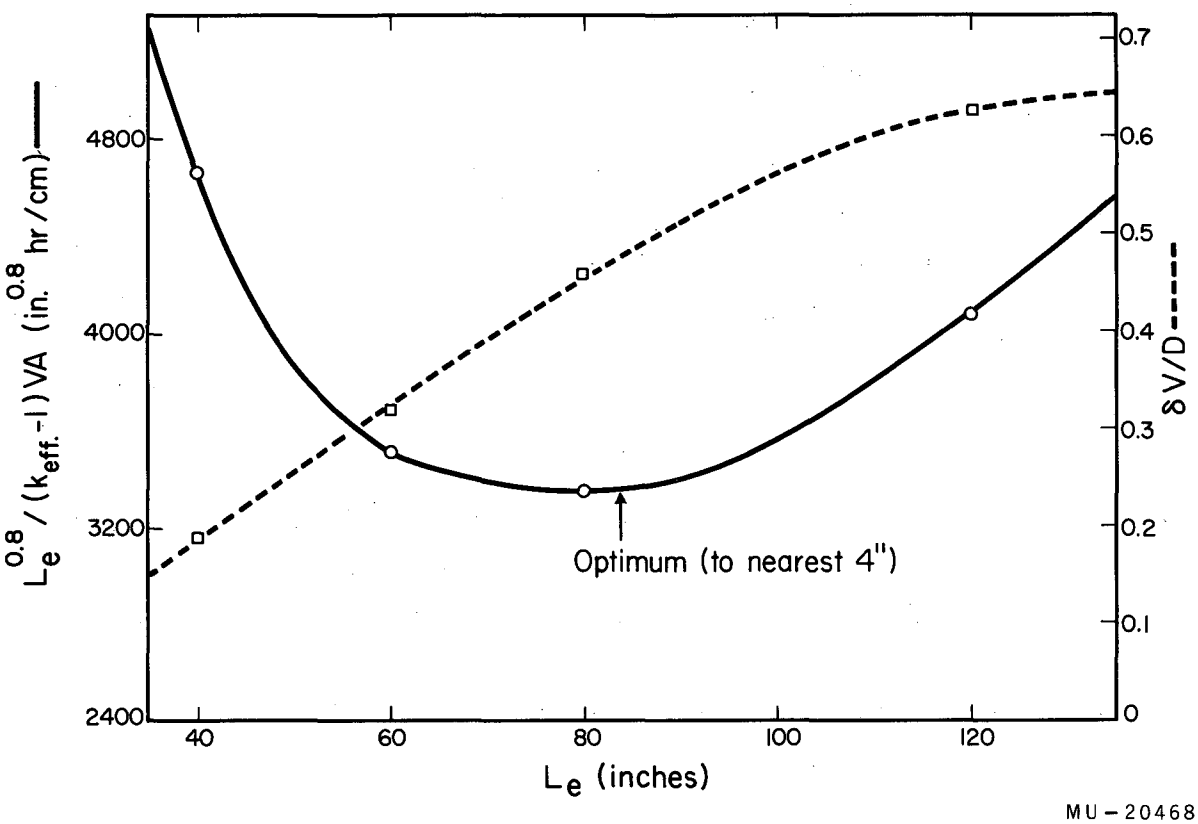

Fig. 80. Relative minimum capital investment necessary for a given production rate of a zone-void refiner. $(L_e)^{0.8}/(k_{eff} - 1)$ V A vs L_e, for δ = 0.05 cm.

Cost Estimation

From the foregoing results, and by the methods of Chilton[104] and Zimmerman and Lavine,[103] costs were calculated for this separation. The detailed calculations are shown in Appendix 6. The results are summarized below:

Installed cost of one refiner	:	$24,100
Total installed equipment cost	:	$1,366,410
Total physical cost	:	$2,190,000
Total project cost	:	$3,940,000
Total capital necessary	:	$4,085,250
Annual cost	:	$1,380,000
Cost per lb. crude naphthalene	:	$2.76.

This shows that zone melting, as described, is too expensive for bulk separation of cheap organic chemicals. However, for small-lot purification of some chemicals, it would be competitive.

Notice, however, that reduction of the boundary-layer thickness would greatly reduce this cost. For a given value of δ V/D and hence k_{eff}, V is incersely proportional to δ. But the production is inversely proportional to V at a constant value of k_{eff}. Therefore, cost goes down almost proportionately to the boundary-layer thickness. New ideas for reduction of boundary-layer thickness are presented in the following chapter.

X. CONCLUSIONS AND RECOMMENDATIONS

At the end of each chapter, specific conclusions concerning the subject of that chapter were made. These are summarized on the following pages. All nomenclature has been introduced previously and is summarized in the table of NOMENCLATURE.

A. Heat Transfer in Zone Melting

The variety of heaters applicable to zone melting is limited only by the worker's ingenuity and imagination. Before making heat-transfer calculations, the size of the zone, size of the tube, rate of zone travel, materials of construction, and heater type and dimensions must be known from other considerations. If these are known, the heater power consumption and position of the zone relative to the heater may be calculated as follows:

1. The axial heat flow out of both ends of the zone is first calculated. An analysis of heat transfer in a moving solid -- such as there is in zone melting -- is shown in Chapter V. The solid-liquid interfaces are safely assumed to be at the freezing point of the material being processed. For a first approximation, the zone is assumed to be equally distributed on both sides of the heater.

2. The heater input to the zone is calculated by noting that the sum of these heat losses is equal to the difference between this heat input and the radial heat loss to the surroundings from the portion of the zone not covered by the heater. [See Eq. (7)]. The size of the heater determines the area available for heat loss to the surroundings, and therefore the necessary heater input to the zone. The zone can be considered to be at the melting point of the material being processed.

3. If the tube is vertical, the position of the zone relative to the heater is calculated from

$$\frac{L_{ch}}{L} = -0.0136 + 0.054 \left[\frac{r\, Q_{tot}}{L\,(q_t + q_b)}\right]^{1/4} . \qquad (25)$$

From this it is seen that L_{ch}, the distance of the upper surface of the zone to the center of the heating surface adjacent to the zone, increases as the length of the zone increases, the radius of the zone's container increases, and the heat out of both ends of the zone decreases.

If the tube is horizontal, the zone will be approximately equally distributed on both sides of the heater. These statements are true only for relatively low rates of zone travel (less than 1 in./hr). For increasing rates of zone travel, the zone will shift with respect to the heater increasingly in the direction of zone travel.

4. If the new zone position affects the heat fluxes, they should be recalculated by repeating steps 1, 2, etc.

5. Based on the heater design the fraction of heater power that is absorbed by the zone is calculated. From this and the previously calculated heater input to the zone, the total necessary heater power is calculated.

An example of this calculation method is given at the end of Chapter V.

B. Total Separation in Zone Melting*

The total separation effected by a single zone pass down a very long, initially uniform charge was found to depend primarily on the equilibrium relations and on the mass-transfer conditions. Two limiting mass-transfer conditions were examined here -- (a) pure diffusional mass transfer, and (b) complete mixing in the bulk zone with only molecular diffusion in the boundary layer at the freezing interface. The mass transfer occurs purely by molecular diffusion only for capillary tubes (less than 4 mm i.d.) under conditions where convection is hindered.

---

*By total separation is meant the total mass in g/cm^2 of the concerned component that has been removed from, or added to, a solid rod (and, hence, added to, or removed from, the zone) of unit cross-sectional area.

Pure Diffusional Mass Transfer

The total separation, $P\, w_o\, \rho_\ell$, is

$$P\, w_o\, \rho_\ell = \int_o^\infty |w_s - w_o|\, \rho_s\, dz = \int_o^L |w - w_o|\, \rho_\ell\, dx = \frac{w_o(1-e^{-p})}{P} L\, \rho_\ell \left|\frac{1-k}{k}\right| \quad (95a)$$

for a constant distribution coefficient, and

$$P\, w_o\, \rho_\ell = \int_o^\infty |w_s - w_o|\, \rho_s\, dz = \int_o^L |w - w_o|\, \rho_\ell\, dx = \frac{w_o(1-e^{-p})}{P} L\, \rho_\ell \left|\frac{e}{w_o} - 1\right| \quad (95b)$$

for eutectic-forming mixtures.

It is seen therefrom, that when no convection takes place the separation increases as:

(a) The length of the zone increases

(b) The velocity of zone travel decreases

(c) The molecular diffusivity increases

(d) The ratio of solid density to liquid density decreases

(e) The liquid density increases

(f) The absolute difference between the initial concentration and the steady-state concentration in the liquid at the freezing interface (e for eutectic-forming mixtures and w_o/k for constant distribution coefficient) increases.

Boundary-Layer Condition, with Free Convection

Under most free-convection conditions the bulk of the zone is well-mixed and the total separation is:

$$P\, w_o \rho_\ell = L\, w_o \rho_\ell \exp\left(-\frac{\delta\, V\, \rho_s}{D\, \rho_\ell}\right) \left|(1/k) - 1\right| \quad (96a)$$

for a constant distribution coefficient, and

$$P\, w_o \rho_\ell = L\, w_o \rho_\ell \exp\left(-\frac{\delta\, V\, \rho_s}{D\, \rho_\ell}\right) \left|(e/w_o) - 1\right| \quad (96b)$$

for eutectic-formers.

The boundary-layer thickness, δ, was correlated by:

$$\frac{\delta}{r} = \frac{a}{|F|\, (r/L)^{0.44}\, (LV/D)^{0.26}}, \quad (84)$$

where $F = Pr^{-1/4} Sc^{1/2} [Gr + (Pr/Sc)^{1/2} Gr']^{1/4}$

for $|Gr| > |(Pr/Sc)^{1/2} Gr'|$, and (85)

$$F = Sc^{1/4} [Gr' + (Sc/Pr)^{1/2} Gr]^{1/4}$$

for $|Gr| < |(Pr/Sc)^{1/2} Gr'|$,

and where the $(w_i - w_\ell)$ in Gr' is given by

$$(w_i - w_\ell) = [(1/k - 1)]w_o \quad [1 - \exp (- \frac{\delta V}{D} \frac{\rho_s}{\rho_\ell})] \tag{86}$$

for a constant-distribution coefficient, and

$$(w_i - w_\ell) = (\epsilon - 1)w_o \quad [1 - \exp (- \frac{\delta V}{D} \frac{\rho_s}{\rho_\ell})] \tag{87}$$

for eutectic-formers. The values of the constant, a, are given in Table XVIII for various situations.

From the above it is seen, qualitatively, that the total possible separation in one zone pass, with free convection, increases as:

(a) the length of the zone increases
(b) the absolute difference between original concentration and steady-state concentration in the liquid at the freezing interface (e or w_o/k) increases
(c) the molecular diffusivity increases
(d) the zone travel rate decreases
(e) the ratio of solid density to liquid density decreases
(f) the liquid density increases
(g) the radius of the tube increases
(h) the kinematic viscosity decreases
(i) the acceleration, g, increases
(j) the absolute difference in the densities of bulk fluid and freezing interfacial liquid increases.

The separation also increases when liquid of greater density (between the bulk zone and liquid at the freezing interface) is produced on top of liquid of lesser density. Table XVIII also shows that insertion of an axial rod or tube of high thermal conductivity into the zone increases the separation.

C. Concentration Profiles in Zone Melting

Pure Diffusional Mass Transfer

If constitutional subcooling* is not significant, the concentration profile resulting from a single zone pass of an initially uniform charge is given by Eq. (64), for pure diffusional mass transfer with a constant distribution coefficient. The profile may be approximated by a plot of the type illustrated in Fig. 59. The various parameters necessary to make such a plot are given in Figs. 60, 61, and 62. For eutectic-forming systems, the profile is given by

$$w_s = 0 \text{ for} \tag{97a}$$

$\tau \leq \tau_0$, and

$$w_s = w_0 \{ 1 - \exp [- (\tau - \tau_0) q] \} , \tag{97b}$$

for $\tau \geq \tau_0$ where

$$1/q = (\epsilon - 1) \left[(1 - e^{-p}) - \left(\frac{\epsilon - 1}{\epsilon}\right) \left\{ 1 - \exp \left[-\left(\frac{\epsilon}{\epsilon - 1}\right) p \right] \right\} \right], \tag{56}$$

and

$$\tau_0 = \frac{(\epsilon - 1)^2}{\epsilon} \left\{ 1 - \exp \left[- \left(\frac{\epsilon}{\epsilon - 1}\right) p \right] \right\}. \tag{57}$$

This says that the distance down a charge that appreciable separation occurs increases as:

(a) the velocity of zone travel decreases
(b) the molecular diffusivity increases
(c) the ratio of solid density to liquid density decreases
(d) the length of the zone increases
(e) the absolute difference in original concentration and steady-state interfacial concentration increases.

*Described in Chapters I and III, and references 47 to 52.

Free-Convection Mixing

With the boundary-layer condition and negligible constitutional subcooling, the concentration profile resulting from one zone pass is given by

$$\frac{w_s}{w_0} = 1 - (1 - k) \exp(- k \frac{z}{L} \frac{\rho_s}{\rho_\ell}) \tag{4}$$

for a constant distribution coefficient, and approximately by

$$w_s = 0$$

$$\text{for} \quad z < L \frac{\rho_\ell}{\rho_s} (\frac{e}{w_0} - 1) \exp(- \frac{\delta V}{D} \frac{\rho_s}{\rho_\ell}) \text{, and} \tag{98a}$$

$$w_s = w_0$$

$$\text{for} \quad z > L \frac{\rho_\ell}{\rho_s} (\frac{e}{w_0} - 1) \exp (- \frac{\delta V}{D} \frac{\rho_s}{\rho_\ell}) \text{,} \tag{98b}$$

for eutectic-forming systems. The actual distribution for eutectic-forming systems will, of course, not have quite this sharp a transition from $w_s = 0$ to $w_s = w_0$, but the exact profile is not known for the above conditions.

Constitutional Subcooling

If constitutional subcooling is appreciable and causes cyclic freezing, the actual concentration profiles will be smeared out more than the foregoing predicts. That is, the initial separation will be smaller but will not taper off as fast as the zone moves down the rod. No method exists, at present, for predicting concentration profiles when constitutional subcooling is important. An estimate for eutectic-forming systems may be obtained from the empirical observation made in Chapter VII that:

$$\frac{L_{eff}}{P_s} (\frac{\rho_s}{\rho_\ell}) \approx 3{,}89, \tag{88}$$

where $w_s = 1$ for $z \geq L_{eff}$.

D. Economics of Industrial-Scale Zone Refining

Optimum Velocity for a Single Pass

When the boundary-layer assumptions hold, and when a single zone is passed through a long, uniform charge, the maximum purification per unit time is obtained when the zone travel rate is given by

$$\left(\frac{\delta V_{opt}}{D}\right)\left(\frac{\rho_s}{\rho_\ell}\right)\left[1 + \frac{1}{k + (1-k)\exp\left[-\left(\frac{\delta V_{opt}}{D}\right)\left(\frac{\rho_s}{\rho_\ell}\right)\right]}\right] = 1. \qquad (92)$$

From this it is seen that the optimum rate of zone travel increases as:

(a) the molecular diffusivity increases

(b) the boundary-layer thickness decreases

(c) the ratio of solid density to liquid density decreases.

However, caution must be observed in determining the optimum rate because the typical rates of zone travel approach that where dendritic growth may be expected. Dendritic growth, of course, will decrease the separation. Therefore the above velocity is actually an upper limit to the optimum velocity, and is the optimum only if growth imperfections, such as dendritic growth, do not occur.

Industrial Equipment

The zone-void refiner,* being continuous (or, at least, semi-continuous) and multistaged, is preferable to ordinary zone melting. A practical cross section for the legs of the refiner is 2 in. wide by 20 ft long, with 2-in. zones and zone spacings. Sketches of such a refiner and (or) a plant layout for utilizing it are shown in Figs. 77 and 78. For separating 500,000 lb/yr of 1%w β-naphthol in naphthalene into 0.1%w and 30%w β-naphthol, a cost of about $2.80 per lb of feed was estimated. This is definitely too expensive for cheap industrial chemicals, but is satisfactory for specialty chemicals or ultrahigh

*This is described in Chapter IX and references 2, 4, and 5.

purification. The total capital necessary for such a plant was estimated to be about $4,000,000. These costs are roughly proportional to the boundary-layer thickness, which indicates the possible economic advantage of reducing this factor.

E. Cooled-Drum Apparatus

A cooled-drum fractional crystallizer* successfully performed a partial separation of mixtures of NaCl and water. Stage efficiencies of nearly 30% were obtained (see the data of Table XX and Fig. 76). It is believed to have commercial possibilities, but needs considerable engineering work to make it a practical reality. The qualitative effects of various operating parameters are discussed in Chapter VII.

F. Recommendations for Future Work

Reduction of Boundary-Layer Thickness

In the economic calculations it was shown that the cost of separating by zone melting drops rapidly with decreases in boundary-layer thickness. In this work it has already been found that the boundary-layer thickness may be reduced by proper choice of conditions and by use of highly conductive materials running axially through the zone. Aside from various methods of physically stirring the zone, the following methods for increasing mixing are recommended for investigation:

(a) Rotate the tube. Centrifugal forces should magnify free-convection effects.

(b) Vibrate the tube, perhaps ultrasonically.

Other Systems

The experimental work on zone melting described in this report was confined to two organic systems. In order to test the general

*This is described in Chapters I and VII, and references 2 and 24.

validity of the results, it is necessary to try other systems. Use of systems with different physical properties would be particularly valuable. For example, low-melting metal alloys would seem to be ideal.

Development of Cooled-Drum Apparatus

Further studies and engineering improvements should be made on the cooled-drum apparatus. It is strongly felt that this equipment has commercial possibilities for cheap separation of bulk materials.

ACKNOWLEDGMENTS

The encouragement, advice, and helpful suggestions of Professor C. R. Wilke throughout this work are gratefully acknowledged. The advice of Professor T. H. Chilton on the economics and design was much appreciated.

The author thanks Professors Wilke, Chilton, and Brewer for reviewing the rough draft of this report.

I especially appreciate the encouragement and the efforts put forth by my wife, Lorraine, during the course of this work. Her help in editing and typing the rough draft was invaluable.

The development of the analytical methods and the performance of the multitude of routine analyses were accomplished by the Analytical Group of the Nuclear Chemistry Division, Lawrence Radiation Laboratory, Berkeley. Thanks are particularly due Mrs. Ursula Abed, who performed the bulk of the analytical work.

The machine work on the experimental equipment was expertly handled by the Accelerator Technicians. The creative suggestions of Mr. G. G. Young on equipment design and construction were especially valuable.

I am indebted to Professor Acrivos for providing the transformation that made possible the analytical solution of the problem of pure diffusional mass transfer in zone melting.

The author is grateful for the financial support provided by fellowships from the General Electric Foundation, the National Science Foundation, and the Dow Chemical Company.

This work was performed under the auspices of the United States Atomic Energy Commission.

APPENDICES

A. Sample Calculation of Experimental Boundary-Layer Thickness

In Chapter VII the method of calculating effective boundary-layer thicknesses from the experimental data for zone melting was described. This method is illustrated by an example calculation on the following pages. The run discussed here is N-44, a β-naphthol–naphthalene run with an initial composition of 10%w β-naphthol. The experimental concentration profile is shown in Fig. 65. The experimental data are V = 0.15 cm/hr, L = 1.2 cm at the end of the run, and L = 2.65 cm at the beginning of the run. The analyses are shown in Table XXI. From this we have

$$P_z = \Sigma\,(1 - w/w_0)\,\Delta Z = 0.372 \text{ cm}$$

$$P_s = \Sigma\,(w_s/w_0 - 1)\,(\rho_s/\rho_\ell)\,\Delta Z = 0.87 \text{ cm},$$

$$\frac{V\,\delta}{D}\,(\rho_s/\rho_\ell) = \ln P/L\,(1 - 1/k) = \ln \frac{0.372}{1.2\,(1 - 1/1.85)} = 0.395 \qquad (78)$$

for the zone, and

$$\frac{V\,\delta}{D}\,(\rho_s/\rho_\ell) = \ln \frac{0.87}{2.65\,(1 - 1/1.85)} = 0.336$$

for the solid.

Therefore, with D = 0.1036 cm^2/hr and (ρ_s/ρ_ℓ) = 1.172, there is obtained δ = 0.198 cm for the zone and 0.169 cm for the solid.

On the other hand, values of $p = LV/D\,(\rho_s/\rho_\ell)$ may be calculated from

$$P = (1 - 1/k)\,L\,\frac{1 - e^{-p}}{p}\,, \qquad (80)$$

from which, by trial and error, the following results, p = 0.854 for the zone and 0.712 for the solid. From this, there yields

$$D = (1.2)(0.15)(1.172)/(0.854) = 0.247 \text{ } cm^2hr$$

for the zone, and

$$D = (2.65)(0.15)(1.172)/(0.712) = 0.654 \text{ } cm^2/hr$$

for the solid.

Table XXI

Analyses of portions of product of run N-44

Estimated z (cm)	Analyses (%w β-naphthol)	Corrected composition (%w β-naphthol)
Standard 10%w sample	9.50	10.0
-0.3 to 0.15	11.40	12.00
0.15 to 0.6	15.25	16.06
0.6 to 1.2	13.51	14.21
1.2 to 1.8	11.11	11.70
1.8 to 2.1	10.24	10.75
10.1 to 10.7 (zone)	6.67	7.03
10.7 to 11.3 (zone)	6.52	6.86
11.3 to 12.3 (bubble)	---	---
12.3 to 12.5	9.48	9.99

These results, typical of those for the other zone-melting runs, demonstrate that the boundary-layer approach definitely gives better results than the pure diffusional mass-transfer approach (since the δ values calculated from zone and solid concnetrations are much closer than the D values).*

*If the D values had been close together, it would not matter, insofar as the usefulness of the approach is concerned, if they were far from the actual D. In such a case these "effective" diffusion coefficients could have been correlated vs the other parameters of importance.

B. Pfann's Equations for Zone-Void Refiners

Pfann has derived the following approximate equations at steady-state for the leg lengths in a zone-void refiner.[2,4,5]

Enriching Section

The enriching section is that leg of the zone-void refiner in which the zones are moving up. The section length (minus about one zone and one void length) is given by

$$L_e = \frac{1}{(0.434)\, B_e} \log \left[\omega \left(\frac{\psi}{\alpha} \right) - 1 \right] , \qquad (99)$$

where α is the enrichment ratio -- the ratio of concentration of "enriched" product to concentration of feed; $(h-L) = L_v$, the void length; B_e is given by $\exp (B_e h) = 1 + B_e L/k_{eff}$,

$$\omega = \frac{k_{eff}}{(1 - k_{eff})\, B_e L} \left[1 - \exp B_e (h-L) \right] ,$$

and

$$\psi = \frac{(h\, k_{eff} - L)}{(h - L)} .$$

Stripping Section

The stripping section is that leg of the zone-void refiner in which the zones are moving down. The section length (minus one zone length and the sum of all the void lengths in the section) is given by

$$L_s = \frac{1}{(0.434)\, B_s} \log \left[\left(\frac{\beta\, \delta - k_{eff}}{\gamma} \right) + 1 \right] , \qquad (100)$$

where

$$\delta = k_{eff} \left(L_v/h \right)^{1 - k_{eff}} ,$$

$$\gamma = \frac{B_s \left[L_v - h \left(1 - k_{eff} \right) \right]}{1 + B_s h - \exp \left(B_s h \right)} ,$$

B_s is given by: $\exp (B_s L) = 1 + B_s h/k_{eff}$.

In general, L_v, h, and L are not the same in the two sections, and k_{eff} is about the same if the zone travel rate is the same in both sections (as generally it is).

C. Economic Calculations

Following are the detailed economic calculations mentioned in Chapter IX. The cost estimation methods and data of Chilton[104] and of Zimmerman and Lavine[103] were used. The cost data from these sources were brought up to date by use of the ENR index (820 now).[105]

Cost of a Single Refiner and Accessories

The Unit

In Chapter IX the dimensions of the refiner were found to be L_e = 84 in., L_s = 2.5 in., zone width = 2 in., and refiner length = 20 ft. A sketch of the refiner is shown in Fig. 77. For corrosion resistance, stainless steel was chosen as the construction material. The dimensions of the unit require about 400 ft^2 of 1/8-in. sheet metal. The cost of the sheet is about 50¢/lb (ENR index = 480).[103] The cost of fabrication and erection is estimated to be roughly twice this (it would be more if only one used were to be constructed, but 56 are required, which provides the economies of near mass production). With a specific gravity of 7.7 for steel,[70] the cost for a refiner is estimated to be:

$$3 \left[\frac{(400)(7.7)(62.4)(0.50)}{(8)(12)} \right] \frac{(820)}{(480)} = \$4,970,$$

which, rounded off, is $5,000.

Heaters

These are about 1-in. wide and 20 ft long and are either the electrical-resistance or steam type. Fourty-four are needed, with two for each zone. If the material cost for each is guessed to be $120, and 10 hr of labor at $10/hr is required to fabricate each one, the cost per heater will be about $220. This assumes that the system is well insulated so that the heat requirements are kept to a minimum. The cost of insulation will be estimated later. The total cost for 44 heaters is, therefore, $9,670. Including a cost of about $300 for the feed-trough heater, this is a total of about $10,000.

Pulling Mechanism

This connects the motor (see below) to the heaters and pulls them alternately up and down (slowly in the direction of zone travel, rapidly one zone length in the opposite direction to pick up the next zone from the adjacent heater). The cost of the instrumentation regulating this mechanism is estimated later, along with the other instrumentation costs. Chilton gives an installed cost of $500 \frac{820}{400} = \$1,025$ for a 1-hp-motor reducer. The present system, being considerably more complex than this, can be expected to cost several times this amount. Consequently, a material cost of $1,000 and a construction time of 40 hr at $10/hr is estimated. This gives a total of $5,000.

Motors

A 1-hp synchronous motor is needed to power the pulling mechanism. It must be synchronous in order to provide a definite, constant speed. According to Chilton, the installed cost is estimated as $310 \frac{820}{400} = \$635$. A 1/4-hp motor is also needed to provide mild stirring in the feed trough (although, if convection currents were sufficient, this would be unnecessary). This is similarly estimated to cost, installed, about $595, giving a total motor cost of $1,230.

Blowers

In the immediate vicinity of the unit some mechanism is needed to remove the heat liberated by the heaters. Free convection along with the building ventilation system would probably be sufficient. For purposes of this estimate, however, it is assumed that four 1/4-hp blowers for each unit are also needed. For the installed cost, Chilton gives $(4)\ (350)\ \frac{820}{400} = \$2,870$. By adding the above, the total installed cost per unit is found to be $24,100.

Total Installed Equipment Cost

Refiners

Fifty-six refiners are required at $24,100 each, for a total cost of $1,350,000.

Storage Tanks

Two 1,000-gal storage tanks are required for the storage of approximately one week's supply of feed and product. Their cost is given by Chilton as $2\ (830)\ \frac{820}{400} = \$3,410$.

Solid-handling equipment, and melter:

Equipment is necessary to transport the feed, which will most likely be a solid, to the refiners. The most convenient method to do this is to melt it and let it flow by gravity feed through steam-traced pipes to the refiners. The cost is estimated to be roughly $5,000.

Total

The total cost of the equipment is estimated to be $1,366,410.

Total Physical Cost

Given as following percentages of Total Installed Equipment Cost:[104]

Process piping and insulation	:	10%
Instrumentation	:	10%
Building	:	25%
Auxiliary facilities	:	10%
Outside lines	:	5%
Total	:	60%

Total Physical Cost . . . . . $2,190,000.

Total Project Cost

Given as following percentages of Total Physical Cost:[104]

Engineering and construction	:	35%
Contingencies	:	30%
Size factor	:	15%

Total Project Cost . . . . . $3,940,000.

Working Capital

Holdup (storage tanks and in-process material) --

137,600 lb at 6¢/lb. $8,520

Other: 10% of Total Installed Equipment Cost[103] . . . . $137,000.

Total Capital Necessary

Working capital plus Total Project Cost. $4,085,250

Annual Costs[103]

Interest	:	(.04) (4,085,250)	= $163,300
Depreciation (7-1/2 years)	:	(.15) (3,940,000)	591,000
Property tax	:	(.02) (2,190,000)	43,700
Insurance	:	(.01) (2,190,000)	21,900
Raw materials	:	(500,000) (0.5)	25,000
Wages: daily need:		8 operators at $4/hr	
		4 maintenance men at $4/hr	
		8 helpers at $3/hr	
		1 supervisor at $12,000/yr	
		1 foreman at $8,000/yr	
		1 secretary at $250/mo	
		1 engineer at $10,000/yr	

Total. $243,100/yr

Fuel, Power, and Steam	:	(0.4) (500,000) (0.1)	= 2,000
Repairs and Maintenance	:	(0.1) (4,085,250)	= 40,853
Overhead: payroll	:	0.15 (243,100)	
general plant	:	0.50 (243,100)	
general office	:	0.10 (243,100)	

Total. . . . . $182,200.

Research, development, patents, etc.:
(.04) (500,000) (0.1) = 2,000

Distributions costs: (.05) (500,000) (0.1) = 2,500

Total: $1,317,553/annum

Contingencies (.05) (1,317,553)

Grand total: $1,380,000/annum

Cost/lb. material processed: $2.76/lb.

NOMENCLATURE

a -- thermal diffusivity, $k/c_p\rho$.

a -- constant.

a_4, a_5, a_6 -- defined in Eq. (19).

A -- cross-sectional area of zone and solid.

A -- $[(1/\alpha) - (1/k_{eff})\exp(B_e L_e/5.3)]$.

b -- constant.

B_e -- defined by $\exp(B_e L) = 1 + B_e L/k_{eff}$.

B_s -- defined by $\exp(B_s L) = 1 + B_s h/k_{eff}$.

c -- constant.

C_j -- jth constant in infinite-series solution.

C_1, C_2, C_3, C_4, C_5, C_6 -- constants.

c_p -- heat capacity at constant pressure.

d -- differential operator.

d -- constant.

d -- thickness of spectrophotometer sample.

D -- diffusion coefficient.

e -- weight fraction of material at eutectic point.

e -- constant.

g -- acceleration due to gravity (taken as positive for flow up, and negative for flow down).

G -- mass rate of flow of material through zone, $VA\rho_s$.

h -- $L_v + L$.

h_b -- mean heat-transfer coefficient for tube below heating chamber surroundings.

h_c -- heat-transfer coefficient from tube inside the chamber to the surroundings.

h_h -- heat-transfer coefficient between heating tape and surroundings.

h_t -- heat transfer coefficient between adjacent layers of heating tape, and between tape and heater tube.

h_T -- mean heat-transfer coefficient for tube above heating chamber to surroundings.

h_z -- heat transfer coefficient between heating tape and zone.

h_{cool} -- heat-transfer coefficient between coolant and inside drum wall.

h_{melt} -- heat-transfer coefficient between solid-liquid interface and bulk melt.

I, I_0 -- emerging and initial light intensity, respectively, in spectrophotometer.

k -- distribution coefficient, w_s/w_ℓ, at equilibrium.

k -- thermal conductivity.

k_a -- thermal conductivity of air.

k_{eff} -- effective distribution coefficient, w_s/w_ℓ.

k_{eff} -- area-weighted average thermal conductivity of glass wall and solid material.

k_{cake} -- thermal conductivity of cake on drum.

k_{drum} -- thermal conductivity of drum material.

k_g -- thermal conductivity of glass tube.

k_s -- thermal conductivity of solid material being processed.

L -- length of capillary tube in diffusion-coefficient determination.

L -- length of zone.

L_b -- length of zone below heating tape.

L_g -- length of glass tube around which heating tape is wrapped.

L_h -- length of heating tape.

L_t -- length of zone above heating tape.

$L_{s,b}$ -- distance of zone above lower surface of heating-tape tube.

$L_{s,t}$ -- distance of zone below upper surface of heating-tape tube.

L_p -- length of flat plate.

L_e -- length of enriching section of zone-void refiner minus h.

L_s -- length of stripping section minus two zone lengths, h, and the sum of the voids in the section.

L_{drum} -- thickness of drum wall.

L_{cake} -- thickness of cake.

L_{eff} -- length of solid over which a separation can be discerned.

L_v -- void length, h - L.

L_{ch} -- distance from the center portion of the heater adjacent to the zone to the upper solid-liquid interface.

$L_{h,zone}$ -- length of heater directly adjacent to zone.

m_j -- jth eigenvalue, $(\lambda_j^2 - p^2/4)^{1/2}$.

M -- molar concentration in moles/liter.

n -- constant.

p -- $LG/DA\ \rho_\ell = LV/D\ (\rho_s/\rho_\ell)$.

P -- either P_s or P_z.

P_s -- total separation in solid relative to initial concentration and to zone density. Defined by Eq. (76).

P_z -- total separation in zone relative to initial concentration and zone density. Defined by Eq. (77).

q -- defined by $(1 - \phi_s) = \exp\ [-q\ (\tau - \tau_0)]$.

q_b -- rate of axial heat conduction into the lower solid interface from the zone.

q_t -- rate of axial heat conduction into the upper solid interface from the zone.

q_{glass} -- rate of axial heat conduction into the glass tube at the bottom and top of the zone.

q_{total} -- total rate of heat transfer from heating tape to tube.

Q_{tot} -- rate of heat transfer from heater to zone.

Q_{waste} -- rate of heat transfer from zone through the side of the tube to the surroundings.

r -- defined by $(\phi - 1) = (\epsilon - 1) \exp(-r\eta)$.

r -- inside radius of zone melting tube.

r_1, r_3 -- radii of outside and inside layers of heating tape, respectively.

R -- outside radius of zone-melting tube.

R_i -- inside radius of heating tube.

R_o -- outside radius of heating tube.

S -- η/p.

t -- time.

T -- temperature.

T -- τ/p^2.

T_c -- temperature of surroundings in heating chamber.

T_b -- temperature of surroundings in lower cooling chamber.

T_T -- temperature of surroundings in upper cooling chamber.

T_m -- melting temperature (or freezing temperature).

T_0 -- temperature at wall.

T_3 -- temperature of inner layer of heating tape.

T_∞ -- temperature in bulk fluid.

T_{cool} -- temperature of coolant flowing through drum.

T_{melt} -- temperature of bulk melt.

V -- zone travel rate.

V_ℓ --mean velocity of liquid in zone, $V(\rho_s/\rho_\ell)$.

V_{opt} -- economically optimal zone travel rate.

w -- weight fraction of component in zone at distance x from freezing interface.

w_i -- concentration of component at wall.

w_ℓ -- concentration of component in bulk fluid.

w_0 -- initial uniform weight fraction of component.

w_s -- weight fraction of component at a distance z from the first material frozen out of the zone.

x -- distance into zone from freezing interface.

x -- concentration in weight fraction.

X_0 -- initial uniform weight fraction in capillary tube.

X_{av} -- average weight fraction in capillary tube at time t after start of diffusion.

X_{bulk} -- weight fraction of medium into which contents of capillary tube are diffusing.

z -- distance along tube from point where solid first came out of the zone.

α -- concentration-densification coefficient, $(1/\rho)\ (\partial\rho/\partial w)_T$.

α -- enrichment ratio for zone-void refiner; ratio of concentration of product of enrichment section to concentration of feed.

α -- extinction coefficient, $(1/d)\log(I/I_0)$.

α_s -- $V\ (\rho\ c_p/k)_{eff}$.

β -- temperature-densification coefficient, $(1/\rho)\ (\partial\rho/\partial T)_w$.

β -- stripping ratio for zone-void refiner; ratio of concentration of product of stripping section to concentration of feed.

β_b -- $2\ h_b/R\ k_{eff}$.

β_c -- $(2\ h_z/k_{eff}R)(r_3/R)$.

γ -- $B_s\ [L_v\beta - h\ (1 - k_{eff})]/[1 + B_s\ h - \exp\ (B_s\ h)]$.

∂ -- partial differential operator.

δ -- boundary-layer thickness at freezing interface.

δ -- $k_{eff}\ (L_v/h)^{1-k_{eff}}$.

Δ -- finite change in a quantity.

ϵ -- e/w_0.

ϵ -- emissivity (radiant heat) of the tube and surroundings.

η -- $xG/DA\ \rho_\ell = xV\ \rho_s/D\ \rho_\ell$.

η -- viscosity, in centipoise.

λ_j -- jth eigenvalue, $(m_j^2 + p^2/4)^{1/2}$.

ν -- kinematic viscosity, in centistokes.

ρ -- density.

ρ_ℓ -- density of liquid.

ρ_s -- density of solid.

τ -- $(t/D)\ (G/A\ \rho_\ell)^2 = (zV/D)(\rho_s/\rho_\ell)^2$.

τ_0 -- τ at which weight fraction first deviates from zero.

$\tau_{us,0.1\%}$ -- τ at which $C_2 = (0.001)C_1$.

ϕ -- w/w_0.

ϕ_s -- w_s/w_0.

$\phi_{s,ext}$ -- extended intercept value of ϕ_s from straight line portion of plot of $\ln |\phi_s - 1|$ vs τ.

ψ -- $\phi \exp (\eta/2)$.

ψ -- $(h\ k_{eff} - 1)/L_v$.

ψ_j -- eigenfunction.

ω -- $[k_{eff}/(1 - k_{eff})\ B_e\ L]\ [1 - \exp (B_e\ L_v)]$.

$\mathrm{erf}(x)$ -- $(2/\pi^{1/2}) \int_0^x e^{-x^2}\ dx$.

erfc (x) -- 1 - erf (x).

exp (x) -- e^x.

Gr -- Grashof number for heat transfer, $(gr^3\beta)(T_0-T_\infty)/\nu^2$.

Gr' -- Grashof number for mass transfer, $(gr^3\alpha)(w_i-w_\ell)/\nu^2$.

$(2hA/L)_0$ -- heat loss rate from edge of heating tape per unit length of tape per degree temperature difference between tape and surroundings.

q/A -- heat rate per unit area transferred through solid cake in cooled-drum apparatus.

q/A -- heat input per unit area to the heating tape.

Pr -- Prandtl number, ν/a.

Rot -- rotameter reading.

Sc -- Schmidt number, ν/D.

ΔH_f -- latent heat of fusion.

ΔT -- degrees of subcooling.

ΔT -- difference in temperature between the melting point of the average mixture in the zone during a run and the average outlet coolant temperatures.

LIST OF ILLUSTRATIONS

BIBLIOGRAPHY

1. H. E. Buckley, Crystal Growth, (John Wiley and Sons, Inc., New York, 1951).

2. W. G. Pfann, Zone Melting, (John Wiley and Sons, Inc., New York, 1958).

3. W. G. Pfann, Trans. Am. Inst. Min. and Met. Eng. 194, 747 (1952).

4. W. G. Pfann, U. S. Pat. 2,739,088 (March 20, 1956).

5. W. G. Pfann, Trans. Am. Inst. Mining Engrs. 203, 297 (1955).

6. W. G. Pfann and R. W. Hamming, Bell Telephone Laboratories, Inc. Monograph 3289, April 16, 1958.

7. W. G. Pfann, U. S. Pat. 2,750,262 (July 12, 1956).

8. W. G. Pfann, U. S. Pat. 2,739,045 (March 20, 1956).

9. L. K. Frevel and L. J. Kressley, U. S. Pat. 2,659,761 (Nov. 17, 1953).

10. D. L. McKay, U. S. Pat. 2,823,242 (Feb. 11, 1958).

11. A. Zarchin, U. S. Pat. 2,821,304 (Jan. 28, 1958).

12. R. A. Findlay and D. L. McKay, Chem. Eng. Prog. Symp. Series 55, No. 25, 163 (1959).

13. D. L. McKay, G. H. Dale, and J. A. Weedman, Ind. Eng. Chem. 52, 197 (1960).

14. M. A. Vela, U. S. Pat. 2,839,411 (June 17, 1958).

15. T. A. Tarr, U. S. Pat. 2,874,199 (Feb. 17, 1959).

16. R. W. Thomas, U. S. Pat. 2,854,494 (Sept. 30, 1958).

17. R. M. Green and J. W. Clark, U. S. Pat. 2,833,835 (May 6, 1958).

18. R. M. Green, U. S. Pat. 2,848,516 (Aug. 19, 1958).

19. J. I. Harper, U. S. Pat. 2,846,292 (Aug. 5, 1958).

20. S. J. Kolner, U. S. Pat. 2,835,598 (May 20, 1958).

21. J. A. Weedman, U. S. Pat. 2,868,830 (Jan. 13, 1959).

22. G. A. William and A. Firth, British Pat. 808,176 (Jan. 28, 1959).

23. J. D. Ratje, U. S. Pat. 2,809,884 (Oct. 15, 1957).

24. Thomas Baron, B.S. Thesis, University of Illinois (1943).

25. K. A. Jackson, Can. J. Phys. 36, 683 (1958).

26. Howard Reiss, Trans. Am. Inst. Min. Eng. 200, 1053 (1954).

27. I. Braun and S. Marshall, Brit. J. Appl. Phys. 8, 157 (1957).

28. Carl Wagner, J. Metals, 154 (Feb. 1954).

29. I. Braun, Brit. J. Appl. Phys. 8, 457 (1957).

30. L. W. Davies, Phil. Mag. 3, 159 (1958).

31. L. Burris, Jr., C. H. Stockman, and I. D. Dillon, Argonne National Laboratory Report ANL-5294.

32. J. A. Burton, R. C. Prim, and W. P. Slichter, J. Chem. Phys. 21, 1987 (1953).

33. V. G. Smith, W. A. Tiller, and J. W. Rutter, Can. J. Phys. 33, 723 (1955).

34. R. N. Hall, J. Phys. Chem. 57, 836 (1953).

35. Jules Pauly, Pierre Süe, Compt. Rend. 244, 2722 (1957).

36. P. Albert, O. Dimitrov, J. L. Héricy, and G. Chaudson, Compt. Rend. 244, 965 (1957).

37. R. D. Burch and C. T. Young, North American Aviation Report NAA-SR-1753 (1958).

38. J. E. Antill, Nuclear Power I, 155 (August 1956).

39. P. Süe, J. Pauly, Andrée Nouaille, Compt. Rend. 244, 1212 (1957).

40. Poul Sorensen, Chem. and Ind. (London), 1593 (1959).

41. J. S. Ball, R. V. Helm, and C. R. Ferrin, Refining Engineer 30, No. 13, C36 (1958).

42. Robert G. Pohl, J. Appl. Phys. 25, 1170 (1954).

43. D. W. Memelink, Philips Research Reports 11, 183 (1956).

44. K. F. Hulme, Proc. Phys. Soc. B68, 393 (1955).

45. W. A. Tiller, K. A. Jackson, J. W. Rutter, and B. Chalmers, Acta Met. 1, 428 (1953).

46. A. I. Landau, in Rost Kristallov, First Conference on Crystal Growth, (Academy of Sciences USSR Press, Moscow, 1957), p. 58. Translated by Consultants Bureau, Inc., New York, 1958.

47. E. L. Holmes, J. W. Rutter, and W. C. Winegard, Can. J. Phys. 35, 1223 (1957).

48. R. H. Doremus, B. W. Roberts, and D. Turnbull, Growth and Perfection of Crystals, (John Wiley and Sons, Inc., New York, 1958), Ch. 4.

49. W. D. Lawson and S. Nielsen, Preparation of Single Crystals, (Butterworth Scientific Publications, London, 1958), pp. 78, 186, 190.

50. R. C. Himes, S. E. Miller, W. H. Mink, and H. L. Goering, Ind. Eng. Chem. 51, 1345 (1959).

51. D. A. Petrov and B. A. Kolachev in Rost Kristallov, First Conference on Crystal Growth, (Academy of Sciences USSR Press, Moscow, 1957), p. 126. Translated by Consultants Bureau, Inc., New York, 1958.

52. M. Tanenbaum, in Semiconductors, N. B. Hannay, Ed., (Reinhold, Publishing Co., New York, 1959), Ch. 3.

53. Ottomar Jäntsch, Neues Jahrbuch für Mineralogie, Monatschefte 47, 205 (1956).

54. G. H. J. A. Tamman, States of Aggregation, (D. Van Nostrand Co., Inc., New York, 1925), Ch. 9.

55. C. S. Lindenmeyer, G. T. Orrok, K. A. Jackson, and B. Chalmers, J. Chem. Phys. 27, 822 (1957).

56. J. B. Hudson, W. B. Hillig, and R. M. Strong, J. Phys. Chem. 63, 1012 (1959).

57. L. F. Fieser and M. Fieser, Organic Chemistry, 2nd Ed. (Heath, Boston, 1950).

58. International Critical Tables, Edward W. Washburn, Ed., (McGraw-Hill Book Co., Inc., New York, 1926).

59. H. Crompton and M. A. Whiteley, J. Chem. Soc. (London), 67, 327 (1895).

60. E. Rudolfi, Z. Phys. Chem. 66, 705 (1909).

61. H. A. Miers and F. Isaac, J. Chem. Soc. (London) 93, 927 (1908).

62. G. Vignon, Bull. Soc. Chim. France (3) 6, 656 (1891).

63. H. Rheinboldt and M. Kircheisen, J. Prakt. Chem. (2) 113, 199 (1926).

64. J. S. Forsyth and J. T. Wood, Trans. Inst. Chem. Eng. 33, 122 (1955).

65. Mason, Rosen, and Swift, J. Chem. Ed. 18, 473 (1941).

66. L. Kofler and A. Kofler, Thermo-Mikro-Methoden, (Verlag Chemie, Weinheim, Bergstrasse, 1954).

67. Walter C. McCrone, Jr., Fusion Methods in Chemical Microscopy, (Interscience Publishers, Inc., New York, 1957).

68. Technological Service Bulletins 6886-A, 6886-B, 6887-A, 6889-C, (Arthur H. Thomas Co., Philadelphia, 1957).

69. Chemical Engineers' Handbook, John H. Perry, Ed., Third Edition, (McGraw-Hill Book Co., Inc., New York, 1950), pp. 213, 214, 153, 161, 131, 143.

70. Handbook of Chemistry and Physics, Charles D. Hodgman, Ed., Thirty-fourth Edition., (Chemical Rubber Publishing Co., Cleveland, Ohio, 1952), pp. 753, 1011, 1019, 1934, 1935, 1937, 1940, 1970, 1971.

71. F. W. Schwab and E. Wichers, J. Research Nat. Bur. Standards 25, 747 (1940).

72. M. P. Mathiew, Chem. Abstracts 47: 10288g,h (1953).

73. A. J. Streiff, A. R. Hulme, P. A. Cowie, N. C. Krouskop, and F. D. Rossini, Anal. Chem. 27, 411 (1955).

74. G. Egloff, Physical Constants of Hydrocarbons, (Rheinhold, New York, 1947), Vol. IV, p. 77.

75. N. S. Kurnakow, Z. für Anorg. Chem. 135, 81 (1924).

76. L. Deffet and G. Vlérick, Chem. Abstracts 38: 4500 (1944).

77. R. S. Jessup, Chem. Abstracts 40: 6330 (1946).

78. R. R. Dreisbach, Physical Properties of Chemical Compounds (American Chemical Society, Washington, D. C., 1955), p. 203.

79. American Society for Testing Materials, Test for Kinematic Viscosity, ASTM Method D445-53T, 1953.

80. M. R. Cannon and M. R. Fenske, Ind. Eng. Chem. Anal. Ed. 10, 297 (1938).

81. W. J. Morris and R. Schnurmann, Chem. Abstracts 44: 3759h (1950).

82. A. Z. Golik and S. D. Ravikovich, Chem. Abstracts 43: 4064i (1949).

83. F. B. Marti, Bull. Soc. Chim. Belg. 39, 590 (1930).

84. H. S. Carslaw and J. C. Jaeger, Conduction of Heat in Solids, 2nd Ed. (Clarendon Press, Oxford, 1959), p. 96.

85. R. C. Reid and T. K. Sherwood, The Properties of Gases and Liquids, (McGraw-Hill Book Co., Inc., New York, 1958), p. 257.

86. K. Hrynakowski and A. Smoczkiewiczowa, Chem. Abstracts 31: 4883 (1937), ibid. 31: 6096 (1937).

87. K. Ueberreiter and H. Orthmann, Z. Naturforsch. 5a, 101 (1950).

88. S. Satō and T. Sogabe, Chem. Abstracts 35: 4275 (1941).

89. D. C. Ginnings and G. T. Furukawa, J. Am. Chem. Soc. 75, 522 (1953).

90. Coffin, Devins, and Dingle, Can. J. Res. 28B, 579 (1950).

91. L. Marchlewski and A. Moroz, Bull. Soc. Chim. France 33, 1405 (1923); ibid. 35, 473 (1924).

92. William H. McAdams, Heat Transmission, (McGraw-Hill Book Co., Inc., New York, 1954), p. 173, Eq. (7-5b).

93. E. M. Sparrow, NACA Tech. Note 3508 (July, 1955).

94. William H. McAdams, Heat Transmission (McGraw-Hill Book Co., Inc., New York, 1954), Ch. 7.

95. C. H. Sorum and E. A. Durand, J. Am. Chem. Soc. 74, 1071 (1952).

96. P. S. Vadilo in Rost Kristallov, First Conference on Crystal Growth (Academy of Sciences USSR Press, Moscow, 1957), p. 109. Translated by Consultants Bureau, Inc., New York, 1958.

97. W. R. Wilcox, Simultaneous Heat and Mass Transfer in Free Convection, UCRL-8807, August, 1959. Chem. Eng. Science (in press).

98. E. F. G. Herington, R. Handley, and A. J. Cook, Chem. and Ind. (London), 292 (1956).

99. William H. McAdams, Heat Transmission (McGraw-Hill Book Co., Inc., New York, 1954), p. 180.

100. William H. McAdams, Heat Transmission (McGraw-Hill Book Co., Inc., New York, 1954), p. 219.

101. Chem. Eng. News 38, No. 3, 19 (Jan. 18, 1960).

102. Chem. Eng. News 37, No. 26, 41 (June 29, 1959).

103. O. T. Zimmerman and Irvin Lavine, Chemical Engineering Costs, (Industrial Research Service, Dover, New Hampshire, 1950).

104. Cecil H. Chilton, Chem. Eng., 97 (June, 1949).

105. Engineering News Record, 109 (Aug. 20, 1959).